# FIBER-WIRELESS INTEGRATED SYSTEMS WITH ULTRA-HIGH CAPACITY LOW-LATENCY AND HIGH-RELIABILITY

A Dissertation
Presented to
The Academic Faculty

By

Feng Lu

In Partial Fulfillment
of the Requirements for the Degree
Doctor of Philosophy in the
School of Electrical and Computer Engineering

Georgia Institute of Technology

May 2018

**FIBER-WIRELESS INTEGRATED SYSTEMS WITH ULTRA-HIGH CAPACITY LOW-LATENCY AND HIGH-RELIABILITY**

Approved by:

Dr. Gee-Kung Chang, Advisor
School of Electrical and Computer Engineering
*Georgia Institute of Technology*

Dr. Mary Ann Weitnauer
School of Electrical and Computer Engineering
*Georgia Institute of Technology*

Dr. Xiaoli Ma
School of Electrical and Computer Engineering
*Georgia Institute of Technology*

Dr. John R. Barry
School of Electrical and Computer Engineering
*Georgia Institute of Technology*

Dr. Umakishore Ramachandran
School of Computer Science
*Georgia Institute of Technology*

Date Approved: February 5, 2018

To my family, my friends and my beloved wife Yun.

## ACKNOWLEDGMENTS

I would like to take this opportunity to express my sincere gratitude to many people who make this dissertation possible.

First, I would like to thank my advisor, Professor Gee-Kung Chang for his continuous support, guidance, motivation, and patience during the past four years. He has shaped and inspired my years at Georgia Tech with his vision, intellectual scope, and uncompromising effort for excellence. It is my greatest honor and pleasure to work with him as his student.

The next thank goes to my dissertation committee members, Prof. Xiaoli Ma, Prof. Mary Ann Weitnauer, Prof. John R. Barry, all from School of Electrical and Computer Engineering, and Prof. Umakishore Ramachandran from School of Computer Science, for their valuable time, insightful comments, suggestions, and approval of my research work.

I am appreciative to my colleagues in the research group. Their unending support, encouragement, and friendship have accompanied me during my wonderful journey at Georgia Tech. Thanks to Dr. Junwen Zhang, Dr. Daniel Guidotti, Dr. Cheng Liu, Dr. Jing Wang, Dr. Lin Cheng, Dr. M. M. Usman Gul, Mu Xu, Hyunwoo Cho, Yahya M Alfadhli, Shuyi Shen, Hyung Joon Cho, Qi Zhou, Rui Zhang, Shuang Yao, as well as many other graduate students, visiting students and scholars. I feel so lucky and proud to have the chance to learn from them and work with them in the team.

I would like to thank my family for all their love, encouragement, and unconditional support. For my parents, who raised me up and shaped me as a considerate and responsible man for the family and society. Finally, and most importantly, special thanks to my beloved wife, Yun Liu. Your support, encouragement, patience and unwavering love were undeniably the bedrock upon which the past ten years of my life have been built, and the most important driving force to make the dissertation possible.

Thank you all.

## TABLE OF CONTENTS

## LIST OF TABLES

## LIST OF FIGURES

## SUMMARY

The "Information Age" is formed by advances in computer networks with the Internet reaching a critical mass of individuals. In the 2000s, the mobile Internet and data connection have experienced exponentially increases after the 3G deployment and Wi-Fi popularity. It is demanding higher capacity, better performance, improved reliability, lower latency and ubiquitous coverage for future wireless communication systems adapting to diverged application scenarios: enhanced mobile broadband (eMBB), ultra-reliable low-latency communications (URLLC) and massive machine type communications (mMTC). With limited average revenue per user (ARPU) for operators and more devices per user, more stringent requirement exists in the cost of devices, as well as network deployment, expansion, upgrading, and operation. The enabling technology behind the overwhelming explosion of the mobile data traffic largely relies on the optical network. It provides high bandwidth and low loss connections from the core network to all types of cells, serving as parts of the radio access network (RAN). Traditional RAN consists of isolated wired and wireless systems, with separate design and optimization. It is not the optimal solution nowadays concerning capital expenditure (CAPEX), operational expenditure (OPEX), performance, latency, reliability, and system capacity. A fiber-wireless integrated system would significantly improve the mobile data network in all these aspects.

This Ph.D. dissertation focuses on system design and digital signal processing (DSP) techniques for the fiber-wireless integrated system and the fiber-wireless channel, to provide higher capacity, improved reliability and reduced latency for next-generation wireless systems. Specifically, the design and optimization are in three aspects: improving the mo-

bile fronthaul (MFH) transmission quality within the physical limitations of the fiber link, in both analog and digital MFH solutions; designing the advanced waveforms adapting to the high-frequency millimeter-wave (MMW) fiber-wireless integrated system; and combining all available electromagnetic (EM) frequency resources in the RAN as the all-spectrum wireless access system.

The current mobile network is based on wireless transmissions using frequencies below 6-GHz. With the introduction of cloud-RAN (C-RAN) and centralized processing, the MFH connecting baseband unit (BBU) cloud and remote radio head (RRH) is an essential network section. Legacy common public radio interface (CPRI) is insufficient concerning capacity and cost requirement of the future 5G system, given that massive multiple-in-multiple-out (MIMO), large-scale carrier aggregation (CA) using an increased bandwidth per channel are necessary. The utilization of more powerful forward error correction (FEC) in the optical link also increases the latency and DSP power consumption. In this dissertation work, different system designs using novel components and advanced DSP schemes are proposed and implemented. For optical multiplexing in the spectral efficient MFH, we apply Fabry-Perot laser diode (FPLD) to enable the low-cost colorless RRH in dense wavelength division multiplexing (DWDM) networks. Besides, the signal peak-to-average power ratio (PAPR) in the analog MFH is reduced using the proposed sub-band phase pre-distortion in DSP. For digital MFH, an adaptive parameter selection scheme in digitization is proposed adapting to varying MFH link conditions, to achieve a high performance without additional requirements to the optical link and the transceiver, or higher DSP complexity/latency due to the more powerful FEC. Both analog and digital MFH solutions are investigated and experimentally demonstrated with enhanced performance in the dissertation work, that operators could choose based on application scenarios and link distances, to provide services with high capacity, reduced latency, and more system power margins.

With increasing data-hungry applications that require high data rate and enhanced device battery life, expanding the wireless channel bandwidth is a promising way to boost up

speed with simple DSP. Given the congested low-frequency channels, higher MMW bands are hot topics for future wireless system deployment. Considering the huge bandwidth and high frequency/time synchronization requirements in case of multi-cell coordination, centralized processing and phonics-assisted up-conversion are the preferred way. With well-established foundations on the physical MMW fiber-wireless integrated system design, this dissertation focuses on the waveform design and optimization adapting to fiber-wireless integrated channel characteristics. For eMBB using CA technology, generalized frequency division multiplexing (GFDM) is proposed to be applied in the fiber-wireless system, to minimize the overhead by frequency guard bands, as well as providing higher tolerance to frequency offsets in both optical and electrical carriers. For eMBB and mMTC, considering the high free-space propagation loss and weak penetration/reflection capabilities by MMW, we proposed the power-division non-orthogonal multiple access (NOMA) in addition to the orthogonal frequency division multiple access (OFDMA). More users with balanced and improved transmission qualities are supported without additional output power. Both downlink and uplink are investigated with synchronized and asynchronous transmissions correspondingly. For URLLC, the orthogonal chirp division multiplexing (CDM) is designed by replacing the frequency kernels in orthogonal frequency division multiplexing (OFDM) to orthogonal digital chirps, for stronger robustness to frequency or time selective interferences/noises, without losing spectral efficiency under some settings. eMBB can also be supported within the same CDM framework, which reduces the DSP complexity and control overheads. These waveforms designed for fiber-wireless integrated systems with diverged application scenarios provide a reference for future mobile data networks.

Ultimately, the wireless frequency is capable of going up to more than 700-THz using current laser and light-emitting diode (LED) technologies. The concept of the all-spectrum wireless system is proposed in this dissertation, to utilize all available spectral resources in the RAN enhancing the data rate and minimize the interference with legacy systems. The centralized processing and C-RAN architecture can reduce the system complexity and

enable inter-band and inter-cell coordination. The all-spectrum coordination is utilized in two applications: user connection and MFH. The user equipment can embed transceivers supporting multiple spectra, from low-frequency to the visible light range. By allocating the traffic with different applications, user categories, and directions to various bands, the overall system capacity is maximized with improved coverage and mobility support. We also design the MFH network serving this all-spectrum access system with minimized resource usage in the optical MFH link. In addition, we propose and demonstrate the visible light communication (VLC) based MFH for indoor signal delivery, as well as converged MMW/free space optics (FSO) schemes using adaptive diversity combining technique (ADCT) and multi-layer function-split. Better reliability is experimentally demonstrated with minimized CAPEX and OPEX.

# CHAPTER 1

# INTRODUCTION AND BACKGROUND

## 1.1 Background and Motivation

With the "Information Age" formed by advances in computer networks when the Internet reaching a critical mass of individuals in the 1990s, the mobile Internet and data connection have experienced exponentially increase after the 3G deployment and Wi-Fi popularity in the 2010s. Broadband mobile networks have enabled information access to the world any time from anywhere to shape the modern society, leading the "Information Age" to a new stage. The global mobile traffic has grown 18-fold in the past 5 years, and will experience a 7-fold increase from 7 exabytes in 2016, to 49 exabytes by 2021 [1], corresponding to 47% compound annual growth rate (CAGR). The global mobile devices and connections are expected to be grown at 8% CAGR. In addition, the application scenario expands to applications that require high reliability and long battery life. It is demanding higher capacity, better performance, improved reliability, lower latency and ubiquitous coverage for future wireless systems [2].

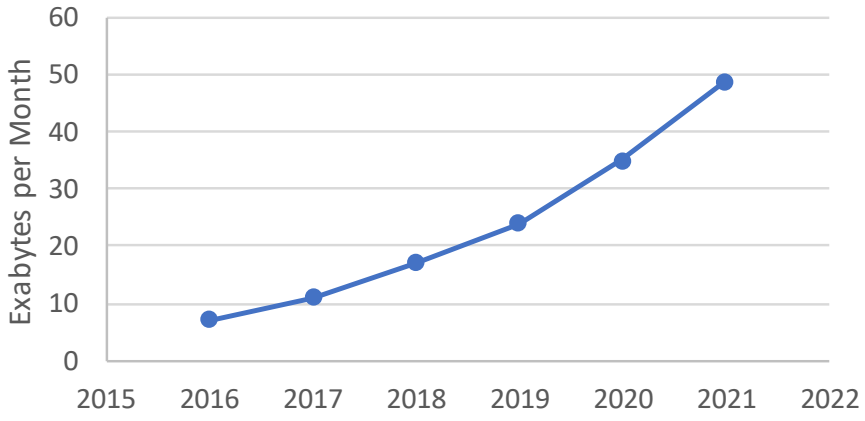


Figure 1.1: Forecast of mobile data traffic by 2021 [1].

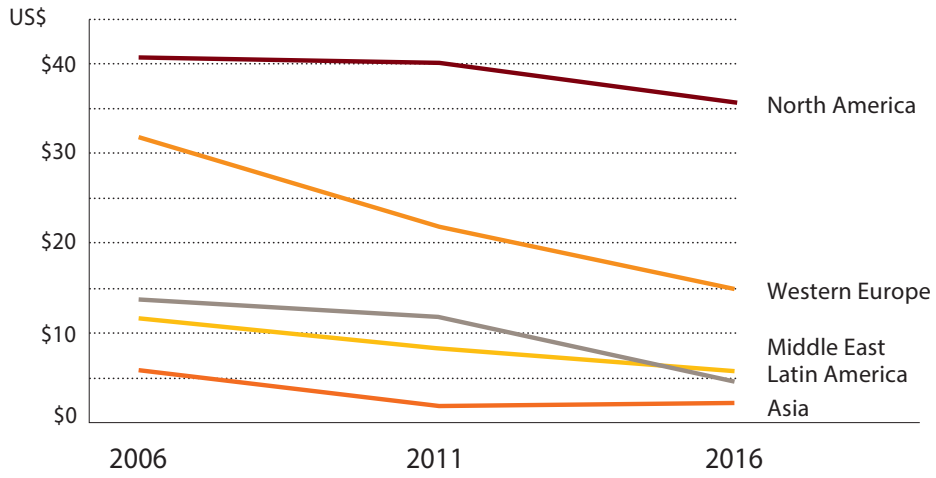


Figure 1.2: Average revenue per user from 2006-2016 [3].

Currently, we observe a gradually decreasing average revenue per user (ARPU) for operators. And the competition from over-the-top (OTT) players are fierce. They offer applications and streaming services directly to consumers through the Internet data service, which have increased their dominance from 2010, even in core communication services such as messaging and voice. Services from Google, Apple, Microsoft and so on have already represent more than 80 percent of all messaging traffic. Many telecommunication operators are facing significant decreases in their basic communication service revenues: drop-offs of as much as 30 percent in short message service (SMS) messaging, 20 percent in international voice, and 15 percent in roaming [3]. As the result, a more stringent requirement exists in the cost of network deployment, expansion, upgrading, and operation, in order to maintain and grow the margin and net income. In addition, the mobile Internet data services plays a more and more important role for the service provider business, comparing with voice and messaging. Other new applications like Internet of things (IoT) will provide huge potential in business growth in the future, with high sensitivity to device cost since the number of devices per user will be increased [4].

The enabling technologies behind the overwhelming explosion of the mobile data traffic mainly rely on the optical networking technology [5, 6]. Since optical fiber was introduced as a promising communication medium by Charles Kao and George Hockham in 1966 [7],

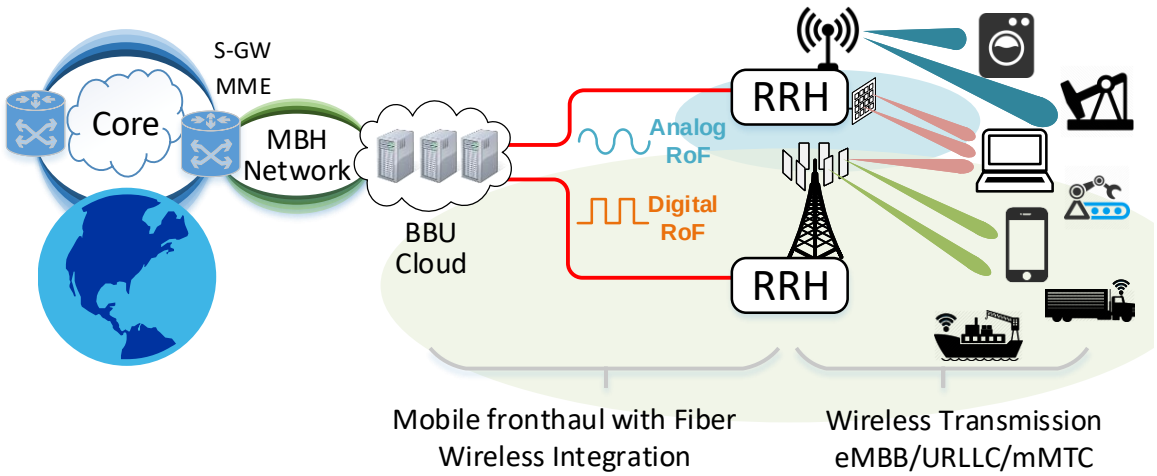


Figure 1.3: Simplified fiber-wireless integrated system model.

it provides high-bandwidth and low-loss connections from the core network to all types of cells, serving as parts of the radio access network (RAN). RAN is the section from the core network to wireless devices. Traditional RAN with fiber or copper wires consists of isolated wired and wireless transmission systems [8]. All processing, modulation, and demodulation are executed in distributed radio heads, called evolved Node B (eNB). Each eNB is complicated and power consuming, with high working condition requirements, making the mobile data network insufficient concerning capital expenditure (CAPEX), operational expenditure (OPEX), power efficiency, and performance. Also, the small channel bandwidth, varying channel conditions and simple DSP limit the data rate and link reliability.

Addressing these drawbacks, it is feasible to integrate optical networks in the mobile system to provide connections to all devices, in an integrated and synchronized manner. A typical fiber-wireless integrated system is shown in Fig.1.3. It consists of three sections from the core network to the user equipment (UE). The mobile backhaul (MBH) connects the service gateway (S-GW) and baseband unit (BBU) clouds, using intensity or coherent optical modulation [9]. All PHY layer functions are executed in BBU clouds, which enables resource sharing, coordination, and virtualization among multiple cells [10]. The mobile fronthaul (MFH) is capable of delivering modulated waveforms between BBU clouds and remote radio heads (RRHs). Finally, the wireless link connects RRHs and UEs with ad-

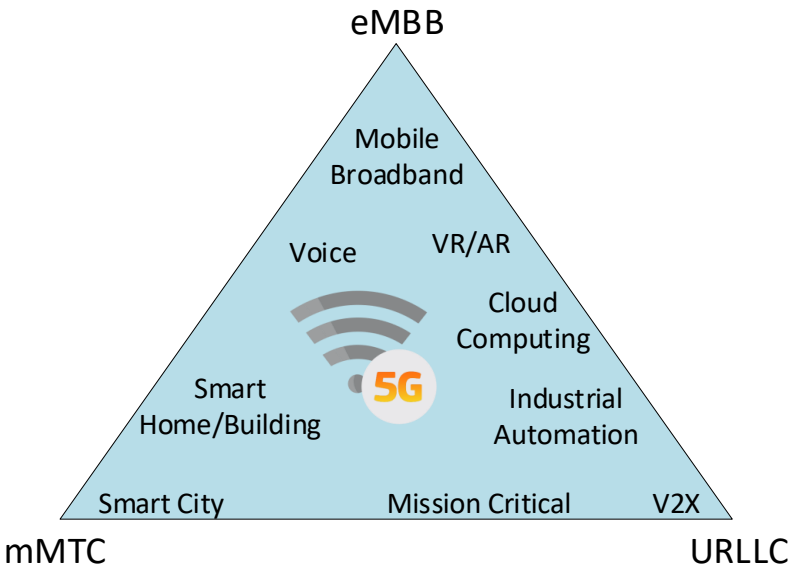


Figure 1.4: Diverged application scenarios defined in 5G.

vanced wireless technologies such as carrier aggregation (CA) and massive multiple-input-multiple-output (MIMO), utilizing multiple bands. This architecture is acknowledged and widely deployed in current Long Term Evolution-Advanced (LTE-A) systems.

With the 5G standardization and its potential deployment after 2020, more application scenarios are discussed in the mobile data network, including eMBB, URLLC, and mMTC as shown in Fig.1.4. The eMBB focuses on applications that require high bandwidth and high traffic density, such as virtual reality (VR), augmented reality (AR) and ultra-high resolution (UHD) high frame rate 4k or 8k video streaming. Intended to support a wide range of services including broadband access in dense areas, in the crowd and vehicles, the first commercial use of the 5G technology is expected to be eMBB to support up to 10-Gbps peak data rate. For broadband access in dense areas, the connection density requirement is 200-2500 users per $km^2$, with a traffic density of 750-Gbps per $km^2$ in the downlink and 125-Gbps per $km^2$ in the uplink. For eMBB in the crowd, like in a stadium, the requirement goes up to 150,000 per $km^2$, and the traffic density is 3.75/7.5-Tbps per $km^2$ for downlink and uplink accordingly [11].

Apart from human-centric eMBB traffic, the machine type communication (MTC) plays

Table 1.1: Key performance indexes in IMT 2020 vision.

| Key Performance Index | | IMT 2020 Performance Requirements |
|---|---|---|
| Per User Performance | Peak Data Rate | >10 Gbps |
| | Minimum Data Rate | >100 Mbps |
| Density | Supported User Density | >1,000,000 Connections / $km^2$ |
| | Supported Traffic Density | >10 Tbps/$km^2$ |
| Latency | | <1 ms End to End |
| Mobility | | Up to 500 km/s |
| Energy Consumption | | 1/10 X Compared to 2010 |
| Service Deployment and Operation | Network OPEX | 1/5 X |
| | Deployment Time | 1/1000 X |

a more critical role in the 5G era, including URLLC and mMTC [12]. mMTC serves the category of service that a massive number of machine-type devices are connected within a limited area. The application includes logging, metering, security monitoring and asset tracking. High connection density up to one million connections per $km^2$ and ultra-high efficiency in power consumption supporting more than ten years of battery life should be supported by this 5G scenario, which presents great difficulty [13]. URLLC emphasis on the reliability and latency performance of wireless transmission, which is suitable for applications that are mission-critical, including but not limited to autonomous cars, wireless industrial control, and drone-related applications [14]. The waveform design of the URLLC service is challenging and problematic since the two features (high-reliability and low-latency) are conflicting, and high mobility should also be considered for better reception performance adapting to the applications [15].

The future fiber-wireless integrated system is shown in Fig.1.5 with multiple application scenarios. All types of devices are supported in the unified fiber-wireless integrated system, including devices requires extremely-high data rate, long battery life or high reliability. To

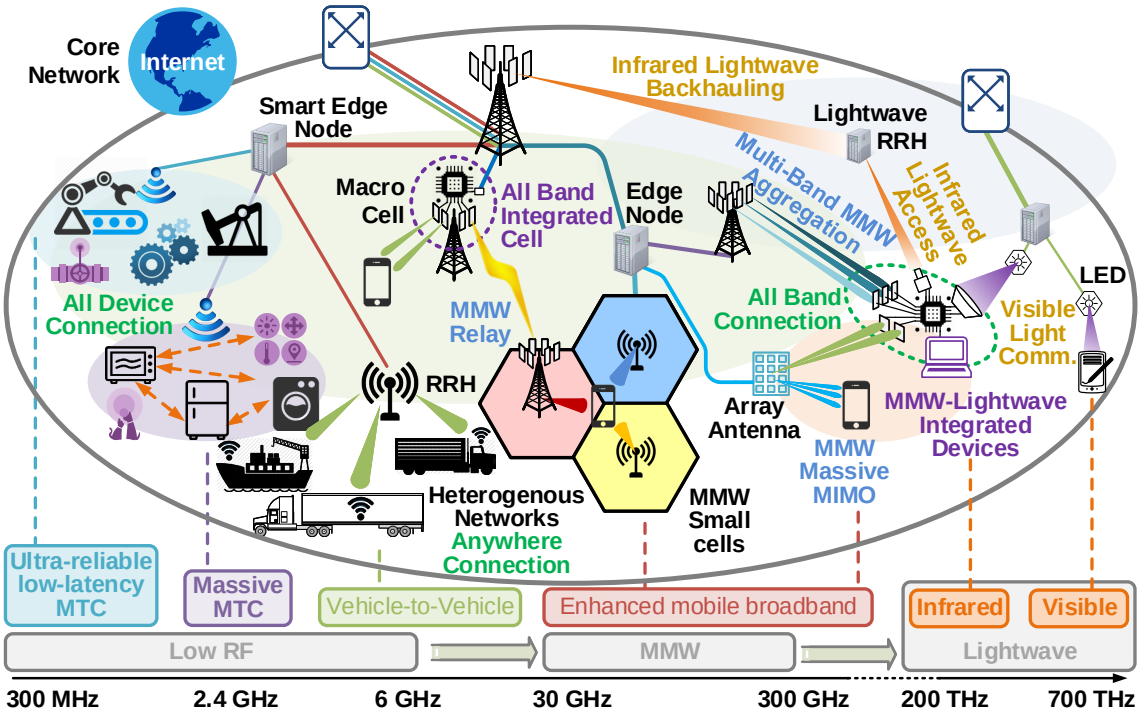


Figure 1.5: Future fiber-wireless integrated system utilizing all spectrum resources

serve a huge number of diversified devices, a comprehensive backbone network is designed, using media including optical fiber, millimeter wave (MMW), free-space optics (FSO) or visible light communication (VLC) links for signal delivery. On top of that, centralized processing is enabled in the BBU cloud. These processing units are capable of some smart computing functions in the edge nodes to reduce the service latency for services benefit from a local decision. Adapting to various scenarios, the wireless frequency range can be extended from sub-GHz to the visible light frequency range of more than 700-THz for connecting user devices, to make use of all available transceiver technologies and achieve the best capacity, density, mobility, coverage, and reliability. All these features contribute to a network that supports all-type device connection, anywhere connection and all-spectrum connection.

Compared with current 4G LTE-A system, using higher wireless transmission bandwidth is an intuitive approach to achieve an increased capacity in the 5G eMBB scenario, by either using enlarged channel bandwidth or combining multiple wireless carriers, known

as CA. The single-channel bandwidth can be doubled, quadrupled or octupled, as current 5G standard proposes. When combined with four CA, the efficient transmission bandwidth can be increased by a factor of up to 32, compared with LTE standards following 3GPP release 8 [16]. The large traffic density in eMBB can also be supported by the capacity gain using multiple-antenna systems, including massive MIMO and beamforming technologies. 5G eMBB will use MIMO technology extensively, as stated currently with up to 32 antenna ports. With massive MIMO and beamforming, operators will be able to deploy 5G base stations on existing sites to achieve a similar coverage using higher frequencies. We can significantly improve the received signal quality thus better power efficiency, signal-to-noise ratio (SNR) and performance are expected. If we consider 160-MHz single channel bandwidth, four CA and 32 MIMO ports, the accumulated wireless bandwidth carried by each small-cell RRH is 20.48-GHz without sectoring, 1024 times of LTE single-input-single-output (SISO). The current common public radio interface (CPRI) based option-8 function-split will need a tremendous bit rate of more than 1-Tbps. The current low-cost optical access network cannot support that huge bandwidth requirement at a reasonable cost with the required distance. Analog radio over fiber (RoF)-based MFH may solve the bandwidth challenge by enabling a one-to-one mapping ratio between the wireless and optical domain, but the linearity and SNR requirements tend to be higher. In addition to increasing the bandwidth, high order modulation (HOM) up to 256-quadrature amplitude modulation (QAM) or 1024-QAM can be applied in eMBB adapting to the increased SNR enabled by high-gain adaptive beamforming, but it needs additional SNR and linearity to maintain higher signal-to-noise-and-interference ratio (SINR) if analog MFH is applied [17].

To enable high traffic density geographically, small cell is a necessary deployment scenario that a huge number of cells are deployed in the limited area both indoor and outdoor, to fully utilize the spatial multiplexing [18]. For the optical network, traditional point-to-point (P2P) MFH connections are hard to deploy, maintain and operate, under this

background, since a huge number of fiber connections will be in each central office (CO). Thus, a proper multiplexing scheme is necessary for optical fibers. Wavelength division multiplexing (WDM) or time division multiplexing (TDM) are mature technologies in optical access networks proposed for MFH. However, the latency generated by time division multiplexing-passive optical network (TDM-PON) scheduling makes it hard to be fit into the 5G low-latency scope. On the other hand, the WDM-PON, especially dense wavelength division multiplexing (DWDM)-PON requires temperature-controlled wavelength-tunable lasers in distributed RRHs, that is costly and hard for RRHs with industrial temperature range.

To obtain higher peak data rate and minimize the digital signal processing (DSP) complexity in the transceiver, expanding the bandwidth by seeking extra spectral resources are the mainstream approach, to use higher MMW, THz or even lightwave frequencies for signal delivery. With larger aggregated bandwidth, it is more challenging to use traditional CPRI based MFH solutions for these wideband applications. Instead, MMW fiber-wireless integrated system is the optimal approach to deliver the signal in its raw waveform format with photonics-assisted up-conversion for better synchronization among different cells in the frequency and time domain. Besides, this approach reduces the device cost in RRH, minimizes the power consumption and can be more stable in distributed cell sites due to the elimination of local oscillators (LOs). However, with the introduction of integration between optical and wireless channels, a new channel is formed which also includes the fiber transmission penalty. More severe frequency selective interferences may be observed in analog MFH, and signal leakage is possible in devices with the multi-band operation. Design of the waveform adapting to the new channel is preferred to achieve the best capacity and performance without changing the mature transceiver architecture. Considering mMTC, a large number of devices are connected to the network using limited resources like subcarriers in the frequency domain or time slots. Current orthogonal frequency division multiple access (OFDMA) cannot draw a right balance between network capacity,

throughput, and quality of service (QoS) control. A new design in the MMW fiber-wireless integrated system to multiplex and separate multiple user data is crucial to support millions of devices in a small area.

When the transmission frequency is further increased from MMW to lightwave frequency range, more stringent requirements on network control and synchronization exist. With narrow beams formed by FSO transmitter, the beam searching and tracking becomes crucial with ultra-high precision, and any prior location information would reduce the latency. Implementing the system in user access is far more than only the P2P link design, a comprehensive network design and resource allocation scheme are preferable to achieve the post-5G system goal with a minimized additional cost to both UE and networks. Besides, the new trend of network densification makes the fiber-only MFH insufficient when more cells are deployed in different environments, that MMW and lightwave can be coordinated to connect cells in the future. As high-frequency transmission schemes, these links are unreliable and expensive, which limits the potential of these technologies.

This dissertation aims to improve the system capacity, reduce the end-to-end latency, and increase the reliability, adapting to different application scenarios in the fiber-wireless integrated system. It provides a reference in both network architecture and DSP design for future 5G and beyond mobile networks. Specifically, the dissertation focuses on the network section from BBU cloud to the UE, including the seamless integration of advanced MFH and wireless transmissions.

## 1.2 Research Background and Challenges

### 1.2.1 Advanced Mobile Fronthaul

Since the proposal of centralized BBU pooling/hoteling and C-RAN concept [19, 20], the optical MFH network becomes necessary to connect distributed RRHs. The function of MFH is to deliver the information of modulated wireless waveforms to and from the RRH, to simplify the RRH DSP and improve the system performance with inter-cell coordination.

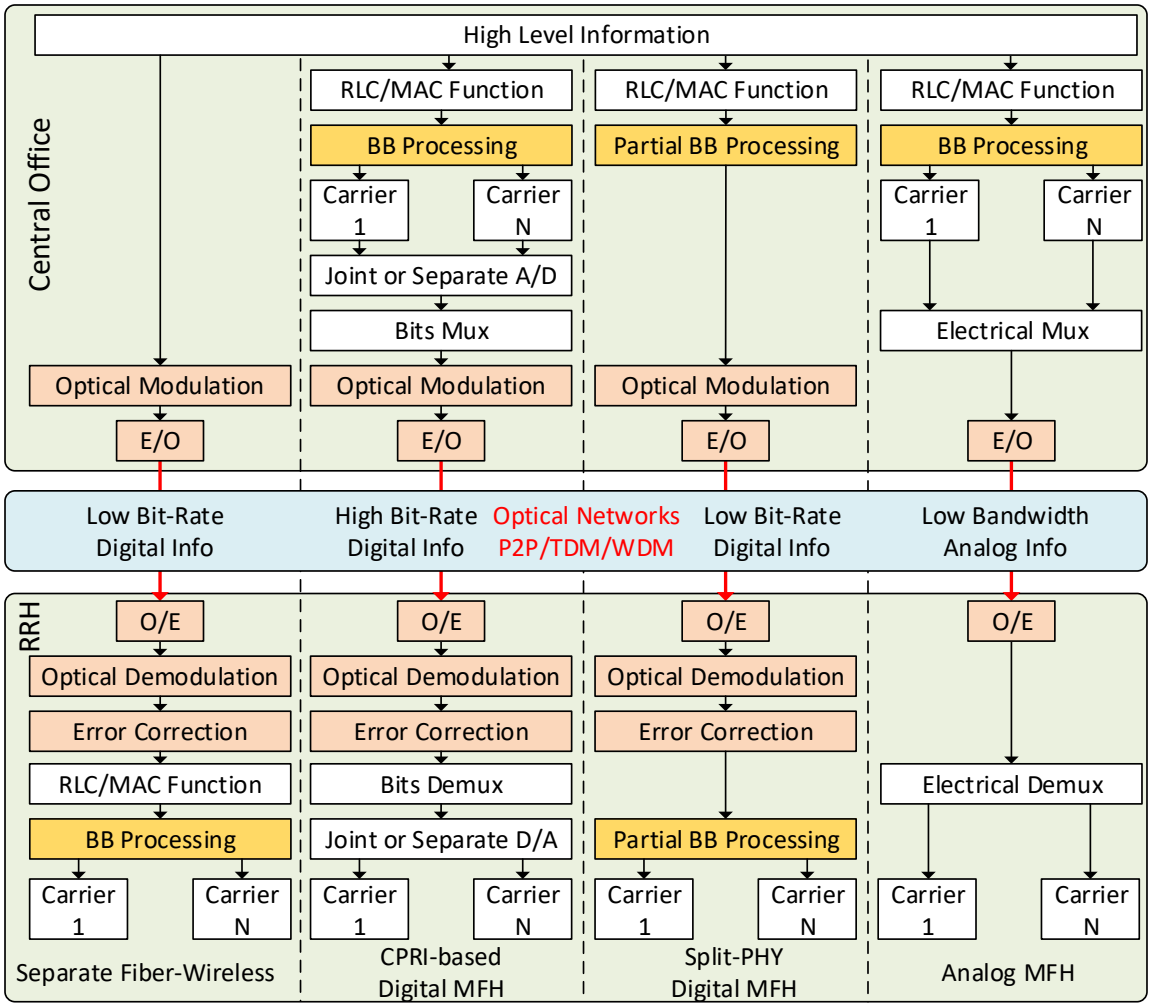


Figure 1.6: Analog and digital mobile fronthaul schemes.

The multi-carrier operation supporting CA and massive MIMO should also be considered as a typical case in 5G [21]. The latency and transmission degradations in MFH are considered as the radio transmission penalty, making the MFH link of high fidelity and latency requirement [22, 23].

The capacity boosting and performance improvement have been a hot topic in optical MFH networks, in particular with the recent 5G era in which wider bandwidth in free-space and more carriers are preferable [24, 25]. Two schemes are mainly discussed and actively investigated in next-generation spectral-efficient MFH: analog MFH and digital MFH, shown in Fig.1.6. Serving multiple RRHs with a tree topology is also actively stud-

ied, using TDM or WDM schemes originally proposed for PON.

*Analog Mobile Fronthaul*

Analog MFH uses the analog radio-over-fiber (RoF) technology for signal delivery and advanced multiplexing [26]. The analog waveforms in wireless transmission are mapped directly to analog samples in the fiber with continuous amplitudes or phases, so the bandwidth in fiber is the same as in wireless, that high spectral efficiency is achieved.

The bandwidth requirement by analog MFH using intensity modulation is shown in (1.1). The $BW_{Ch}$ is the wireless bandwidth each channel, and $BW_{GB}$ is the bandwidth of guard bands in frequency domain reserved in MFH. $N_{MIMO}$, $N_{MIMO}$ and $N_{Sector}$ are the number of MIMO streams, aggregated carriers, and sectors correspondingly.

$$BW_{MFH} = (BW_{Ch} + BW_{GB}) \times N_{MIMO} \times N_{CA} \times N_{Sector} \tag{1.1}$$

The modulation and multiplexing used in analog MFH are widely investigated. To serve multiple carriers for multiple sectors, CA or MIMO, electrical multiplexing is mandatory for multiple wireless carriers sharing one laser source, since the laser is typically one of the most expensive components in the transmitter.

Frequency division multiplexing (FDM) or multi-intermediate frequency (IF) over fiber is one of the state-of-the-art technology in this field, with several publications on simulation, experimental verification and field trials [27, 28]. Different carriers are mapped in fiber with varying IFs by intensity modulation with intensity modulators (IMs) or directly modulated lasers (DMLs). With pure analog or digital filtering on the receiver side, carriers can be separated and extracted with minimal latency and very small jitter [29]. Multi-service MFH and bi-directional MFH have been explored with co-existence of MMW and below 6-GHz bands [30, 31].

TDM provides another approach for electrical multiplexing, by cascading wireless samples for different carriers in the time series [32]. It reduces the receiver complexity, consid-

ering that multiple LO frequencies are needed in FDM. However, it has a higher requirement for the time synchronization with increased latency, if still using traditional wireless frame scale multiplexing. Sample-wise TDM is developed to reduce the latency from symbol level to sample level, corresponding to 99.95% latency reduction in LTE [33].

The analog MFH provides ultimately high spectral efficiency, and the frontend complexity is reduced with simplified functionality. It makes the purely analog processing possible in RRH. Both FDM and TDM MFH schemes suffer from fiber and transceiver nonlinearity, generated with its principle of transmitting analog samples with continuous amplitudes. For example, the signal delivered in FDM based analog MFH is multi-band orthogonal frequency division multiplexing (OFDM) signals, which has high peak-to-average power ratio (PAPR) compared with current modulation formats widely used in optical links, like on-off keying (OOK) or pulse amplitude modulation-4 (PAM-4).

Digital or analog pre-distortion in analog MFH have been studied to mitigate its performance degradation, with extra DSP or circuits in both transmitter and receiver [34, 35, 36]. If we can slightly change the transmitted waveform in MFH, a series of technologies can be applied to reduce the signal PAPR [37]. The high peaks of multi-band OFDM signals are generated when multiple subcarriers are added with similar phase and carried symbols. If we can change the format or placing of different carriers or modifying some symbols, the PAPR can be reduced significantly. These technologies include coding schemes [38], in which some measures are taken to reduce the occurrence probability of the same phase of the signal symbols. Other approaches exist like partial transmission sequence (PTS) [39, 40] and selective mapping (SLM) [41]. For PTS method, the input data block is partitioned into disjoint sub-blocks, and we can use one of the methods to partition: adjacent partition, interleaved partition, or random partition. Two major issues exist for PTS: high computational complexity and the large overhead generated by delivering optimal phase values. Sharing the similar idea, in SLM, the input data sequences are multiplied by each of the phase sequences to generate alternative input symbol blocks, based on the criteria to min-

imize the signal peak power. Tone reservation (TR) and tone injection (TI) are two other efficient schemes, that both transmitter and receiver reserve a subset of tones for generating the compensation signals for the high power peaks [42, 43]. Those subcarriers (tones) are not used for data transmission, but only for PAPR reduction as overheads. The tone mapping should be stored in both transmitter and receiver. It wastes some spectral and power efficiency due to the introduction of non-data-transmission subcarriers. All schemes as mentioned in this paragraph require some modifications to user devices, making it hard to be deployed in current LTE and future 5G systems, that the device is hard to be changed adapting to our optimization for MFH. Moreover, even with these nonlinearity compensations and PAPR reduction schemes, the linearity requirement for analog MFH is still higher than digital MFH, so linear transmitters, and receivers are preferred.

Another drawback is the noise aspect. Due to the nature of analog transmission and analog processing in RRH, it is very hard to error detection or correction in analog MFH. Forward error correction (FEC) does not work here, and the most applicable noise removal technique is by filtering. To achieve high SNR fulfilling the 3GPP requirement, higher power transmitter and low noise figure (NF) amplifiers are preferred, which adds the system cost. Meanwhile, the link reliability is limited, that any optical link degradation should generate signal penalties in the wireless domain, such that delicate optical channel monitoring schemes should be accompanied. Considering these limitations and its high capacity feature, the analog MFH is suitable for cells that covers a large area, potentially supports multiple sectors.

*Digital Mobile Fronthaul*

Digital MFH offers another approach for digital delivery of analog waveforms. It converts the analog waveform into digital bits based on some algorithm, then uses optical modulation again in the MFH link. Separating the wireless and optical modulation provides benefits including the capability for optimizing the transmission quality in fiber without

Table 1.2: Required CPRI data rate and number of 100G wavelengths.

| Antenna Ports | Channel Bandwidth | CPRI Data Rate | Number of 100G Wavelengths |
|---|---|---|---|
| 8 | 20-MHz | 8-Gbps | 1 |
| | 160-MHz | 64-Gbps | 1 |
| | 1-GHz | 400-Gbps | 4 |
| 32 | 20-MHz | 32-Gbps | 1 |
| | 160-MHz | 256-Gbps | 3 |
| | 1-GHz | 1.6-Tbps | 16 |
| 256 | 20-MHz | 256-Gbps | 3 |
| | 160-MHz | 2-Tbps | 20 |
| | 1-GHz | 12.8-Tbps | 128 |

modifying the wireless standards. Also, more commercial products can be easily modified and fit into the MFH application.

The mainstream technology in the digital MFH domain is CPRI [44]. The purpose of CPRI is to allow replacement of a cable connection between a radio transceiver and a base station so that the connection can be made to a remote and more convenient location. By digitizing the wireless in-phase and quadrature components, the analog waveform modulated for wireless transmission can be converted to digital bits with Nyquist digitization. As a technology since Global System for Mobile Communication (GSM) deployment, CPRI is simple but extremely spectral inefficient when scaling up to the 5G service with extended bandwidth, massive MIMO and CA. Shown in Table. 1.2, more than 100 wavelengths using 100-Gbps per wavelength may be required with 1-GHz bandwidth and 256 antenna ports. The specification is possible in MMW array of sub-array antennas. Using higher rate links employing pulse amplitude modulation (PAM-4) or discrete multi-tone (DMT) is necessary, but the increased channel bit error rate (BER) directly degrades the CPRI performance.

Other compressed CPRI schemes can reduce the data rate by down-sampling, partial sampling [45, 46], nonlinear companding [47], differential coding [48] and other techniques [49]. Down-sampling aims to remove the dependency from OFDM oversampling in CPRI, that a 1.7 over-sampling rate is set by default; partial sampling reduces the digitiza-

tion bits but still fulfill the error vector magnitude (EVM) requirement, at the cost of losing some system margin; and nonlinear companding utilizes the distribution of OFDM amplitude samples, using mu-law [50], A-law [51] or Lloyd algorithm. The compressed CPRI still shows advantages including low cell site complexity, low latency, and small jitter, over other digital MFH technologies.

Given the scalability challenge from the legacy CPRI/compressed CPRI, the industry and academia realize that a more efficient digital MFH technology is required for 5G. A critical point that must be resolved before the technology moves forward is the function split separating which Layer 1, 2, and 3 functions reside in the RRH, and which of these processing functions reside at the BBU. With at least some Ethernet functions placed in the RRH, aggregation and statistical multiplexing can take place before data hits the MFH network. It potentially reduces the link bit rate requirement. It is critical due to the massive deployment once standardized [52].

Most of the split function options are digital MFH-based, and only option-8 function split is compatible with analog MFH. Among the digital options, MAC-PHY split [53] and split-PHY processing (SPP) have been demonstrated in papers [54]. It provides a high compression ratio, and can still reuse some existing digital optical infrastructure. How-

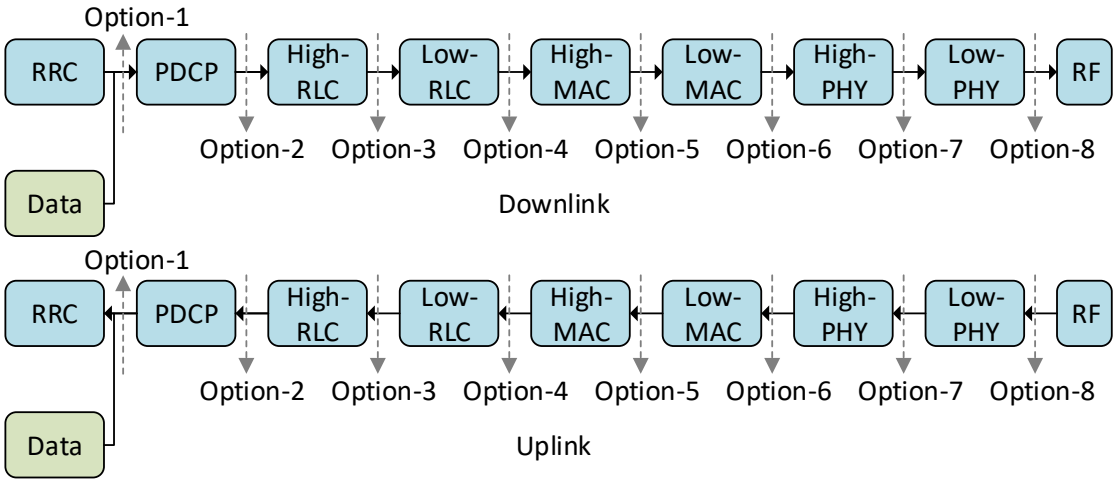


Figure 1.7: Different options of function split

ever, it is incompatible with inter-cell coordination under some configurations limiting the system capacity. Other function split options are also discussed. As one implementation of function split, next-generation fronthaul interface (NGFI) is an MFH interface actively developed and standardized. It redefines the baseband processing split between BBU and RRH, hence redetermining the positioning of eNB stack components between them. According to China Mobile who introduced the terminology NGFI, BBU is redefined as radio cloud center (RCC), and RRH becomes Radio Remote System (RRS). The NGFI envisions a revised point-to-multi-point network. Another element radio aggregation unit (RAU) is introduced connecting the radio cloud center (RCC) and several cell sites. The traditional MFH is divided into MFH I and MFH II based on the current proposal, with different capacity and latency requirements on the optical network.

Apart from purely digital MFH, schemes are proposed to combine the benefit of analog and digital MFH, like the Delta-Sigma modulation in MFH [55, 56, 57]. It draws a balance between performance and spectral efficiency. The transmitter linearity requirements are relaxed since the transmission signal is usually OOK or PAM-4 signal with low PAPR. It is actively developed in LTE and data over cable service interface specification (DOCSIS) signal delivery [58].

With more powerful DSP capability in RRHs supporting digital MFH, the multiplexing is easier compared with analog solutions, that packet-wise information separation can be implemented. However, in most papers, the digital signal and system architecture design are optimized separately. The modulation, multiplexing and coding schemes in MFH is not coupled with the MFH application, generating a room for improvement by joint optimization. Other DSP-based split PHY schemes are moving towards the distributed architecture with increased RRH complexity and introduction of additional network layers, which contradicts the C-RAN original intention. Moreover, the digital MFH has uncontrollable latency due to the framing and buffers if using legacy Ethernet or PON architecture to load the MFH traffic, making it extremely hard to fit into the 5G frame. With features including

low-cost, high-stability and comparably low-capacity, the digital MFH is suitable for small cell RRHs.

*Optical Multiplexing for Mobile Fronthaul*

Except for the aforementioned electrical multiplexing, optical multiplexing schemes are discussed in recent research for optical MFH with a tree topology, since high-density small cells are expected to be deployed in the 5G system extensively [25]. Existing TDM-PON has been proposed for low-cost connections to RRHs. However, the shared bandwidth and uncontrollable latency with Next-Generation Passive Optical Network 2 (NG-PON2) [59] or Ethernet Passive Optical Network (E-PON) cannot power the 5G service sufficiently, considering the microsecond level latency requirement and more than 100-Gbps data rate. Also, the sensitivity limited split ratio increases the number of trunk fibers from each BBU or CO, which adds the system complexity.

These limitations from TDM-PON makes WDM or DWDM more feasible [60], which all enable a dedicated optical channel with improved capacity and reduced latency. In DWDM MFH, each RRH is connected to the BBU with a dedicated wavelength, that a logical connection is built without sharing bandwidth with other RRHs. It provides higher connection speed, reduced latency, and small jitter. It is also easier to operate. However, the light source in uplink is one of the most challenging parts. Since a colorless RRH is feasible, tunable distributed feedback (DFB) laser or self-seeded reflective semiconductor optical amplifiers (RSOAs) can be implemented in RRHs [61]. However, DFB laser is costly in high-density RRHs, especially when wavelength tunability and stability are required. Besides, the tunable DFB laser can hardly cover the whole C band, making the supported RRHs per trunk fiber is limited using the standard channel spacing of 50-GHz or 100-GHz. Reducing the optical channel spacing may be another solution, it needs more advanced DFB with improved frequency stability, which adds the cost significantly. RSOA is preferable only in digital links since the spontaneous noise degrades the signal significantly

in fiber-wireless MFH. This issue remains to be solved by this research work.

### 1.2.2 Millimeter-Wave Transmissions with Fiber-Wireless Integration

In the mobile Internet era, the wireless operation using high channel bandwidth with increased spectral efficiency is preferable. More CA [62] and larger scale massive MIMO [63] provides higher data rates to serve the proliferation of smart mobile devices and data-hungry applications, including UHD video streaming, 3D applications, VR, mobile AR, and real-time cloud computing [64, 65, 66].

*Network and Physical Architecture*

In 5G standardization process, FCC approves the study on 27.5-29.5, 37-40.5, 47.2-50.2, 50.4-52.6, and 59.3-71 GHz as potential candidates [67]. The high frequency and expanded bandwidth enable its potential to support targeted 10-Gbps peak downlink rate and accommodate the exponential traffic increase [2]. Moreover, the high frequency and large attenuation in free-space transmission provide high spatial density, low inter-cell interference (ICI) and minimized interference with legacy services [68].

On the other hand, the wireless local area network (WLAN) moves towards MMW as complementary technologies for indoor access. With the 7-GHz license-free bandwidth, the 60-GHz V-band provides a large opportunity for new wireless services. Comparing with 160-MHz bandwidth enabled by channel bonding in 802.11ac at 5-GHz [69], the huge bandwidth of 2.16-GHz in 802.11ad provides 4.62-Gbps using single carrier (SC) modulation or 6.76-Gbps data rate using 64QAM-OFDM [70]. The data rate of 802.11ay goes up to 176-Gbps by bonding four 802.11ad channels and utilizing $4 \times 4$ MIMO and HOM of 256-QAM [71]. Other IEEE projects including the NG60 also emphasize to improve the wireless transmission on the V-band [72].

With the high oxygen absorption peak on 60-GHz [73], moving the operation frequency to W-band (75-110-GHz) provides lower loss, improved coverage, and broader bandwidth

[74]. With high baud-rate single-carrier or OFDM modulation, the W-band wireless transmission has been recorded with more than 400-Gbps data rate using technologies including MIMO, polarization multiplexing and DSP-based receiver [75, 76]. Due to the recent maturity of optical and electrical devices on higher frequencies, wireless transmissions on D (110 to 170-GHz) and THz bands are also investigated and demonstrated [77, 78].

Also, photonic-assisted high-frequency wireless signal generation and delivery are extensively explored as the foundation of MMW fiber-wireless integration [79, 80]. It is currently a mainstream technology in V, W, D, H and THz bands signal generation since the availability and stability of electrical high-frequency devices are still low [81, 82]. Taking advantages of the large bandwidth in fiber, the signal up-conversion is done by mixing in the wide-band photo-detector (PD) between two light waves. Other technologies in the microwave photonics field are widely investigated for a more seamless integration between the optical and wireless domain, using polarization multiplexing, frequency doubling/quadrupling/octupling, advanced optical modulation biasing, nonlinear effects and so on [83, 84, 85]. These technologies as mentioned above lay the foundation of the physical system design for a fiber-wireless integrated system.

*DSP and Modulation for MMW Fiber-Wireless Integrated Systems*

Given the digital modulation and multiplexing scheme design, current MMW systems still use legacy OFDM [86] or SC modulations [87], like the 802.11ad. Considering the shrunk wavelength, weaker multi-path, and narrow beams with high-gain antennas [68], these schemes originally designed for low-RF or coherent optical communications are not suitable to achieve the maximal performance and capacity.

Other wireless studies from both industry and academia on advanced modulation formats are extensive, including generalized frequency division multiplexing (GFDM)[88, 89, 90], filter-bank multi-carrier (FBMC) [91, 92], universal-filtered multi-carrier (UFMC) [93, 94], weighted overlap and add (WOLA)-OFDM [95, 96] and so on. They provide reduced

out of band (OOB) leakage by different approaches, to minimize the interference to adjacent channels. Hence, reduced guard bands can be used to reduce the overhead in the frequency domain. Meanwhile, the robustness with residual carrier frequency offset (CFO) is enhanced. The overhead in the time domain is also reduced with optimized or removed cyclic prefix (CP). However, all these research are focused on the low-RF bands, leaving the gap in MMW waveform. With high attenuation transmission characteristics in 60-GHz MMW band and horn antennas applied with narrow beams, the large and deterministic radio power difference also makes the orthogonal multiplexing and multiple access schemes inefficient and unreliable. Even with advanced beamforming, this issue still exists if a large number of users are supported by a single antenna or antenna array.

Moreover, the state-of-art research in modulations and multiple access schemes are designed for the wireless system only, without considering the fiber-wireless integration. The additional fiber link provides benefits above but also generates signal degradations and reduce its reliability, which should be taken into consideration. Besides, the 5G is regarded as a multi-scenario standard, which should serve three applications including eMBB, URLLC, and mMTC. Current modulation is designed mainly for eMBB emphasizing on capacity improvement [97], that more research on other applications should be carried out by this dissertation in fiber-wireless integrated systems.

### 1.2.3 All-Spectrum Wireless Communication and Coordination

In mobile data networks, the MBH and MFH are relying on the optical fiber connection, which provides high-capacity and low-loss channels from the CN to the antenna sites. On the other hands, the data delivery between antenna site and users are based on low-frequency or MMW wireless communications. It provides mobility and good coverage. However, both schemes have challenges in deployment and operation.

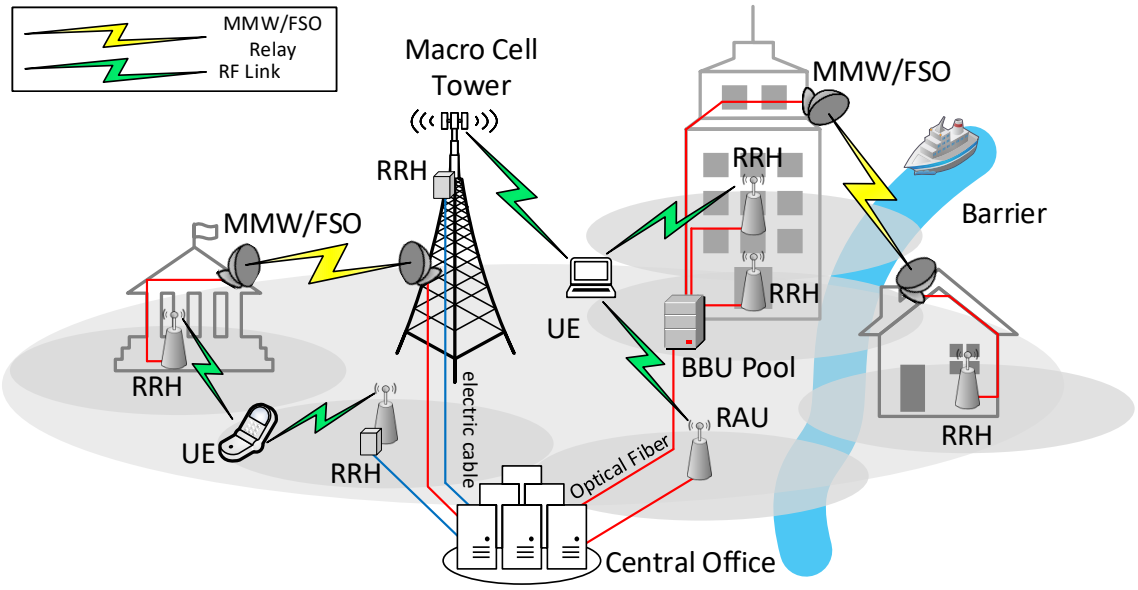


Figure 1.8: Mobile fronthaul with relays using MMW or FSO technologies.

*All-Spectrum Communication for Mobile Fronthaul*

For the fiber link, it is extremely costly to deploy new fibers in the field, and typically the cost is several hundreds of thousands of dollars per mile in urban environments. For indoor fiber installation, it is also difficult in existing infrastructures. A high cost is expected even the fiber length is typically limited. Considering these factors, in scenarios like long-distance deployment, covering a geographic barrier or installation in existing buildings, wireless technologies carrying MFH or MBH traffic is critical in the highly centralized network. Several techniques are discussed: FSO, microwave technologies including MMW, and light-emitting diode (LED)-based VLC technologies.

FSO is a mature optical technology that relies on a laser to send a very high bandwidth information data through wireless channels. Based on current DML technology, more than 25-GHz bandwidth is available [98], and higher bandwidth is demonstrated with external modulation. It is natively compatible with the other optical section of backhaul/fronthaul links, since the only difference between fiber and FSO transmission is the transmission media. And no DSP or signal conversion is necessary for the relay node. Considering the

standard single mode fiber (SSMF) characteristics, O band or C band are typically used, while communication using other visible bands is demonstrated [99, 100], with reduced fiber distances. FSO can utilize mature and widely available optical transmitter, receiver and amplifiers, which is another huge advantage over other wideband wireless connections using MMW or THz bands. Ultra-high frequency wireless communication beyond 300-GHz does not have mature devices and integration technologies, which also leads to higher power consumption. By using either coherent or intensity modulation-direct detection (IM-DD) based modulation, the FSO link can easily carry multi-Gbps data over a long distance to these hard-to-reach RRHs or BBUs. As a general optical-wireless transmission link, the FSO is compatible with both analog MFH or other digital-based functional split formats, that does not need modifications to the mobile fronthaul frontends.

The MMW mobile fronthaul places a wireless overlay in densely populated heterogeneous networks where MMW small cell base stations are integrated into 5G networks. The link aims to extend the network capacity massively at a reasonable cost and transparent to end users. By increasing the wireless signal frequency to more than 30-GHz, the available channel bandwidth is significantly expanded to multi-GHz, capable of delivering the increased traffic generated by 5G networks. So, a seamless convergence of the fiber and MMW MFH and backhaul is feasible, in which the MMW RoF technology plays an important role as relays [101]. The signal delivered by the fiber is in the analog waveform as transmitted in the MMW band, such that no complicated and high-speed DSP and digital modulation is necessary to the relay node. Also, the precise LO used in wireless communication can even be eliminated since the up-conversion is done at the central site, making the fiber-wireless mobile fronthaul link more stable and robust to the environment.

MMW, THz, and FSO have attracted attention for research with low-cost, abundant bandwidth, high deployment flexibility, and fast deployment. However, the high-frequency EM-wave signal is vulnerable to atmospheric attenuation due to absorption, scattering, and turbulence, as well as other losses such as geometrical, pointing and optical losses in the

Table 1.3: Comparison between available transmission technologies using different spectral resources.

| | Centimeter Wave | Millimeter Wave | Infrared Free-Space Optics | LED-Based Visible Light Communications |
|---|---|---|---|---|
| Frequency Range | 0.3-30 GHz | 30-300 GHz | Around 190-THz | 400-700 THz |
| Channel Bandwidth | Several MHz | Several GHz | 25/50/100 GHz | N.A. |
| Modulation Bandwidth | Several MHz | Several GHz | >10-GHz | <100-MHz |
| Coherent Transmission | Yes | Yes | Yes | No |
| Channel Bonding | Yes | Yes | Yes, WDM | Yes, RGB WDM |
| Transmission Distance | High | Medium | High | Low |
| Coverage | High | Medium | Low | Low |
| Transceiver Complexity | Low | Medium, Symmetric | Medium, high for transmitter | Ultra-low |
| Existing Standards | 3G, 4G LTE-A, 5G phase 1, 802.11a/b/g/n/ac/ax | 5G phase 2, 802.11ad/ay | | IEEE 802.15.7 |
| Application | User Access, MFH, MBH | MFH, MBH | MBH | |

link [102]. They have limited delivery distance due to the comparably high propagation loss, and impairments from weather and atmospheric conditions. Converging fiber and wireless links has been a hot research topic, considering that the typical distance for mobile fronthaul and backhaul can be beyond 10-km. So, most of the distance should still be covered by the fiber. When there is an obstacle in the path, like a river, a canyon or private property, one or multiple wireless technologies can be deployed. To further improve the wireless transmission quality, especially with possible weather conditions, combining multiple wireless techniques within the fiber-wireless framework is a promising approach.

Owning to the drastically different channel response in FSO and RF links, those complementary transmission characteristics are exhibited under different conditions [103, 104].

Therefore, the hybrid link with both FSO and MMW transmission will be a good solution for joint deployment. Several studies have been reported about the hybrid MMW/FSO link design, such as hardware or software switching schemes based on the availability of channels and joint bit-interleaved coding schemes between channels [105]. To avoid the complexity of real-time feedback, QAM level adaptive diversity combining technique (ADCT) can be used to combine the information from both channels and obtain the symbols with improved SNR [106].

Most of the above scheme is designed for outdoor links. For indoor coverage, the wireless fronthaul link is also critical, because of the need for high-density small cells in open public spaces, like open offices, stadium or libraries. It is challenging for the MMW or FSO to be deployed in a high-density scenario, due to the cost and deployment challenges. These wireless transmission technologies utilize narrow beams, that require fine alignment in installment, and are sensitive to vibrations, especially for FSO.

*User Access with All-Spectrum Communications*

As for user access, the 5G has requirements for capacity, latency, and reliability. However, based on currently available technology and components, it is very hard to fulfill all the requirements simultaneously. Similarly, multiple technologies and transmission bands can be utilized for user access to serve various user types and scenarios, as the data pipe between antenna units and user devices.

High capacity required in eMBB needs large bandwidth channels with better power efficiency, making the high-frequency channels feasible since there are wider channels available. To achieve a similar data rate, so the number of MIMO streams can be reduced to simplify the receiver DSP. Otherwise, the MIMO decoder is still complex with high power consumptions with the current MIMO technology, using either linear or nonlinear decoding algorithms [107, 108].

However, the penetration and reflection capability by these MMW, THz and FSO chan-

nels are weak due to the short wavelength and antenna design. As directional beams, most of the transmissions require line of sight (LoS) operation, that limits the service range and coverage of each small cell, especially for indoor applications. These schemes are also hard to serve massive users with high mobility, like users in a car or a high-speed train. It is due to that the physical and electrical beam tracking schemes are hard to implement and control with reduced wavelength.

From another aspect, to serve users with long distances in an outdoor environment, the service quality is sensitive to the weather conditions, that limits its feasibility. As a result, the high-frequency wireless access technology is more feasible as data pipe with indoor stationary users for eMBB. Among these technologies using high frequencies, the availability and stability of transceivers vary. The FSO transmitter is simple when embedded in RRH, and it is natively compatible with the fiber fronthaul networks. So FSO more feasible in the downlink with beamforming and tracking technologies [109, 110]. However, it requires temperature control precisely for the laser, making it hard to be integrated into the UE. The FSO transmitter is also power consuming. On the other side, the receiver for FSO is stable, making it possible for users to incorporate PD as the receiver. Besides, transceivers running at low-frequency and MMW band are more mature with integrated circuits and RF frontends available [111]. Hence, it is viable for RF/MMW frontends to be embedded in the UE and serve as the uplink transmitter.

For other channels delivering control signals, it is hard to use the unreliable high-frequency channels that suffer from transmission quality. Instead, the low-frequency below 6-GHz channel is more feasible with its extensive coverage and better penetration capability. Since the data rate for the controlling channel is low, each low-frequency band can support a large number of users, making it easy for multi-user synchronization. These signals broadcasted by the macrocell can be used for multi-small-cell coordination. Also, its broad coverage makes it possible for these low-frequency bands to serve mMTC.

To serve some location-based services (LBSs), as well as supporting beamforming,

the precise position of UE is needed [112]. Current GPS based solution cannot provide adequate coverage indoors, and other Wi-Fi sniffer schemes have a low precision, which cannot serve the purpose [113, 114]. Instead, it is proposed to use a LED-based VLC network to provide the positioning system [115, 116]. Thanks to the ultra-low-cost LED chips as transmitters, and it is viable to deploy high-density anchor cells to support the service. In the receiver, traditional or machine learning based DSP methods are proposed to calculate the device location in centimeter precision. Low computational complexity and high precision are demonstrated [117, 118]. By using the prior positioning information, the beam scanning and sweeping are significantly simplified with reduced latency when the initial connection is built.

When all the spectral resources and technologies are combined, a complete architecture of the all spectra wireless access system is formed, fulfilling all requirements in 5G and beyond standards by the unified fiber-wireless system. All types of devices can be supported simultaneously, including bi-directional data-hungry smartphone and laptops, smart sensors and meters, mission-critical car/drone-related devices and so on.

Current technologies lay the foundation of each wireless link that communication schemes using separate bands are well studied and implemented, including the modulation, synchronization, equalization, and decoding. However, when combining multiple spectral resources in the integrated system, a complex system is formed, with potentially large control overhead and latency. Considering the time offset and jitter, it is also hard for multiple bands to coordinate, like MMW/FSO coordination. A complete system-level design with fiber-wireless integration is necessary, considering the backbone network design and resource allocation, as well as the UE design and optimization, to achieve the maximal performance, capacity, and reliability.

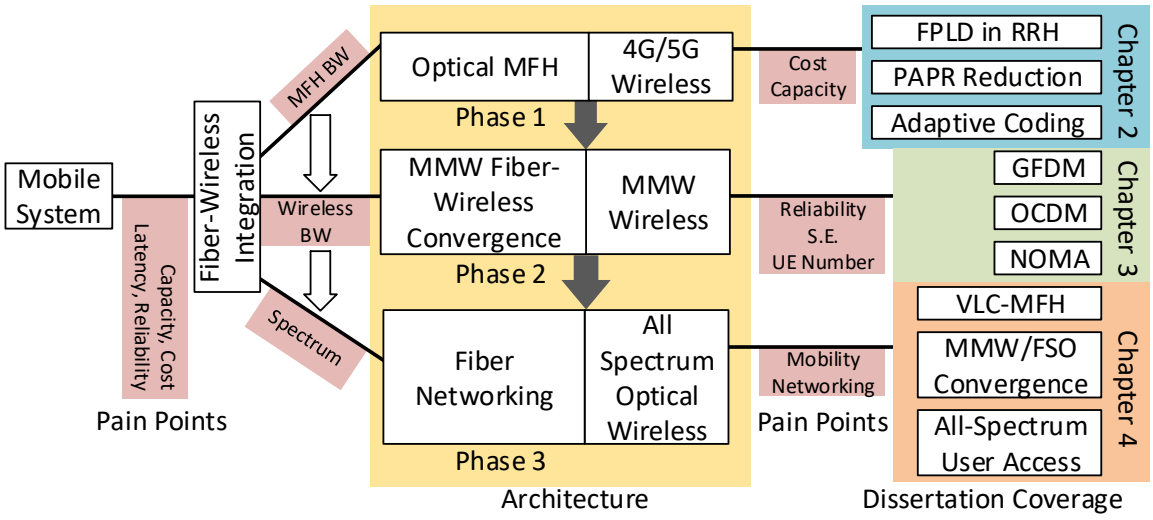


Figure 1.9: Logic and organization of dissertation works.

## 1.3 Organization of Dissertation

### 1.3.1 Logic of Dissertation Work

The logic and organization of the dissertation work are shown in Fig. 1.9. With the proliferation of mobile devices, the traditional mobile data network cannot fulfill the capacity, CAPEX/OPEX, latency, and reliability requirements. Fiber-wireless integration provides the only solution in the long term. In our view, the research and implementation of the fiber-wireless integrated system have three phases.

The first phase of implementation is based on the 4G/5G air interface and fiber MFH. The 5G is expected to be commercialized in 2020, with the standards coming close to be fixed. Moreover, for current 4G LTE-A and 5G phase one shortly, still below 6-GHz frequency channels are used [119]. The mobile data network can reuse the current MFH architecture. Considering the LTE-A standard is fixed for years, and the 5G NR is close to being standardized, the air interface is hard to be modified if we target on good user device compatibility. Hence, for this implementation phase, we investigate the MFH technologies only, with advanced network and DSP design. The research on analog MFH, digital MFH as well as DWDM-based network transceiver design is included.

The second phase of the fiber-wireless integrated system is the MMW converged system. To resolve the very congested channel allocation limitation, as well as minimize the interference with existing systems. The transmission bands can go up to MMW to further expand the system capacity. However, considering the huge channel bandwidth coupled with CA and MIMO, it is challenging to serve each cell with traditional digital MFH. Instead, analog fiber-wireless integration is more feasible. Adapting to the new MMW fiber-wireless integrated channel, we design advanced modulation formats and multiple access schemes, also fitting into different application scenarios newly defined in 5G: eMBB, URLLC, and mMTC.

The ultimate phase of fiber-wireless integration is what we proposed as the all-spectrum communication system. Since each wireless transmission band has limitations with current technology in either DSP or transceiver design, combining multiple frequency bands is feasible. Here we combine a wider range of frequency bands from sub-GHz to multiple hundreds of THz. We focus on the research of all-spectrum MFH and all-spectrum user access. A comprehensive system design minimizing the resource usage while still fulfilling the future requirement is executed. The system capacity is maximized, with improved reliability in the presence of channel degradations.

### 1.3.2 Dissertation Organization

The dissertation is organized as follows.

After the introduction to research background and challenges in Chapter 1, Chapter 2 shows the work for optical MFH to improve the fiber-wireless integrated system in phase one. With analog MFH, we show the research of PAPR reduction without the need to modify wireless user devices. For digital MFH, we propose the adaptive digitization and parameter selection in the advanced PAM-4 MFH, significantly improving the capacity and power margin. With high-density small cell deployment, a novel weak-resonant cavity Fabry-Perot laser diode (WRC-FPLD) is proposed in the RRH transmitter to solve the pain

point.

In Chapter 3, the work on advanced modulation of MMW fiber-wireless integrated system is presented. For MMW CA operation with reduced guard band, we proposed and demonstrated GFDM. Considering the increased reliability requirement, another modulation OCDM is designed for both eMBB and URLLC scenario. Finally, the PD-NOMA is proposed in the MMW fiber-wireless system for better performance and more user supported. Both synchronized downlink and asynchronous uplink are investigated.

The research of all-spectrum fiber-wireless system is presented in Chapter 4. The all-spectrum MFH research covers both indoor and outdoor applications. For indoor, we propose the LED-based VLC links for MFH, supporting high-density small cells with low-cost features. For outdoor application, a converged MMW/FSO solution is further enhanced with the novel inter-dimensional modulation and combination technologies developed. We designed and implemented the all-spectrum user access schemes with minimized resource usage and maximized capacity. The centralized architecture would significantly enhance the feasibility of the proposed all-spectrum fiber-wireless system.

The contributions of the research work are summarized in Chapter 5. Future research opportunities are also discussed in this chapter.

# CHAPTER 2

# ADVANCED OPTICAL MOBILE FRONTHAUL

In this chapter, we present the dissertation work on the advanced MFH. It is for the phase one implementation of the fiber-wireless integrated system, which should be paired with the 4G/5G air interface. Both analog and digital MFH are investigated.

## 2.1 PAPR Reduction in Multi-Band Analog Mobile Fronthaul

Multiple technologies have been proposed in the future wireless communications including MIMO and CA. Those technologies require multiple wireless carriers for a single cell-site. Hence high data rate links are needed in the MFH if we continue using CPRI, which increases the deployment cost dramatically. Instead, it is proposed to use the multi-IF-over-fiber architecture, that multiple wireless carriers are multiplexed in different IFs and delivered to the RRH.

All wireless carriers are processed and fully modulated in the centralized BBU pools. The analog waveforms are mapped to different IFs and delivered to the RRH. By this efficient MFH, we reduce the bandwidth requirement and make the system compatible with future 5G networks that require more carriers to each RRH. With simplified RRHs, the power consumption and cost is also reduced, contributing to a greener network.

However, with higher spectral efficiency, the requirement for channel quality in optical MFH is also higher, especially for linearity. OFDM modulation is used in LTE-A downlink. One of the shortcomings in OFDM is its high PAPR. This challenge becomes greater if we aggregate multiple OFDM streams at IFs in MFH. It decreases the signal-to-quantization noise ratio (SQNR) of the analog-to-digital converter (ADC)/digital-to-analog converter (DAC) while degrading the power efficiency of the transmitter.

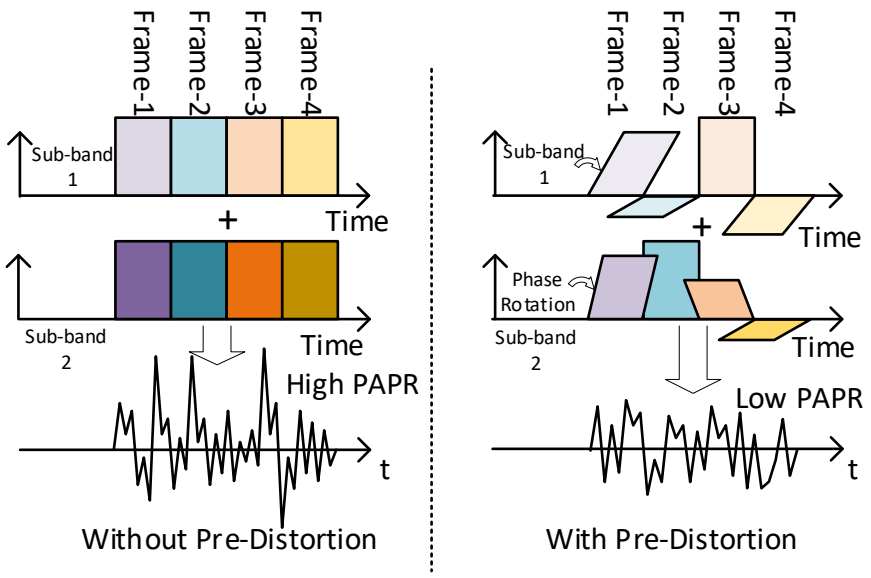


Figure 2.1: Current direct multi-band combination (left) and proposed phase pre-distortion scheme for reduced PAPR (right).

### 2.1.1 Principle of Sub-band Phase Pre-Distortion

The OFDM signal has high PAPRs when compared to single-carrier systems, due to multiple subcarriers accumulated. The PAPR is defined in (2.1). $x(t)$ is the samples in time domain inside one symbol or frame, corresponding to symbol/frame PAPR. Moreover, with multiple OFDM streams multiplexed in the frequency domain, the PAPR in MFH is higher due to more subcarriers aggregated. The peak sample in MFH is generated when the peaks of multiple sub-bands are aligned in time and phase.

$$PAPR = 10\log_{10}\{\max[x(t)x^*(t)]/E[x(t)x^*(t)]\} \tag{2.1}$$

Hence, we propose a pre-distortion scheme to shift the phase of the peaks and arrange them to neutralize the MFH peak value, as shown in Fig. 2.1 [120]. Without processing, the time domain PAPR can be high, shown on the left; with our proposed phase rotations on different sub-bands with the time-domain granularity of wireless frames, the PAPR can be reduced, shown on the right.

To calculate and modify the phase of each sub-band signal, typically complex multipli-

ers are needed, which is resource-hungry and time-consuming. We convert the phase search to delay search, in which only adders are required. $a_{i,m}(t)$ is the QAM symbol stream for $i$-th sub-band and $m$-th subcarrier, without considering cyclic prefix (CP) here.

$$\begin{aligned} s(t+\Delta t_i) &= \mathrm{Re}\sum_{i=1}^{k}[\sum_{m=0}^{N-1} a_{i,m}(t+\Delta t_i)e^{j2\pi BW(\frac{m}{N})(t+\Delta t_i)}e^{j2\pi f_{IF,i}(t+\Delta t_i)}] \\ &\approx \sum_{i=1}^{k}\sum_{m=0}^{N-1}\mathrm{Re}[a_{i,m}(t)e^{j(2\pi f_{i,m}t+\varphi_{i,m})}], -N/2+1 \le m \le N/2 \end{aligned} \tag{2.2}$$

$$\varphi_{i,m} = 2\pi(\frac{m}{N}BW + f_{IF,i})\Delta t_i = \begin{cases} \approx 2\pi\Delta t_i f_{IF,i} = \varphi_i, f_{IF,i} \gg BW \\ = 2\pi\Delta t_i f_{i,m} = \varphi_{i,m}, else \end{cases} \tag{2.3}$$

By shifting the $i$-th sub-band signal with delay $\delta t_i$, phase pre-distortion is generated following (2.2) and (2.3). In (2.2), the approximation can be made because the OFDM symbol duration is significantly larger than the time shift. In (2.3), two cases are discussed here: with IFs significantly greater than the sub-band bandwidth, the time delay generates a unified phase shift to subcarriers in the specific sub-band; for other sub-bands, linear phase shifts among subcarriers are generated. The phase shifts generated by delay can be well compensated in existing OFDM receivers in both scenarios.

$$Delay = \arg\min_{\Delta t}(\max[|x_1(t) + x_2(t+\Delta t)|]) \tag{2.4}$$

In MFH, a huge number of sub-bands need to be combined. To reduce the latency and DSP complexity, a binary searching tree is proposed for the combination process. In each optimized combination process, we combine two streams into one following the criteria to minimize the maximal absolute sample value, as (2.4) suggests. Instead of searching the whole possible phase space for a global minimum, we only search with the proposed binary tree for higher DSP efficiency. Though the global PAPR minimal may not be achieved,

the computational complexity is significantly reduced from $M^N$ to $MLog_2(N)$ ($M$ is the search points, $N$ is the number of sub-bands), and no more multipliers are needed.

The pre-distortion processing is working as Fig. 2.2 shows. After baseband OFDM generation, all sub-bands are up-converted to the assigned IFs digitally. Then the proposed binary combination tree is implemented for PAPR reduction on the wireless frame and all sub-bands. For layer-1, all original sub-band streams are combined in pairs to generate intermediate streams. At layer-2, all intermediate streams are combined again with optimized delays, and so on. At each layer, the number of streams is reduced to half. The scheme works following a layer by layer manner and terminates when only one stream is generated, which is the final stream with optimized phases (delays) that has the reduced PAPR. The extra clock cycles needed by the searching tree is the product of search point and the number of layers. For 32-point, 5-layer delay search serving 32 sub-bands, about 160 additional clock cycles are needed, generating less than 2-us extra latency running on field-programmable gate array (FPGA)/application-specific integrated circuit (ASIC) at a 100-MHz clock rate.

$$\Delta t_{i,m} = 1/[f_{IF,i} + (m/N)BW] \tag{2.5}$$

$$R_{i,m} = 1/(N \times f_{IF,i}/BW + m) \tag{2.6}$$

Two issues may raise from the phase pre-distortion: synchronization and channel estimation. Time synchronization precision is impaired because of the different delays added to the sub-bands. These delays are little comparing to the OFDM symbol duration, with absolute value in (2.5) and relative value in (2.6). $m$ the subcarrier index and $N$ is the number of subcarriers. We assign the first sub-band as the anchor band and adjust the delay of other bands according to it. For other bands, $f_IF > 1.5BW$. So for LTE with $N$ equal to 1200, we have $R < 0.09\%$. The CP can fully compensate this delay offsets.

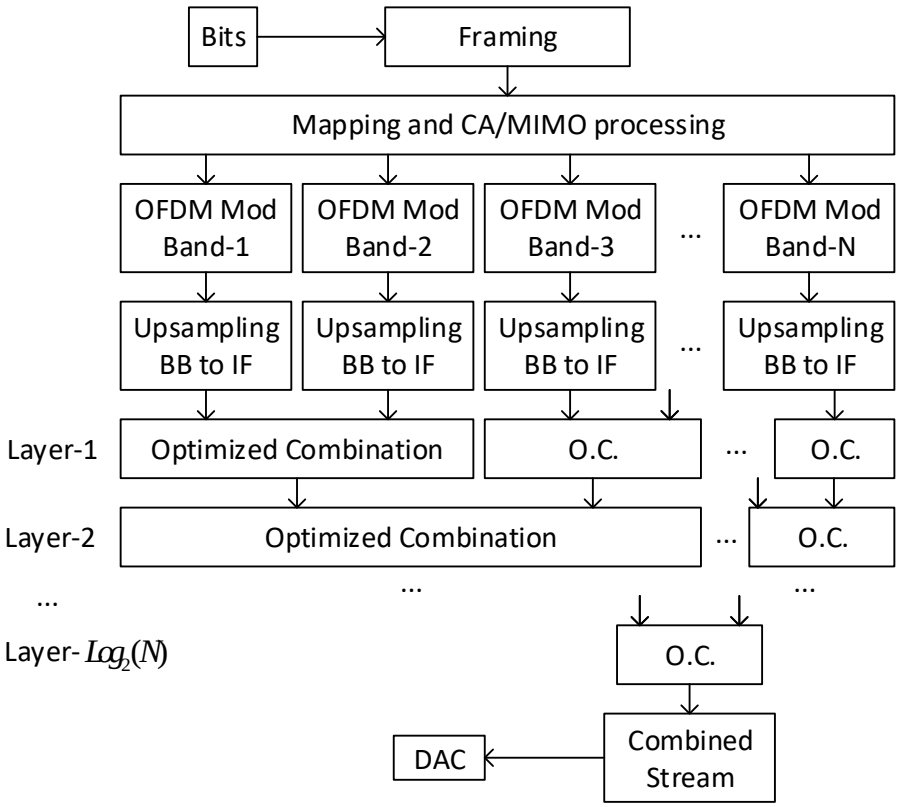


Figure 2.2: Principle of proposed phase optimized combination and binary searching tree.

For the 5G system with a wider bandwidth than LTE, the IF should also be increased to avoid interference between sub-bands in MFH. The scheme should still work since the ratio between bandwidth and IF are not changed much. The delay search window requirement changes with carrier IF (longer window for low IFs, a shorter window for high IFs). However, we use a unified search window with all sub-bands for simplicity and DSP efficiency. A significant PAPR reduction can be achieved even the delay search window cannot cover full $2\pi$ phase rotations for all sub-bands. We can optimize the search window for a balance between latency, performance and multi-path resistance in wireless transmission.

The channel estimation issue is solved by existing DSP in the wireless device. The estimation is working within wireless frames, and we apply a unique phase or linear phase shifts in subcarriers within the sub-band inside each frame. Hence, any existing channel estimation method can see the phase rotations as part of the wireless channel response

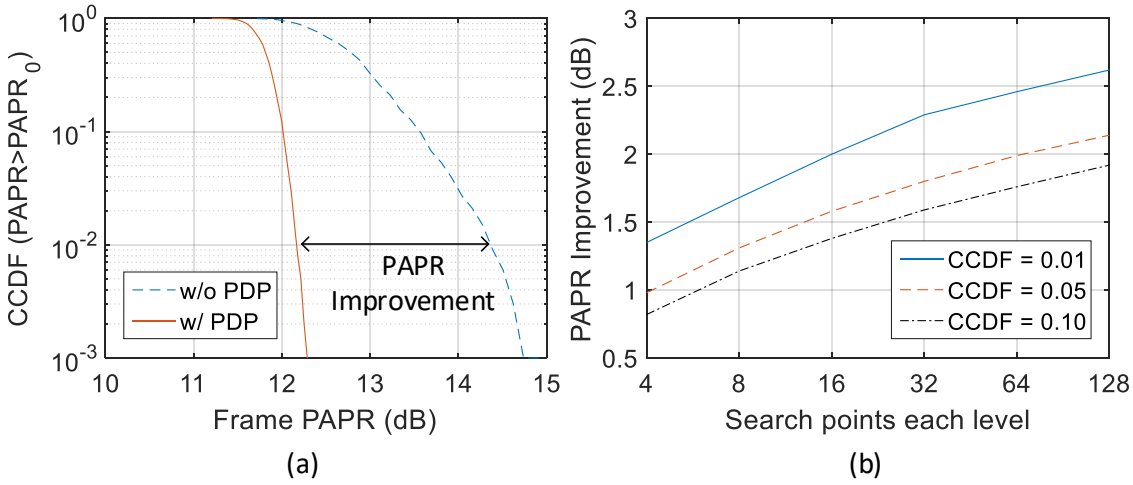


Figure 2.3: Simulation results. (a) CCDF of PAPR with and without proposed phase predistortion. (b) PAPR improvement with different searching window.

and fully compensate the distortion. Also, the introduced phase distortion does not affect MIMO or CA operation.

### 2.1.2 Simulations

Adapting to new applications including IoT/MTC and higher operation frequency, OFDM with fewer subcarriers is feasible due to lower DSP complexity and weaker channel multipath. The frame length is reduced for MTC efficiency. The bandwidth of each sub-band is set to 20-MHz, consisting of 32 subcarriers with 12.5% CP. The MFH carries 64 sub-bands, with 5-MHz guard band spacing. Each frame consists of 12 OFDM symbols, providing lower latency and better compatibility to short packet transmission than LTE. 64-QAM symbols are used.

The simulation results are shown in Fig. 2.3(a) with 32 search points each level. The comparison between different searching points is shown in Fig. 2.3(b). Results show that a larger window has better performance. Meanwhile, we need a higher amount of calculation, and a larger delay is generated. With only 32 search points each level (0.8% of symbol duration), we can achieve 2.2-dB PAPR reduction at 1% complementary cumulative distribution function (CCDF). So, 99% of the OFDM frames have PAPR smaller than 12.2-dB,

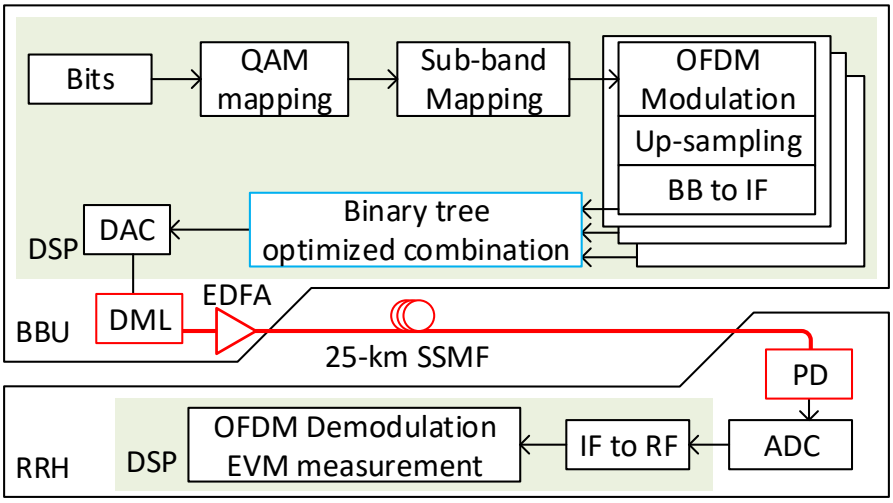


Figure 2.4: Experimental setup.

while the value can be 14.4-dB without the proposed scheme.

### 2.1.3 Experimental Setup and Results

Fig. 2.4 illustrates the experimental setup. A low-cost IM-DD link is built to verify the feasibility of the proposed scheme for MFH PAPR reduction.

With random bits going into the system, bits go through QAM mapping, sub-band and subcarrier mapping, and finally goes to individual sub-band OFDM modulation modules. After upsampling and conversion to IFs, the proposed scheme is applied. Getting the optimized multi-IF signal, the digital samples go through DAC and converted to the optical signal by a DML. The optical signal is amplified by an Erbium-doped fiber amplifier (EDFA) before transmission. With 25-km single mode fiber, the signal is detected and sampled in RRH.

In RRH DSP, the samples are converted from IF to RFs. OFDM streams are demodulated through time synchronization for each frame, CP removal, frequency synchronization, Fast Fourier transform (FFT), and QAM slicing. A cross-correlation based time synchronization is used with the first sub-band, and the synchronization information is shared with

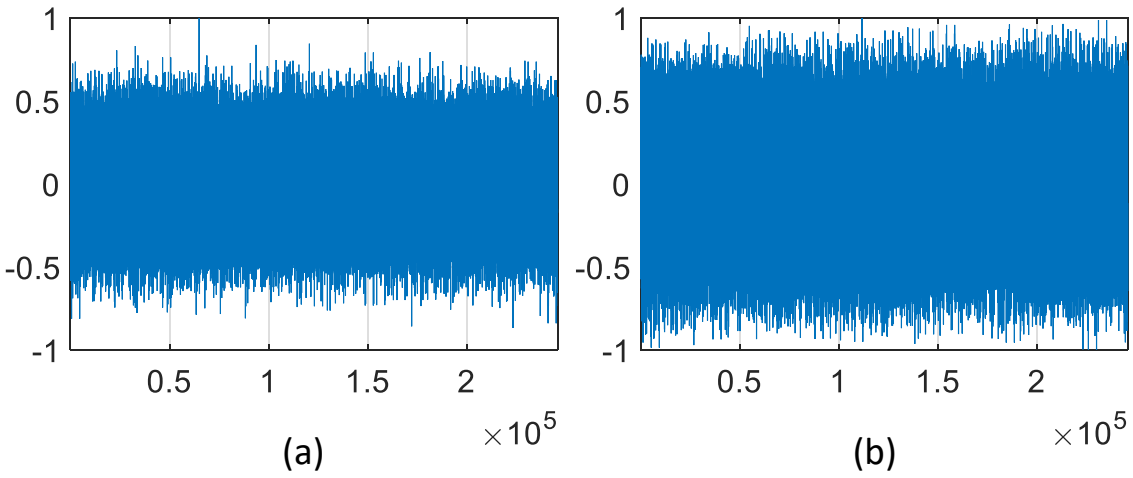


Figure 2.5: OFDM samples (a) without and (b) with pre-distortion.

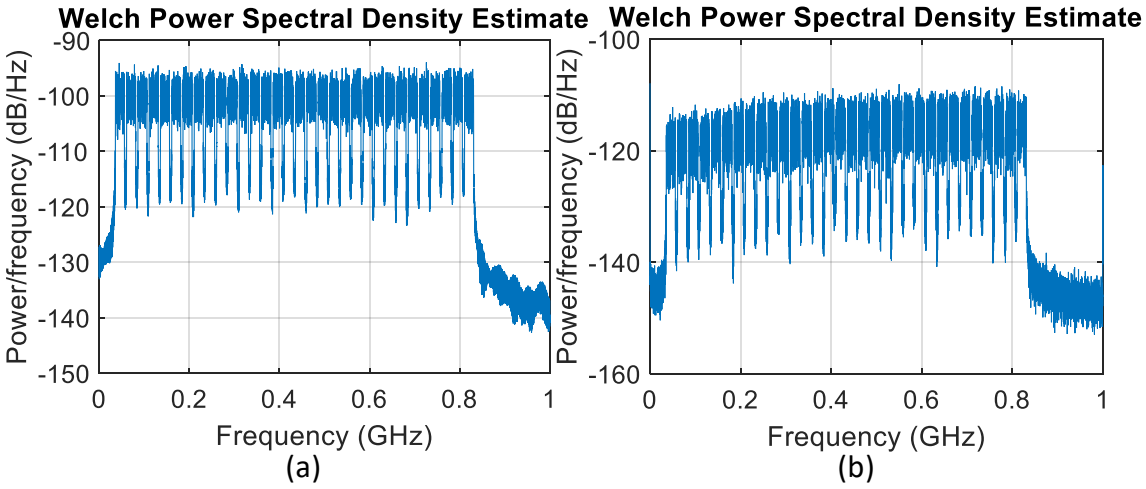


Figure 2.6: (a) Transmitted and (b) received spectrum in the experiment.

all sub-bands. A pilot pattern similar to LTE is applied. Time domain averaging and frequency domain interpolation is utilized in the channel estimation. When compared with LTE receiver, no additional process is applied to recover the pre-distorted stream.

For the signal, we test MFH streams consisting of 32/64/128 sub-bands. Identical to simulation settings, the data bandwidth of each sub-band is 20-MHz, with guard bands of 5-MHz. A guard band of 36.25-MHz is allocated around DC to reduce the impact by interference and noise at low frequencies. The bandwidths are 831.25-MHz, 1.631-

GHz and 3.231-GHz for 32/64/128 sub-bands. All sub-bands use 64-QAM modulation. The time domain signal without and with pre-distortion are shown in Fig. 2.5(a) and (b) accordingly. The transmitted and received spectrum is shown in Fig. 2.6.

The experimental results are shown in Fig. 2.7. Three different settings of 32, 64 and 128 sub-bands are experimentally verified. The data stream without pre-distortion is shown with the same setup for comparison. To fairly compare the system performance with different PAPRs, we use the optimized DAC output level for various signals, that we sweep the DAC output levels and choose the best performance one to measure.

Fig. 2.7(a) shows the result with 32 sub-bands, which can support 88 massive MIMO and four CA, or 4 $\times$ 4 MIMO and eight CA. To fulfill the requirement of 8% EVM by 64-QAM, a received optical power of -0.8-dBm is needed without using proposed pre-distortion, and can be reduced to -2.8-dBm applying pre-distortion. A 2-dB sensitivity improvement is achieved with the same optical link.

The results of 64/128 sub-bands are shown in Fig. 2.7(b). Both settings exceed the 4G LTE-A requirement for 64-QAM. To serve 64-QAM with 64 sub-bands, the proposed method can improve the sensitivity from 0-dB to -1.2-dB. A future proven 128 sub-bands setting are verified with a sensitivity of 0.5-dBm, which is sufficient to support 8 $\times$ 8 MIMO and 16 CA.

Finally, 25-km of single-mode fiber is added between BBU and RRH. Due to the high spectral efficiency and small signal bandwidth, we observe a negligible penalty after fiber transmission.

Experimental results validate the feasibility of the proposed pre-distortion scheme generating multi-IF OFDM signal in spectral efficient analog MFH with reduced PAPR.

## 2.2 Adaptive Digitization and Channel Coding for Digital Mobile Fronthaul

Common public radio interface (CPRI)-based MFH solution cannot fulfill the 5G requirement due to very high data rate requirement. CPRI compression techniques are investigated

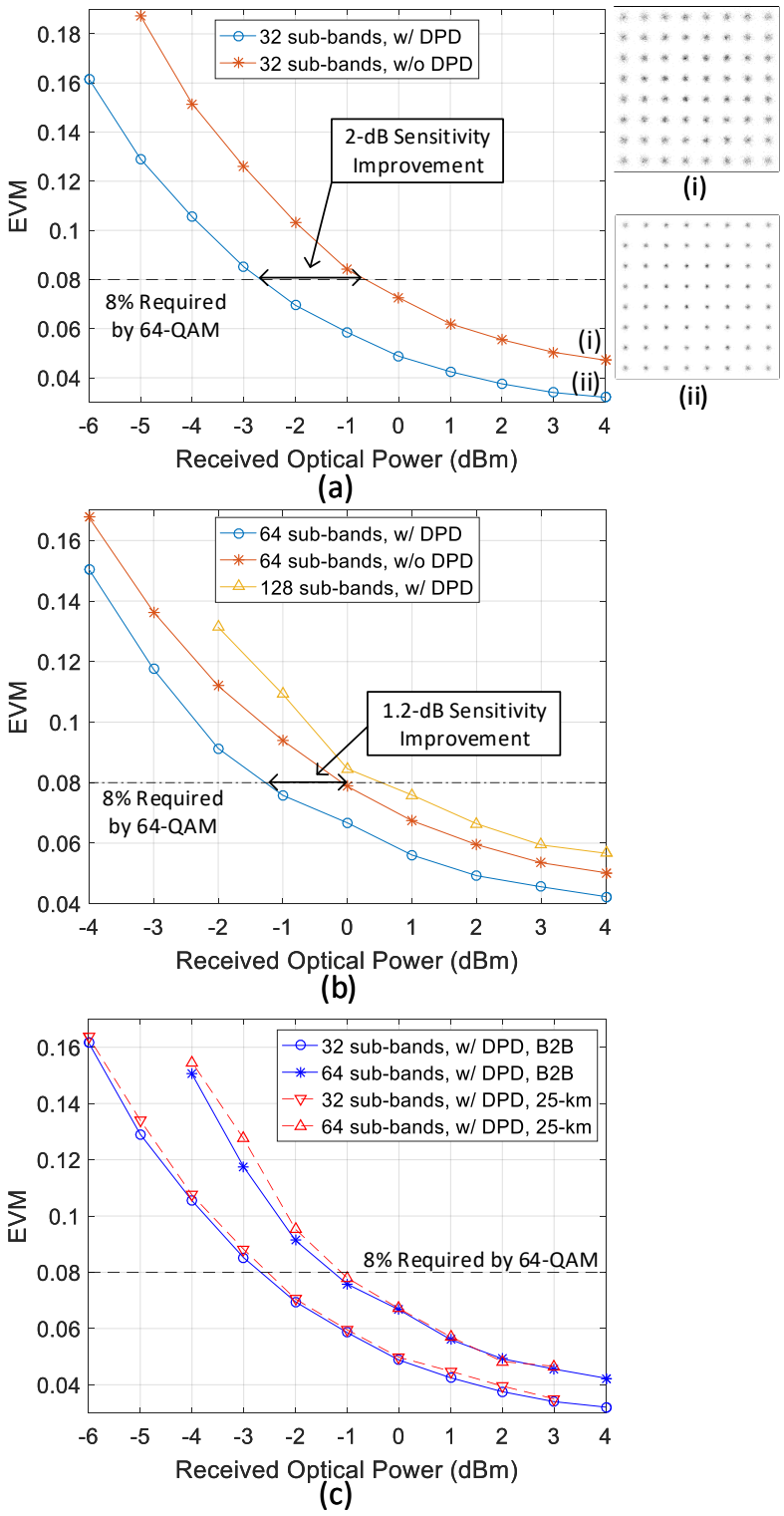


Figure 2.7: Experimental results. (a) Results with 32 sub-bands and (b) with 64/128 sub-bands. (c) Results with 25-km fiber transmission. (DPD: digital pre-distortion)

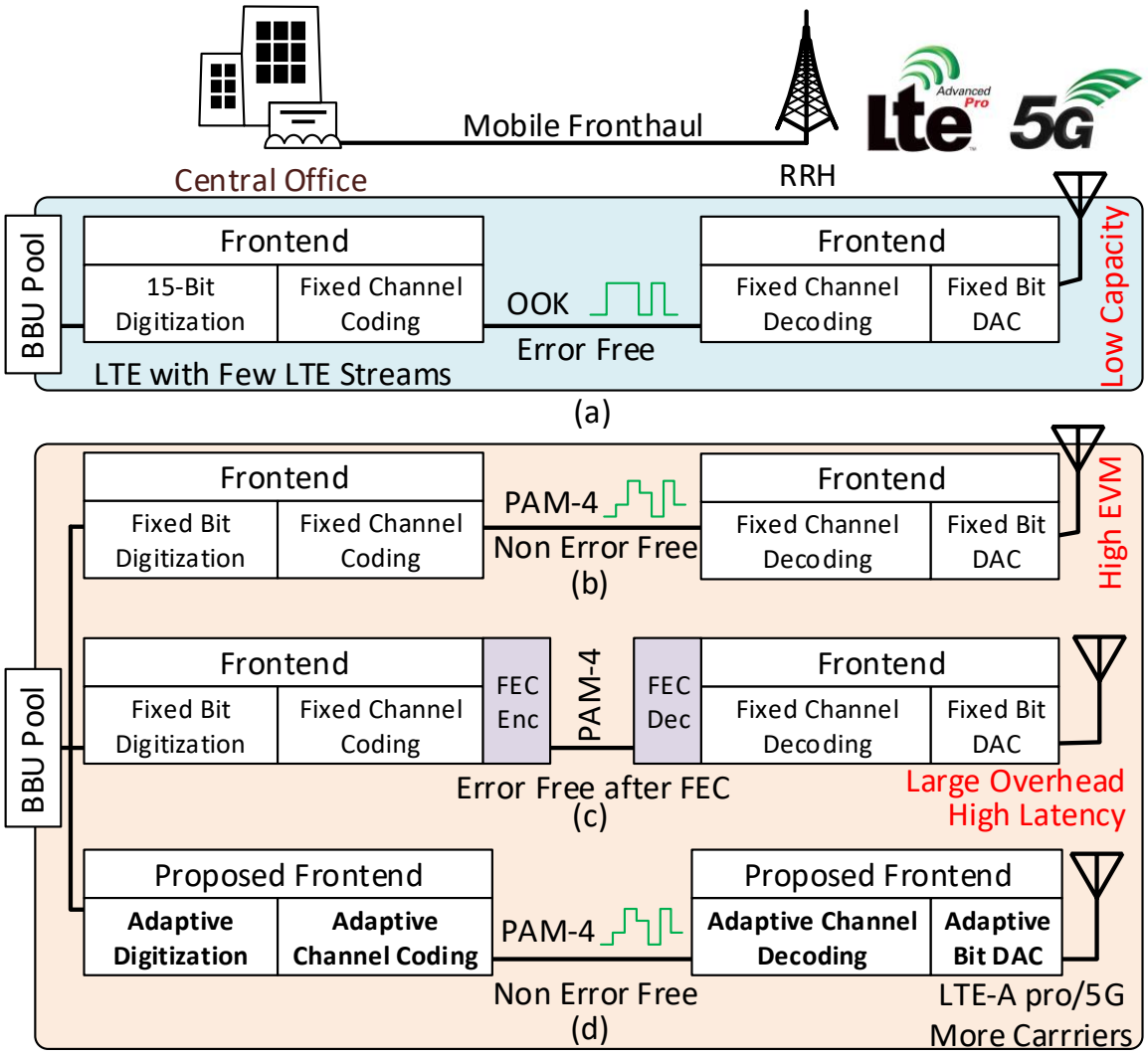


Figure 2.8: (a) LTE MFH serving few carriers with OOK link, fixed bit digitization and coding. LTE-A pro/5G MFH with more carriers using PAM-4 MFH (b) with fixed bit digitization and coding generating performance degradation, (c) using extra FEC generating extra delay, and (d) using proposed adaptive digitization and channel coding. (Enc: encoder, Dec: decoder)

and researched, including reducing the sampling rate, reducing the number of levels in digitization, nonlinear companding before digitization and so on. These techniques can reduce the line rate by more than 50%. With them, still more than 100-Gbps line rate is needed for a full capability transmission defined in 3GPP release 13.

Current OOK based optical links are hard to serve the number of carriers defined in LTE-A Pro and 5G, even with compressed CPRI. PAM-4 is promising for its high line rate

and spectral efficiency in MFH. Comparing with current low baud rate OOK, PAM-4 transmissions have increased BERs due to the reduced energy per bit and increased transmission penalties. On the other hand, the CPRI performs best with low BER links due to the fixed Reed-Solomon (RS) FEC with low overheads and a large number of digitization levels, shown in Fig. 2.8(a). Transmission errors in PAM-4 link finally degrade the EVM using current schemes, as Fig. 2.8(b) shows. In current CPRI, all parameters are fixed under all channel conditions, making the system unusable under some conditions, especially with increased line bit rates. Introducing another layer of FEC provides error-free links between frontends [shown in Fig. 2.8(c)], but requires more transmission overheads in the optical link and generates extra latency, which is not feasible in 5G where low-latency is a key feature.

### 2.2.1 Adaptive Digitization and Channel Coding

The current CPRI digitizes the in-phase and quadrature waveforms into bits, adds control words, finally applies RS channel coding. All the parameters including digitization bits and channel coding rates are fixed under all conditions. It works efficiently with low BERs since CPRI uses 15-bit digitization and a small coding overhead of only 3% in the 64b/66b setting. With 10-Gbps OOK optical link, it is easy to achieve error-free transmission, generating very low carrier EVMs due to the small quantization and clipping noise. However, as we upgrade the MFH link to high baud rate PAM-4 or discrete multi-tone (DMT) links, it is very hard to maintain error-free transmission due to the reduced Euclidean distance between amplitude levels and increased inter-symbol interference (ISI) generated by the limited bandwidth. Even with the receiver equalizer, the degradation cannot be eliminated.

Hence, we propose to use adaptive digitization and channel coding based on the MFH optical link condition to achieve an improved performance [121].

*Adaptive Digitization and Channel Coding Rate*

With relatively high channel BERs measured after the optical link, the very low channel coding overhead and simple coding scheme cannot correct these errors generated. The channel BER is defined as the BER measured after optical link equalization, without any FEC decoding. Under such conditions, there is no value in providing high digitization bits, since the channel coding cannot provide reliable information on each of the sampling bits. Instead, we propose to reduce the digitization bits so that a higher coding overhead can be provided with the same line data rate. For example, 15-bit digitization (with 1-bit control word) with 64b/66b coding rate has the same output data rate as 7-bit quantization with 51.5% overheads. The high overhead provides a strong capability of correcting errors, hence making the 7-bit digitization reliable even with high channel BERs.

However, low digitization bits generate high quantization noises, which cannot be reduced with improved BER. It leads to a high EVM floor. As a result, it is crucial to determine the optimal number of bits and coding rates applied under different channel BER conditions.

*Variable Channel Coding for High and Low Bits*

From another aspect, the noise in the wireless carrier generated by error bits after FEC can be expressed as (2.7).

$$n_i = (C \times 2^{i-N+1})^2 \propto 4^i, i \in [0, N-1] \tag{2.7}$$

$n_i$ is the noise generated by the $i$-th bit error; $C$ is the linear clipping level before digitization; $i$ is the bit index with the least significant bit (LSB) as the first index; $N$ is the total number of digitization bits.

It can be observed that the $i$-th bit error generates 6-dB lower noise than the $(i+1)$-th bit error. It is feasible if we give higher priorities to transmit high indexed bits and lower

priorities for low bits. With channel coding, assigning more coding overheads to the high indexed bits (referred to as high-bits, with the index from $N/2$ to $N-1$) can provide us improved performance even the overhead for low indexed bits (referred to as low-bits, with the index from $0$ to $N/2-1$) is shrunk.

### 2.2.2 Proposed Scheme and Simulations

Combining both adaptive and variable coding schemes, we have a series of parameters to change and optimize, including the number of digitization bits and coding rates for high-bits/low-bits. Adapting to different BERs, we can choose the option with the lowest EVM to use.

Considering the compatibility of CPRI, we still use RS with the same coding overhead of 64b/66b. As the development of DSP, the potential MFH applications with low-density parity-check (LDPC), Turbo codes or other coding schemes could share the similar adaptive scheme, since FEC with more overheads provides higher BER improvement with properly designed codes [122]. Similar performance and capacity improvement should be observed with coding schemes other than RS as a result.

In CPRI options beyond 7A, the sampling bits and control words firstly go through 64b/66b to 256b/257b transcoder, then is fed into the 514b/528b encoder. Each I/Q sample has 16-bits information including the 1-bit control word. 320-samples generate 5120-bits and are added up to 5140-bits after transcoder, finally makes 140 parity bits with the encoder. A total of 5280-bits is transmitted in the optical link.

In this paper, we use compressed CPRI with 3/4 down-sampling, nonlinear companding, and partial sampling to reduce the data rate and quantization noise, which are all well-established technologies to reduce the bit rate requirement of OFDM digitization.

The MFH delivers LTE carriers of 20-MHz channel bandwidth. The data bandwidth of each carrier is 18-MHz consisting of 1200 subcarriers, with 15-kHz subcarrier spacing following 3GPP release-8. Two settings are introduced in the paper, based on 8-bit and

16-bit digitization referred to as high-compression and low-compression settings. Under each of the setting, multiple options are designed with variable bits and coding rates. All options under the same setting generate the same data rate from each wireless carrier. The codeword and message length with high-compression are shown in (2.8)-(2.10), with $N$ is the number of bits in digitization.

$$CW_H = Round[64 \times N + (1056 - 128 \times N) \times p]$$
$$p = \begin{cases} 0.5 & Constant\ coding \\ 0.9 & Variable\ coding \end{cases} \tag{2.8}$$

$$CW_L = 1056 - CW_H \tag{2.9}$$

$$MSG = 64 \times N \tag{2.10}$$

The proposed DSP and coding flow of high-compression setting is shown in Fig. 2.9. The input is LTE OFDM streams of 20-MHz bandwidth. After 3/4 down-sampling, the sampling rate is reduced from 30.72-MS/s to 23.04-MS/s. Then every 640 complex samples are grouped and separated into in-phase and quadrature components. Two channels are independently clipped and companded. After that, the digitizer converts samples with continuous amplitude to discrete levels. Then, the high-bits and low-bits from I/Q streams are separated and recombined as the input to high/low-bit encoders. The input codeword lengths of high/low bit encoders are shown in (2.8) and (2.9), with 10-bit word width. Finally, the outputs of both encoders are combined, and one frame of 10560-bits is generated.

On average, each I or Q sample generates 8.25-bit information with high-compression, including both the sampling bits and coding overheads. For the constant coding scheme, the high and low bits all share the overhead evenly providing the same error correction

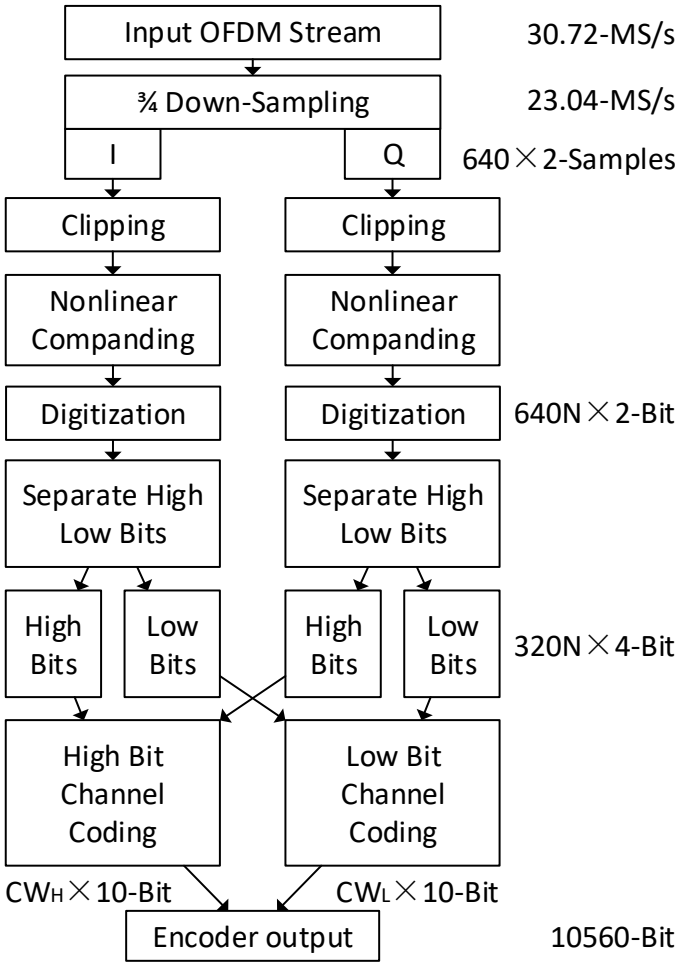


Figure 2.9: DSP flow of proposed adaptive digitization with variable channel coding for high/low bits. ($N$ is the number of digitization bits)

ability; in the variable coding scheme, low-bits use 10% of the overhead budget, and high-bits use the rest 90% overhead budget. The allocation of coding overheads is determined by $p$ in (2.8). For instance, for 8-bit digitization with variable coding, high bits use 512b/541b coding, and low bits uses 512b/515b coding.

The bar graph of all available options with the high-compression setting is shown in Fig. 2.10(a). 2, 4, 6, 7 and 8-bit digitization are available. 7-bit option is only in constant coding, while other options can have either constant or variable coding. Options are referred to as the labels from 2C to 8V. From up to down, the bar series denotes low sampling bits, low-bit coding overheads, high-bit coding overheads and high sampling bits. The same

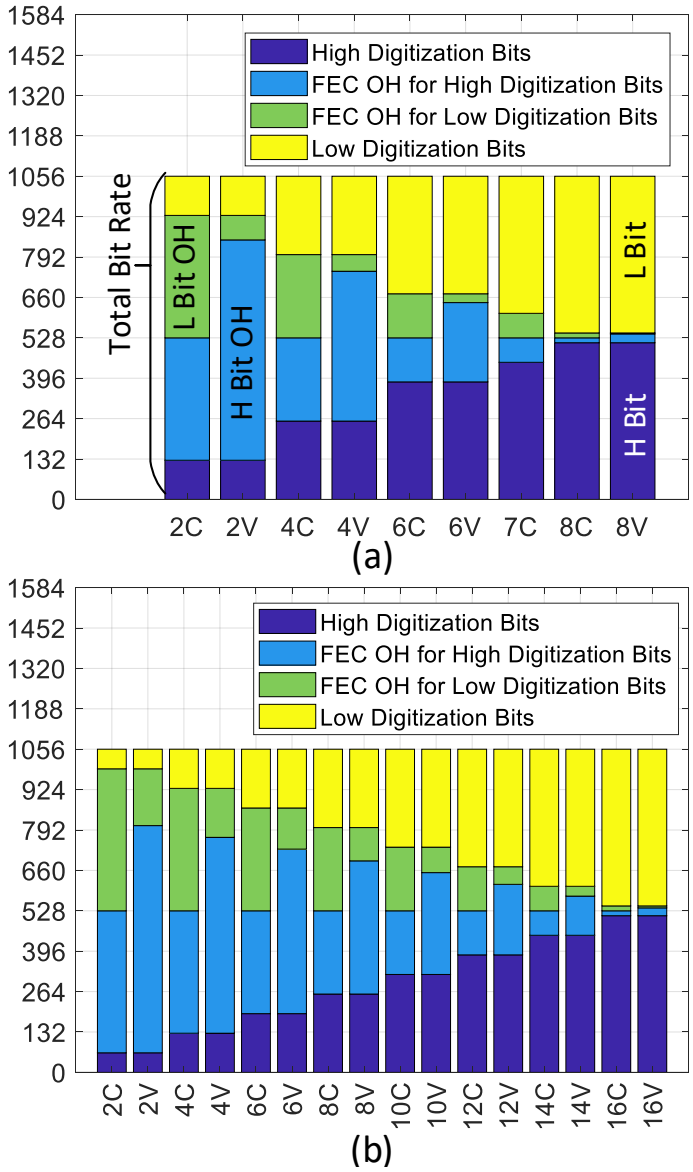


Figure 2.10: Available digitization bits and channel coding rate options of (a) high-compression and (b) low-compression settings. The bars from up to down denote low sampling bits, low sampling bit coding overheads, high sampling bit coding overheads and high sampling bits. (C: constant coding, V: variable coding, OH: overhead)

accumulated bar height infers that the packet length with all options is constant 10560-bits.

We extend the maximal digitization bits to 16-bit, referred to as the low-compression setting. No nonlinear companding is used. In the variable coding scheme, high-bits use 80% of the overhead. All options are listed in Fig. 2.10(b). The output bit rate is doubled comparing with high-compression from I/Q digitization. Hence 21120-bits deliver 640

complex samples, doubling the bits from the high-compression setting.

The proposed scheme is also capable of delivering control words. All control words use 64b/66b channel coding. The bit rate by control words is in (2.11).

$$R_{CW} = 30.72Mbps \div 64b/66b \times 2 = 63.36Mbps \tag{2.11}$$

So, the accumulated bit rate with high-compression settings is shown in (2.12). It is only 36.1% of the CPRI option 7, and 43.8% of option 7A and beyond. Similarly, the bit rate is calculated as (2.13) with the low compression setting.

$$R_H = 23.04MS/s \times 8Bit/S \div 64b/66b \times 2 + 63.36Mbps = 443.52Mbps \tag{2.12}$$

$$R_L = 23.04MS/s \times 16Bit/S \div 64b/66b \times 2 + 63.36Mbps = 823.68Mbps \tag{2.13}$$

To determine the option to use under varies optical link conditions and channel BERs, we run a series of simulations for the high-compression setting. Still, RS FEC is used for compatibility and low latency. The generator polynomial is the default value by Matlab communication toolbox under all coding setups.

Simulation results are shown in Fig. 2.11(a), with x-axis the channel BER without FEC. With more digitization bits, the curve slope is smaller, which is generated by the weaker capability of error correction with low overhead FEC. However, these options have lower EVM floor, because of the reduced quantization noise when the post-FEC error-free transmission can be achieved. With each additional digitization bits, the EVM floor can be reduced by 6-dB. Also, the variable channel coding options generate a three-section slope curve: the right high slope is generated by the high overhead coding with high-bits; the middle section is by low overhead coding with low-bits, and the left flat section is with the post-FEC error-free transmission.

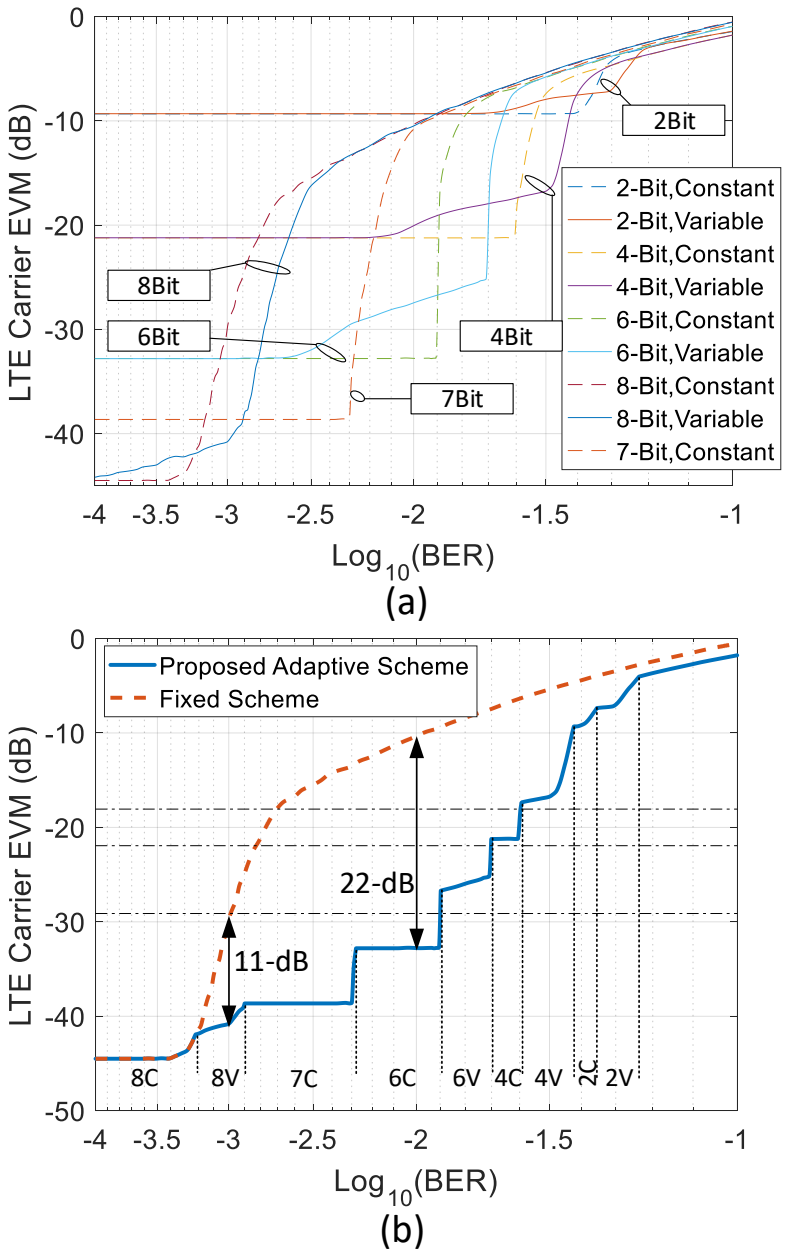


Figure 2.11: (a) Performance of all options with high-compression. Comparison between current fixed and the proposed adaptive/variable scheme with (b) high-compression.

Combining the lowest value of all options under each BER, we have the performance of the proposed adaptive scheme, shown in Fig. 2.11(b). Reference lines of 3.5%, 8% and 12.5% corresponding to 256-QAM, 64-QAM, and 16-QAM are shown. Options chosen are marked on the figure. All nine available options have their corresponding BER ranges,

covering the BER from 5% to 0.01%. As a comparison, the result using fixed bit digitization and channel coding is also presented. To serve wireless services using 16-QAM, the proposed scheme requires 2.5% raw BER from the optical MFH, while the current scheme needs a very low BER of 0.2%. The proposed scheme can also increase the BER threshold from 0.16% to 2%, and from 0.1% to 1.3%, to fulfill the requirement by 64-QAM (8% EVM) and 256-QAM (3.5% EVM). 22-dB/11-dB EVM improvements are observed with 1%/0.1% BER.

Simulation results on options of the low-compression setting are shown in Fig. 2.12(a). With the adaptive scheme performance in Fig. 2.12(b), only eight options of 2V, 4V, 4C, 6V, 6C, 8C, 10C, and 12C are necessary to cover the BER from 7% to 1.3%, obtaining EVM as low as -60-dB. Huge performance gain can be achieved: for 16-QAM, BER requirement is relaxed from 0.15% to 4%; from 0.12% to 3.2% with 64-QAM; and from 0.09% to 3% with 256-QAM. The proposed scheme reduces the EVM from -7-dB to less than -60-dB under 1% raw BER.

Our proposed adaptive scheme outperforms the fixed digitization and coding scheme due to more available options. Moreover, the best performance gain is observed between 3.1% to 0.03% raw BER, with EVM improvements as high as 25/53-dB for high/low-compression settings. Since the optical channel is stable over time, the options are updated with very low frequencies (once in hours/days), generating negligible overhead, latency, and traffic interruption to the network.

### 2.2.3 Experimental Setup and Results

A low-cost IM-DD testbed is set up to verify the feasibility of the proposed scheme in a PAM-4 optical platform.

The experimental setup is shown in Fig. 2.13. For the high-compression setting, the output from the encoder is 10560-bits regardless of which option is chosen. The time duration corresponding to the frame in wireless is 27.78-us. The information from control

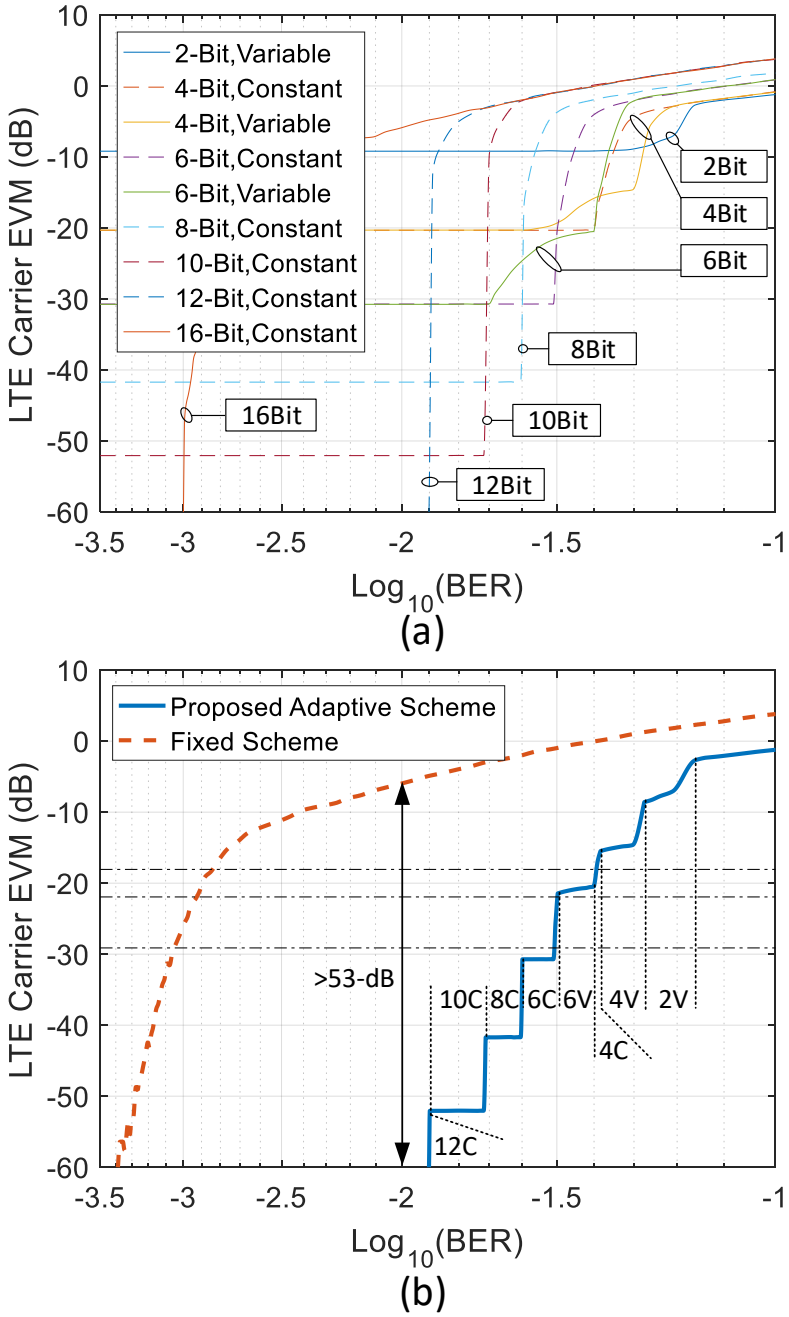


Figure 2.12: (a) Performance of all options with low-compression. Comparison between current fixed and the proposed adaptive/variable scheme with (b) low-compression.

words is cascaded, adding 1760-bits to the frame. All bits are fed into the PAM-4 modulator, outputting 6160 symbols. Then, 128 PAM-4 symbols are added as the training sequence for the equalizer, with about 2% overhead. Each frame has 12576-bits or 6288-symbols.

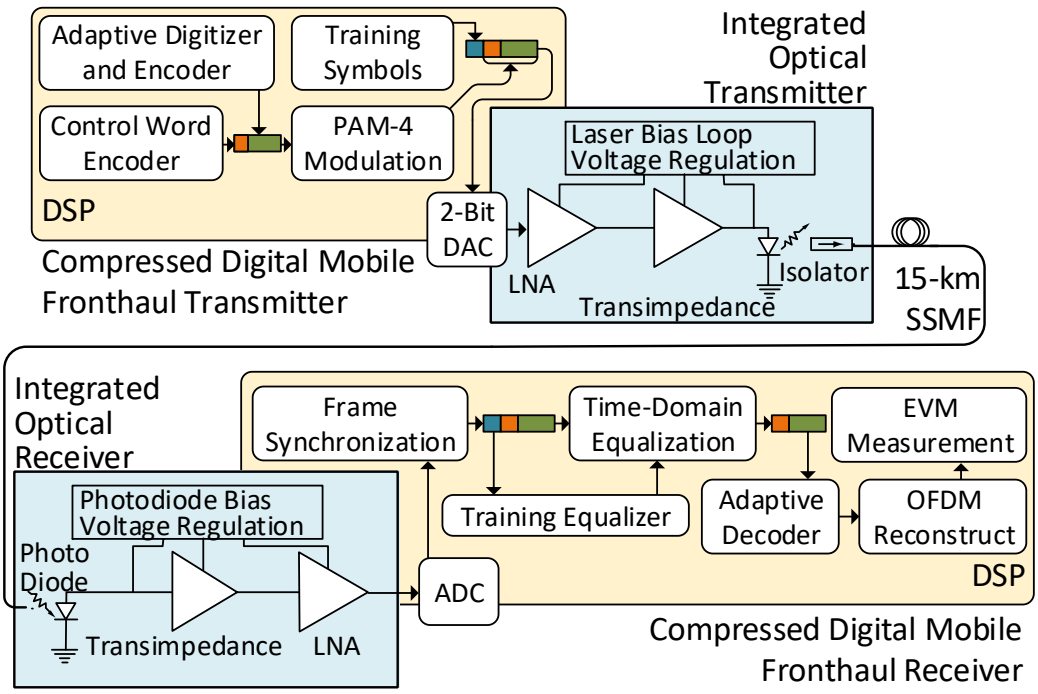


Figure 2.13: System framing and experimental setup.

The overall line rate in the optical transmission for each LTE carrier is 452.736-MHz with the high-compression setting including transmission overhead. For the low-compression setting, the data rate from symbol sampling doubles, resulting in a total bit rate of 832.896-Mbps for each LTE carrier, including about 1% training sequence overhead.

After framing, the digital signal is sent to a DAC. Since no oversampling, pre-distortion or digital shaping is applied, the DAC only has 4-level outputs. Then, a directly modulated laser (DML) based integrated optical transmitter is used for electrical to optical (E/O) conversion. The integrated transmitter consists of a low noise amplifier (LNA), a trans-impedance amplifier (TIA) and a laser. After 15-km fiber transmission, an integrated optical receiver consisting of a PD, a TIA and an LNA is used for signal reception.

The electrical signal is fed into an ADC. The training sequence is used for frame synchronization and equalizer training. Then, the time-domain equalizer of 21-taps is applied on PAM-4 symbols. After PAM-4 demodulation, we use the decoder to retrieve the information for OFDM samples and control words. Then, we reconstruct the OFDM waveform

Table 2.1: Experimental Results of MFH Capacities

| ROP | Setting | LTE Modulation | Max Allowed Capacity | | Capacity Gain |
|---|---|---|---|---|---|
| | | | Adaptive Coding | Fixed Coding | |
| -4 dBm | High Compression | 16-QAM | 106 | 81 | 31% |
| | | 64-QAM | 106 | 78 | 36% |
| | | 256-QAM | 99 | 76 | 30% |
| | Low Compression | 16-QAM | 57 | 42 | 36% |
| | | 64-QAM | 57 | 42 | 36% |
| | | 256-QAM | 57 | 40 | 43% |
| -9 dBm | High Compression | 16-QAM | 86 | 60 | 43% |
| | | 64-QAM | 82 | 58 | 41% |
| | | 256-QAM | 77 | 55 | 40% |
| | Low Compression | 16-QAM | 51 | 31 | 64% |
| | | 64-QAM | 50 | 30 | 66% |
| | | 256-QAM | 47 | 28 | 68% |

from multiple MFH frames and measure the wireless carrier EVM as the metrics. For all measurements, we firstly transmit ten measurement frames to estimate the channel BER. Then the optimal option is selected [using criteria described in Fig. 2.11(a) and 2.12(a)], transmitted and measured.

In the setup, the ADC has a variable sampling rate between 12-GS/s and 24-GS/s, and the DAC is running on a fixed 40-GS/s. The low-cost optical link is designed for 10-Gbps OOK transmission. The 3-dB bandwidth with DAC, optical transmitter, optical receiver and ADC is 6-GHz, 11-GHz, 10-GHz and 13-GHz correspondingly. The setup is capable of 48-Gbps PAM-4 transmission.

*Capacity Experimental Results*

We sweep the transmitter baud rate to change the MFH bit rate using PAM-4 modulation. We test both high-compression and low-compression settings, under -4-dBm and -9-dBm received optical power (ROP). Results are shown in Fig. 2.14. Reference lines of 12.5%, 8%, and 3.5% corresponding to the requirement of 16-QAM, 64-QAM, and 256-QAM are added. Using the same physical link, the energy for each bit decreases with the increment

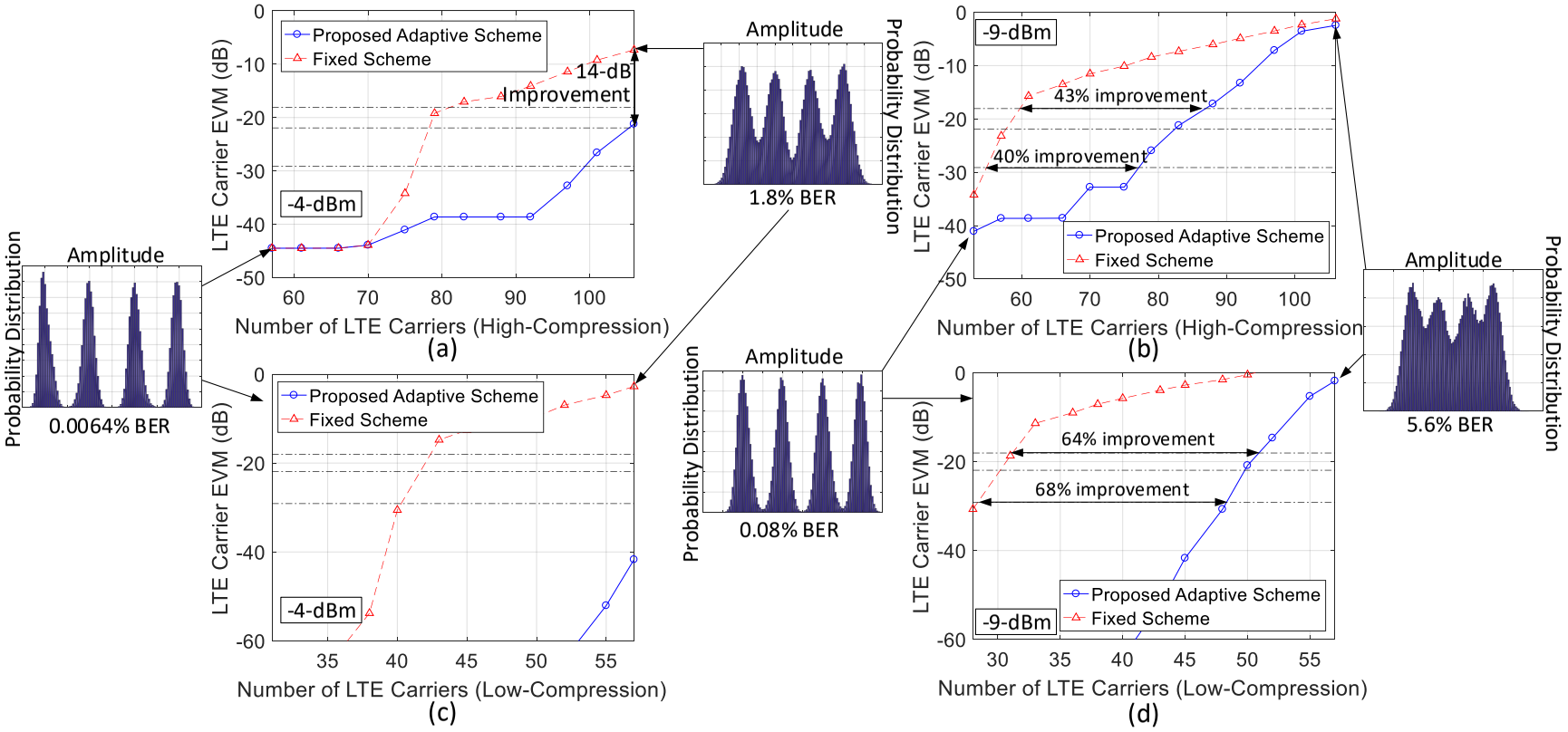


Figure 2.14: Experimental results with varying LTE carrier capacities. Performance with high-compression setting under (a) -4-dBm ROP and (b) -9-dBm ROP. Performance with low-compression setting under (c) -4-dBm ROP and (d) -9-dBm ROP. Probability distributions of equalized symbols are shown in insets.

of the data rate. Moreover, the ISI is severer with higher baud rate due to the limited bandwidth. Hence, the channel BER increases as a result of the increased data rate. The maximal allowed number of LTE carriers by both settings are shown in Table 2.1, under -4-dBm or -9-dBm ROP.

Fig. 2.14(a, c) show the EVM under -4-dBm ROP after 15-km fiber transmission. With high-compression results in Fig. 2.14(a), our proposed scheme can serve 64-QAM with the maximal 106 LTE carriers, enough for 8×8 MIMO and 13 CA with another 2×2 MIMO carrier. Under the same condition, the EVM with the traditionally fixed scheme is -8-dB. 14-dB EVM improvement is achieved. Using the low-compression setting, results are shown in Fig. 2.14(c). The adaptive scheme with -4-dBm ROP has a very low EVM of -41-dB when delivering 57 carriers, a huge improvement of 38-dB from the -3-dB EVM with the fixed scheme. The capacity gain with low-compression is between 36% and 43%. It has more potential for capacity boosting if we keep increasing the baud rate since the EVM of 57 carriers is only -41-dB.

Similar results are obtained under -9-dBm ROP shown in Fig. 2.14(b, d), 40% to 68% capacity gain can be observed depending on different QAM mappings used and settings applied.

*Sensitivity Experimental Results*

The sensitivity results are shown in Fig. 2.15 and Fig. 2.16. All measurements are executed after 15-km fiber transmission. We test three bit rates in the optical link: 24-Gbps, 36-Gbps, and 48-Gbps corresponding to the capacity of 53/79/106 LTE carriers with high-compression, and 28/43/57 with low-compression.

Fig. 2.15 show results with high-compression. With 53 carriers, we observe 2-dB to 3-dB sensitivity improvement by applying the proposed adaptive scheme. At -10-dBm ROP, the EVM improvement is 20-dB. The reduction of EVM is slower with the increment of ROP for the fixed scheme. As a result, the high-compression with 79 carriers can never

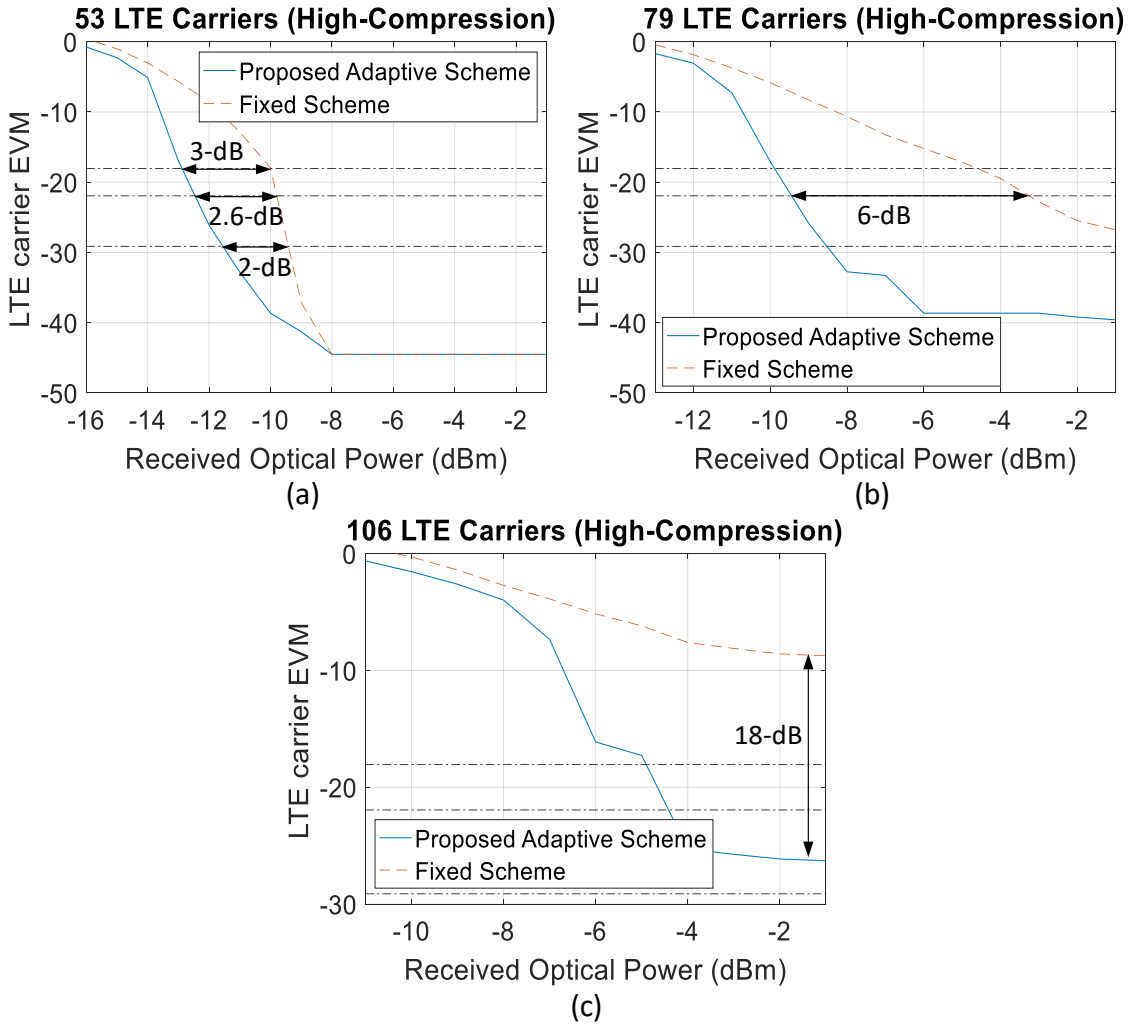


Figure 2.15: Experimental results on system sensitivity. Performance with high-compression setting with MFH capacities of (a) 53, (b) 79 and (c) 106 LTE carriers.

fulfill the 256-QAM requirement; while the adaptive scheme can achieve less than 3.5% EVM with ROP greater than -8.5-dBm. The sensitivity improvement is 6-dB for 64-QAM. For the full capacity of 106 carriers, the fixed scheme has an EVM floor of more than -10-dB. On the other hand, the adaptive scheme can serve 16-QAM and 64-QAM when the ROP is greater than -5-dBm or -4.5-dBm.

Results with the low-compression setting are shown in Fig. 2.16. The sensitivity gain is about 4-dB with 28 carriers and is increased to 9-dB with 43 carriers corresponding to 64-QAM. With the highest capacity of 57 carriers, the -5-dB EVM provided by the fixed

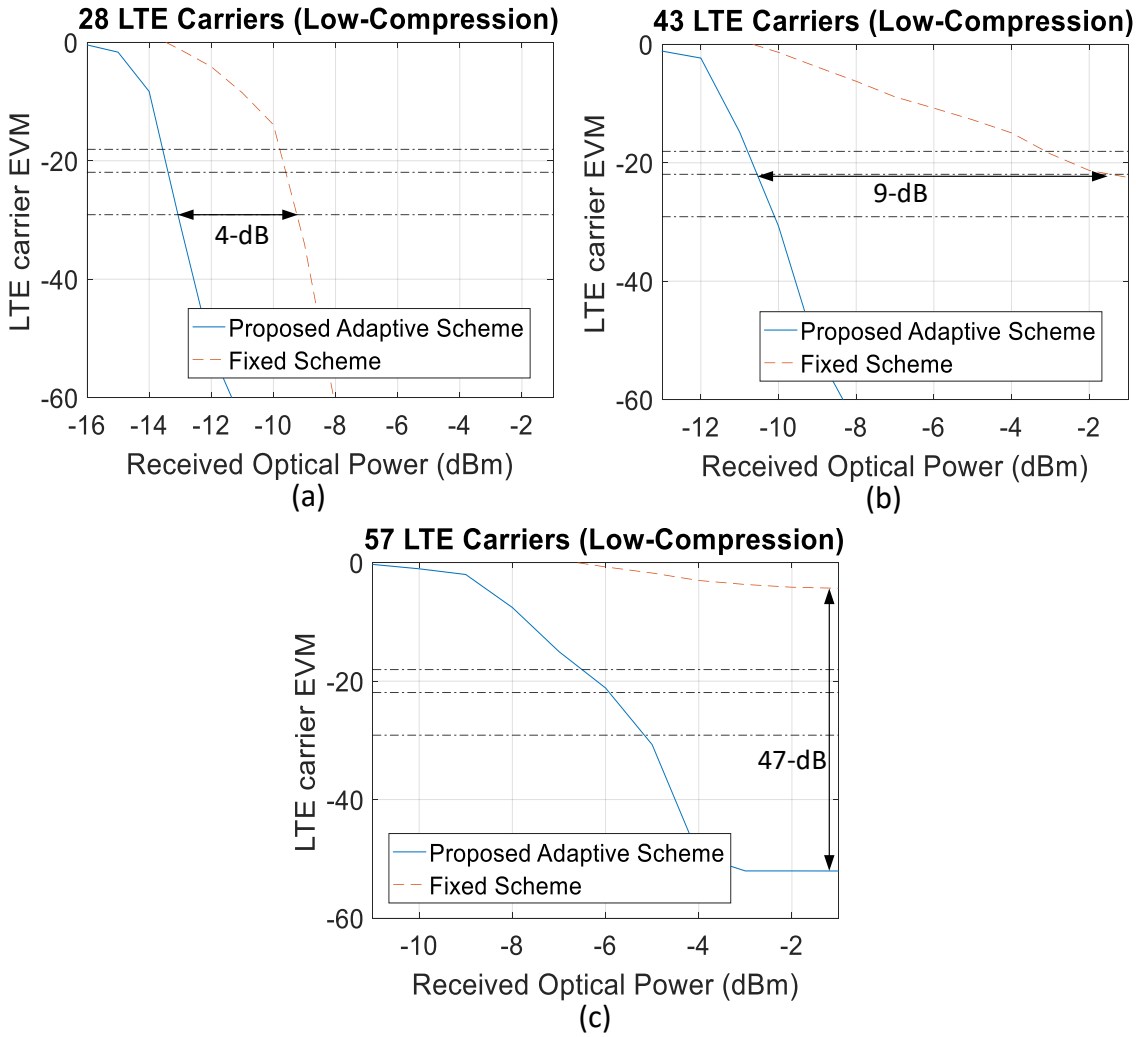


Figure 2.16: Experimental results on system sensitivity. Performance with low-compression setting with MFH capacities of (a) 28, (b) 43 and (c) 57 LTE carriers.

scheme is too high for any LTE services, while the proposed method significantly reduces the EVM to -52-dB. The EVM improvement is 47-dB with -1-dBm received power.

The capacity increment and sensitivity improvement by the proposed adaptive scheme are verified using the specific experimental setup, but similar conclusions can be drawn with other system setups or modulations. Because the proposed scheme is applied before optical modulation and after optical demodulation, which is independent of the PAM-4 modulation and optical platform. Under any link conditions with different BERs, the improvement

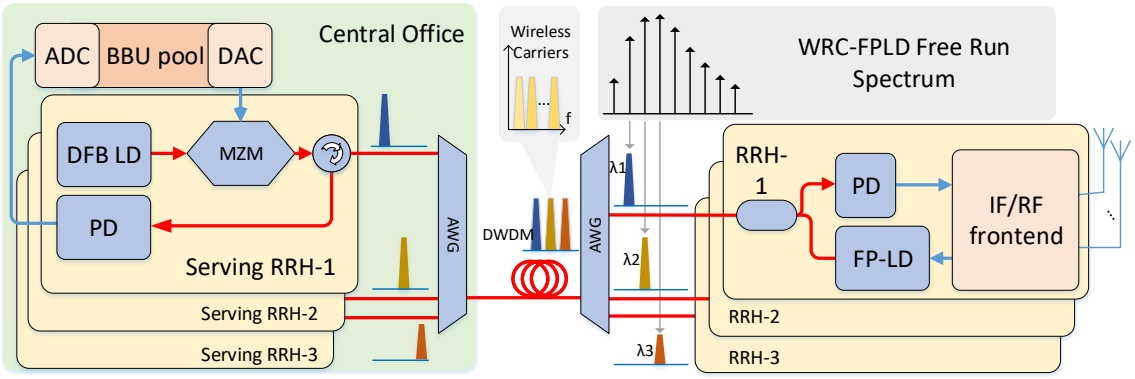


Figure 2.17: Schematic of proposed bi-direction mobile fronthaul with low-cost colorless WRC-FPLD.

should be observed within the channel BER range, as Fig. 2.11(b) and 2.12(b) show.

## 2.3 WRC-FPLD in DWDM Mobile Fronthaul

Fiber-wireless integration technology is developed and widely researched as one approach to reduce the bandwidth requirement, that analog radio waves are transmitted between BBUs and RRHs in the fiber using FDM. Each carrier only occupies 20-MHz. This approach provides high spectrum efficiency, transparency to wireless standards, and reduces the RRH cost and complexity significantly.

Challenges are still present from uplink light source, which previously most proposed mobile fronthaul uses DFB laser or RSOA based RRH, employing direct or external modulation for uplink. DFB laser is costly in high-density RRHs, especially in DWDM fronthaul where wavelength tunability and stability are required. RSOA is preferable only in digital links since the spontaneous noise degrades the signal significantly in fiber-wireless fronthaul.

### 2.3.1 WRC-FPLD in Mobile Fronthaul Uplink

The proposed scheme is shown in Fig. 2.17 [123]. Both uplink and downlink signals are transmitted in analog waveforms, which enables modulation/demodulation centralization

in BBU to reduce the RRH cost. Carriers are multiplexed on IFs and transmitted to RRH for downlink. For the uplink, the received raw waveforms after RF/IF conversion are sent back to BBU in analog waveform too. Only simple analog frontend for filtering and analog RF/IF conversion is necessary for RRH. The high spectral efficiency makes it possible for low-cost low-bandwidth devices to support a high volume of carriers required by massive MIMO and enhanced CA.

In fiber transmission, DWDM architecture is introduced that one trunk fiber from BBU serves multiple RRHs, with data to/from RRHs multiplexed in the wavelength domain. As a mature technology, DWDM keeps the mobile fronthaul scalable, reliable, flexible, delay controllable, and future-proofed. Multiple DFB lasers at different DWDM channels are deployed in BBU as the downlink light source.

For the uplink, the DFB laser with a broad modulation bandwidth can be used. However, to achieve colorless RRH, a wide wavelength tunability is necessary, making tunable DFP lasers expensive for high-density RRHs. Another approach with directly modulated RSOA does not apply to the fiber-wireless integrated mobile fronthaul because the spontaneous emission of RSOA induces a strong intensity noise, which seriously degrades the channel quality for radio signal transmission and increases the EVM. Instead, low-cost WRC-FPLDs are proposed to be deployed in RRHs. Modified from conventional FPLD that has fewer longitudinal modes and does not favor colorless applications, the WRC-FPLD is developed with multi-mode lasing, the broadened gain spectrum and a higher tolerance to wavelength drift from the injected light. In the proposed scheme, the downlink light carries data and also serves as the seed light for injection-locking (IL) in RRH. Traditionally it is not a feasible approach because the high optical modulation depth with OOK in downlink generates severe performance degradation for uplink. However, the penalty is less due to the high PAPR and linearity requirements of multi-band OFDM in downlink, making the equivalent modulation depth in seed light lower, and provides better perfor-

mance in the uplink.

$$B_c \approx \frac{1}{Delay} = \frac{1}{LD\Delta\lambda} = \frac{1}{LD[(n-1)d\lambda + d\lambda_s]} = \begin{cases} \frac{1}{LD(n-1)d\lambda}, n > 1, free\_running \\ \frac{1}{LDd\lambda_s}, n = 1, injection\_locked \end{cases} \tag{2.14}$$

Additionally, IL keeps the uplink wavelength strictly the same as downlink without complex control mechanism, making the system agile and easy to operate. The only locked mode makes the RRH natively compatible with DWDM, and increases the equivalent wireless coherent bandwidth significantly, shown by (2.14) with $B_C$ for coherent bandwidth. $d\lambda$ and $d\lambda_s$ are the wavelength spacing corresponding to WRC-FPLD mode spacing (73-GHz) and signal bandwidth (2-GHz), with $L$ for fiber length, $D$ for fiber dispersion and n for the number of modes with high optical powers. Considering the mode spreading is greater than 10-nm without IL in WRC-FPLD, we could extend the coherent bandwidth from below 250-MHz (corresponding to only about ten streams with guard bands) to beyond 100-GHz without dispersion compensation, assuming a 25-km fiber transmission over C-band in mobile fronthaul.

### 2.3.2 Experimental Setup and Parameters

The experimental setup is shown in Fig. 2.18. 70 OFDM carriers are generated by the offline DSP and a 12-GS/s digital to analog converter (DAC). After an electrical amplifier, the downlink signal is fed into a Mach-Zehnder modulator (MZM). Then the light is amplified with an erbium-doped fiber amplifier (EDFA) and transmitted through 25-km single mode fiber (SMF). In RRH, the lightwave firstly goes through a 50/50 splitter and is fed into a PD. Another branch is to the WRC-FPLD for IL. Optical spectra with or without IL is shown in Fig. 2.19. The uplink electrical signal generated by DSP and 12-GS/s DAC drives the WRC-FPLD for direct modulation. Back to BBU, the uplink signal is separated by the circulator, amplified with an EDFA, and detected by another PD. All recovered electrical

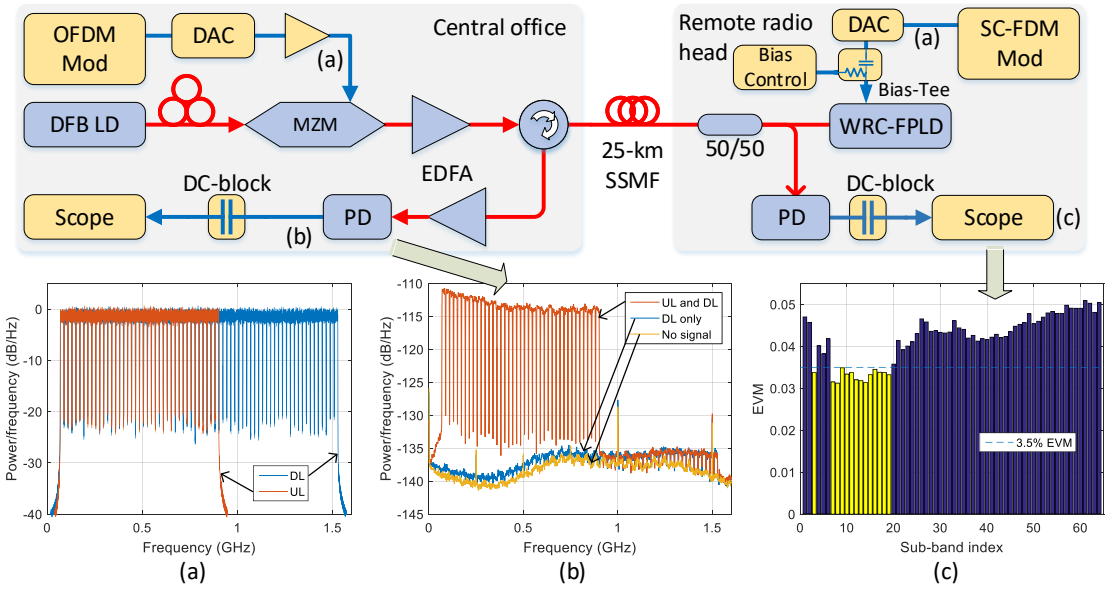


Figure 2.18: Experimental setup. (a) downlink/uplink electrical spectra. (b) Received electrical spectra in uplink. (c) Received downlink EVM for all carriers.

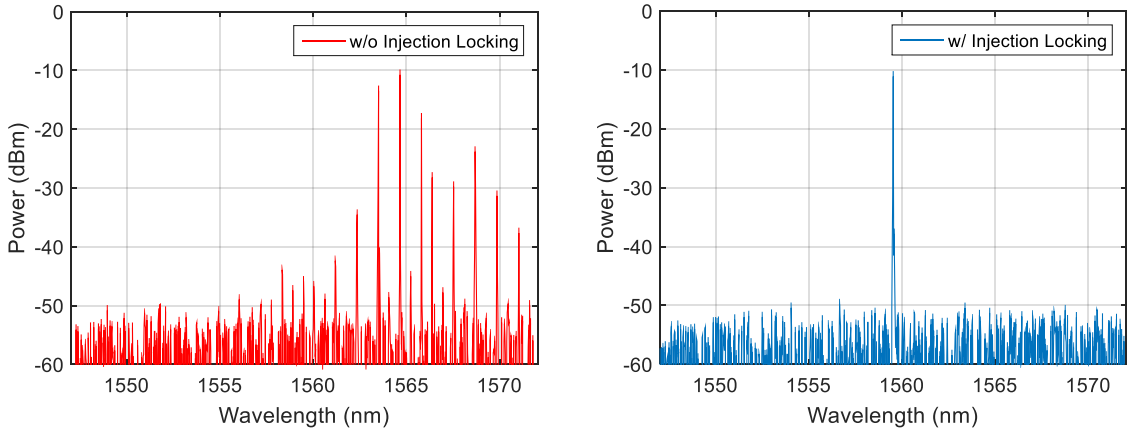


Figure 2.19: Optical spectra with (right)/without (left) injection-locking.

signals are sampled by a scope and demodulated offline. The received uplink spectrum after PD is shown in Fig. 2.18(b) with varies conditions. Comparing the downlink only and no signal curves, the downlink signal leakage reduces the uplink SNR by less than 3-dB.

Out of 70 downlink carriers, 64 are selected by channel quality and used to serve 88 MIMO and 8 CA, which exceeds the current LTE-A standard. The uplink signal is 40 carriers using single-carrier frequency division multiplexing (SC-FDM). 32 carriers with

best channel conditions are selected for uplink 4 $\times$ 4 MIMO and 8 CA. All uplink and downlink carriers are with bandwidths of 18-MHz following LTE standard using 64-QAM, with guard-bands set to 2.88-MHz between carriers allowing analog filtering and frequency conversion in RRH. The generated uplink/downlink spectra are shown in fig. 2.18(a). Leaving 69.12-MHz at DC, the downlink/uplink signals have accumulated bandwidths of 1527.84/901.44-MHz. Varying EVMs across carriers at different IFs are generated. An example is shown in Fig. 2.18(c) with downlink. In the following section, all EVMs are calculated regarding the maximum EVM carrier-wise. For example, Fig. 2.18(c) suggests a maximum EVM of 5.1%, guaranteeing all carriers suitable for 64-QAM transmission. 14 out of 64 carriers are with EVMs below 3.5% for 256-QAM.

### 2.3.3 Results

All EVMs shown in Fig. 2.20 are the maximal EVMs carrier-wise, which is the EVMs of carriers operated in the worst condition. For the downlink, different modulation depths and ROPs are tested, as well as 25-km fiber transmission, shown in Fig. 2.20(a, b). The EVMs for different optical modulation depths are shown in Fig. 2.20(a). The modulation depth is shown by the external electrical attenuator between downlink DAC and amplifier. Three attenuations are tested: 12-dB, 20-dB and 26-dB. With higher attenuation, the input electrical power is lower, so is the optical modulation depth. From results, with a too high attenuation (low modulation depth), the system is noisy and has higher EVM. 1.2/5.2-dB ROP penalties are generated between 20/26-dB and 12-dB attenuation at 8% EVM. For too low attenuation, like 12-dB, the system works better with low ROPs due to the increase modulation depth but has higher EVM floor by nonlinearity in the amplifier and MZM. From IL aspect, lower modulation depth generates better uplink performance due to the clearer seed light. There is a 1.8-dB ROP difference between 25-km fiber transmission and optical back-to-back (B2B) with 8% EVM and uplink services, as shown in Fig. 2.20(b).

Optical back-to-back and 25-km transmission are tested for uplink. The downlink sig-

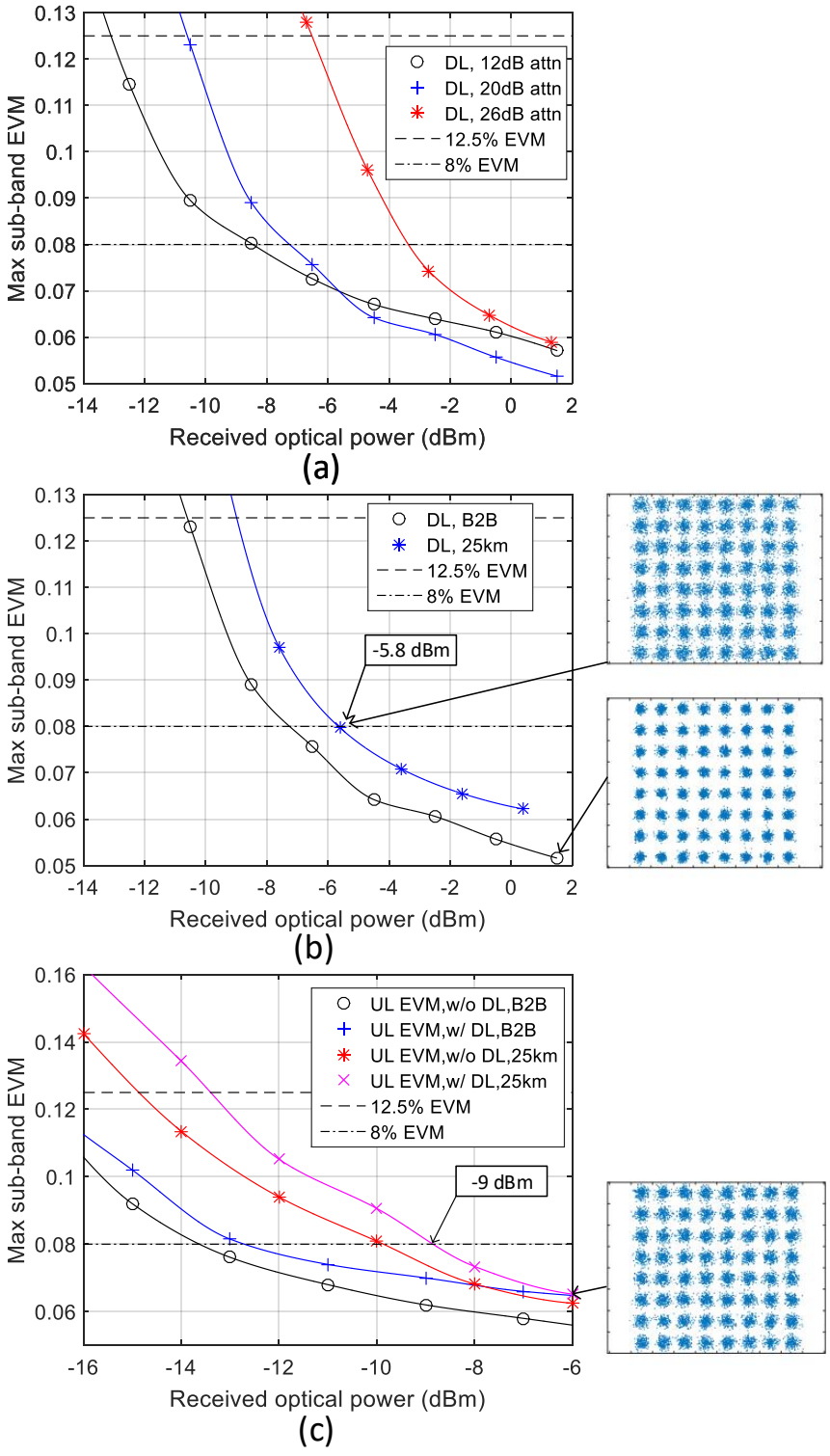


Figure 2.20: Experimental results: (a) downlink EVM with different modulation depths; (b) downlink EVM with fiber transmission; (c) uplink EVM

nal is fixed with 20-dB attenuation and 0 dBm optical power at RRH, so the injection power is -3 dBm. From Fig. 2.20(c), 1-dB ROP difference is generated with/without downlink signal, which suggests that the reuse of downlink light as seed light generates a tolerable penalty. With 25-km fiber transmission, the required ROP for 8% EVM is 4-dB higher than optical B2B.

The proposed mobile fronthaul provides low EVM performances for bi-directional transmission for high-density small cell RRH deployment. If the downlink/uplink ROPs are greater than -5.8/-9 dBm, the mobile fronthaul could deliver 3GPP release 12/13 bi-directional services to RRH 25-km away with all carrier EVMs below 8%, which is the requirement for 64-QAM.

## 2.4 Summary

In this Chapter, we present the research in MFH for improved capacity and reliability in the phase 1 implementation of fiber-wireless integrated systems.

We have proposed a novel pre-distortion scheme to reduce the PAPR in spectral efficient MFH for 5G networks using analog MFH schemes. This proposed pre-distortion is feasible because all introduced processing power is centralized in the BBU, and no additional modifications are necessary for the user device. We replace the phase search with delay search and use a binary searching tree scheme to reduce the computational complexity. The PAPR can be reduced by 2.2-dB at 1% CCDF, without introducing remarkable latency. The experimental results show significant sensitivity improvements with proposed pre-distortion under 32/64 sub-bands setup, to fulfill the requirement by 64-QAM. The results validate the feasibility of the proposed pre-distortion scheme generating multi-IF OFDM signal in spectral efficient MFH with reduced PAPR.

Adapting to the digital MFH schemes, we propose an adaptive scheme on the digitization bits and channel coding rates according to the optical channel condition. Adapting to the channel BER, we can dynamically change the digitization bits and channel coding

rates. The coding overhead for high-bits and low-bits can also be different for improved performance. The adaptation does not change the output channel bit rate. In simulations, we discuss different adapting schemes and obtain options with their selection criteria. We set up a PAM-4 MFH testbed from low cost electrical and optical devices, with varying data rates from 24-Gbps to 48-Gbps. Comparing with current CPRI on OOK links, the MFH spectral efficiency is increased by 5.5 times. When compared with other PAM-4 based compressed digital MFH, the sensitivity gain is 2 to 9-dB, and the wireless EVM is significantly reduced. The proposed scheme should have similar performances and capacity improvements with other channel coding schemes, system setups, and optical modulations.

As for optical multiplexing and high-density small cell support, we have proposed a novel bi-directional mobile fronthaul architecture with low-cost, high spectral efficiency and high flexibility features enabled by WRC-FPLD in RRH. It is compatible with DWDM colorless RRH for spatial densification. The FPLD provides high stability when properly injection locked, with improved coherent bandwidth and reduced chromatic dispersion penalties.

With features of high spectral efficiency, scalability, reliability, and performance, we believe proposed MFH technologies are promising for MFH in the phase 1 implementation of fiber-wireless integrated systems.

# CHAPTER 3

# WAVEFORM FOR MILLIMETER-WAVE FIBER-WIRELESS INTEGRATED SYSTEM

In this chapter, the research work of advanced modulation and multiple access schemes are shown adapting to the fiber-wireless integrated channels introduced by the second phase of fiber-wireless integration: MMW fiber-wireless integrated system.

Adapting to different 5G application scenarios, three modulation and multiple access schemes are designed and developed, shown in Table 3.1. During the verification of different MMW waveforms, we applied various MMW generation schemes with optical technologies.

## 3.1 Generalized Frequency Division Multiplexing for Millimeter-Wave Carrier Aggregation

To meet strong demands for wireless broadband services from mobile users, CA technology is introduced by 3GPP to support high data rate transmission over wide frequency bandwidths. Compared with other technologies introduced by LTE-A such as MIMO and coordinate multi-point, CA combines more bandwidth to increase data rates and has lower requirements on channel quality and DSP complexity. Currently, CA technology is based on OFDM modulation, which exhibits high out-of-band radiation in standards for high data rate operation and low mobility scenarios (for example, Wi-Fi). Therefore, large guard

Table 3.1: Coverage of proposed waveforms in the 5G application scopes.

| Application Scenario | eMBB | URLLC | mMTC |
|---|---|---|---|
| Key Performance | Data Rate | Reliability and Latency | Device Density |
| GFDM | | | |
| OCDM | | | |
| PD-NOMA | | | |

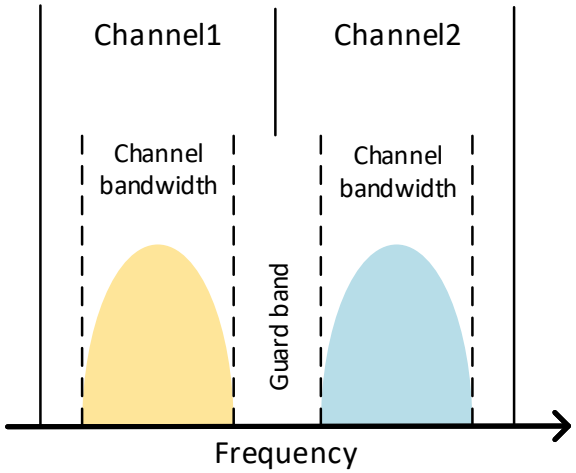


Figure 3.1: Channels and guard-bands for intra-band carrier aggregation.

bands are required to protect adjacent channels: in 802.11n/ac, more than 15% guard bandwidth is required to safeguard a 20-MHz legacy mode, as shown in Fig. 3.1. Thus the spectrum efficiency is severely hampered by the guard bands. Furthermore, due to the congestion in the traditional UHF spectrum, it is costly for operators to provide extra bands to support CA. The wide available bandwidths over unlicensed MMW bands provide tremendous opportunities for service expansion and CA deployment.

### 3.1.1 Principle of generalized frequency division multiplexing

Generalized frequency division multiplexing (GFDM) is a PHY concept initially developed to exploit spectrum white spaces for wireless transmission. It has been proposed and widely investigated for its deployment flexibility and ultra-low out-of-band radiation, as Fig. 3.2 shows. GFDM modulation alleviates harmful interference to adjacent channels. Hence it can reduce the guard band in CA operation and increase spectrum efficiency without affecting existing services on adjacent channels. Comparing with OFDM, GFDM has lower overheads and is more suitable for the low multipath characteristic in MMW bands. We propose to use the GFDM modulation in the MMW bands for reduced overhead in Ca operation [124].

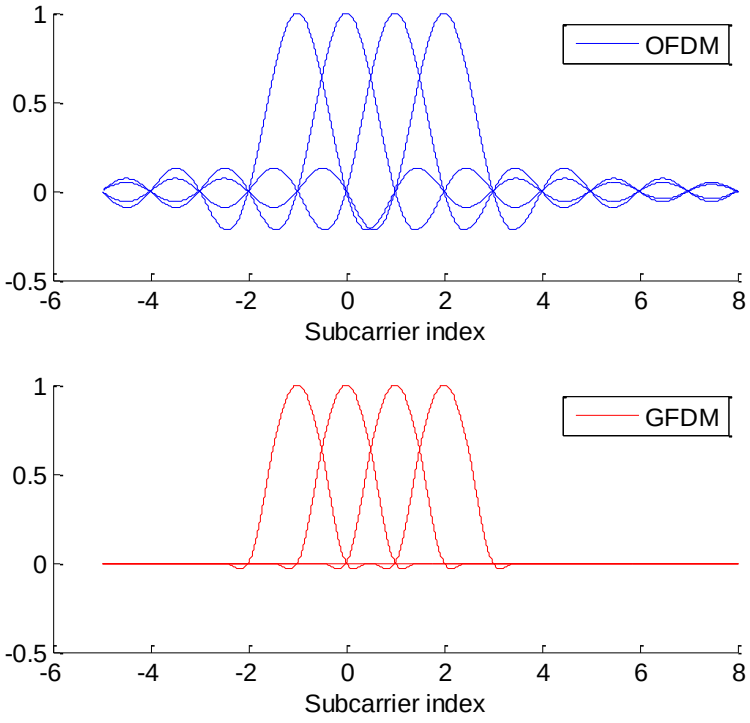


Figure 3.2: Spectrum comparison of GFDM and OFDM.

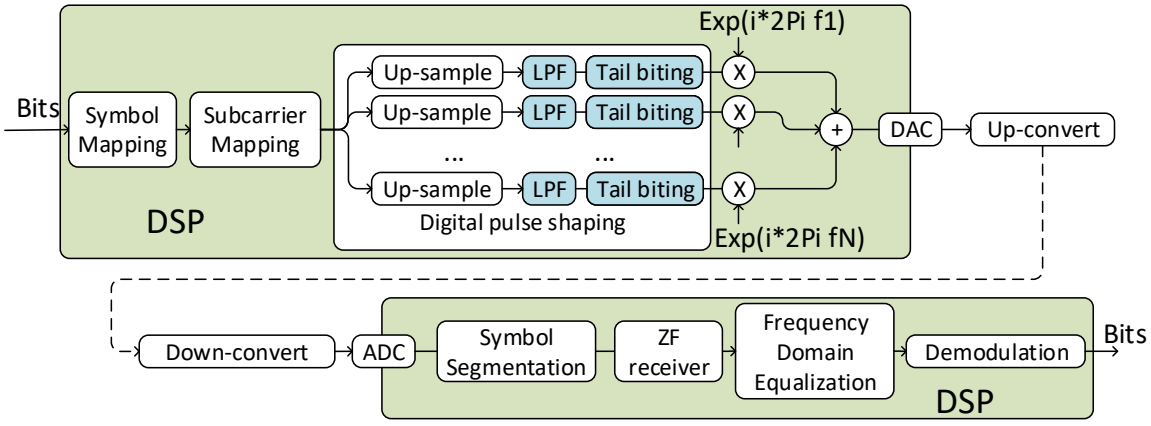


Figure 3.3: DSP flow of GFDM transmitter and receiver.

GFDM is a multi-carrier modulation scheme using digital shaping filter bank. The transmitter and receiver structure is shown in Fig. 3.3. Each subcarrier is modulated using QAM formats, pulse-shaped subcarrier-wise and up-converted individually in DSP. Hence, GFDM can be interpreted as a parallel single-carrier using the cyclic prefix (SC-CP), with

more controllable out of band radiation. The output samples can be denoted as (3.1).

$$X(k) = \sum_{n} [s(n,k) * g_{TX}(k)] e^{i2\pi k f_n} \tag{3.1}$$

$s(n,k)$ is the up-sampled QAM symbol on subcarrier $n$ and time slot $k$. $g_{TX}(k)$ is the low pass filter coefficient. $f_n$ denotes different carrier frequencies and is normalized regarding signal occupying bandwidth $B$. Operator $*$ denotes convolution operation for filter shaping to $k$. Circular shaping filters are used in GFDM to create tail biting and prevent rate loss from shaping filter tails in the transmitter. We apply CP for frequency-domain equalization. After DSP, the output stream for the component carrier (CC) is digital-to-analog converted, low pass filtered, and mixed to digital IFs.

Since the subcarriers in GFDM are not orthogonal but exists mutual interference among subcarriers, FFT based receiver is not applicable. Instead, a ZF receiver is used. The GFDM modulation can be expressed by a more general modulation matrix $M$, so $X = MD$. $D$ is the transmitted symbol block. M is corresponding to GFDM modulation. Usually, some subcarriers on the band edge are not transmitting symbols but used as the guard band. Thus $M$ can be simplified to a non-square matrix: $M_s$. For $M_s$, there exists its pseudo-inverse ${M_s}^+$ if the columns of $M_s$ are linearly independent.

$$\hat{D} = {M_s}^+ X_r \tag{3.2}$$

The received symbols can be recovered by (3.2), where $\hat{D}$ is the recovered symbols, and $X_r$ denotes received samples in the time domain. The quality of the ZF receiver strongly depends on the properties of ${M_s}^+$, which is affected by the filter shape, time slot lengths, and other GFDM parameters.

At the receiver, the analog wave is first down-converted to baseband, then digitized using ADC. After time offset (TO) and CFO estimation and removal, samples are converted back to QAM symbols by a digital ZF receiver with a frequency-domain equalizer.

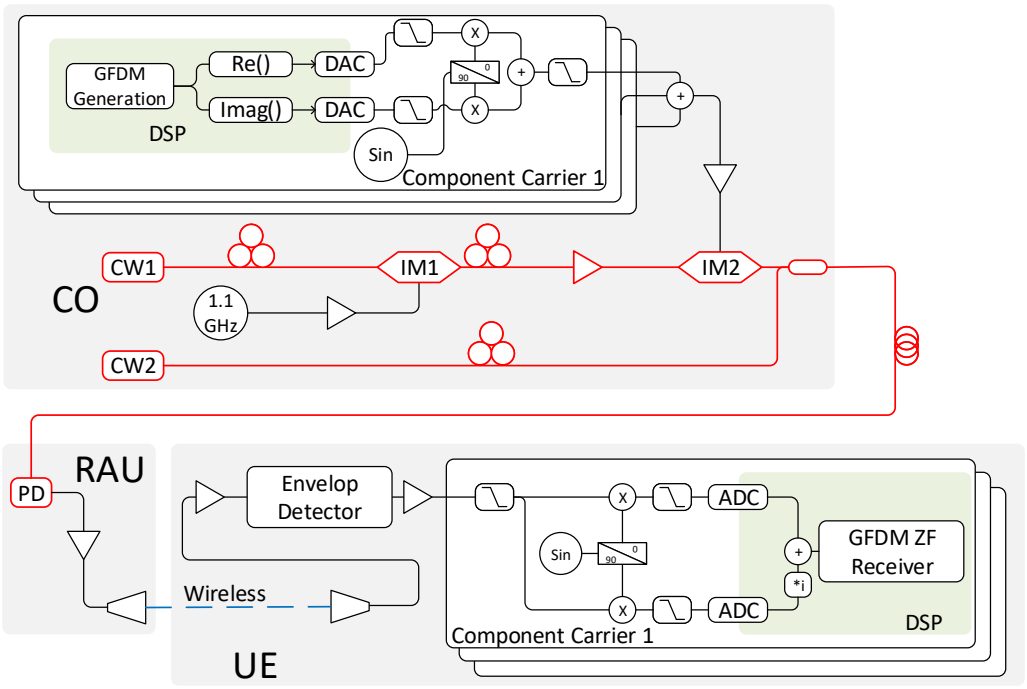


Figure 3.4: Experimental setup of GFDM CA with fiber-wireless integration.

### 3.1.2 Experimental setup

The experimental setup is depicted in Fig. 3.4. Two continuous-wave optical signals from DFB lasers with 60-GHz frequency spacing are used for MMW generation. One optical signal (from CW1 in Fig. 3.4) is applied to an intensity modulator (IM1 in Fig. 3.4), which is driven by a 1.1-GHz sinusoidal wave to generate three optical carriers. The lightwave is then amplified by an EDFA and applied to another IM (IM2 in Fig. 3.4). IM2 is driven by a combination of three 40-MHz CC signals centered at IFs of 450 MHz, 490 MHz, and 530 MHz, respectively. Each CC is generated by a FlexRIO FPGA adapter module (FAM) from National Instruments. Inside each FAM, the IQ samples are converted into analog waves using two DACs. After low pass filters (LPFs), the IQ signal is up-converted to IF to drive IM2. The three FAMs are controlled by one PXIe-8133 controller and driven by separate Virtex-5 FPGA chips. Finally, 18 optical CCs are generated and combined with CW2, as shown in Fig. 3.5.

After fiber transmission, the signal is detected by a 60-GHz PD, amplified by a high-

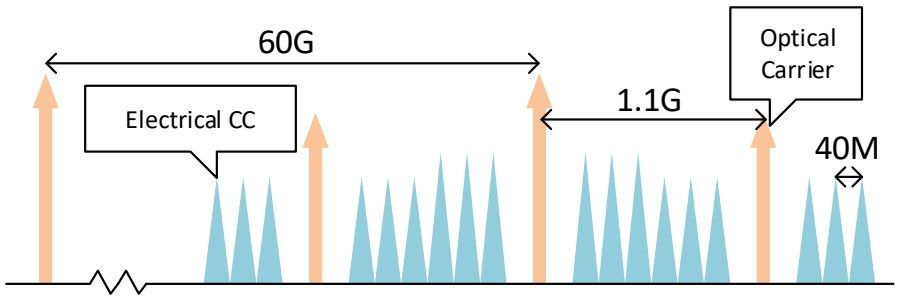


Figure 3.5: Band allocation of 18 bands in GFDM CA.

bandwidth amplifier, and radiated by a horn antenna with a 15-dBi gain. After 2-meter LoS wireless transmission, the MMW signal is received by another horn antenna in UE. The signal is then amplified and down-converted by an ED. The signal is received by another FAM. Similar to the FAMs in the transmitter, the receiver FAM has an IF down-converter, ADCs, and LPFs. By choosing different IF frequencies, we can receive and analyze signals from different CCs. Finally, the symbols are recovered by a digitally implemented ZF receiver with a frequency-domain equalizer.

In the experiment, the bandwidth of each channel is 40 MHz, consisting of 64 subcarriers with 625-kHz spacing. 52 subcarriers carry data, and the other 12 subcarriers are used as guard bands. Therefore, the guard band is 3.75 MHz each side by default. All subcarriers use 16-QAM mapping. We also use OFDM modulation of the same parameters to compare EVM performance under different conditions with GFDM modulation.

### 3.1.3 Experimental Results

We first test the received-optical-power performance. By changing the input optical power of PD, different EVM is observed. During the test, the wireless link is fixed to two meters, with all CCs center frequency 40 MHz apart. The EVM performance of OFDM is also tested as a comparison. Fig. 3.6(a) shows the experimental results. A 15-km fiber is then added and tested, causing no significant performance degradation compared with the back-to-back transmission, shown in Fig. 3.6(b).

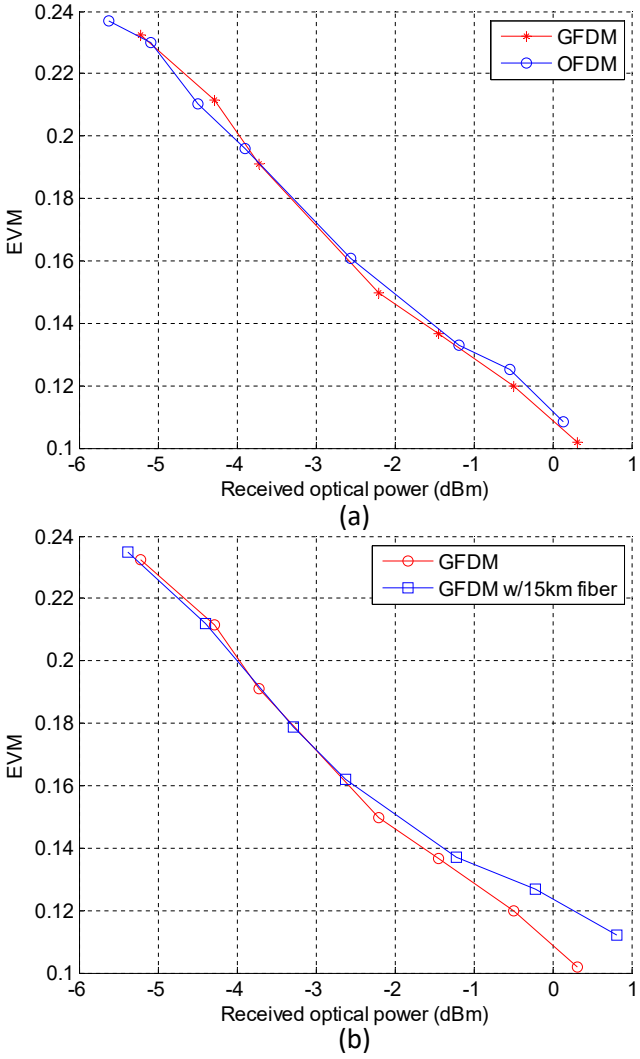


Figure 3.6: Experimental results of GFDM CA with fiber-wireless integration. Sensitivity results with (a) back to back and (b) 15-km fiber.

Different CC center frequency spacing (or guard bandwidth) is tested. With 0 dBm received optical power, we reduce the electrical CC spacing by changing the center frequencies from the three transmitter FAMs, while keeping the optical carrier spacing fixed. The results are shown in Fig. 3.7(a-b). CC1 and CC3 receive CC2s interference from either high or low-frequency side, while CC2 is impacted on both sides. The performance degradation is more severe for CC2, as shown in Fig. 3.7(b). From Fig. 3.7(a-b), an improvement of 3% in EVM is observed when guard band is reduced to 2-8 subcarriers.

Reduced optical carrier spacing is also tested. By adjusting the input signal frequency

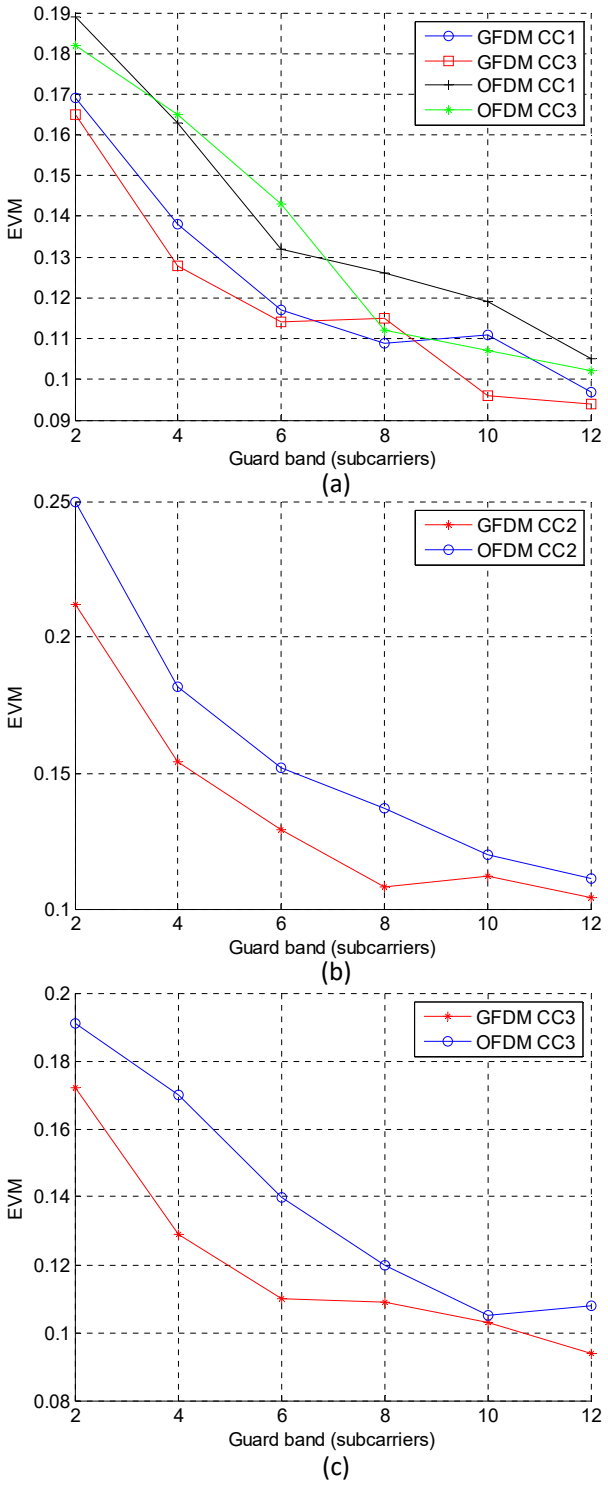


Figure 3.7: Experimental results of GFDM CA with fiber-wireless integration. With different (a-b) guard bands between electrical generated CCs (c) guard bands between optical generated CCs.

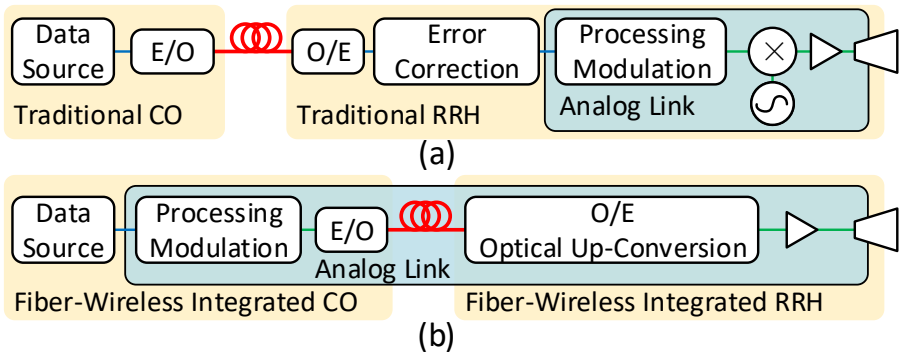


Figure 3.8: System architecture of (a) traditional distributed RAN and (b) RAN with fiber-wireless integration.

of IM1, different guard bandwidths between CC3 and CC4 are generated. Only CC3 is impacted due to reduced optical carrier spacing, as shown in Fig. 3.7(c). Similar to reduced electrical guard bands, reducing guard bands between optical generated CCs lead to a 3-4% EVM gain for GFDM modulation when the guard band is reduced to 2-6 subcarriers.

## 3.2 Orthogonal Chirp Division Multiplexing for Ultra-Reliable Low-Latency Communications

The fiber-wireless integrated design enables simple RRH by utilizing MMW up-conversion in PDs and centralizing DSP to the CO. It reduces the RRH cost and increases the spectral efficiency in fiber transmission. However, it presents new challenges in system performance and reliability. The traditional architecture is shown in Fig. 3.8(a) with isolated fiber and wireless transmissions. By error correction after the fiber transmission, the analog link is minimized and only exists in the RRH, guaranteeing the radio signal quality. On the other hand, fiber-wireless integrated architecture extends the analog link from RRH to CO, including the fiber transmission. Any signal degradation in the fiber will result in an impaired wireless signal. The errors generated in the analog fiber link is hard to be corrected.

As more wireless backhaul and fronthaul links running on MMW bands, as well as extended analog links in fiber-wireless systems, frequency selective interferences and noises

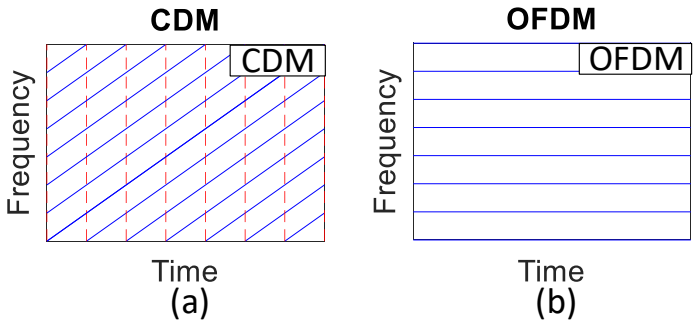


Figure 3.9: Frequency profile of (a) orthogonal CDM and (b) OFDM.

can be observed, making the system unreliable. Especially, with OFDM or single-carrier modulation, the bandwidth equals to the QAM symbols transmitted over a unit time if we do not consider CP. For URLLC with low data rates, the signal bandwidth is small comparing to the available channel bandwidth in MMW, making it risky if the small bandwidth is overlapped with existing services or high noise floors. Some subcarriers can be impaired severely with the interferer. Schemes including bit-loading need prior channel information, which is not applicable in highly dynamic situations with low-latency requirements. Also, with constant frequency selective interferences, the repetition cannot improve its reliability. Hence, OFDM cannot fulfill the reliability and latency requirements in 5G URLLC.

### 3.2.1 Principle of Orthogonal Chirp Division Multiplexing

$$BER_i = \frac{4(1-\frac{1}{\sqrt{M}})}{Log_2 M} Q[\sqrt{\frac{3}{(M-1)}\frac{P_s}{n_i}}] = BER(\frac{P_s}{n_i}) \tag{3.3}$$

Instead of subcarrier kernels with constant frequency in OFDM [shown in Fig. 3.9(b)], we propose to use the orthogonal digital chirps with varying frequency to spread the interference power to all modulation kernels, shown in Fig. 3.9(a) [125]. With the relationship between SNR and BER of $i$-th subcarrier/subchirp, we have the $BER_i$ in 3.3. $M$ is the number of constellation points, $N$ is the number of subcarriers/subchirps, $P_s$ is the power of each subcarrier/sub-chirp, and $n_i$ is the noise/interference power on $i$-th subcar-

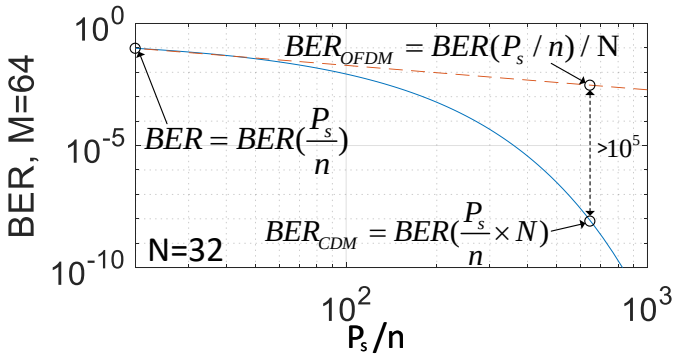


Figure 3.10: 64-QAM BER under varying $p_s/n$, with comparison between CDM and OFDM.

rier/subchirp.

$$BER_{OFDM} = BER(P_s/n)/N \tag{3.4}$$

$$BER_{CDM} = BER(P_s \times N/n) \tag{3.5}$$

With a narrow band interference with power $n$ impacting a single subcarrier, the BER is reduced by a factor of $N$ in OFDM, since the narrowband interference is only impacting a single subcarrier and all other subcarriers are still error free. The BER for CDM is shown in (3.5) because the interference power is spread over all subchirps, so the noise power is reduced by a factor of $N$ in each symbol. An example is shown in Fig. 3.10 with 32 subcarriers/subchirps and 64-QAM. An improvement of $10^5$ is achieved with the concave function $BER(x)$. We observe that the CDM has improved performance and reliability with the same narrow band interference or noise. Exchanging the time and frequency division, it can be derived that CDM has stronger reliability combating burst interferences in time division than single carrier modulations. The CDM has better performance in fiber-wireless systems with uneven noise floors in frequency division or burst noises in the time

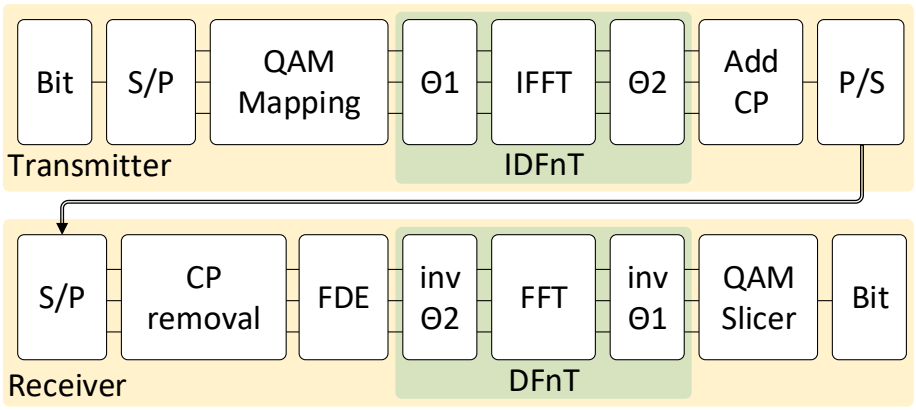


Figure 3.11: Transmitter and receiver DSP for chirp division multiplexing.

division.

$$\Phi(m,n) = 1/\sqrt{N} \times e^{-j\pi/N \times (m-n)^2} \tag{3.6}$$

The digital kernel of CDM is shown in (3.6); $m$ and $n$ are the sample index and subchirp index correspondingly [126]. With a similar expression with the kernel of subcarriers in OFDM, we can still apply inverse fast Fourier transform (IFFT)/FFT in the transmitter/receiver shown in Fig. 3.11 with the full DSP flow. The only difference is that CDM needs quadratic phases as (3.7) and (3.8), adding $O(N)$ complexity. The overall DSP complexity is similar to OFDM with $O(N \times Log(N))$. We still use CP with a frequency division equalizer (FDE).

$$\Theta_1(n) = e^{-j\pi \times n^2/N} \tag{3.7}$$

$$\Theta_2(m) = e^{-j\pi \times m^2/N} \tag{3.8}$$

To maintain the orthogonality of subchirps in CDM, the number of subchirps cannot exceed the product of symbol duration and signal bandwidth. However, the bandwidth of CDM is independent of the number of subchirps used, compared with the fact that

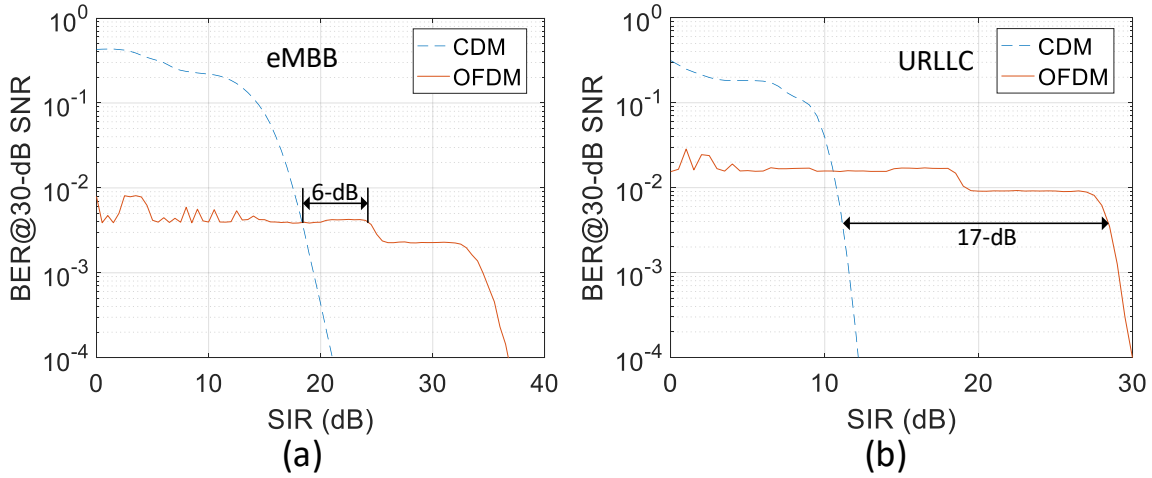


Figure 3.12: Simulation results. BER results with narrow band interferer in (a) eMBB and (b) URLLC.

the bandwidth of OFDM reduces as the number of subcarriers decreases. Two modes are introduced in this letter: eMBB utilizes all subchirps providing the same spectral efficiency as OFDM, using orthogonal dense CDM. CDM is working as a multiplexing scheme in eMBB. URLLC only uses fractional orthogonal subchirps for enhanced reliability, as sparse CDM, which works as a spreading technique.

### 3.2.2 Simulations

We run a series of simulations showing the improved performance by CDM, as well as its tolerance to residual CFOs and TOs. The signal has 64 subcarriers/subchirps. eMBB uses all resources carrying data, while URLLC uses 25% of the resources. All subcarriers/subchirps apply 64-QAM mapping. The simulation has an SNR floor of 30-dB.

First, we introduce an interferer with single frequency overlapped with both CDM/OFDM signals and sweep the signal to interference ratio (SIR). Using 3.8e-3 BER as the threshold, we can tolerate 6-dB higher interference power in eMBB, and 17-dB higher interference power in URLLC, shown in Fig. 3.12.

Then, different residual CFOs are added before demodulation. In Fig. 3.13(a), both CDM and OFDM are sensitive to the CFO with identical degradations in eMBB. For

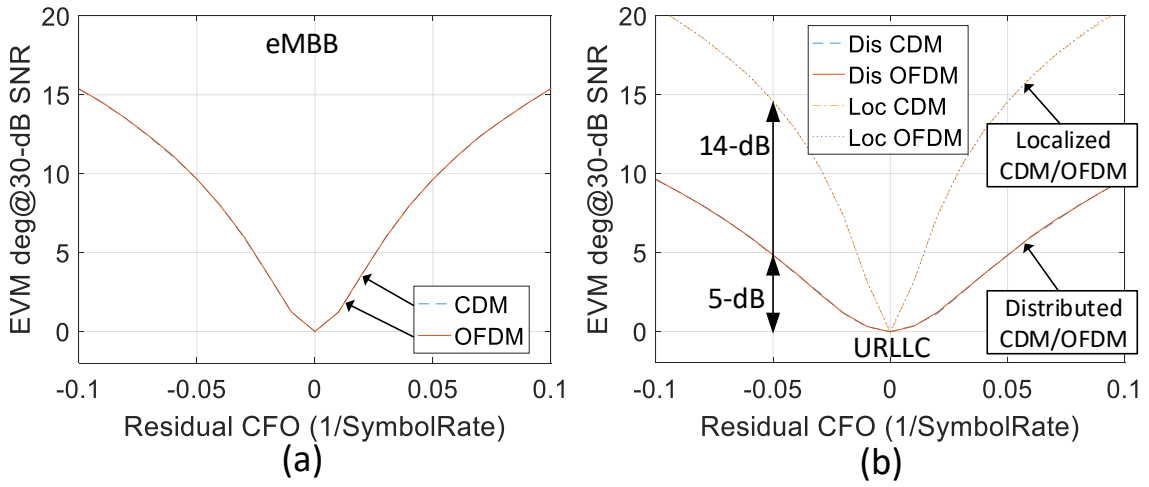


Figure 3.13: Simulation results. EVM degradations with residual CFO in (a) eMBB and (b) URLLC.

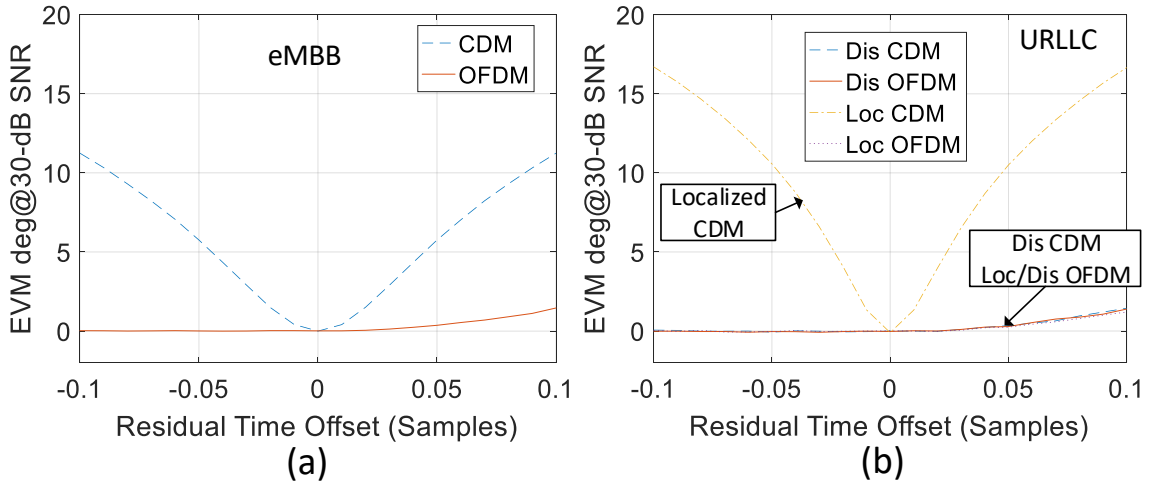


Figure 3.14: Simulation results. EVM degradations with residual time offsets in (a) eMBB and (b) URLLC.

URLLC with sparse CDM, we introduce two chirp allocation schemes. For distributed mode, the CDM utilize distributed chirps with index [0, 3,..., 60]; the CDM utilizes [0,1,...,15] indexed chirps in localized mode. Because that the adjacent subchirps do not have interference power in the presence of CFO, we have improved performances with the distributed mode. 5/14-dB EVM degradations are generated by $0.05/SymbolRate$ CFO with distributed and localized modes, for both CDM and OFDM.

Finally, we test the modulation response to TOs, with results in Fig. 3.14. OFDM is

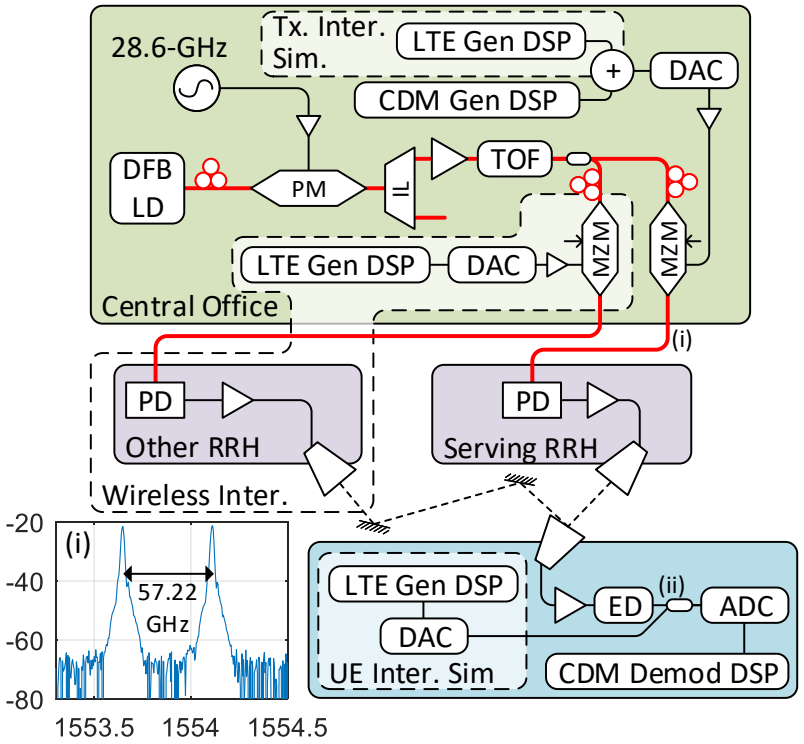


Figure 3.15: Experimental setup of the MMW fiber-wireless system with CDM and interferences.

known for its strong capability in TOs with CP, observed in the flat line from -0.1 to 0. The 0 to 0.1 degraded EVM is because the sampling offset is outside CP, which can be solved by timing advance. However, for CDM in eMBB, more degradations are generated by the varying frequency kernels. In URLLC, the CDM shows similar performance with OFDM if we use the distributed mode.

In simulations, we show that the CDM has better BER performances than OFDM with a narrowband interferer. If we select distributed mode in URLLC, CDM/OFDM have the same degradations. However, CDM is more sensitive to TO in eMBB. This TO can be easily compensated by the FDE in the receiver with CP, or we can simply switch back to OFDM in the eMBB scenario by assigning $\Theta_1$ and $\Theta_2$ to ones.

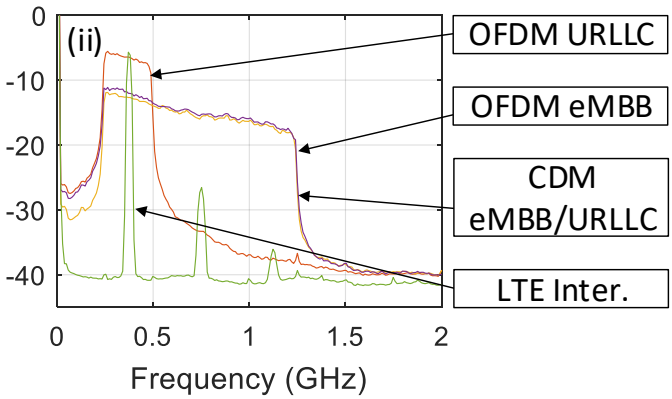


Figure 3.16: Received electrical spectra of CDM and OFDM with various applications.

### 3.2.3 Experimental Setup and Results

We set up a 60-GHz fiber-wireless transmission system, with another optical generation scheme with bias insensitive phase modulation, shown in Fig. 3.15. A single DFB laser with a phase modulator (PM) driven by 28.61-GHz sinusoidal signal is used for MMW generation. Then, first order lightwaves with 57.22-GHz spacing are selected by a 33/66-GHz interleaver. After a tunable optical filter, the IF-CDM signal is modulated by a Mach-Zehnder modulator (MZM). In RRH, the lightwave is directly converted to electrical signal by a PD and transmitted by an amplifier and horn antenna with 25-dBi gain. After 6-ft wireless link, in the user equipment, we use an envelope detector for down-conversion. Finally, the received IF-CDM signal is sampled by an oscilloscope, equalized and demodulated offline.

Interferences from three sources can be added to the system: the transmitter interference is added before DAC in CO in the digital domain; the receiver interference is added by combining signal and interference before scope in the electrical domain, and the wireless interference is introduced by a parallel RRH transmitting on the same frequency.

The signal transmitted is IF-CDM. The signal bandwidth is kept 1-GHz, consisting of 64-subchirps in eMBB, using 64-QAM and 12.5% CP; the IF is 750-MHz, with 5.33-Gbps data rate. For a comparison, OFDM carrying the same data rate using 64-QAM with

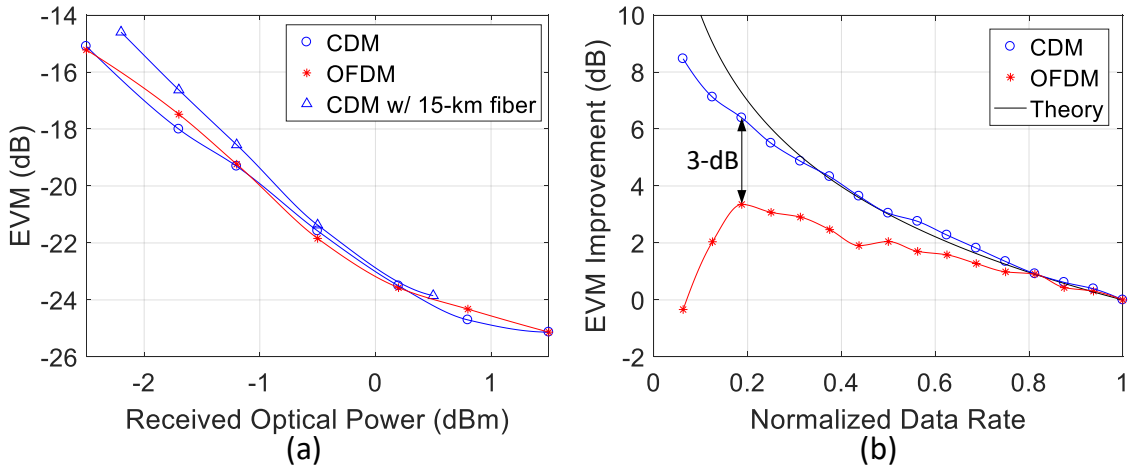


Figure 3.17: Experimental results with (a) optical sensitivity, (b) EVM improvement with reduced data rate.

identical IF is introduced. However, we also test URLLC with reduced data rate. For CDM, the sparse CDM still have a 1-GHz bandwidth, while OFDM has shrunk bandwidth. The IF for OFDM becomes $(250 + BW/2)$-MHz. The received spectra of CDM/OFDM under eMBB and 25% data rate URLLC is shown in Fig. 3.16. All interferences use LTE with 18-MHz bandwidth and varying IFs, simulating multi-service co-existence in transmitter/receiver, or MMW fronthaul links in 60-GHz bands.

The experimental results are shown in Fig. 3.17 and Fig. 3.18. First, we test the sensitivity of CDM/OFDM using eMBB configuration, with results in Fig. 3.17(a). CDM and OFDM show similar sensitivity performances, with negligible penalties by 15-km fiber. Then, we gradually reduce the number of subchirps/subcarriers carrying data to simulate URLLC with varying data rates, to measure the EVM improvement (reduction) with results in Fig. 3.17(b). The improvement should be identical with additive white Gaussian noise (AWGN). However, we observe a gap between OFDM and CDM, which increases to 3-dB if we only use 12 subchirps/subcarriers. It is generated by the higher noise floor with lower IFs. For some data rates, the CDM curve is beyond the theoretical line, which is generated by imperfect baseline EVM measured in eMBB.

Then, three types of interferences from the transmitter, receiver and wireless signal-

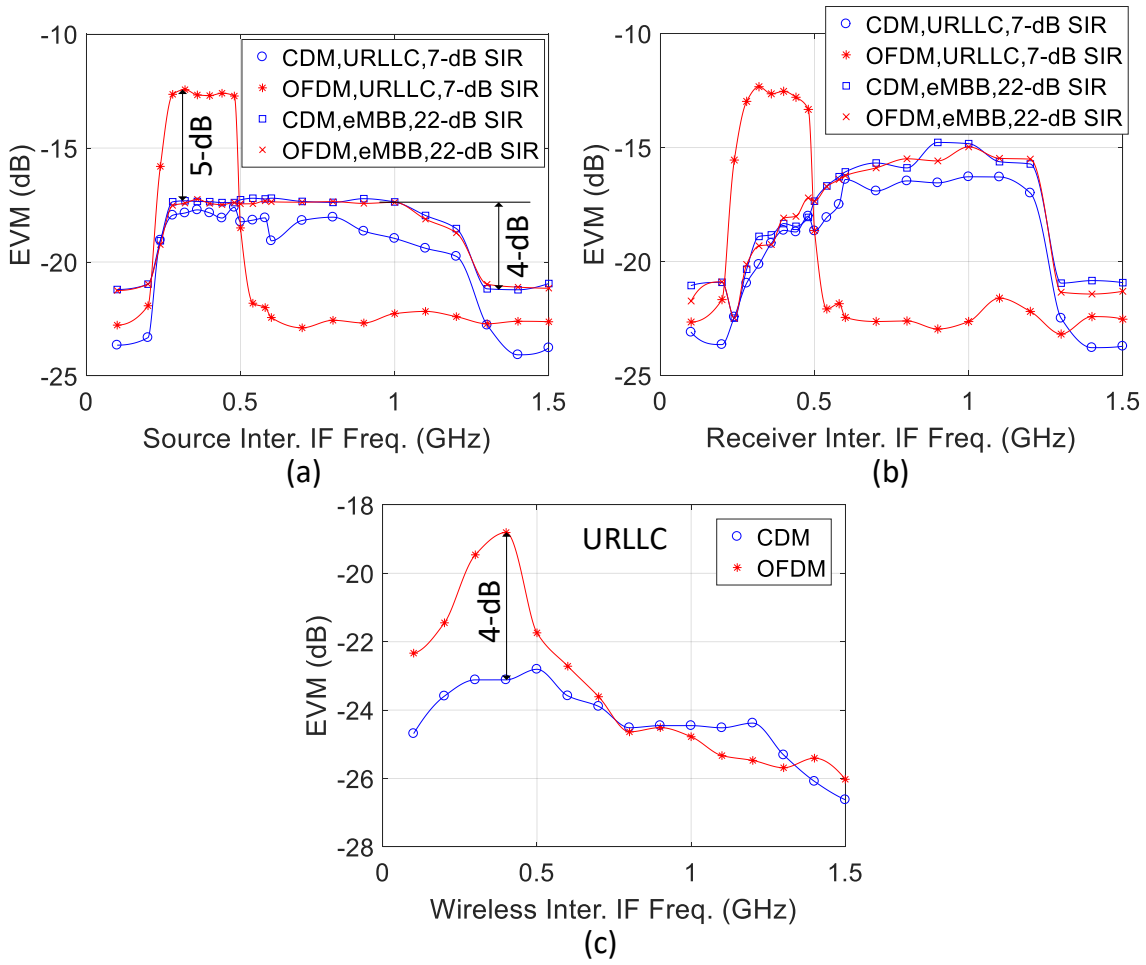


Figure 3.18: Experimental results. EVM performances with (a) transmitter interferences, (b) receiver interferences and (c) wireless interference.

ing are applied. In Fig. 3.18(a) with transmitter leakage, in eMBB, if the interference is overlapped with signal bandwidth with 22-dB SIR, 4-dB penalty is generated for both CDM/OFDM. On the other hand, under URLLC providing 25% of the data rate and 7-dB SIR, the CDM provides reliable EVM under -17.5-dB, but OFDM can have beyond -13-dB EVM if interfered. The receiver side interference shows similar degradations in Fig. 3.18(b). The received signal has lower power density at high IF due to limited bandwidth, so a higher degradation is generated by an high-IF interference. Finally, a wireless interference is introduced in the free-space with varying IFs. Results are shown in Fig. 3.18(c) with URLLC and we observe up to 4-dB EVM improvement for sparse CDM when the

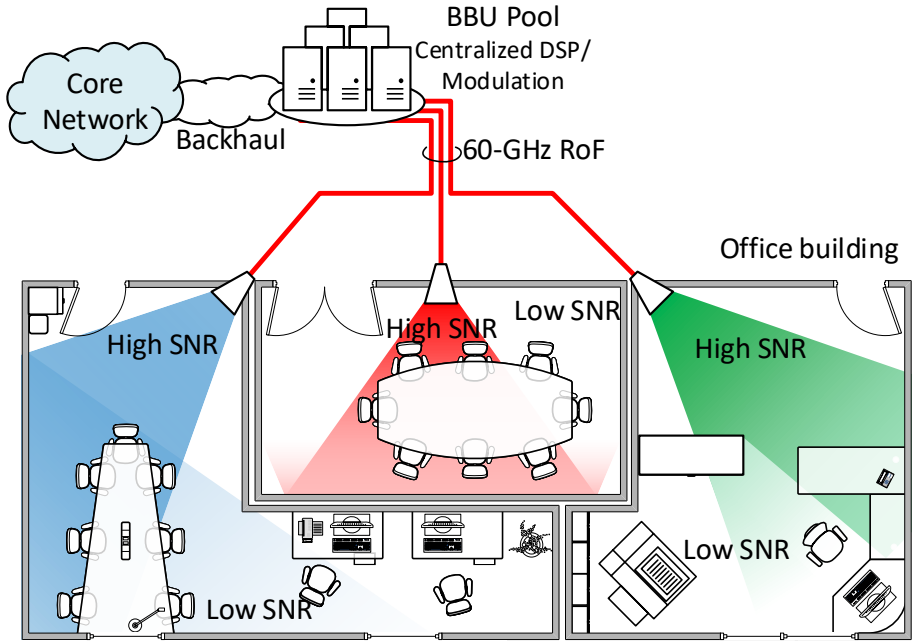


Figure 3.19: Typical MMW applications in one floor of an office building with various channel conditions.

interference is at 400-MHz IF and fully overlapped with both signals.

### 3.3 Power Division Non-Orthogonal Multiple Access

Due to the huge bandwidth and high operation frequency, the cost of each 60-GHz MMW RRH is more expensive than current APs working under LTE or 802.11 n/ac. As a result, it is hard to deploy 60-GHz MMW RRHs in high densities (e.g., multiple RRHs inside one room). On the other hand, the exponentially increased volume of mobile users will lead to high user densities, especially in urban areas with new applications including the mMTC and eMBB. Consequently, it is expected that each MMW RRH will simultaneously serve a large number of users.

Typically, users served by one RRH are located at different places, and have various channel conditions, as shown in Fig. 3.19. The 60-GHz transmission is more susceptible to obstacles and antenna misalignment. Furthermore, the penetration capability of 60-GHz is not as strong as that of existing Wi-Fi spectrum; any obstacles in the channel can cause

severe degradation in received power. Moreover, the antenna gain changes with the device orientation. Combining all those factors, the users served by one RRH are with varies reception qualities, which causes different SNRs, EVMs, BERs and therefore different QoS if using OFDMA.

3G mobile communication systems use non-orthogonal direct sequence-code division multiple access; whereas 4G-LTE uses OFDMA. To serve multiple users under different conditions, LTE systems use adaptive modulation control (AMC) to assign high order modulation formats to users with high SNR (e.g., 64-QAM, 256-QAM), and low order QAMs to low-SNR users [e.g., Binary phase-shift keying (BPSK), quadrature phase-shift keying (QPSK)]. Nevertheless, due to the low spectrum efficiency of low-SNR users, the significant part of low spectral efficiency resource blocks decreases the overall system efficiency.

### 3.3.1 Principle of Power-Division Non-Orthogonal Multiple Access

Non-orthogonal multiple access (NOMA), is a scheme for multiplexing and modulating multiple data streams into a single symbol stream of higher spectral efficiency, with varying reception qualities to different users. In this section, we focus on downlink NOMA.

Existing research of MMW systems aims to improve the performance of each user individually, which limits the MMW cell coverage and power budget significantly due to the increased SNR requirement of modulation formats with higher spectral efficiency. In real situations, not all users are at cell edges or under severely impaired channels. As a result, some users with high SNR may have margins of power budgets. Instead of using only time/frequency OFDMA to multiplex multiple data streams, NOMA utilizes an additional non-orthogonal power domain for multi-user access to achieve better performance and fairness. As a result, compared with one orthogonal resource block serving one user in OFDMA, in NOMA, one resource block can serve multiple users [127]. The goal is to optimize the performance of all users as a whole group, rather than to improve the performance of each user. The user group is defined as all users that share one orthogonal resource block

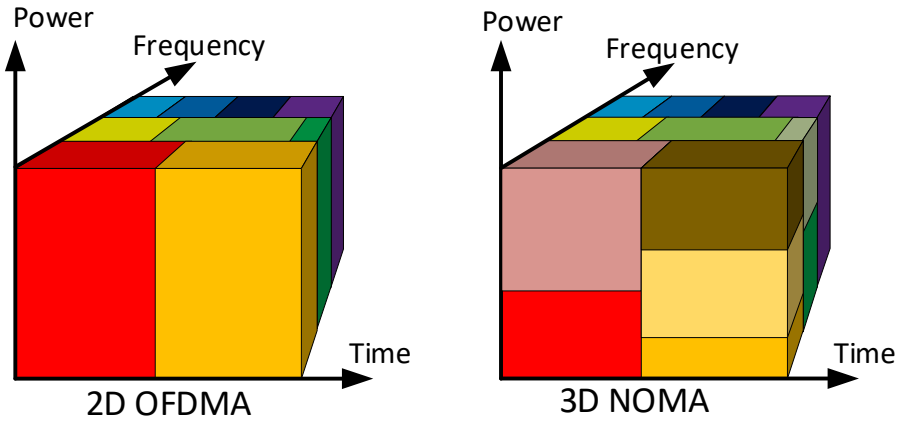


Figure 3.20: Non-orthogonal multiple access and OFDMA resource blocks.

(time and frequency slot).

$$S = \sum_{k} T_k \sqrt{P_k} \tag{3.9}$$

In Fig. 3.20, the left-hand side figure shows the current OFDMA scheme, with data multiplexed in two dimensions: frequency and time. By orthogonal subcarriers the in the frequency domain and cyclic prefix (CP) in the time domain, there is no interference introduced between data to different users. We add a third dimension in the power domain for multiplexing, as shown by the right-hand side of Fig. 3.20. The symbols are formed following 3.9. $T_k$ is the transmitted symbol to $k$-th user, and $P_k$ is the corresponding transmission power to $k$-th user; $N$ is the number of users. All symbols are combined according to a predetermined power ratio.

$$SINR_k = \frac{P_k |h_k|^2}{P_{\text{int}} + N_k} = \frac{P_k |h_k|^2}{\sum\limits_{i>k} P_i |h_k|^2 + N_k} \tag{3.10}$$

By power domain multiplexing, more users can be served within a certain frequency and time range. More importantly, since the noise is added in the power domain, by adjusting the power allocation among different users, we can equalize the equivalent SINR of each user without changing any physical layer parameters, such as transmission power

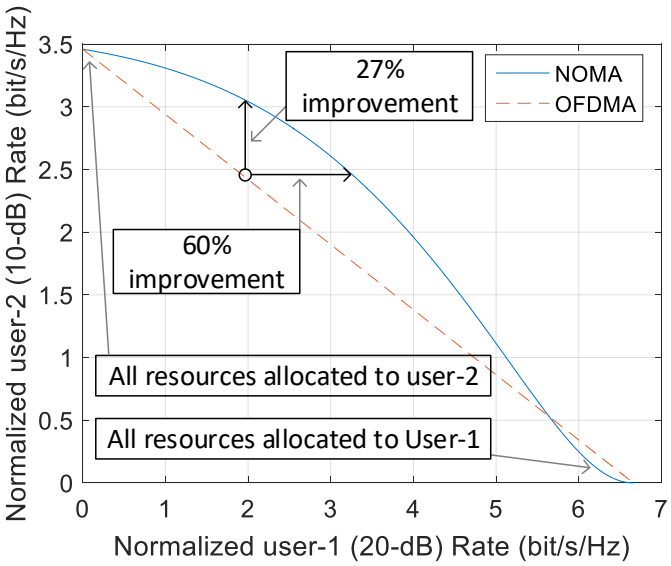


Figure 3.21: Capacity comparison of NOMA and OFDMA.

and channel conditions, as (3.10). Supporting more users is also a key-enabling feature for future-proof soft-defined radio in mMTC.

The equivalent SINR for each receiver is shown in (3.10). $P_k$ is the power allocated to the $k$-th user, with $N_k$ the receiver noise. In NOMA, one receiver can remove the interference with greater allocated power than itself, so $P_{int}$ is the interference power from other users that we cannot remove. Moreover, we assume there is no error for prior symbol decisions during successive interference cancellation (SIC). Then we can get the capacity to each user as (3.11).

$$R_k = B \times Log_2(1 + \frac{P_k|h_k|^2}{\sum\limits_{i>k} P_i|h_k|^2 + N_k}) \tag{3.11}$$

A theoretical capacity calculation result is shown in Fig. 3.21. We compare the capacity of NOMA and OMA systems. A two-user environment is calculated by 3.11, with SNR of 10-dB and 20-dB. We sweep the resources (frequency or time in OMA, and power in NOMA scheme) allocated to each user. From Fig. 3.21, rates are the same when all resources are allocated to either user. However, when serving both users with fairness

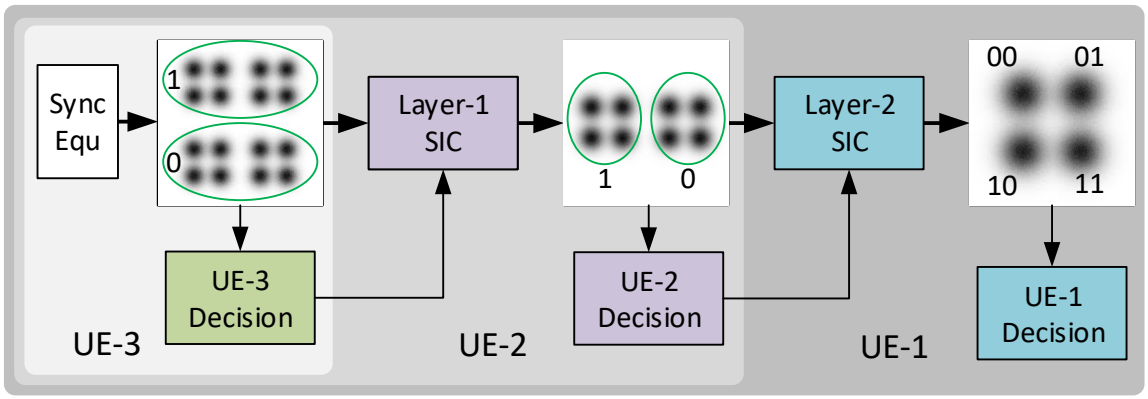


Figure 3.22: Example of 3-layer successive interference removal operation in PD-NOMA.

control, NOMA shows a higher capacity. Results show 27% and 60% capacity gain for users of 20/10-dB SNR at rates of 2/2.4-bit/s/Hz, without losing the capacity to the other user.

In NOMA scheme, resource blocks multiplexed in power domain are non-orthogonal; the interference from other users needs to be removed. Successive interference cancellation technology is introduced in the DSP-based receiver for interference removal. Inside receivers, the SIC receiver needs to decode all data streams whose fractional power ratio is higher than the receivers power, then subtracts the interference from original symbols. The SIC is working on a level by level manner, so the receiver should remove the interference from the data stream with the largest power, then remove the interference from the second largest, and so on. After complete SIC, the receiver can decode the bits transmitting to the actual receiver as QAM symbols.

An example is shown in Fig. 3.22. In each symbol, two bits information is assigned to user-1, one bit is assigned to user-2, and another bit is assigned to user-3, accumulating 4 bits per symbol that has 16 constellation points. Firstly, the received waveform needs to be converted to constellations by synchronization, equalization and other operations including FFT in OFDM. Then, the user-3 does the slicing treating the constellation as BPSK. After that, the interference from user-3 is canceled by SIC using user-3 results. Then user-2 applies BPSK demodulation. After that, the last user applies another SIC and finally decodes

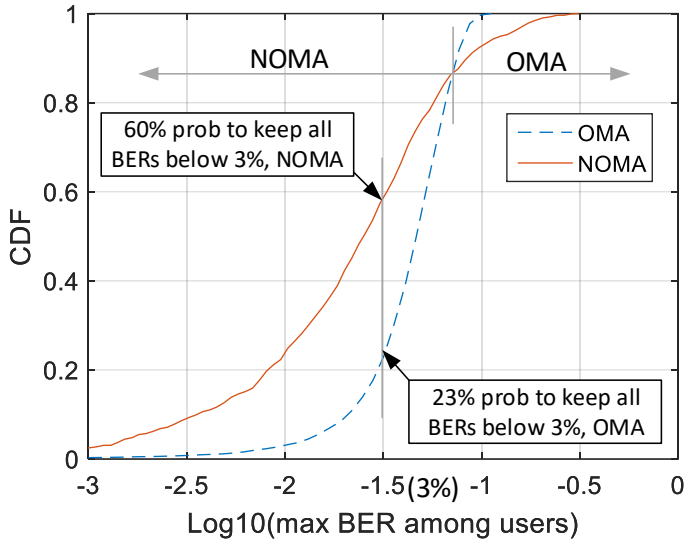


Figure 3.23: CDF of worst-user BER using NOMA and OFDMA.

the residual QPSK signal. With more layers of SIC applied, the signal quality is degraded more since we reduce the power by removing the interference. Different DSP processes are implemented in different receivers, which adds the DSP complexity, but can be overcome by advanced DSP design and manufacturing.

To better show the benefits from NOMA and SIC, a simulation of BERs among a set of randomly placed users are executed. For simplicity and fairness in showing the performance gain of BER by the worst user, we assign the same data rate to all users. Nonetheless, different user data rate can also be supported by NOMA, which is demonstrated in the experiments. Four users are randomly moving inside a 5m5m room all requesting 1-bit/s/Hz normalized rate, with the transmitter placed in one corner of the room. The channels are modeled as LoS channels with $n = 2$ and $\sigma = 0.5$ using isotropic antennas, as measured from . We assume a 25-dB SNR received at $d_0 = 1m$. We analysis the maximal received BER of users, which is the BER measured under the worst channel. From the CDF curve in Fig. 3.23, the probability of achieving lower BER is significantly improved with NOMA. For example, under the simulation setting, we have 60% probability to maintain all user BERs under 3% BER, while the probability is reduced to 23% with OMA. However, we

observe that OMA has better performance than NOMA in the high BER region, which is due to the gray mapping from more constellation points to each user. The software-defined radio (SDR) allows us to switch back to OMA mode under those cases.

NOMA is applied to the constellation symbols in synchronized downlink, which means it can be applied to any QAM-based modulations, includes single-carrier modulation, OFDM, SC-FDMA and other advanced modulation formats including GFDM, FBMC, and UFMC. Furthermore, in multi-carrier modulations, the PAPR is sensitive to the number of subcarriers but not the symbols carried by each subcarrier, such that the NOMA signal has no additional requirement on the system linearity and the effective number-of-bits (ENOB).

However, severe performance and security issues are raised if we multiplex data only in power domain. The number of users supported is limited by the constellation points per symbol. For example, only eight users can be supported with 256 constellation points. On the other hand, the sensitive information leakage issue is severe since the users with more layers of SIC needs to decode the data for other users. This security issue can be partially resolved by software encryption. However, we propose to use both non-orthogonal and orthogonal resources for multiple access in the physical layer to solve the issue. In that case, the user data can be distinguished by time, frequency and power such that massive users can be supported by one NOMA stream simultaneously. Moreover, the users with high-security requirements are served through exclusive orthogonal resource blocks, which are not multiplexed on top of other users. Meanwhile, non-sensitive user data are multiplexed in power domain for higher spectral efficiency and performance.

### 3.3.2 Fractional Transmission Power Allocation

We exploit an additional power domain for multiplexing. The power ratio is defined as $[p_1, p_2, ..., p_n]^T$, and can be adjusted continuously, such that the performance with different users is optimized. The user data rate is sensitive to frequency and time allocation; the performance (BER) is sensitive to power ratios. Without loss of generality, we consider

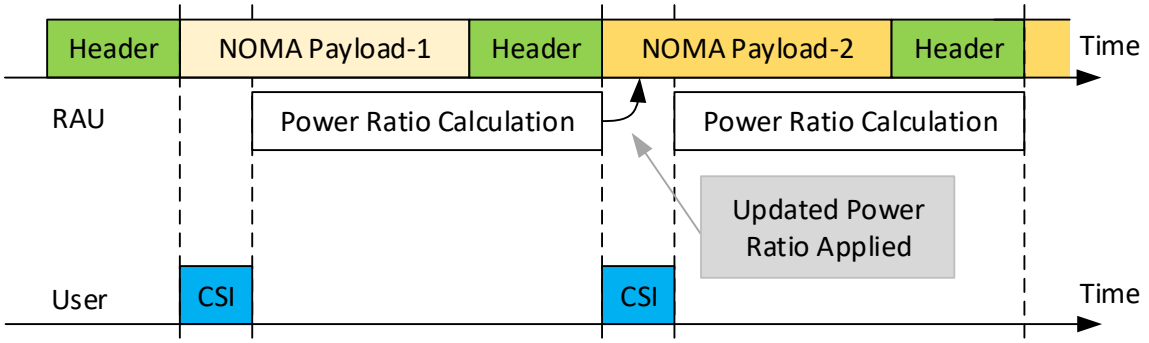


Figure 3.24: Channel state information feedback and calculation timeline.

the power ratio allocation inside one frequency/time resource block. Here we discuss the algorithm determining downlink NOMA power ratios.

We design a closed loop system with channel state information (CSI) feedback from all users through the uplink. We can use either NOMA or OMA in the uplink.

An example scheme is shown in Fig. 3.24. At the beginning of each frame, a header using OFDM and standard QAM mapping is broadcasted in the downlink. The header also helps for frame synchronization and channel estimation. By measuring the quality of received header, the receiver should have an estimation of reception quality. Right after the quick estimation, a CSI packet is sent back to the transmitter. After collecting all CSIs from all users, the transmitter starts calculating the power ratio. The received BER is a function of SNR, requested data rate and fractional power ratios for all users, as (3.12) suggests.

$$BER = f(SNR, Mod, PR) \tag{3.12}$$

We assume that only the white Gaussian noise is observed. $BER$, $SNR$, $Mod$, and $PR$ are all multi-dimensional vectors. $Mod$ indicates the modulation level or spectral efficiency to each user. The lengths of vectors are the number of users. The objective is to get the power ratio such that the BER vector can fulfill some fairness criteria. One we want to achieve is the fairness of BER, that the best fairness is achieved when all users have the identical BER.

Calculation of the power ratio of a dynamic wireless system needs to be fast since we want the system to be responsive to any channel fluctuations (e.g., moving devices or moving obstacles). The best case is that we calculate the power ratio within one frame, so the updated power ratio can be applied to the next NOMA payload, as Fig. 3.24 shows. The delay allowed for calculation is less than a frame length, which is stringent.

$$\Delta PR_n = -\nabla_{PR}\mathrm{var}[f(PR_n)] \tag{3.13}$$

$$\beta_n^{FR} = \frac{\|\Delta PR_n\|^2}{\|\Delta PR_{n-1}\|^2} \tag{3.14}$$

$$S_n = \Delta PR_n + \beta_n^{FR} S_{n-1} \tag{3.15}$$

$$PR_{n+1} = PR_n + \alpha S_n \tag{3.16}$$

The look-up table (LUT) or brute-force search is a good solution when the user number is small and the search space is limited. Massive pre-calculated data are stored in the BBU pool, and shared by several NOMA DSPs. However, when the number of users increases, it is hard to store the whole LUT since the data volume increases exponentially with the user number. Instead, we use a conjugate gradient method in the optimization problem with Fletcher-Reeves updating [128]. By setting the objective function to the variance of BER vector, we execute the iteration-based algorithm following (3.13)-(3.16), with search direction updated as $s_n$. $\alpha$ is the line search result from either exact line search or inexact line search. We start the algorithm with (3.17), and terminate the iteration when objective function value is smaller than a pre-determined threshold.

$$S_0 = \Delta PR_0 = -\nabla_{PR}\mathrm{var}[f(PR_0)] \tag{3.17}$$

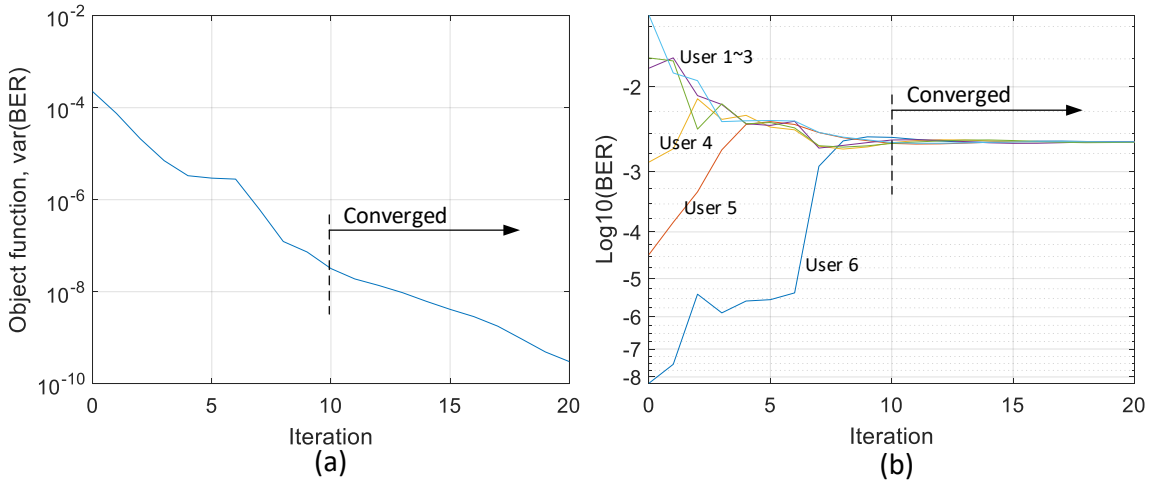


Figure 3.25: (a) Object function value and (b) BERs for different users during iterations.

An iteration example is shown in Fig. 3.25(a, b). The scenario is that six users share 64 constellation points, carrying 1-bit to each user per symbol. Since the user number is large for each orthogonal resource block, we are simulating an extreme case with the largest optimization dimension, which tends to take the longest time to converge. The SNRs for users are 15/18/21/24/27/30-dB. At iteration 0, users have very different BERs. As the iteration goes on, the BERs are converged since the variance of BERs is reduced. By using the updated power ratio, we make use of the margin by the best users (user-5/6) to compensate the other users (user-1/2/3). We improve the BER performance of user-1 from 3.8e-2 to 2.5e-3. By reducing the power to user-6, the best BER is increased from 5.7e-9 to 2.5e-3, which is tolerable since the FEC is necessary for wireless channel coding to correct the burst errors. On the other hand, improving the BER of the lowest-SNR user is significant since it enables us to use FEC with lower overhead, and increases the net data rate. In Fig. 3.25, the system achieves fast convergence after only ten iterations.

### 3.3.3 Uplink Asynchronous Transmission

In the downlink, since the signal is generated in centralized BBU, the signal to all users are natively synchronized with joint processing. However, when considering the uplink transmission, the additional time synchronization requirement adds latency and DSP complexity

in the user devices, if the synchronized transmission is still necessary.

On the other hand, asynchronous uplink transmission can significantly reduce the latency [129]. So, we extend the research to enabling asynchronous transmission in the uplink with PD-NOMA [130].

$$SINR_k = \frac{P_k|h_k|^2}{P_{\text{int},k} + N_k} = \begin{cases} \dfrac{P_{k,DL}|h_k|^2}{\sum\limits_{i>k} P_{i,DL}|h_k|^2 + n_{UE,k}}, & Downlink \\ & \sum\limits_k P_{k,DL} \le P_{\max,RRH} \\ \dfrac{P_{k,UL}|h_k|^2}{\sum\limits_{i>k} P_{i,UL}|h_i|^2 + n_{OLT}}, & Uplink \\ & P_{k,UL} \le P_{\max,UE} \end{cases} \tag{3.18}$$

If we sort the user index by descending power ratio, the equivalent SINR for uplink and downlink are in 3.18, extended from 3.10, with $P_k$, $h_k$ and $n_k$ for the transmission power, path response and noises corresponding to the user with index $k$. We do not consider SIC error. For the downlink, all UE share the power from one antenna, so the sum of the power allocated should be within the transmitting power, and the power ratio is determined by the digital power ratio embedded in the transmission waveform only. To balance the performance of different users with different path losses, usually, we assign a greater power to the user with a higher path loss and lower ROP. In the uplink, the power allocation is limited by the output power in each user individually. The power ratio is determined by both the transmission power and the path loss. With a higher loss, typically we assign smaller power ratio, to make full use of the path loss difference and maximize the received power in the RRH antenna.

Two types of PD-NOMA are introduced. For downlink synchronized PD-NOMA, information for different users is multiplexed in the constellation level, as the previous section illustrated in detail, and the OFDM symbols are all synchronized, as shown in Fig. 3.26(a). It means the SIC is applied after OFDM demodulation. For asynchronous PD-NOMA used in uplink, the SIC is applied directly to the waveform, since the OFDM symbols for differ-

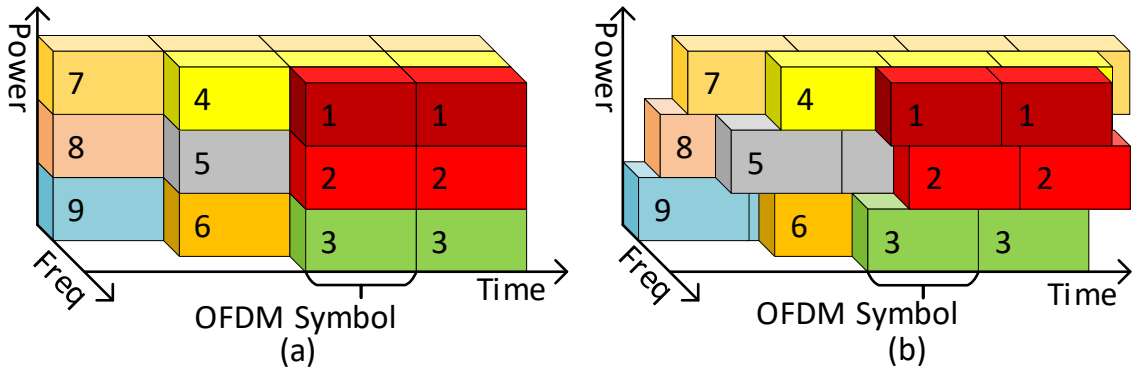


Figure 3.26: (a) Synchronized PD-NOMA in downlink and (b) asynchronous PD-NOMA in uplink, with numbers corresponding to different user resources.

ent users are not synchronized [shown in Fig. 3.26(b)] and a single FFT window can never recover all user data.

An example of synchronized/asynchronous PD-NOMA decoding with SIC decoder is shown in Fig. 3.27. Without loss of generality, we assume an application of three users with each user requiring 2-bits per symbol. We refer the user-1, user-2, and user-3 to the user with highest, intermediate and lowest power ratio. The transmitted power ratio associated with each user is [0/-7/-14]-dB. It is chosen because based on QPSK modulation each user, it needs at least 6-dB granularity for correct SIC between layers. The extra 1-dB is reserved for the performance gradient between users fitting into different sensitivity requirements.

For asynchronous PD-NOMA in the uplink, all decoding is in the centralized BBU. Single OFDM is not applicable because the beginning of OFDM symbols from different users are not aligned that severe interference is generated not only between users but also between symbols and subcarriers. Inter-symbol and inter-subcarrier interference cannot be handled by constellation-level SIC. So, the received constellation on high-level decoding is blurred and cannot be used in decoding the lower level information. Instead, SIC is working on the waveform level. Firstly, user-1 does OFDM demodulation, and retrieve the information from this user. After that, it reconstructs the waveform transmitted from user-1, by using the decoding result, channel estimation, and time synchronization information. After SIC by subtracting the user-1 waveform from the received waveform, BBU can do

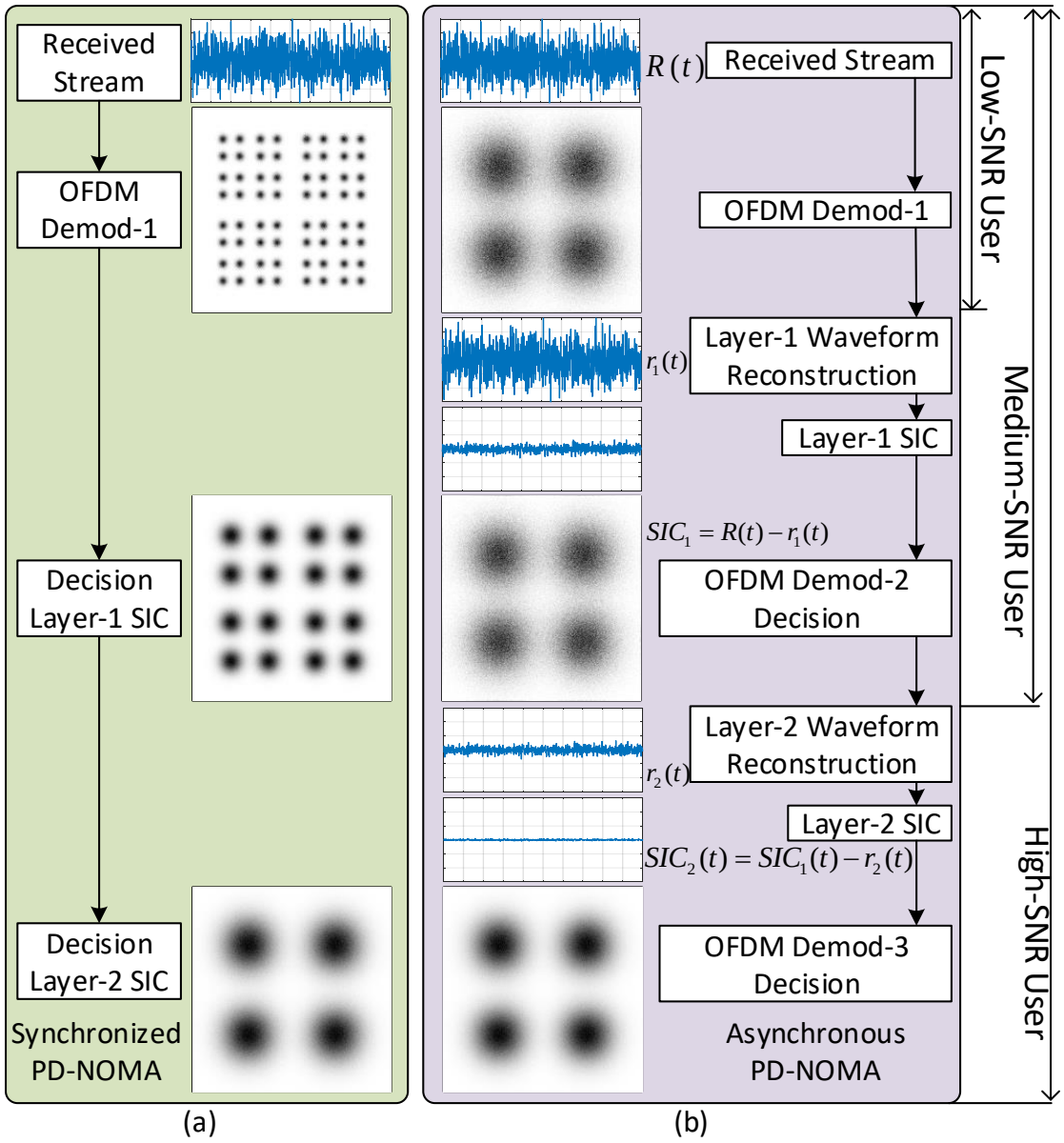


Figure 3.27: Flow chart of (a) synchronized PD-NOMA with constellation level SIC and (b) asynchronous PD-NOMA with waveform level SIC

time synchronization again and demodulate the OFDM signal for user-2. Then, the user-2 information is retrieved and removed. Finally, BBU demodulates the OFDM signal after removing the interference from user-1 and user-2, and retrieves the information from user-

3. Since all DSP is centralized in BBU, the additional DSP complexity is tolerable.

$$Power\ Ratio = \begin{cases} \begin{bmatrix} P_{1,DL}|h_m|^2 \\ ... \\ P_{N,DL}|h_m|^2 \end{bmatrix} = \begin{bmatrix} P_{1,DL} \\ ... \\ P_{N,DL} \end{bmatrix}, & Downlink \\ & at\ m^{th}\ user \\ \begin{bmatrix} P_{1,UL}|h_1|^2 \\ ... \\ P_{N,UL}|h_N|^2 \end{bmatrix}, & Uplink \\ & at\ RRH \end{cases} \tag{3.19}$$

Typically, the user with fewer levels of SIC (higher power ratio) has better performance. The performance difference can be adjusted by changing the power ratio, which is measured at the receiver. For the downlink, the power ratio is determined by the power ratio defined in the waveform; for the uplink, the power ratio is determined by both the PA output powers and their path losses, shown in equation 3.19. If we increase the power allocated for one specific user, the performance with this user will be improved, but the performance for other users will be degraded. By adequately mapping the user to different SIC levels and controlling the power ratio, we can have an optimized and improved performance for all users with minimized FEC overhead.

### 3.3.4 Simulations

In simulations, we introduce OFDMA as a comparison. To achieve the same spectral efficiency, no guard band is reserved in OFDMA, so the interference between subcarriers may be observed if the OFDM symbols from users are not synchronized. To cancel the interference from other users due to non-orthogonality, OFDMA-SIC is also compared in the simulation. The principle of OFDM-SIC is like NOMA-SIC that we can decode the information from the high-power user, and recover the waveform from the specific user incorporating the channel estimation information. Then, the waveform is subtracted from

the original received one to remove its interference to other adjacent frequency users. After that, lower-power users can demodulate the residual signal with reduced interferences.

We control the power ratio on the receiver side. So, the same simulation model can be used for both uplink and downlink. We show the BER under synchronized scenario to simulate the downlink [using the SIC decoding scheme in Fig. 3.27(a)], and the BER under full unsynchronized scenario (OFDM symbols from different users arrives the RRH with half of the OFDM symbol duration interval) simulating the worst case of asynchronous transmission in the uplink [using the SIC decoding scheme in Fig. 3.27(b)]. The real uplink performance should be between the synchronized scenario and fully unsynchronized scenario.

Each label in Fig. 3.28 and Fig. 3.29 marks two curves, corresponding to the synchronized and fully asynchronous BER performance. Under some circumstances, both curves are overlapped.

To simply and clearly show the results, we simulate the system with two users. Each user requires 2-bits per symbol, accumulating 16 constellation points each symbol. The system uses OFDM consisting of 32 subcarriers, and 12.5% CP is used. For OFDMA scheme, each user is assigned 16 subcarriers. We assume it is a ROP sensitive system that the electrical noise in the receiver is dominating the system noise. Fig. 3.28(a), 3.29(a), and 3.30(a) show the performance of the high-power-ratio user, corresponding to the higher path loss user in downlink, or lower path loss user in the uplink. Fig. 3.28(b), 3.29(b), and 3.30(b) show the performance with the other low-power-ratio user.

We firstly simulate SNR performances, in Fig. 3.28. The power ratio difference is set to be 12-dB. We sweep the received SNR to show the performance. The required SNR for the high-power-ratio user with 3.8e-3 (corresponding to 7% overhead hard-decision FEC requirement) is 7.3-dB to 8.1-dB for PD-NOMA. Comparing with 8.5-dB to 8.8-dB requirement with OFDMA, 0.7-1.2-dB SNR improvement is observed. For the low-power-ratio, we can reduce the SNR requirement from 20.7-dB to 17.7-dB, comparing

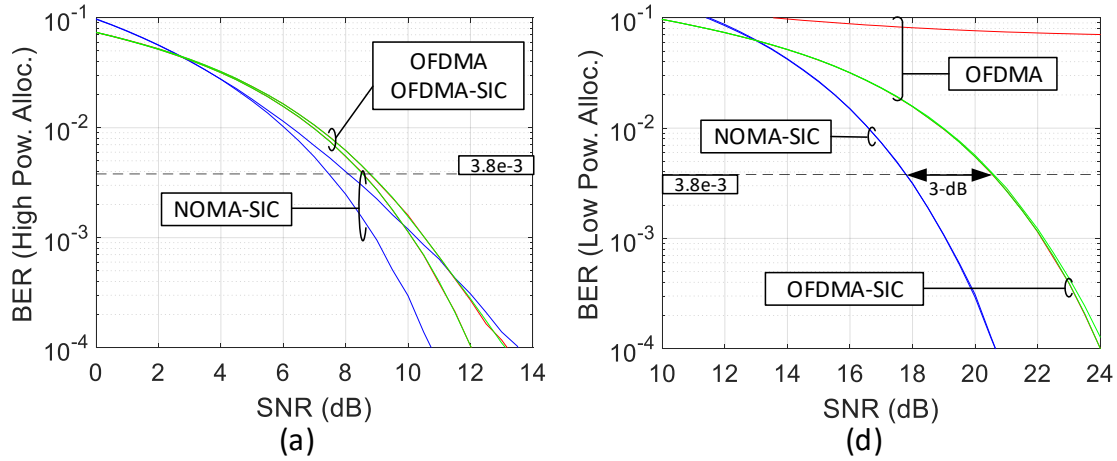


Figure 3.28: Simulation results. SNR results with (a) high-power-ratio user and (b) low-power-ratio user.

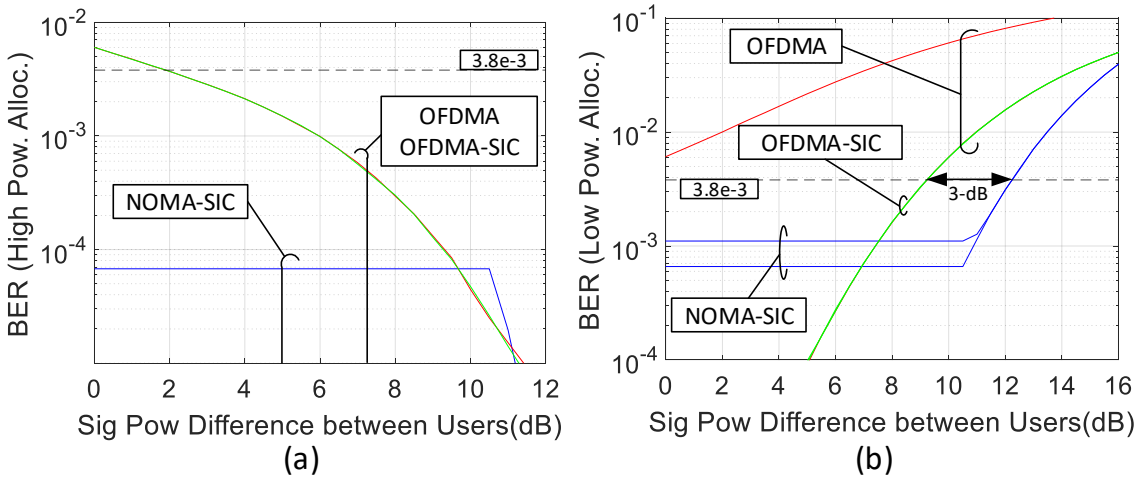


Figure 3.29: Simulation results. Extra path loss results with (a) high-power-ratio user and (b) low-power-ratio user.

with OFDM-SIC. If no SIC is used in OFDMA, a very high BER floor (>6%) is observed when fully unsynchronized, which is generated by the leakage from the high-power users, making the scheme unusable.

Fig. 3.29 shows results with varying power differences. In PD-NOMA, the BER is minimized at a specific power difference. The power difference is defined as the power difference between the high-power-ratio user and the low-power-ratio user. If the low-power-ratio user's power is greater than the optimal (the power difference is smaller than

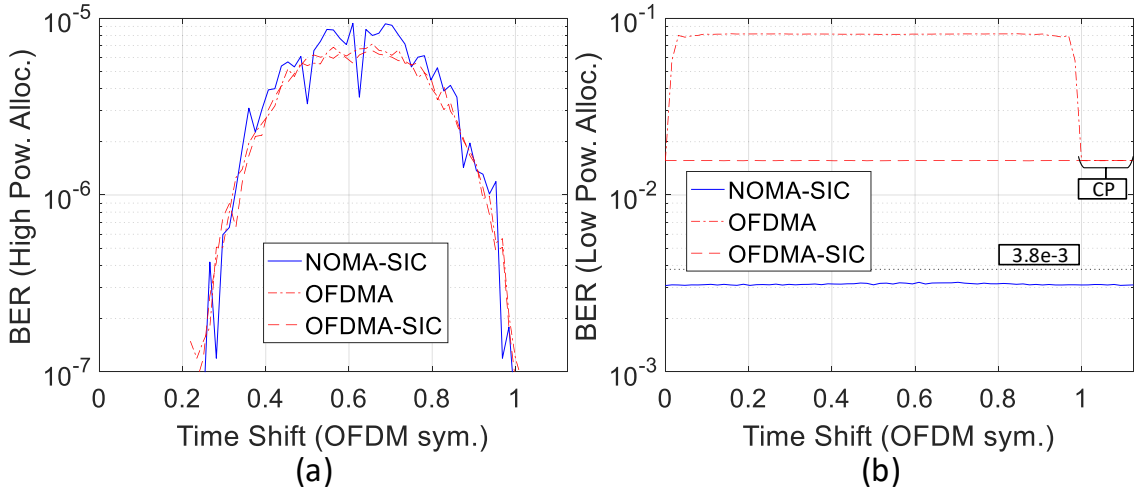


Figure 3.30: Simulation results. Synchronization results with (a) high-power-ratio user and (b) low-power-ratio user.

the optimal equivalently), the high-power-ratio user performance will be degraded, thus the SIC performance will be impaired for the low-power-ratio user. If it happens, we reduce the output power of low-power-ratio user intentionally to achieve the best performance. In simulations, we fix the SNR of the high-power-ratio user at 18-dB and vary the power to/from the other user. The optimal power difference is 10.5-dB, so the BER keeps constant in PD-NOMA if the power difference is below 10.5-dB. For the high-power-ratio user in Fig. 3.29(a), below 1e-5 BER is observed if both users are synchronized. If they are fully unsynchronized, PD-NOMA can always keep the BER below 3.8e-3, but the OFDMA with/without SIC can never achieve this performance when the power difference is within 2-dB. Because users with similar powers using OFDMA have severe interference to others due to the leakage if not synchronized. For the low-power-ratio user, NOMA can improve the power difference tolerance from 9.2-dB to 12.2-dB. A 3-dB improvement is observed.

Depending on how well users are synchronized, different BERs can be observed for both users. When both users are synchronized, best performance can be observed; when their offset is half of the OFDM symbol duration, the worst performance is generated, due to expanded constellations and noisy training symbols. The synchronization performance

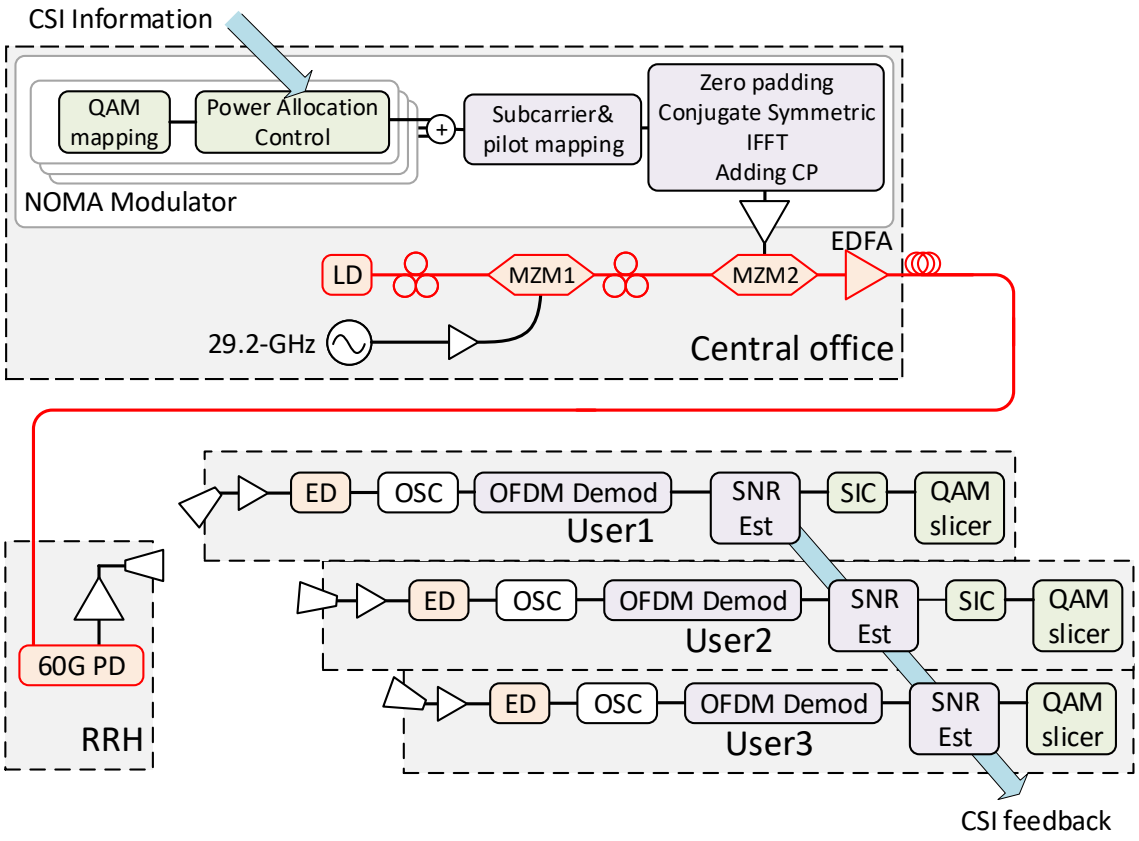


Figure 3.31: Experimental setup of MMW fiber-wireless integration using PD-NOMA.

is shown in Fig. 3.30. The SNR is 18-dB, with 12-dB power ratio difference. The time shift is swept between 0 to 1.125 (including CP). For the downlink, the time shift is always 0; for uplink, any offsets can be generated with the same probability. From results, the high-power-ratio user can always achieve very low BER below 1e-5. Still, slight performance degradation is observed with offsets in all schemes. However, for the low-power-ratio user, PD-NOMA can keep the BER below 3.8e-3, while OFDMA-SIC/OFDMA BER can be beyond 1%/7% if the time shift is greater than CP.

### 3.3.5 Experimental Setup and Results

*Experimental Setup*

In this subsection, we demonstrate an end-to-end system for 60-GHz OFDM-NOMA transmission through the fiber-wireless integrated system. We set up a testbed consists of a BBU,

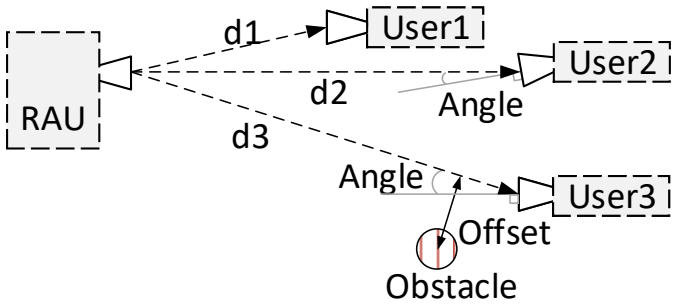


Figure 3.32: User location settings in experiments.

an RRH, and three wireless end users, shown in Fig. 3.31. Due to the limitation of lab devices, we only experimentally verify the feasibility of downlink synchronized PD-NOMA.

In the experiments, we use IF-OFDM modulation to carry NOMA symbols. The data are carried by 512 subcarriers, aggregating 1-GHz bandwidth, with 1.953-MHz subcarrier spacing. Zero-padding generates 250-MHz DC guard bands around 60-GHz central frequency. The IFFT/FFT size is 2048 after conjugate symmetric expansion. After that, a 128-point cyclic prefix is added. All the DSP processing are centralized in the BBU, simulated by offline processing. The samples are converted to analog waves by an AWG running at 10 GS/s.

The optical signal comes from a DFB laser centralized at 1553.97-nm. A double-sideband DSB-OCS method is applied by an MZM (MZM1 on Fig. 3.31) and 29.2-GHz sinusoidal electrical signal source. Then the NOMA-IF-OFDM signal is modulated by another MZM (MZM2 on Fig. 3.31). Amplified by an EDFA, the optical signal is fed into an SSMF-28 of 25-km length. In the RRH, the optical signal is received by a PD of 60-GHz bandwidth. Amplified by a 60-GHz PA, the signal is transmitted through the RRH antenna. Those antennas are of 25-dBi gain.

Three physically identical users are tested in the experiments. Inside each user, after the receiving antenna, an envelope detector is used for down-conversion from radio frequency (RF) to IF. A real-time oscilloscope samples the waveform at 10 GS/s. After that, a modified OFDM receiver with frequency/time synchronization, channel estimation, and

equalization is implemented, but we replace the traditional QAM slicer to NOMA SIC receiver. Before SIC, we estimate the EVM of the received signal and send it back to the BBU for calculating the power ratio of the next frame, using conjugate gradient nonlinear optimization method described in the previous section. Positions of users are shown in Fig. 3.32. We test a typical scenario that user-1 is under the best channel condition and requires the highest data rate of 2-Gbps. User-2 and user-3 request 1-Gbps each. All three data streams are independent, and generates 4-Gbps rate in total. We test the performance on power domain multiplexing, so each NOMA symbol carriers 4 bits: two bits to user-1, one bit to user-2 and one bit to user-3.

As a comparison, 16-QAM OFDM of the same OFDM parameters is tested, providing the same system data rate. To serve three independent users, OFDMA is used for 16-QAM constellation so that data to different users can be distinguished in time or frequency domain.

*Sensitivity Results*

We first test the BER performance under different received optical powers. Without changing the gain of the power amplifier (PA) and low-noise amplifier (LNA), we sweep the optical power into the PD. During this test, we cut the CSI feedback, and relative power ratios at the transmitter are fixed at a typical value of [0, 4.95, 4.95]-dB corresponding to user-1, user-2, and user-3. The results are shown in Fig. 3.33 with 4-feet wireless channels. Fig. 3.33(a) shows the performance with the optical back-to-back and Fig. 3.33(b) shows the performance with 25-km fibers.

OFDMA carrying four bits per symbol are tested as the baseline performance. Comparing the performance between NOMA and OMA (OFDMA), we observe that the UE-1 performance is degraded because of the biased power allocation and higher data rate since the power allocated to user-2 and user-3 are significantly higher than user-1. Under the test case, we assign the same power to user-2 and user-3, so the performances for user-2/3 are

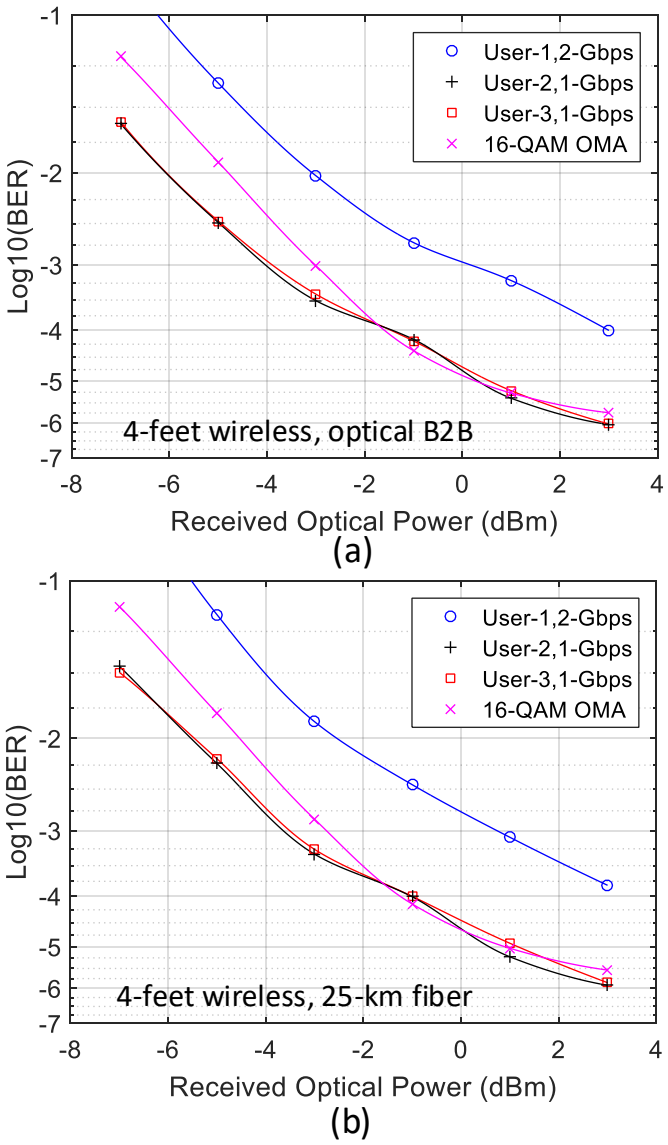


Figure 3.33: Experimental results with different received optical power (a) back-to-back and (b) with 25-km fiber.

similar, which outperform OFDMA. At -1 dBm received optical power, we achieved 1.9e-3, 4.5e-5 and 6.3e-5 BER for user-1, user-2 and user-3. A 25-km fiber is added between the BBU and the RRH to extend the service range by this 60-GHz RoF system. Negligible penalties are observed by adding the 25-km fiber in the system.

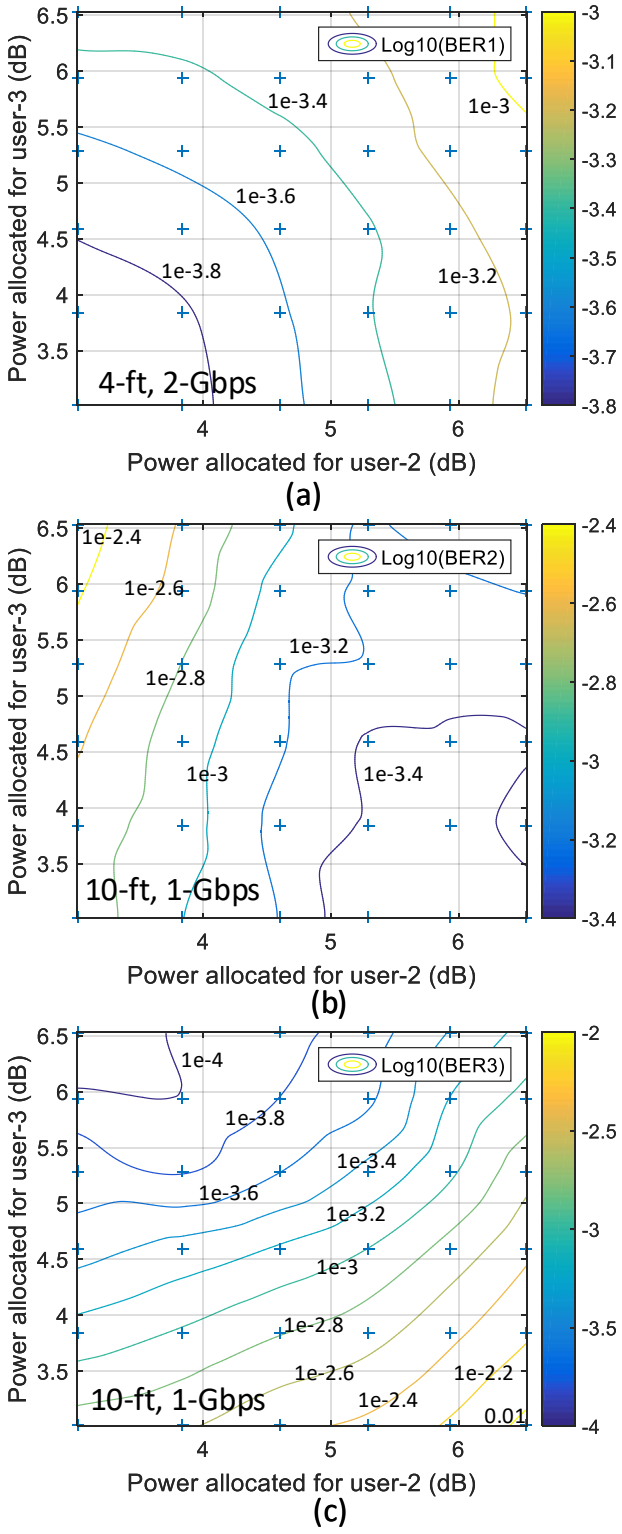


Figure 3.34: BER contour of (a) user-1 at 4-feet with 2-Gbps (b) user-2 at 10-feet and (c) user-3 at 10-feet distance.

*Power Ratio Sensitivity Result*

Unlike OFDMA that we can only change the modulations to adjust the received BER for a fixed transmission power, NOMA provides more dimensions of freedom since the power ratios can be continuously tuned to adjust the BER to each user. The dimension of power ratio is N-1, with N equal to the user number in the user group. A 2- dimensional space is generated in the 3-user system. Still, with the feedback loop opened, we sweep the power ratios to user-2 and user-3. We show the results as BER contours, in Fig. 3.34. All powers are normalized by the power of user-1. The plus marks indicate the experimental result points, and we use cubic interpolation to generate BER values covering the whole configuration space. We test the user-1 with a 4-feet wireless link, and user-2, user-3 with 10-feet links. The received optical power is 1-dBm.

Since the power ratio is normalized by user-1 power, the higher the power allocated to user-2 and user-3, the lower power is allocated to user-1. From Fig. 3.34(a), with higher power allocated to either user-2 or user-3, the BER for user-1 is increased. When the power of user-2 and user-3 is between 3-dB and 6.5-dB, the BER for user-1 is between 1e-3 and 1.5e-4. For user-2, the BER decreased with increased power allocated to it. It complies with the vertical lines on Fig. 3.34(b). By increasing the power ratio to user-2 from 3-dB to 6.5-dB, we improve the BER performance of user-2 from 4e-3 to 3.9e-4. Similarly, the performance of user-3 increases with more power allocated to it. Hence, the result by user-3 can be tuned between 1e-2 and 1e-4.

Under this setup, NOMA provides us an additional two-dimensional parameter tuning space that can adjust the performance of the downlink system. For example, for a [0, 3, 3]-dB power ratio, the BERs are 1.6e-4/1.78e-3/1.8e-3, which is biased since the SNR for user-1 is significantly higher than the others. If we set the power ratios to [1, 5.3, 5.3]-dB, a rough BER balance is drawn that the user BERs are 5e-4/6.4e-4/4e-4. As a result, we improve the user-2 BER from 1.78e-3 to 4e-4, user-3 BER from 1.8e-3 to 4e-4 by allocating more power to user-2 and user-3. However, the user-1 BER is slightly increased

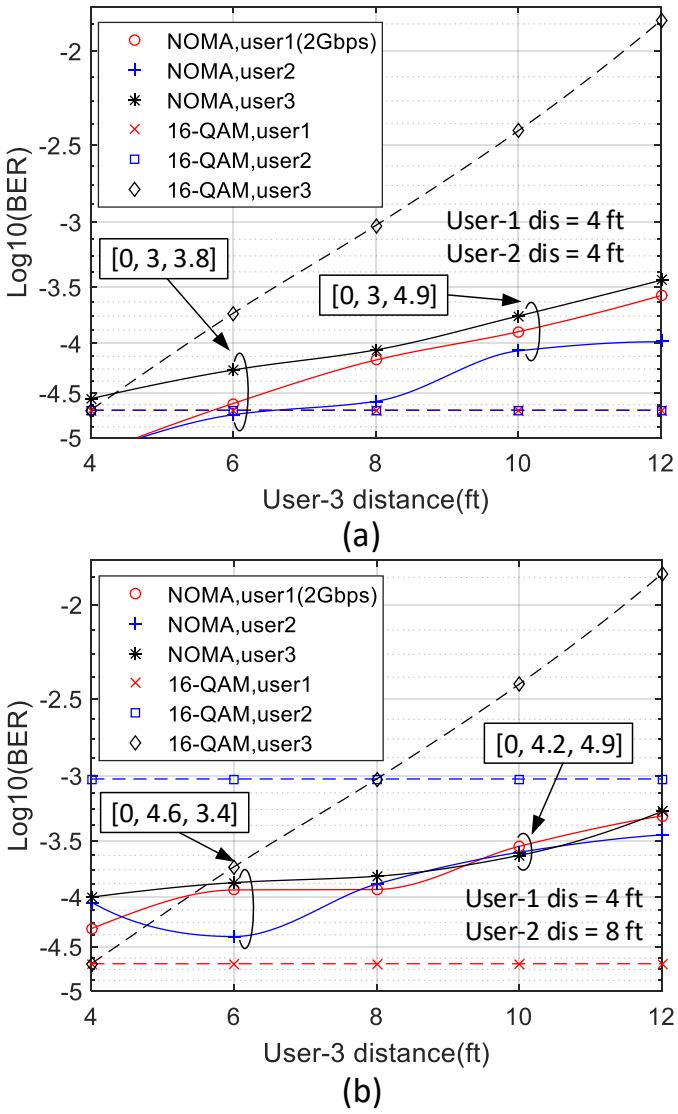


Figure 3.35: Experimental results for user distance test: (a) user-1 and user-2 are at distances of 4-feet; (b) user-1/2 are at distances of 4/8-feet.

from 1.6e-4 to 5e-4.

*User Distance Result*

We fix user-1 location and change the distance to the other users. User-1 requiring 2-Gbps rate are at the best channels, with a distance of 4-feet. For user-2, we change two locations with distances of 4-feet and 8-feet, simulating the user at good or intermediate channels. We refer the case of 4-feet links as the first setting and 8-feet links as the second setting. Under

both cases, we sweep the distance of user-3 from 4 to 12 feet, and measure the received EVM of three users, calculate the power ratio to balance BER of the system, apply the updated power ratio, and finally measure the BERs of three users using updated NOMA payloads. Results are shown in Fig. 3.35(a, b). We measure the OFDMA performance as a comparison, at the same locations. Since the BERs of users are independent, the BER curve is flat for user-1/2 with 16-QAM OFDMA.

By adaptive power ratio adjustment, the BER of three users becomes more similar. Under the first setting, the BER for user-3 is reduced, while the BERs for user-1/2 are increased; under the second setting, the BER for user-2/3 are reduced, while the BER for user-1 is increased. More power is allocated to user-3 if it is impaired more: the power ratio is [0, 3, 3.8]-dB for users of distances of 4/4/6-feet, and is updated to [0, 3, 4.9]-dB for 4/4/10-feet under the first setting. If we set the BER threshold to 1e-3, we expand the allowed user-3 distance from 8-feet to more than 12-feet for the first setting. Similar conclusions can be made with the second setting, that NOMA scheme can expand the user-3 distance by more than 4-feet. At 4/8/12-feet distances for user-1/2/3, the BER of the worst performance user is improved from 1.8e-2 to 4.2e-4 by NOMA.

*Antenna Angle Result*

We test the case with different receiving antenna angles. Because of the horn antennas we used for transmission and reception, any orientation offsets will cause antenna gain degradations. This test simulates the cases with dynamic users that no mechanism can guarantee the antenna orientation or antenna gain. The user-1 angle is fixed at 0-degree, and user-2 antenna angle is fixed at 0-degree (the first setting) or 10-degrees (the second setting). We sweep the angle of user-3 and measure the BER of all three users after adaptive power ratio adjustment. Results are shown in Fig. 3.36. All users are at distances of 4-feet.

Larger antenna angle leads to more severe antenna misalignment, and higher channel loss is observed. The BER for all three users is converged due to the converged power ratio

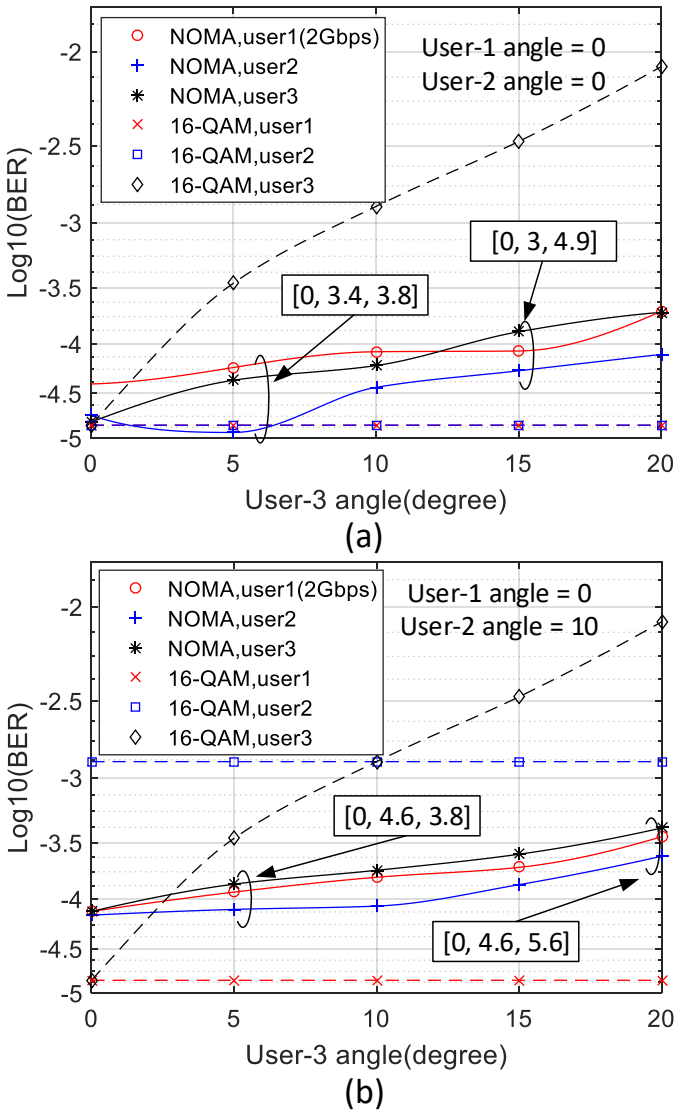


Figure 3.36: Experimental results for angle test: (a) User-1/2 receiving antenna are fully aligned. (b) User-1 angle is 0-degree; user-2 angle is 10-degrees.

calculation iterations. For example, the BER using NOMA is measured as 2e-4, 1.3e-4 and 2.5e-4 with 0/10/15-degree angles, comparing with 1.6e-5, 1.3e-3, 3.2e-3 using OFDMA. Setting the threshold to 1e-3 BER again, NOMA can compensate any impairments within in 20-degree angle for user-3 under both settings, while OMA can only provide good services when all user angles are smaller than 10-degree. A 10-degree or 100% relative improvement on antenna angle using with 25-dBi horn antenna is experimentally verified. In real scenarios with wider antenna beam, the orientation tolerance is larger concerning the ab-

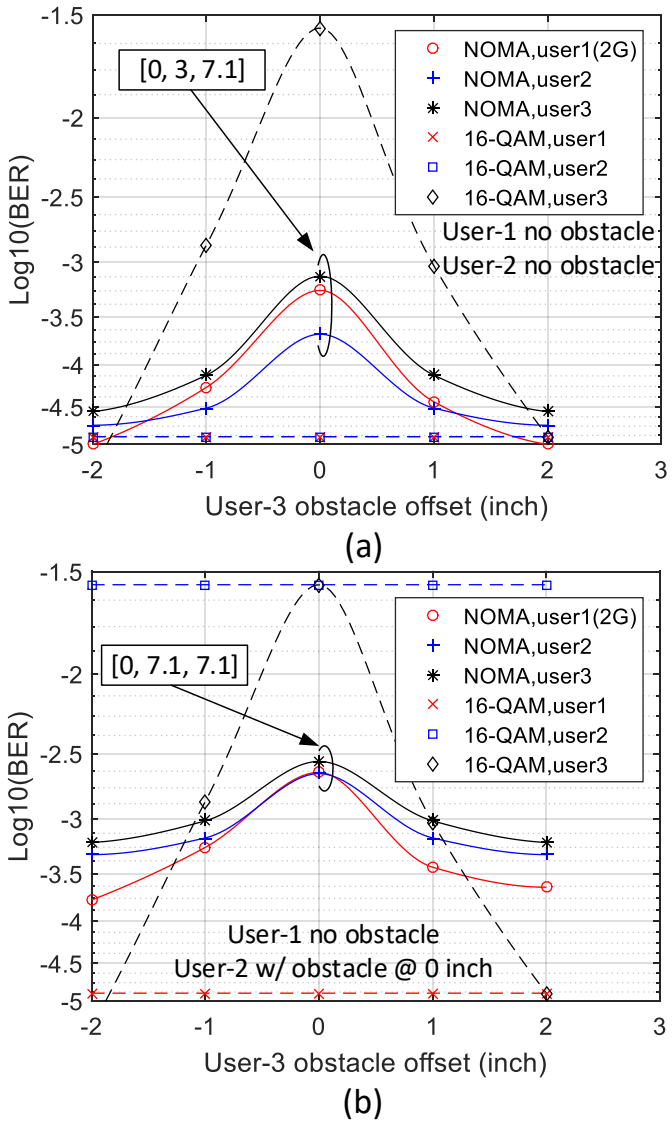


Figure 3.37: Experimental results for obstacle test: (e) user-1/2 are with LoS channels, (f) user-1 are with LoS channel, user-2 are fully shaded.

solute values, while the trend is similar that the NOMA scheme can effetely improve the transmission quality with users that have antenna misalignment.

*Obstacle Test Result*

Obstacles full of water are put in front of the receiving simulating the scenarios that obstacles may appear in front of the receiving antenna. The distance between the antenna and the obstacle is 5-inches. The diameter of the obstacle is 3-inches. For user-1, no obstacle is

set, and it has a LoS channel. For user-2, either with (referred as the first setting) or without obstacle (referred as the second setting) are tested. All users are at 4-feet distances without antenna angles. We change the location of the obstacle of user-3, measured by the offset by the wireless channel central line, shown in Fig. 3.32. With 0-inch offset, the obstacle is put in front of the receiving antenna. When the absolute offset is greater than 2-inch, the degradation by obstacles is negligible.

Results are shown in Fig. 3.37(a, b). Under the first setting, two users are under LoS channels, and only user-3 are impaired. By OFDMA scheme, the BER is increased to more than 1% for an obstacle with 0-inch offset. Instead, the BER is maintained under 1e-3 with NOMA scheme after power ratio calculation. The resulted power ratio is [0, 3, 7.1]-dB that a significant portion of the power is allocated to user-3 for compensating the impaired channel. Under the second setting that user-1 is under LoS channel and user-2 is fully shaded, the performance for all users is degraded. Especially, for any position of the user-3 obstacle, the user-2 BER is beyond 1% because of the independence of three users in OFDMA. However, with NOMA the BER can be improved to below 3.2e-3, with power ratio set to [0, 7.1, 7.1]-dB that large powers are allocated to user-2/3. As a result, in the obstacle test, more than one order of magnitude BER improvement is achieved for the extreme cases.

## 3.4 Summary

We show these works related to the second phase of implementation in this chapter. Adapting to the new channel and trends in MMW fiber-wireless integrated systems and channels, we design various modulations and multiple access schemes for the three major applications defined in 5G: eMBB, URLLC, and mMTC.

For eMBB, have proposed a GFDM modulation based photonic-assisted CA method using both optical and electrical carriers for component carrier generation. To minimize guard bands and increase spectrum efficiency, GFDM modulation with zero forcing re-

ceiver is applied. GFDM is similar to OFDM but with shapes subcarriers. It significantly reduces the overhead in the frequency domain by guard bands. We have experimentally aggregated $18 \times 40$-MHz-component carriers in MMW and achieved a high-quality signal transmission with significantly improved EVM. Designed for URLLC, but also compatible with eMBB, we proposed to use orthogonal chirp division multiplexing (CDM) in MMW fiber-wireless integrated systems. By replacing orthogonal subcarriers in the frequency division to orthogonal digital chirps, this novel modulation supports both eMBB and URLLC by tuning the sparsity of chirps. Without losing spectral efficiency or performance in eMBB, it is proven to be more robust to interferences and system degradations in URLLC while still be DSP efficient. It is verified by theoretic derivations, simulations as well as experimental demonstrations. Up to 5-dB EVM improvement is verified experimentally using the testbed with the presence of interferences.

For both eMBB and mMTC, we have proposed to use the NOMA scheme with SIC receiver in 60-GHz MMW fiber-wireless integrated system for multiple access. NOMA optimizes the users as user groups. It improves the reception quality and reliability by dynamic power resource sharing and allocation. DSP based SIC receivers are implemented in the receiver for interference removal. Moreover, the combination of OMA and NOMA is proposed to overcome supported user number limitation and security issue by NOMA. A fast iteration-based conjugate gradient nonlinear optimization method is applied to the fractional power ratio updating process, to fast adapting to the dynamic channel conditions. In addition, both synchronized and asynchronous PD-NOMA are investigated for downlink and uplink transmissions.

In the experiments to evaluate advanced modulations and multiple access schemes, we have used three different techniques for MMW generation with fiber-wireless integration. They all use the centralized MMW generation, such that the high-frequency LO is centralized in the BBU for downlink. Each LO is shared by multiple MMW RRHs, eliminating the CFO between nearby RRHs. It makes possible for the MMW coordinated multi-point

Table 3.2: Comparison with different MMW generation schemes involved in the dissertation.

| | Direct Modulation | Independent Light Beating | Phase Modulation, Using 1st Order Carriers | Intensity Modulation, with OCS |
|---|---|---|---|---|
| LO Frequency | $f_c$ | N.A. | $f_c$/2 | $f_c$/2 |
| Extra Device Required | IM | Laser | PM, Interleaver | IM |
| Device Bandwidth Required | High | Low | Medium | Medium |
| Stability | Medium | Low | High | Low |
| Limitations | Power penalty from CD, High modulator bandwidth | Narrow Line-Width Laser, Stable Laser Frequency Required | Extra Interleaver | Bias and Driving Voltage Sensitive |

(CoMP). In GFDM experiments, we use independent light sources with a specific frequency spacing, that the MMW is generated by beating between the two in PD. In CDM demonstration, a bias-insensitive PM paired with interleaving is applied to select the first order optical carriers. The PM is driven by an LO with a specific frequency $f_c/2$. In the PD-NOMA verification, we use intensity modulation at a specific bias point for optical carrier suppression (OCS). A comparison is listed in Table 3.2. Traditional direct modulation widely used in low-frequency RoF system is also listed. Based on device availability, system stability requirement and available LO frequencies, different optical MMW generation techniques should be chosen accordingly.

# CHAPTER 4

# ALL-SPECTRUM FIBER-WIRELESS INTEGRATED SYSTEM

In this section, we present the work to utilize the EM-wave of all frequency ranges based on currently available technologies. Specifically, we integrated low RF, MMW, FSO using lasers with infrared output, and VLC by LED. The fiber link is also included to be compatible with the fiber-wireless integrated architecture.

The application of all-spectrum communication can be categorized into two sections within the dissertation scope: for MFH and user access. With MFH related applications, both sides of the link are implemented and operated by the service providers (SPs). Moreover, the mobility requirement and battery life tend to be lower compared to user access. On the other hand, the user access scenario is more sensitive to the power consumption of the user devices. Still, high capacity, high reliability with low latency should be achievable for both applications.

For all-spectrum MFH, we present the research of VLC link technology with advanced pre-equalization for indoor applications, and the converged MMW/FSO with inter-dimensional modulation and diversity combining for outdoor applications. For all-spectrum user access, we propose and demonstrate the complete network architecture and UE design as a candidate for beyond 5G wireless communications.

## 4.1 Visible Light Communication for Indoor Mobile Fronthaul

In future wireless networks, spatial densification is necessary to support thousands of devices with excellent service qualities and high data rates in a small range, which requires an enormous amount of RRHs in the particular area, especially in urban areas and indoor environments, like open offices, classrooms, libraries, exhibition halls and other public open spaces. Multiple cells should be deployed in each space to increase the data rate to each

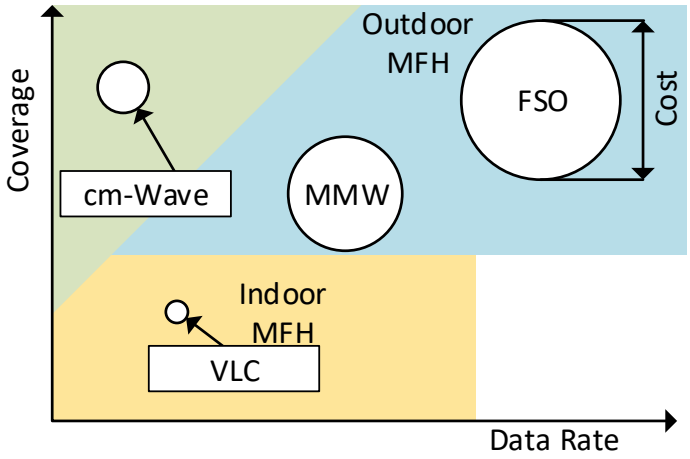


Figure 4.1: Comparison of multiple communication bands and their applications.

user. With more cells operating on the same band in a small area, the capacity and performance are limited due to the ICI in the cell edge. To deal with the ICI and increase the channel diversity, wireless network MIMO with coordinated cells is proposed and developed in addition to traditional single cell MIMO. Each user is served by all RRHs within its range, such that no strict cell edge exists in the network. To enable inter-cell coordination, a tight synchronization in time and frequency division is required among all RRHs in the network. The fiber-wireless integrated architecture can fulfill this stringent requirement.

As one of the strongest candidate for future MFH, analog MFH transmits wireless carriers in its raw waveform, by using different IFs for multiple carriers. Utilizing low bandwidth optical/electrical devices in RRH, the MFH cost is significantly reduced with better tolerance to chromatic dispersion, as shown in the work in Chapter 2. Still, fiber needs to connect all RRHs, and all RRHs must have optical devices. In the spatial densified indoor network with more RRHs in a small space, it is impractical for those fiber-connected RRHs to be deployed in a massive amount, especially for indoor installation in existing infrastructure due to the extra fiber deployment.

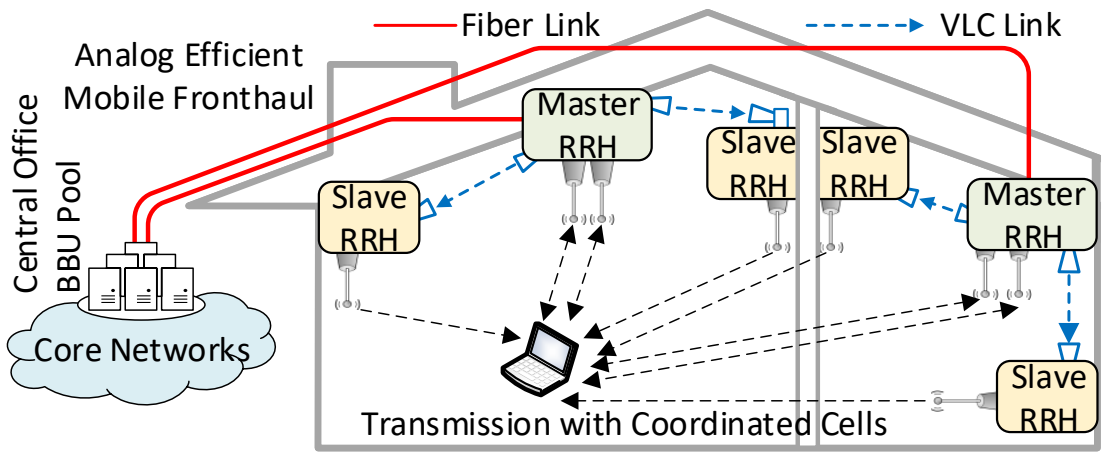


Figure 4.2: Spectral efficient mobile fronthaul with low-cost VLC links.

### 4.1.1 Proposed Architecture

The system architecture is shown in Fig. 4.2 [131]. Two tiers of RRHs are introduced in the proposed architecture. The first tier of RRH is connected to fiber MFH networks, referred to as master RRHs, with a direct fiber connection to the BBU pool in the CO. For the fiber transmission between the CO and the master RRH, we use multi-IF RoF technology. Multiple wireless streams for network MIMO and CA are multiplexed in different IFs over the fiber. The master RRH uses a PD to receive all carriers: some of the carriers are for the master RRH itself, other carriers are for adjacent slave RRHs. Inside the master RRH DSP, we separate wireless carriers by digital filters. Carriers for this master RRH are directly up-converted to the RF for wireless transmission. Carriers for the other tier of RRH, slave RRHs are down-converted to a low IF and fed into LED transmitters. Signals are delivered to slave RRHs by VLC links. Like the waveform in fiber, we use the raw wireless streams for transmission, which also makes purely analog slave RRHs possible without DSP. In these slave RRHs, the VLC signal is detected by detectors operated on visible light, and directly up-converted to the RF for wireless transmission.

Since one master RRH can serve multiple slave RRHs, most of the RRHs in the proposed architecture is slave RRHs that do not require any wired signaling, DSP, nor devices

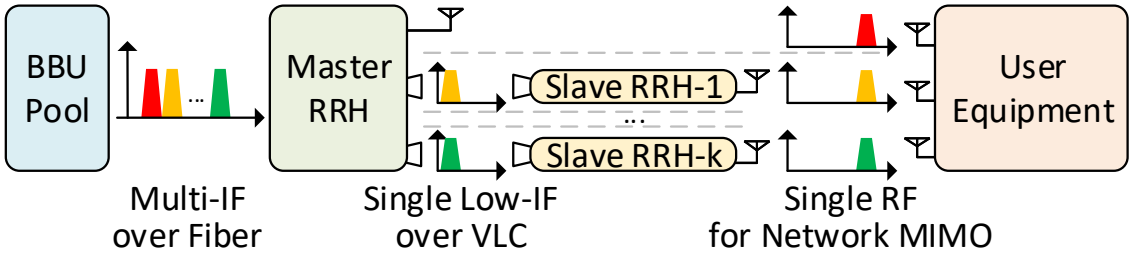


Figure 4.3: Frequency bands allocation in fiber, VLC links and MIMO operation.

for the fiber connection. The deployment and maintenance cost of the network is significantly reduced for these RRHs. With purely analog processing, it also saves power, reduces the latency and provides better time synchronization. The network flexibility and extension capability are improved significantly since new slave RRH deployment does not require any signal wiring, we just need electricity to run additional slave RRHs.

However, several issues exist in VLC links with current technology. VLC needs LoS channels to operate, which can be solved in the MFH since the link is between two RRHs that are typically mounted on indoor ceilings, within one large open space. These channels can be hard to be interrupted by moving objects on the floor. Another challenge is the limited mobility by directional beams, which does not exist in our system since the RRHs are always stationary. The distance and bandwidth can be expanded by pre-equalization or using a lens and reflector to concentrate the light beam. Better PCB design and impedance match should also increase the bandwidth with little extra cost.

Comparing with other wireless MFH solutions including MMW and FSO, the VLC link is more cost effective with sub-dollar LED chips. Moreover, it does not occupy any of the valuable MMW spectra which is actively discussed in 5G standardization. The VLC link is also easier to deploy and operate, compared with FSO, due to the wider beam by LED and lens.

### 4.1.2 Centralized and Distributed Pre-Equalization

Due to the limited bandwidth of LED, receiver, and PCB design/manufacturing in the low-cost VLC link, transmitter side pre-equalization is needed. It is also feasible since the RF signal should have a balanced performance among all subcarriers, without any processing in low-cost slave RRHs. Hence, the transmitted signal should have higher power densities with higher frequencies to compensate the strong low-pass effect in the channel. High pass filters in DSP or analog circuits can do the pre-equalization but require extra resources including DSP complexity, power consumption, and heat dissipation.

This dissertation work introduces two pre-equalization schemes with centralized/distributed processing. In the centralized pre-equalization, the pre-equalization is processed in the BBU pool. The waveform transmitted in the fiber is pre-equalized according to the VLC link response. In the distributed pre-equalization, the pre-equalization function is completed in the master RRH, so the waveform in fiber is uncompensated.

$$EVM_{i,Distributed} = \frac{n_{optical}|H_{pre,i}|^2|H_{VLC,i}|^2 + n_{VLC}}{P_{tx}|H_{fiber,i}|^2|H_{pre,i}|^2|H_{VLC,i}|^2} \tag{4.1}$$

$$EVM_{i,Centralized} = \frac{n_{optical}|H_{VLC,i}|^2 + n_{VLC}}{P_{tx}|H_{fiber,i}|^2|H_{pre,i}|^2|H_{VLC,i}|^2} \tag{4.2}$$

The final EVM at the slave RRH for the $i$-th subcarrier is shown in (4.1) and (4.2) for distributed/centralized pre-equalization correspondingly: $P_{tx}$ is the transmitted subcarrier power; $H_{fiber}$ is the fiber channel response (including transmitter and receiver response); $H_{VLC}$ is the VLC link response (including transmitter and receiver response); $H_{pre}$ is the pre-equalization filter response; $n_{optical}$ and $n_{VLC}$ are the noises in optical receiver and VLC receiver on each subcarrier correspondingly. The fiber channel is relatively flat in frequency division, and the product of $|H_{VLC}|$ and $|H_{pre}|$ is a constant since the pre-equalization filter should compensate the VLC channel. The distributed pre-equalization scheme provides a more balanced EVM performance among the subcarriers; while the centralized scheme

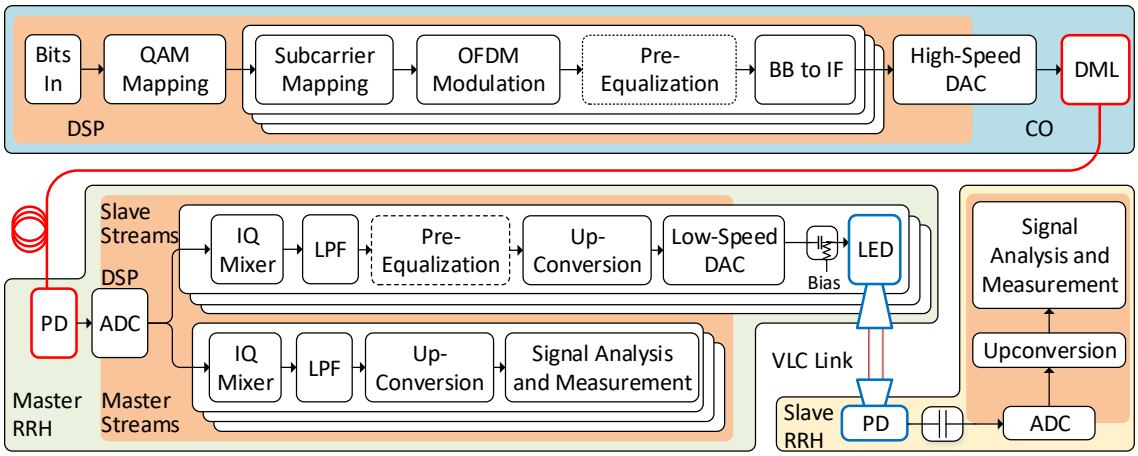


Figure 4.4: Experimental setup of advanced MFH with VLC links.

has imbalanced EVMs since the pre-equalized signal has an impaired performance after the fiber transmission. Lower frequency subcarriers have amplified EVMs due to the lower transmitting power into the fiber.

However, since DSP resources or analog circuits are needed in pre-equalization, the centralized scheme can reduce the master DSP complexity, which is feasible regarding network cost. We need to properly design the system with different applications and performance requirements.

### 4.1.3 Experimental Setup and Results

We set up an MFH testbed with master and slave RRHs including spectral efficient fiber MFH and low-cost VLC links, shown in Fig. 4.4. A low-cost intensity modulation-direct detection (IM-DD) fiber link is implemented. Both centralized and distributed pre-equalization are implemented and compared.

The bits firstly go to QAM mapping. Then, independent streams are generated by conventional OFDM modulation. No precoding is used in the experiment. The setup is capable of MIMO signal transmission with additional MIMO processing. The processing will not affect the MFH performance. If centralized pre-equalization is applied, the signal then goes through a digital high-pass filter for pre-equalization with these carriers to slave

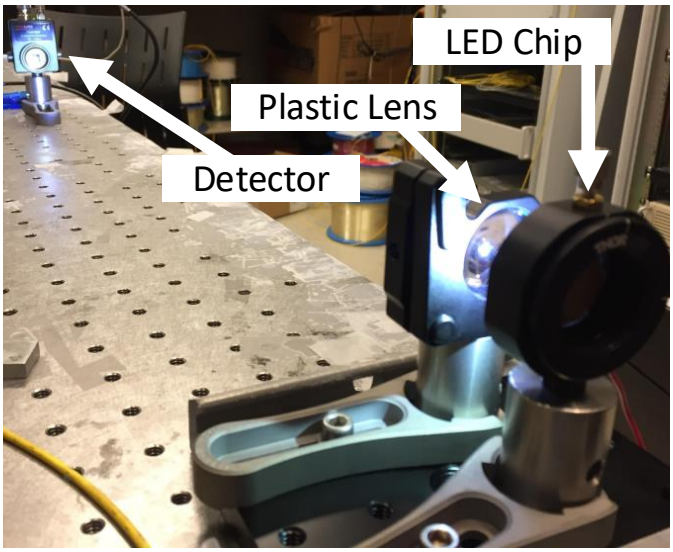


Figure 4.5: Low-cost VLC links for connection between master/slave RRHs.

RRHs. Different wireless streams are mapped to varies IFs and converted to electrical waveforms by a high-speed DAC. The electrical signal is then fed into a DML.

After 25-km fiber transmission with single mode fiber, the optical signal is then detected by a PD. The signal is sampled by an oscilloscope, and fed into the master RRH DSP. Then, different carriers are down-converted through digital IQ mixers, low-pass filtered and down-sampled. The baseband signal is generated with reduced sampling rate. For those carriers to the master RRH, the signal is directly up-sampled, up-converted to the RF and analyzed digitally.

For other carriers to slave RRHs, a pre-equalization filter is applied if we use the distributed pre-equalization scheme. Baseband samples are up-converted to a low IF for VLC transmission. Then the electrical signal is amplified by a PA. A DC bias is combined with a bias-tee, then the signal directly drives a low-cost, off-the-shelf white LED chip by CREE. The bias current is about 120-mA. With a plastic lens, the light wave is transmitted through a 1-ft wireless VLC link in Fig. 4.5. With a silicon amplified detector, the signal is received with another scope. After that, wireless signals at the radio frequency are generated after up-conversion and analyzed by an OFDM demodulator. The VLC link wireless distance

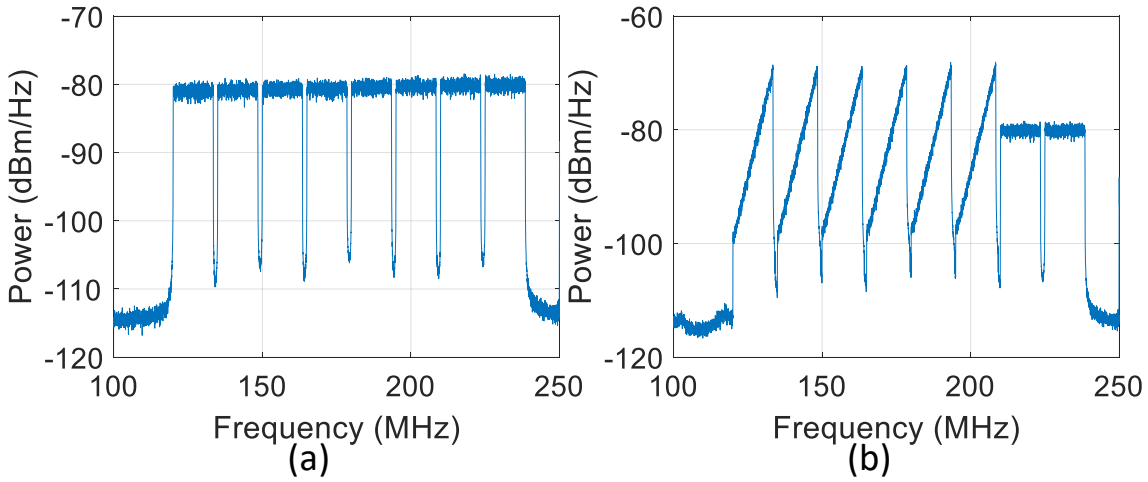


Figure 4.6: Received electrical spectrum after fiber link with (a) distributed pre-equalization and (b) centralized pre-equalization.

can be further extended by using an additional reflector in the transmitter or using a detector with higher sensitivity.

We use the standard LTE waveform with 13.5-MHz data bandwidth, which is widely deployed in current LTE network. With 15-kHz subcarrier spacing, each carrier consists of 900 subcarriers. A 6.25% CP is inserted between OFDM symbols. In the multi-IF MFH in fiber, we reserve 1.5-MHz guard bands to protect adjacent carriers. In fiber, a guard band of 120-MHz is reserved around DC, since our optical link response starts at 100-MHz. In the VLC link, the DC guard band is set to 750-kHz to reduce the signal bandwidth.

We measure the MFH serving one master RRH and six slave RRHs. One VLC link is used in the experiment due to the limited lab equipment. We measure different slave-RRH performances by feeding different input carriers extracted from the master-RRH DSP. Eight independent carriers are transmitted in the fiber, serving downlink eight CA or 88 MIMO if using an additional MIMO precoder. The received spectrum after fiber transmission is shown in Fig. 4.6(a, b), with distributed or centralized pre-equalization. The spectrum after the VLC link is shown in Fig. 4.7(a, b), without or with pre-equalization. Since the setup is software-defined, we can dynamically arrange the carriers and designate them to master/slave RRHs. By default, the lower six carriers in fiber are for slave RRHs, and the

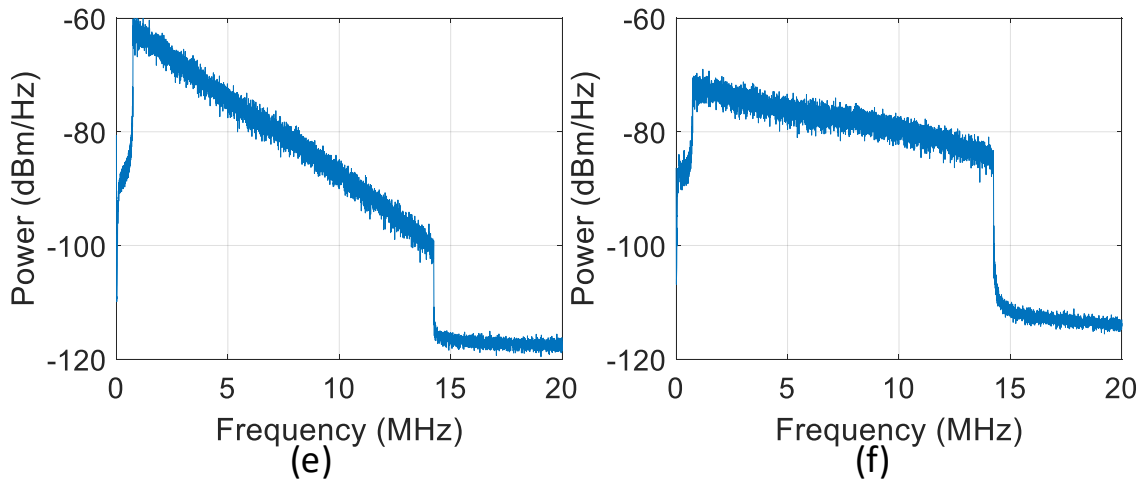


Figure 4.7: Received electrical spectrum after VLC link (a) without pre-equalization and (b) with pre-equalization.

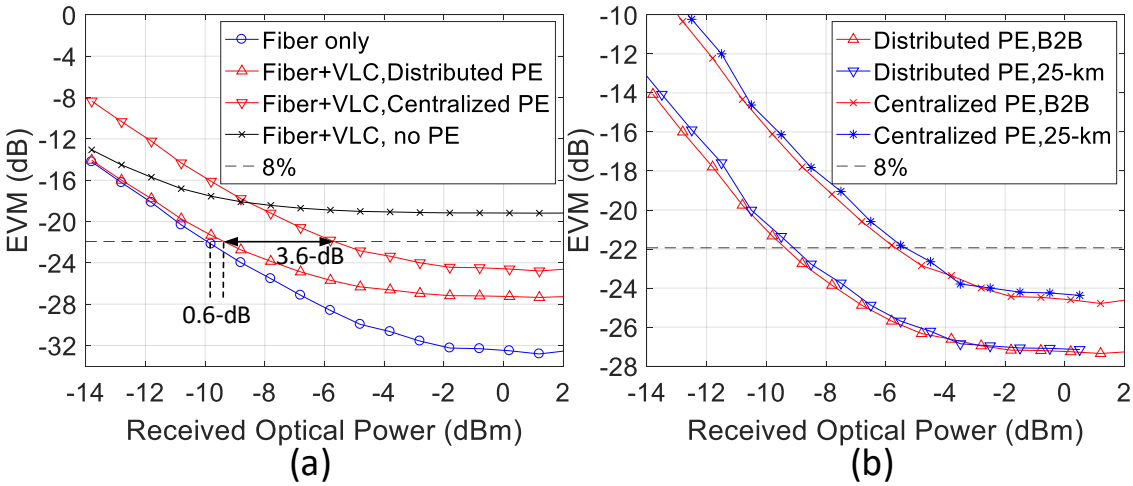


Figure 4.8: Experimental results. (a) Received optical power sensitivity. (b) Sensitivity with optical back to back and 25-km fiber.

higher two carriers are for the master RRH.

Experimental results are shown in Fig. 4.8. The ROP sensitivity performance is shown in Fig. 4.8(a). The fiber only curve illustrates the performance of master RRH that does not include VLC links. The other three curves are for cascaded fiber and VLC transmissions. We test scenarios of centralized/distributed pre-equalization, as well as no pre-equalization performances. From results, the VLC link generates a small penalty of 0.6-dB to achieve 8% EVM required by LTE-A 64-QAM modulation, if we use the distributed pre-

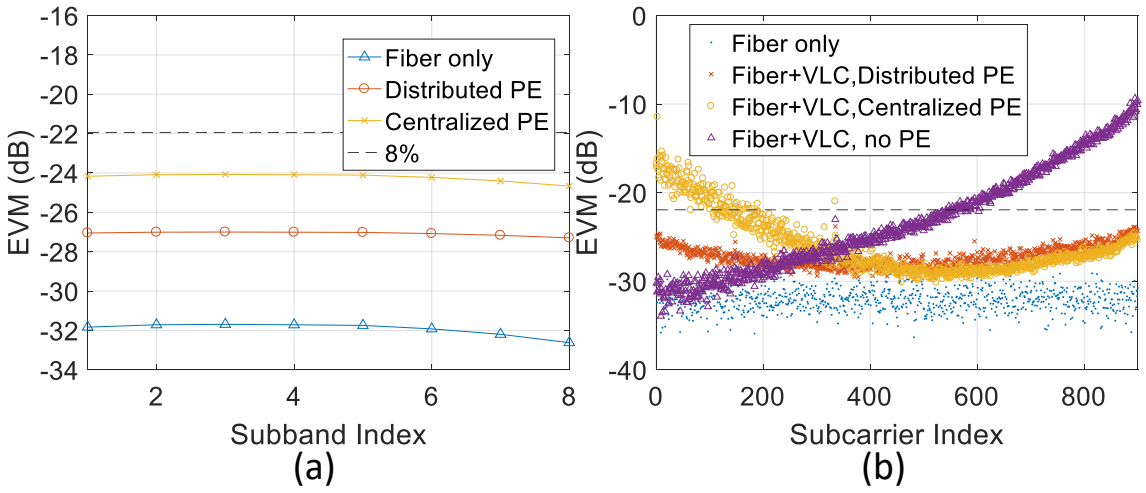


Figure 4.9: Experimental results. (a) EVM performances with wireless carriers. (b) Subcarrier EVM performances.

equalization scheme. The centralized pre-equalization generates another 3.6-dB sensitivity penalty. The required ROP for distributed/centralized pre-equalization are about -9.3-dBm and -5.7-dBm. If we do not apply any pre-equalization, the system has an EVM floor of more than -19.3-dB, which cannot fulfill the 64-QAM requirement.

25-km single mode fiber transmission is measured and compared with optical back to back performance. Negligible penalties are generated due to the fiber transmission, because of the high spectral efficiency and small bandwidth in fiber.

The performance of each wireless carrier is measured. EVMs of all carriers should be below the 8% threshold defined in 3GPP. With 0.2-dBm ROP, the EVM of each wireless carrier is shown in Fig. 4.9(a), with centralized/distributed pre-equalization. Even no optical pre-emphasis is applied, the EVM difference is within 0.5-dB. A consistent performance can be observed among all carriers due to the limited bandwidth in fiber.

A more precise EVM measurement in subcarrier-level is applied. Results are shown in Fig. 4.9(b) with 0.2-dBm ROP and the lowest-IF carrier. Without pre-equalization, EVMs of higher-indexed subcarriers increase dramatically to more than -10-dB, due to the reduced power received. With centralized pre-equalization, lower subcarriers have higher EVMs due to the impaired performance with pre-equalized fiber transmission. The distributed

pre-equalization provides the best performance that all subcarrier EVMs are below 8%.

The result complies with our previous derivation that the distributed pre-equalization should have a better performance comparing with centralized pre-equalization.

## 4.2 Inter-Dimensional Modulation and Advanced Coding for Reliable All-Spectrum Mobile Fronthaul

In some situations, fiber deployment is extremely costly and geographically challenging, as the link to cover a geographic barrier (river, canyon and so on) or to cross private property. Wireless mobile fronthaul would benefit concerning cost reduction, scalability, and flexibility from alternative MMW and FSO technologies. Also, the MFH wireless connections should be able to deliver extra system information including controlling bits for radio heads or additional traffic generated by wired users.

### 4.2.1 Network Architecture

Adapting to small cell applications, the RRH is close to users. Those RRHs are wirelessly connected to relay nodes by MMW/FSO links. However, both technologies using high-frequency transmission are sensitive to the channel conditions. Considering the different transmission absorption characteristics under various atmospheric and weather conditions, as well as their various modulation and antenna design, converged MMW/FSO technologies are proposed and demonstrated to enhance the reliability.

ADCT shows better performance, reduced latency, and improved reliability than hard switching schemes. However, most current ADCT schemes use the same modulation that ignores the different transmitter/receiver architecture and availability of commercial products that adhere to existing standards. For MMW, the DSP and frontend chips are actively developed with high linearity designed for multi-carrier modulations including OFDM but have limited bandwidth. For FSO, the optical transceiver is available with limited linearity for single carrier modulations including PAM, with a wider bandwidth of more than

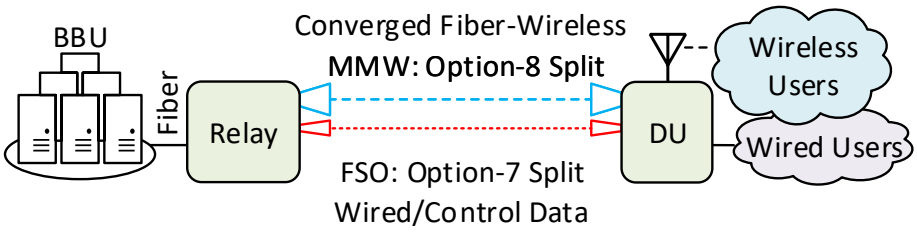


Figure 4.10: Multi-layer function split in converged fiber-wireless mobile fronthaul with FSO/MMW links.

10-GHz typically.

The system architecture is shown in Fig. 4.10 [132]. All the high-layer wireless data is processed in the centralized BBU. Then, most of the distance from BBU to the DU is covered by fiber. For the last mile/feets, a flexible converged fiber-wireless link is deployed to cover the distance where the fiber is unavailable. However, since the available single technology including MMW and FSO are sensitive to the atmospheric and whether impairments, using both techniques simultaneously provides a more practical approach to a reliable service.

Due to different device characteristics in the MMW/FSO transceiver, we propose the inter-dimensional ADCT based on various modulation formats. OFDM is delivered in the MMW link because the link has high linearity but limited bandwidth. OFDM fits this frame well with increased spectral efficiency but high PAPR. We propose to use the analog 5G waveform delivered in MMW. It is an option-8 function split since all the functions are completed before the MMW link in downlink including low-PHY. For FSO, the optical link suffers more from nonlinearity but has a wider bandwidth. Single carrier modulation is preferable, and the PAM is widely used in optical networks. In the proposed scheme, we transmit PAM signals serving the 5G MFH. However, PAM symbols only embed amplitude information but not phase. Hence, we utilize two PAM symbols to deliver one QAM symbol in 5G, for in-phase and quadrate amplitudes accordingly. After receiving and recovering the PAM, assembling the QAM, we still need the low-PHY including IFFT and CP insertion. So, the FSO link is an option-7 function split. The PAM level in FSO for

MFH is changed according to the QAM level in the wireless interface.

### 4.2.2 Inter-Dimensional Adaptive Diversity Combining with Repetition Coding

After recovering the QAM symbols from both links, the ADCT is applied. It combines symbols based on an optimized ratio to obtain superior performance than each link. Besides, because the FSO link provides much higher symbol rate, we have the redundant bandwidth to apply repetition coding to improve the system performance further. The combined symbol is expressed as S in (4.3). $S_{FSO,I,i}$, $S_{FSO,Q,i}$ and $S_{MMW}$ are the recovered PAM models from FSO for I, Q (with multiple repetitions indexed i) and the received QAM symbols from MMW accordingly. $\alpha$ is the weight when combining, based on the estimated signal noise level, as (4.3) suggested. $N$ is the number of repetitions. With more repetitions, the wireless EVM tends to be smaller, at the cost of reducing the residual data capacity for wired user or control information. We need to properly design the repetition coding for balance.

$$S = \sum_{i=1}^{N} \alpha_i (S_{FSO,I,i} + iS_{FSO,Q,i}) + (1 - \sum_{i=1}^{N} \alpha_i) S_{MMW} \tag{4.3}$$

$$\alpha_i = (1/{EVM_{FSO,i}}^2)/[\sum_{i=1}^{N} (1/{EVM_{FSO,i}}^2) + 1/{EVM_{MMW}}^2] \tag{4.4}$$

To optimize the EVM of combined symbols, maximal ratio combining (MRC) is applied. Symbol weights are inversely proportional to the recovered EVM square. If the noise and interference from multiple bands/repetitions are independent, the combined symbol SNR is the sum of all component QAM SNRs. After acquiring combined QAM symbols, the low-PHY is executed, and finally, the 5G OFDM waveform is delivered to the RF-frontend.

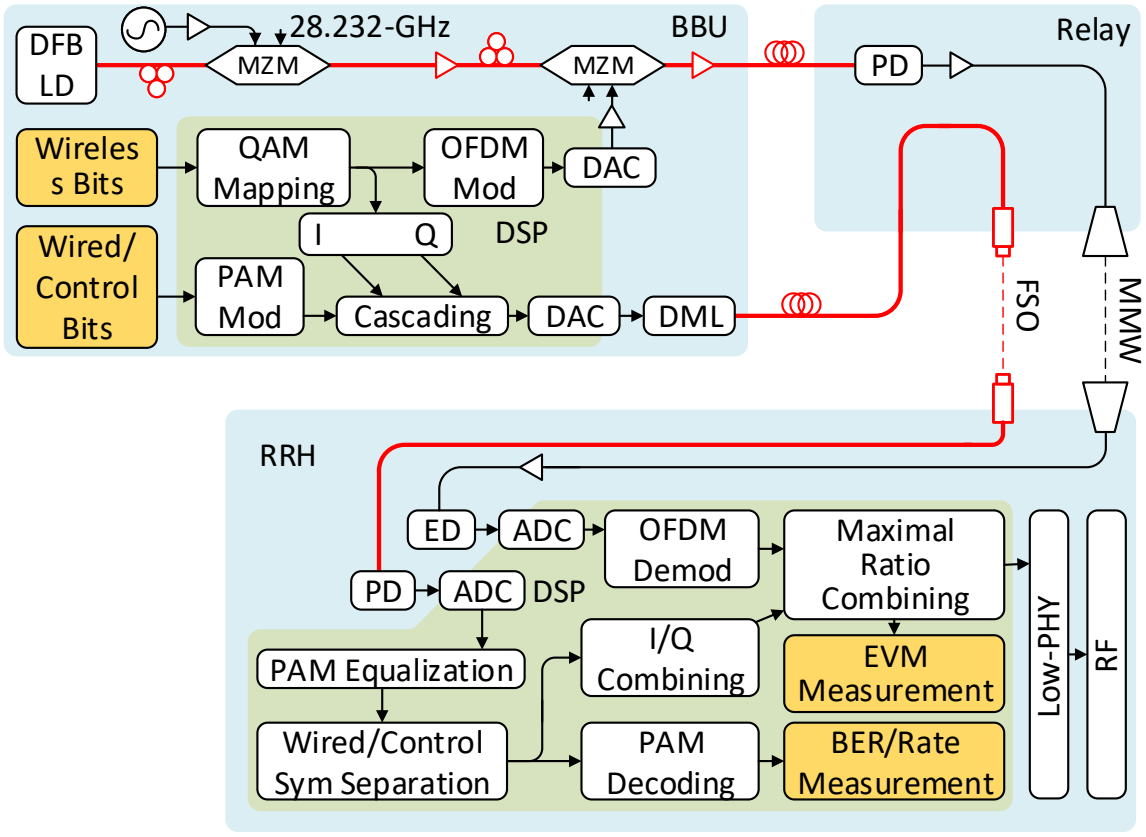


Figure 4.11: The experimental setup of converged MMW/FSO links using inter-dimensional adaptive diversity combining technique.

### 4.2.3 Experimental Setup and Results

The experimental setup is shown in Fig. 4.11. For the MMW physical link, a DFB-LD connected to MZM driven by the 28.232-GHz signal is used for MMW carrier generation at 56.46-GHz. Then, another MZM is connected for data modulation. After 13.875-km DSF, the optical spectrum is shown in Fig. 4.12. Moreover, a high-bandwidth PD is deployed for optical signal detection. A PA and horn antenna with 25-dBi gain are used for MMW signal boosting and transmission in the relay node. In the RRH, a symmetric horn antenna, an LNA, and an ED are applied for detection and down-conversion, paired with an ADC. In the FSO link, we use an IM-DD scheme. A DML is utilized for signal generation and PAM modulation. In the relay node, we use a fiber-coupled collimator for signal transmission. In the RRH, a PD and another ADC is applied.

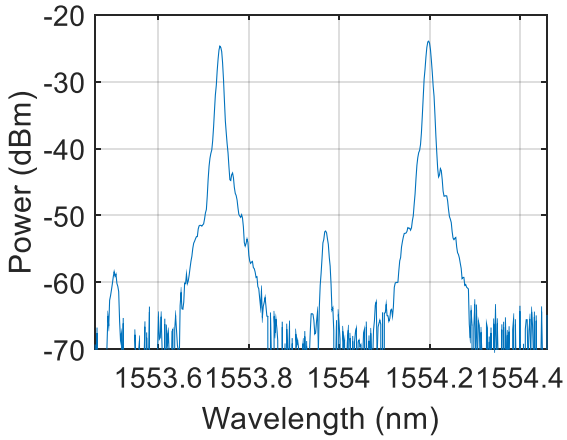


Figure 4.12: Received optical spectrum in the relay node.

In DSP, both wireless and wired/control bits are fed into the transmitter DSP. For wireless information, we map it into different QAM symbols. After that, we use a digital OFDM modulator and a DAC to drive the optical modulator in the MMW link. The same QAM symbols are split into I/Q and cascaded with PAM-4 symbols carrying wired user data. Then, another DAC is driving the DML in the FSO link. In MMW receiver, we do OFDM demodulation and blind EVM estimation. For the FSO receiver, we equalize the PAM stream and separate different information to wired user bits and wireless symbols. Each two PAM symbols are assembled to a QAM, and the EVM is also blindly estimated. Finally, we combine the QAM symbols from both links and multiple FSO repetitions using the optimized parameter and measure the EVM of combined QAM symbols. The BER of the wired user bits is also measured from the FSO PAM link. In MMW, the OFDM bandwidth is 576-MHz with 480-kHz subcarrier spacing following current 5G agreement, with 5.88% CP. For FSO, we use 12-GBaud PAM: the fixed user always uses PAM-4, while the wireless traffic is carried by PAM-4/8 depending on whether 16/64-QAM is used. The MMW link transmits 542.1M QAM symbols per second, so it needs 1.084-GBaud rate for each repetition in FSO. The FSO link can support a maximal of 11 repetitions for significant EVM reduction in the wireless symbols.

The experimentally measured MMW power sensitivity is shown in Fig. 4.13(a). Ref-

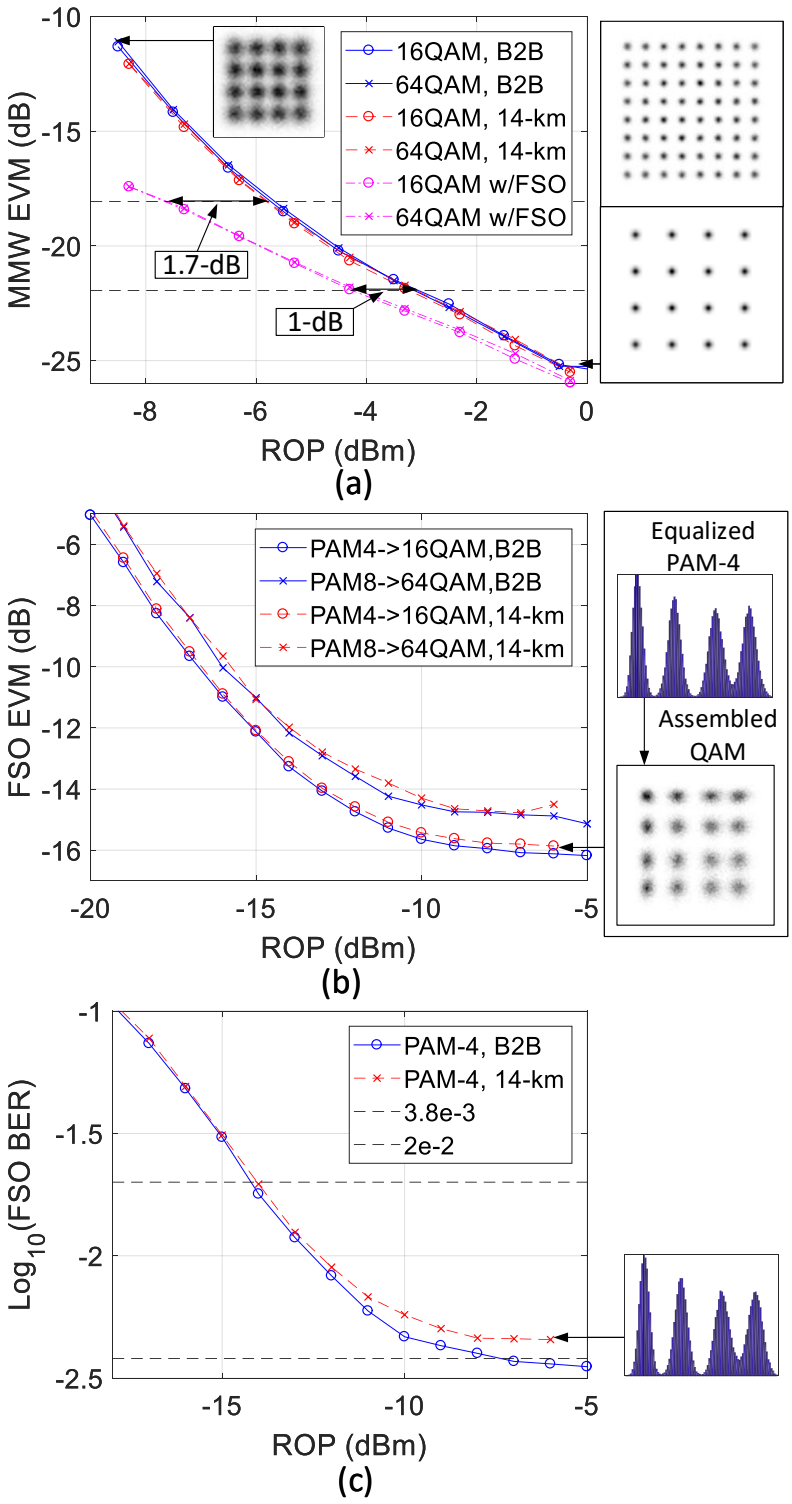


Figure 4.13: Experimental results. EVM sensitivity performance in (a) MMW and (b) FSO link. (c) BER sensitivity in the FSO link.

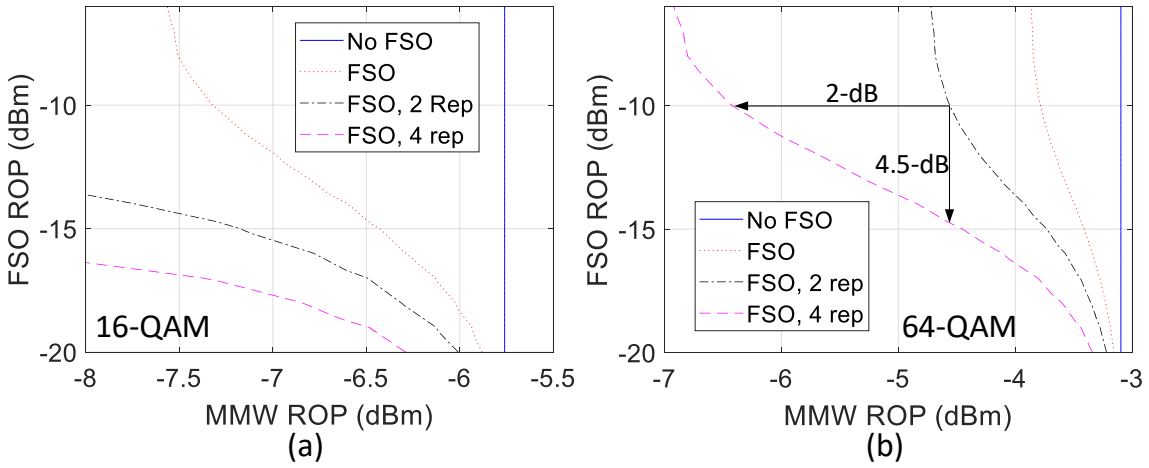


Figure 4.14: ROP tolerance for (a) 16-QAM symbols and (b) 64-QAM symbols.

erence lines of 12.5% and 8% EVM as the requirement for 16/64-QAM by 3GPP are presented. Without FSO, the single MMW can fulfill the requirement at -3/-5.5-dBm ROP accordingly. Both 16/64-QAM OFDM shows similar performance, and 14-km fiber generates a negligible penalty. With the FSO link at -6-dBm ROP, even without repetition, 1/1.7-dB sensitivity improvement is observed for in MMW link. Similarly, the FSO sensitivity is shown in Fig. 4.13(b, c). The EVM of PAM converted QAM symbols is presented in Fig. 4.13(b). Due to the high baud rate, the EVM cannot fulfill the 3GPP requirement with single FSO link. The performance difference between PAM-4/8 is due to the PAPR difference. In Fig. 4.13(c), the BER of wired users can be maintained below 3.8e-3/2e-2 when ROP is greater than -7/-14-dBm back to back. A slight penalty is measured with the fiber transmission in the low BER range.

Then, we apply the proposed inter-dimensional ADCT and repetition coding. We simplify the complex atmospheric and weather degradations as power penalties for easy quantification. The ROP tolerance for both links is shown in Fig. 4.14(a, b) with 16/64-QAM. These figures show boundaries under various repetition coding. For each boundary, if the channel condition falls into the upper right part with larger ROP, the system works with good performance. With more repetitions, the top right area expands as the boundary moves downwards in Fig. 4.14(a, b), which suggests a more reliable link. For example,

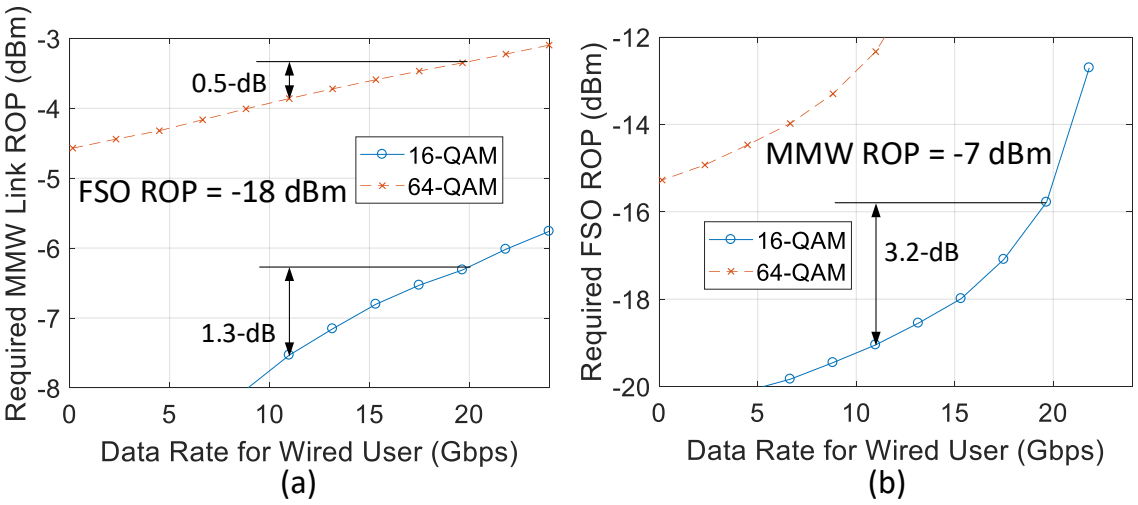


Figure 4.15: Required ROP for (f) MMW and (g) FSO link with varying data rates for wired users.

if we increase the repetition from 2 to 4 times in FSO, we can improve the sensitivity by 2/4.5-dB for MMW/FSO links serving 64-QAM.

Finally, we show the required ROP for MMW and FSO in Fig. 4.15(a, b), under different repetition coding. Higher data rates reserved for wired users shrink the available resource and energy for wireless QAM symbols, so higher ROP is required for both links to fulfill the wireless EVM requirement. For instance, we can reduce the required MMW link ROP by 1.3/0.5-dB if we fix the FSO ROP and reduce the rate for wired users from 19.66-Gbps to 10.99-Gbps. Similarly, 3.2-dB sensitivity improvement is observed for the FSO link. Based on the channel conditions, we can adaptively tune link sensitivities by changing the repetition coding, to deal with varying weather and atmospheric conditions in MFH.

## 4.3 All-Spectrum User Access with Optimized Network and User Device Design

In this section, we apply the proposed all-spectrum wireless access technologies to the final user access section, which is the logical link between the radio heads and the user devices. It is challenging due to the high complexity of both network architecture, synchronization, and coordination, as well as user device design. For user devices, the requirement of battery

life, DSP efficiency, and stability under changing environments are high.

A total of 4 bands or band groups are included in the proposed all-spectrum system: low-frequency centimeter-wave bands from sub-GHz to 30-GHz, high-frequency MMW from 30-GHz to 300-GHz, infrared FSO links operating at around 192-THz, and VLC with frequency up to more than 700-THz.

Among them, the VLC technology with LED transmitters can only support intensity modulation due to the incoherency. The LED cannot support single frequency output, so the I and Q cannot be separated. More importantly, with massive production for the illumination application, the cost of the LED chip is extremely low. Sub-dollar chips with multi-watt output are available on the market. It makes it possible to deploy high-density LED cells to serve as both communication anchors and lights. However, for communication applications, the LED modulation bandwidth is low, typically less than 100-MHz without pre-equalization, which is discussed in detail in Chapter 4.1.

On the contrary, the FSO, as another lightwave communication technology, provides the ultra-high modulation bandwidth of more than 10-GHz easily, which can be converted to more than 100-Gbps with PAM or DMT modulation. Coherent optical transmission is also supported by this scheme using narrow line-width lasers. However, the coherency of the laser makes the EM wave beam very narrow and hard to be aligned. Using optical beam forming maybe one solution, but prior location information down to centimeter precision level is necessary. Besides, the high power consumption and temperature sensitivity make it hard to be integrated into battery-powered user devices.

For other conventional wireless communication frequencies: cm-wave and MMW, the selection is between capacity and coverage. With lower operation frequency, the penetration capability tends to be higher, with much-improved coverage thanks to the reduced propagation loss. The disadvantage of these bands is the very congested channels. On the other hand, MMW provides wide channel bandwidth with minimized interference with existing standards, at the cost of limited coverage and mobility.

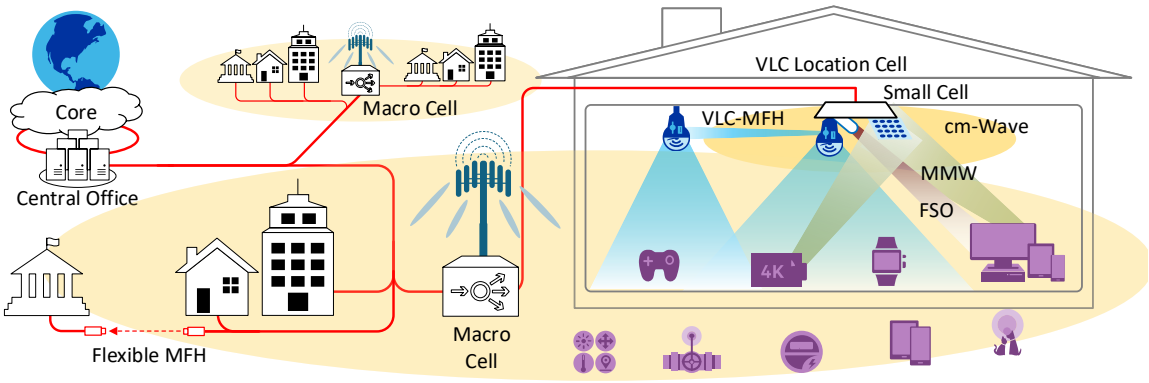


Figure 4.16: Proposed network architecture of all-spectrum wireless access.

### 4.3.1 Proposed Network Architecture

The proposed network architecture is shown in Fig. 4.16. Four types of cells are included in the completer network architecture.

For wide area coverage, the macro cell is preferred with the low-frequency operation. It covers both indoor and outdoor, mainly serves the eMBB and mMTC applications. This cell type is more useful in rural areas. The data rate for eMBB application by this cell type cannot be extremely high, but can still be fit into the minimal per-user data rate requirement in Table. 1.1 due to the limited user density. For mMTC application, the cm-wave technology provides large coverage and enough capacity for those sensor related applications.

In the urban scenario, we design the small cell RRH specifically for indoor coverage with ultra-high capacity, which embeds multiple transceivers including FSO, VLC, MMW, and cm-wave. For eMBB users, the uplink data is carried by MMW, which supports multi-GHz channel bandwidth. When coupled with MIMO and CA, the latest specification can go up to 176-GHz with 802.11ay. Moreover, the MMW frontend chips and DSP are mature with modem IC available, with reasonable power consumption. The antenna design is compact and mature, making the MMW suitable for high-speed uplinking. For the downlink, FSO provides higher peak data rate and can save the valuable spectral resource of MMW. As mentioned, the optical or mechanical beamforming can precisely align the narrow beam

to users. Other diffusive beam generation technologies can loosen the beamforming requirement, but still, precise location information is preferred to avoid the time-consuming beam sweeping process with initial connection.

For precise positioning, current GPS system cannot support indoor service, neither can it provide enough precision. We utilize the VLC positioning technologies with high density LED anchor cells. So the VLC cell is designed indoor with high deployment density, which can also serve as illumination purposes. However, due to the signaling requirement, these cells should be still connected to the fiber backbone network.

All three types of cells should be connected to the fiber MFH network. Enabled by the heterogeneous MFH of multiple standards and various cells, the centralized C-RAN like architecture can still be used. Similarly, the BBU processes all data streams to all types of user devices. Due to the advanced architecture, the physical waveforms from different cells at distributed locations can be easily synchronized, such that better coordination and control are achieved.

### 4.3.2 Experimental Demonstration Setup

We set up a testbed demonstrating the feasibility of proposed all-spectrum wireless access system, with fiber-wireless integrated MFH. The target is to minimize the resource usage, to fulfill the capacity, coverage and reliability requirements.

To minimize the wavelength usage, the carriers for macro cell and VLC cell share one laser source. The signal is carried by different IFs. In the cell site, the optical signal is detected jointly; then a simple separation DSP is applied. The FSO uses another dedicate wavelength for signal delivery.

For the cm-wave and VLC downlink, the DSP generates multiple OFDM signals at designated IFs. After the DAC, the signal drives an integrated optical transmitter based on DML. It consists of one LNA, one TIA, and a wide-band DML, shown in Fig. 4.17(a). For FSO downlink, the DSP generates OFDM or PAM-4 signal; then a high-speed DAC is

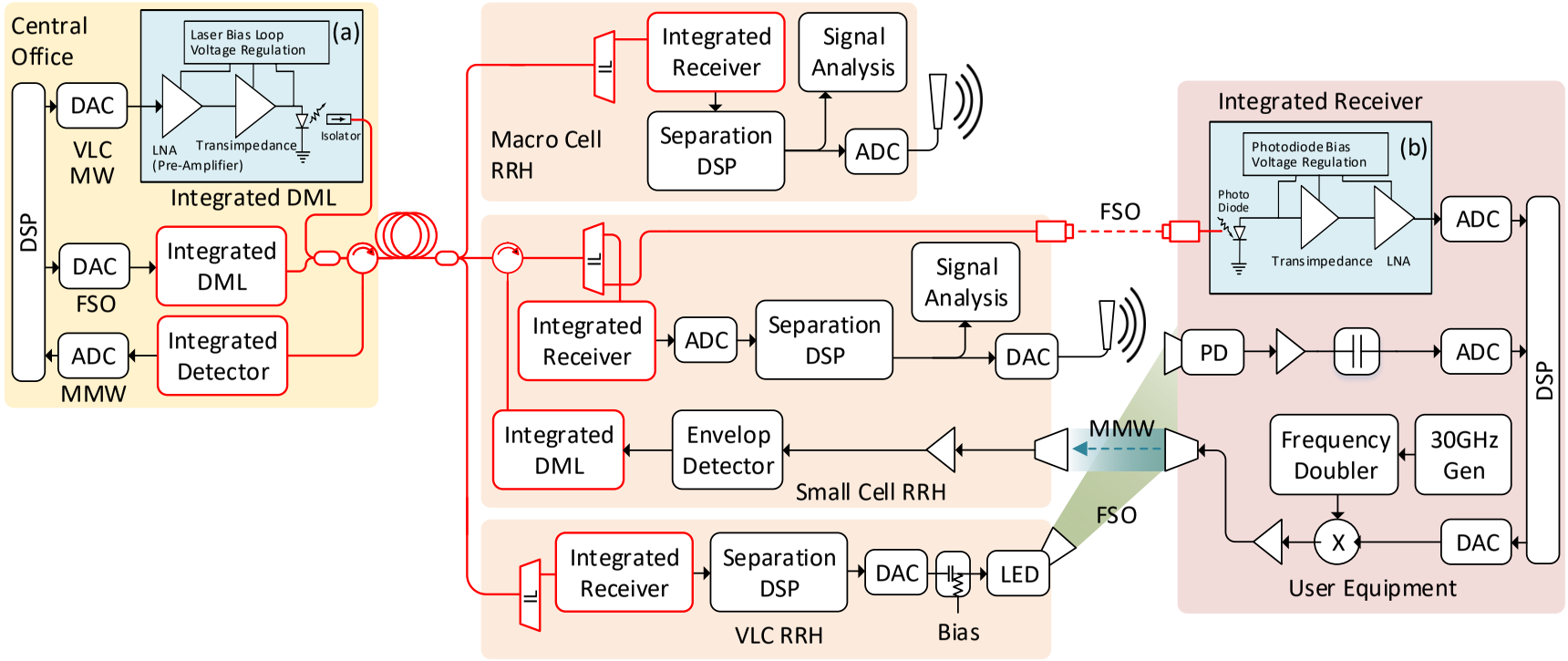


Figure 4.17: Experimental demonstration setup of the proposed all-spectrum fiber-wireless integrated system. (Architecture of (a) integrated optical transmitter and (b) integrated optical receiver. )

applied to drive another similar optical transmitter centered at a different center frequency about 30-GHz apart. After coupling both wavelength signals, the optical signal is fed into the fiber.

In the macro cell RRH, an interleaver is used to filter out the signal. Then, a PD is applied for signal detection. The electrical signal contains the information for both macro cell cm-wave and VLC, multiplexed in the frequency domain. A simple filtering is applied to filter the cm-wave information; then it is digitally up-converted. We cannot evaluate the wireless transmission using low-frequency bands since they are mostly licensed. Instead, we measure the signal quality at the wireless transmitter side, using EVM criteria.

Similarly, the VLC cell shares a similar architecture, with a LED transmitter replacing the traditional antenna. A PD operating at visible wavelength range is working as the receiver in the user device. A DSP is applied with signal synchronization and equalization. Hence, we evaluate the end to end performance, with BER as the metrics.

The small cell RRH consists of multiple transceivers. The interleaver separates the two wavelengths: the upper branch is shared by VLC and cm-wave, processed as describes in the macro cell and VLC cell; the lower branch is dedicated for wideband FSO. Since the wavelength are shared by both fiber transmission and FSO, the downlink transmitter is a simple fiber collimator. In the receiver, another collimator as the antenna is used, and couple the signal into fiber. After that, a PD and receiving DSP are utilized, and the information is extracted finally.

For the eMBB user uplink, the 60-GHz MMW resource is used. The signal is generated by DSP and DAC in the user device. Then the signal is up-converted to V-band with a 60-GHz carrier and a mixer. After the passive mixer, a PA is utilized to boost up the signal, and then it is transmitted by the horn antenna. In the small cell, the signal is collected by another horn antenna, and amplified by an LNA. Then, it is down-converted with an ED and converted to the optical signal with another integrated optical transmitter. Back in the BBU pool, the uplink MMW signal is detected and measured.

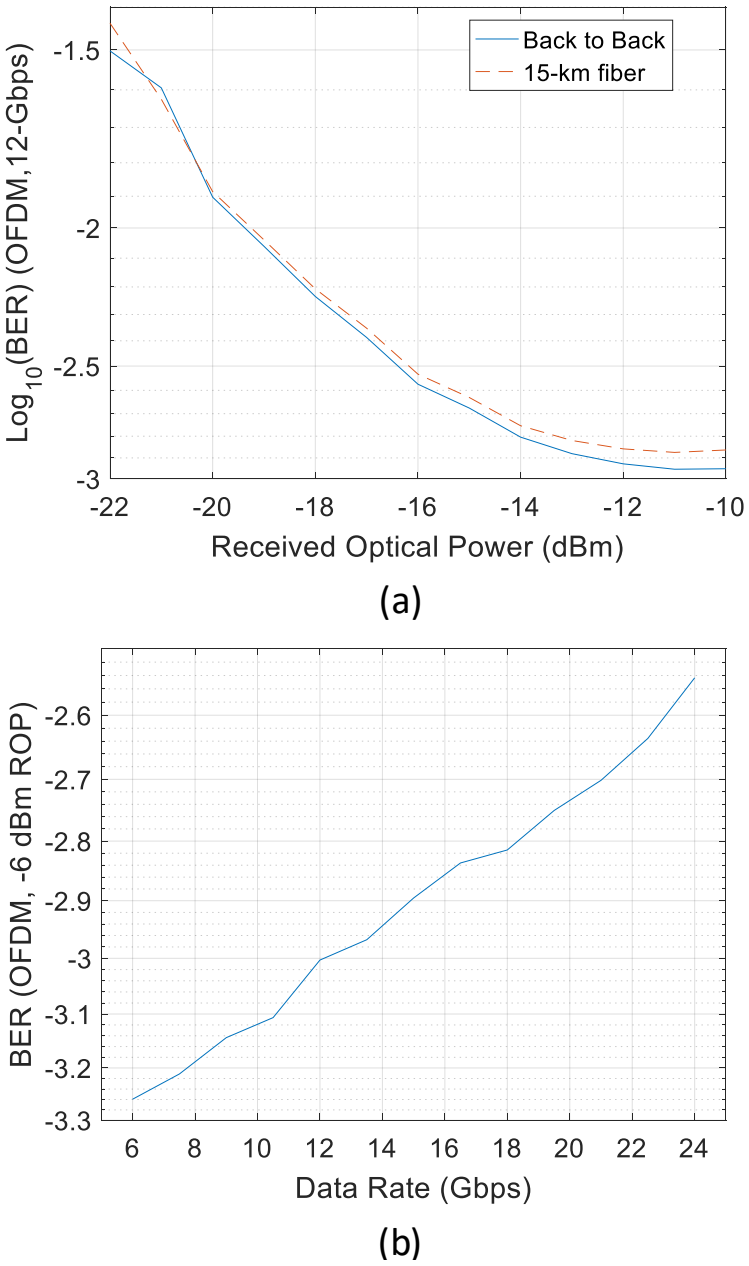


Figure 4.18: Experimental result of FSO downlink using OFDM modulation. (a) Sensitivity result. (b) Data rate result.

The system supports three independent downlink data streams: cm-wave, VLC and FSO, and one uplink data stream: MMW. All data streams are capable of being synchronized or jointly managed since they are all handled by centralized DSP in BBU pool. Two optical transmitters are utilized for downlink, and another one is used for the uplink. In the user device, no laser or any temperature sensitive components are necessary, making the

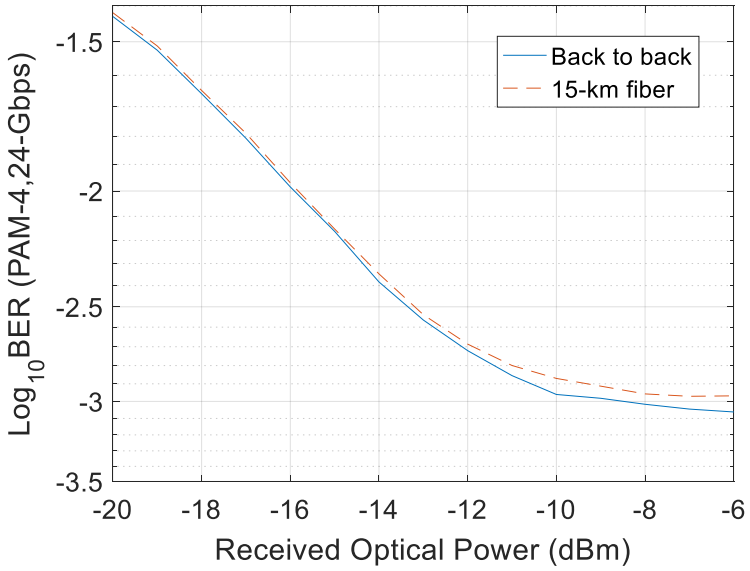


Figure 4.19: Experimental result of FSO downlink using PAM-4 modulation.

scheme more stable.

### 4.3.3 Measurement Results

We first measure the downlink FSO link performance, using OFDM modulation. Fixing the modulation to 16-QAM and bandwidth to 3.2-GHz, the sensitivity results are presented in Fig. 4.18(a), delivering 12-Gbps data rate excluding the CP overhead. Less than 0.13% BER is achieved with back to back condition. A very small penalty is generated with the 15-km fiber transmission. Then we sweep the bandwidth to vary the data rate, at -10-dBm ROP. As expected, higher data rate leads to impaired BER performance. However, tolerable channel BER of less than 0.32% is achieved with 24-Gbps channel rate.

Then, we replace the modulation to PAM-4, which is a better fit to high-speed optical links, due to its reduced PAPR and increased transmission power. At 12-Gbaud, equivalently 24-Gbps, the sensitivity is shown in Fig. 4.19. Slightly improved performance is observed. With -10-dBm ROP and 24-Gbps data rate, the OFDM provides a BER of 0.29%, while PAM-4 BER is 0.1%.

For the MMW uplink, we use widely commercialized OFDM modulation. Chang-

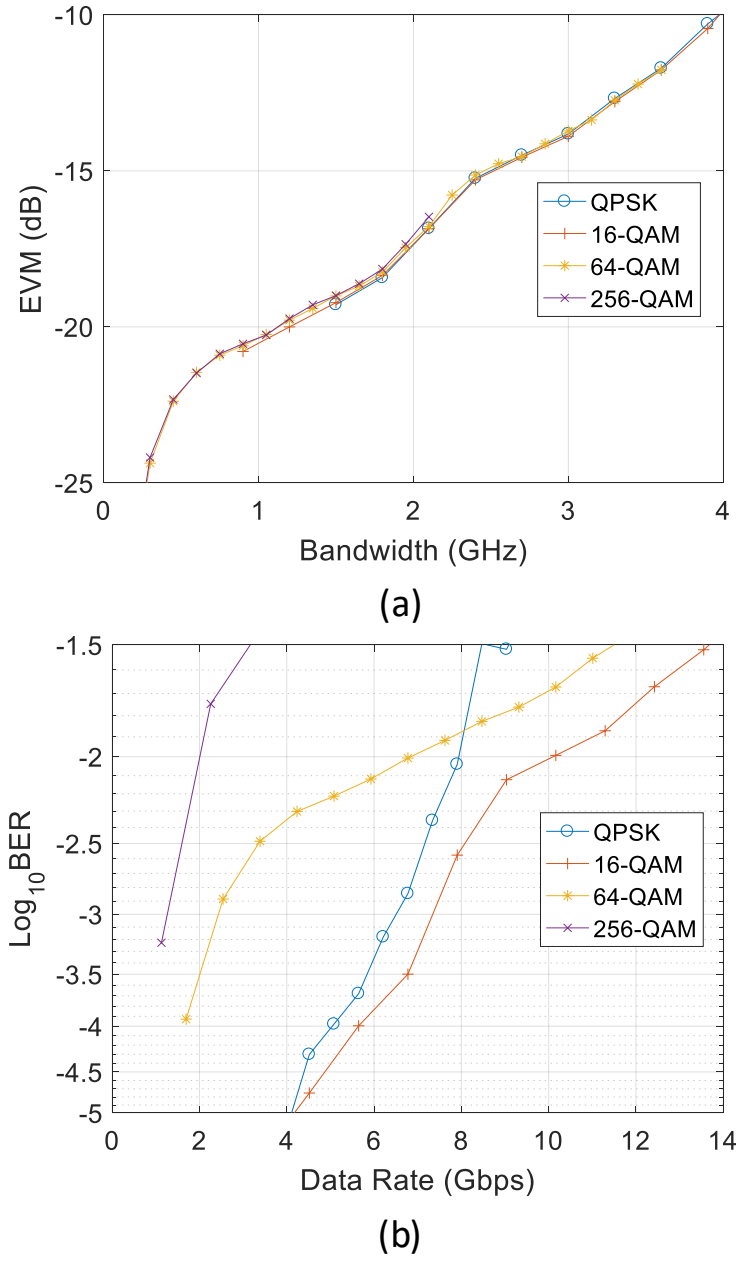


Figure 4.20: Experimental result of MMW uplink. (a) EVM and (b) BER performance with various bandwidth.

ing different signal bandwidth, we measure the EVM performance, shown in Fig. 4.20(a). Comparing between multiple QAM levels from QPSK to 256-QAM, the EVM performance is very similar with the same signal bandwidth. Up to 4-GHz channel bandwidth is evaluated. Then, we test the BER performance, with different QAM levels. Comparing among them, 16-QAM is the optimal QAM mapping with the lowest BER given the data rate

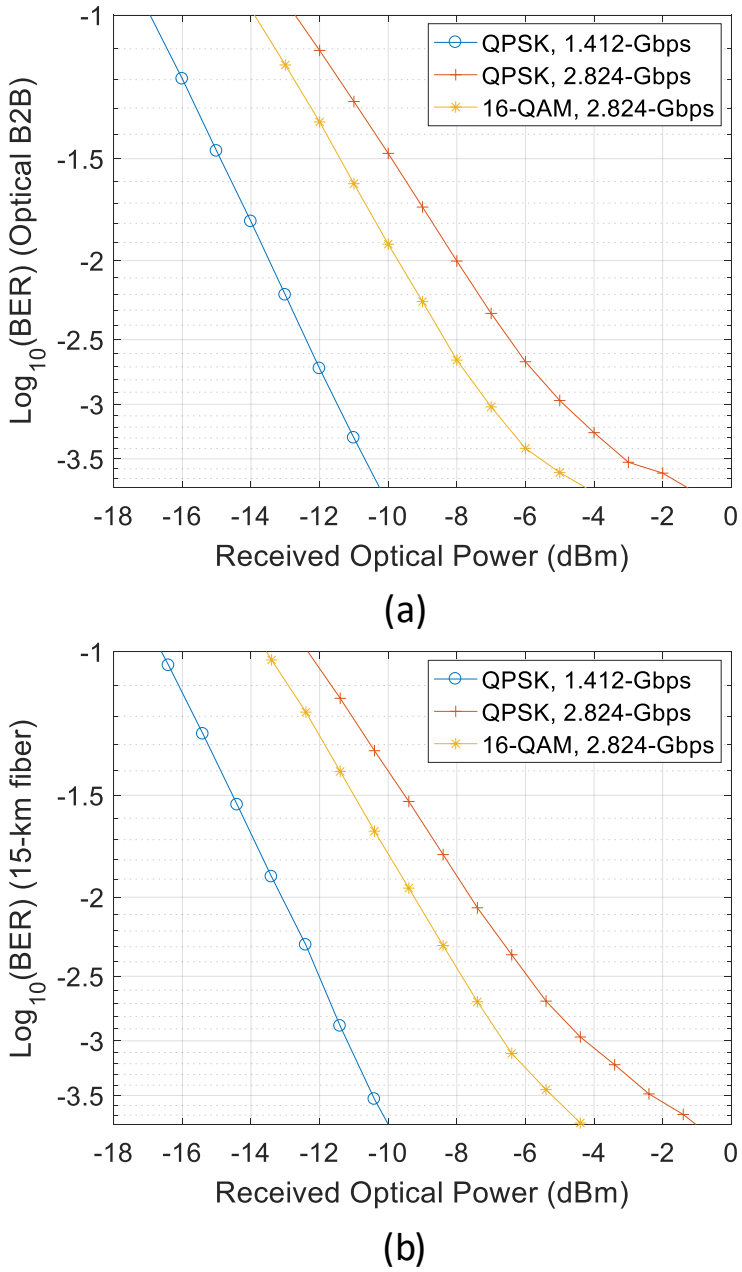


Figure 4.21: Experimental result of MMW uplink sensitivity, under (a) back to back and (b) 15-km fiber transmission.

requirement, as the red curve is always the lowest.

The MMW uplink sensitivity test is also measured, with results in Fig. 4.21. With 6 feet wireless distance, we measure the BER performance. The power is measured in BBU before PD. As expected, the 16-QAM provides the best performance and BER sensitivity. Comparing with QPSK doubling the bandwidth, we observe about 2-dB sensitivity

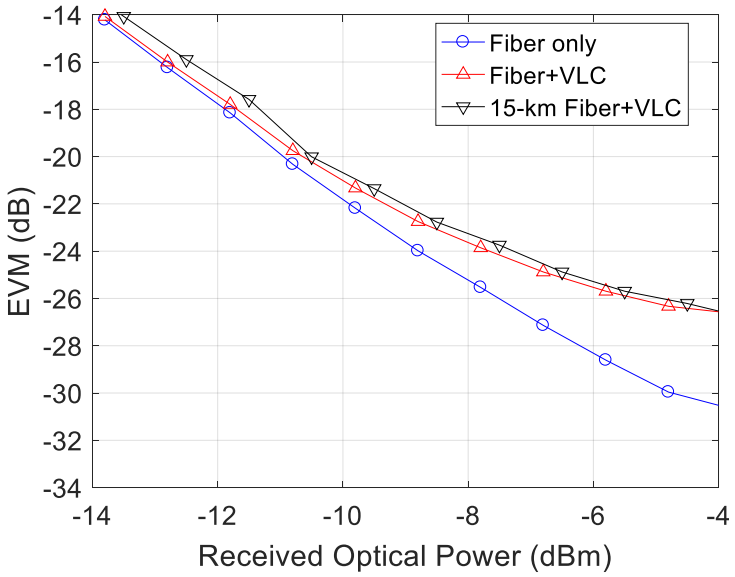


Figure 4.22: Experimental result of cm-wave downlink.

improvement with the same channel bandwidth.

The cm-wave signals powering macro cells are tested with analog MFH, with results shown in Fig. 4.22. Only MFH results are presented, without wireless transmission. Using 20-MHz OFDM signal following LTE standard, we test the back to back scenario and 15-km fiber transmission as well. EVM lower than -30-dB is measured, enough to power 256-QAM modulation. As described in Chapter 4.1, VLC link can be applied with pre-distortion. We test this scheme with VLC MFH using distributed pre-distortion technology, generating 4-dB penalty in Fig. 4.22. Here we implement and test the analog MFH, but the digital MFH can still be supported. The digital signal can be delivered in the base-band format, while other VLC traffic is carried with higher IFs for proper separation.

Lastly, the VLC link end-to-end transmission is implemented with fiber-wireless integration. The signal bandwidth is 13.5-MHz, using OFDM modulation carrying various QAM symbols from 16-QAM to 1024-QAM. A proper digital pre-distortion is applied in the RRH separation DSP, referred as distributed pre-distortion in Chapter 4.1.2. It provides the best performance under fiber-wireless integrated system architecture. The ROP is measured at the VLC RRH shown in Fig. 4.23. With different ROP, significantly different

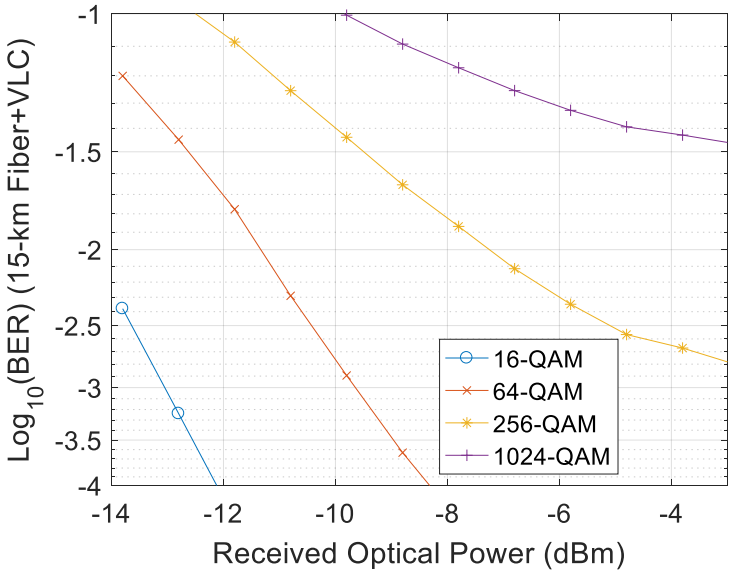


Figure 4.23: Experimental result of VLC downlink.

performance is measured. A proper trade-off between the data rate and BER should be made.

## 4.4 Summary

In this Chapter, we proposed the concept of the all-spectrum fiber-wireless integrated system. The system can utilize all spectral resources based on the application and device requirements. It can be categorized into all-spectrum MFH and all-spectrum user access.

For all-spectrum MFH, we have proposed a novel hybrid MFH architecture combining spectral efficient fiber MFH and low-cost VLC links to support cell coordination in a spatial densified network. With multi-tier master-RRHs and slave-RRHs, the deployment and operating cost of the network are significantly reduced, which has higher performance and flexibility, as well as better network extension/upgrading capability. Both centralized and distributed pre-equalization are proposed, investigated and compared. In the experiment, we demonstrated the MFH network delivering eight independent streams serving one master RRH and six slave RRHs with eight CA or $8 \times 8$ network MIMO. The system with either distributed or centralized pre-equalization has a good performance suitable for

64-QAM modulation. For outdoor all-spectrum MFH, we propose an inter-dimensional ADCT in the converged MMW/FSO wireless MFH link. Adapting to different transceiver characteristics and channel features, we propose to adaptively combine the frequency division symbols in the MMW link and time division symbols in the FSO link. Also, the repetition coding technique has been implemented to improve the system performance further. The experiment verifies the feasibility of the proposed scheme by delivering both 5G wireless symbols and additional payload for wired users, with extra tunability between performance, capacity and power margin.

Then, we propose the all-spectrum wireless access system. A complete system architecture and band allocation scheme are proposed and designed, adapting to the key performance requirements by IMT 2020 and the available transmission technologies. Bi-directional transmission supporting various applications are implemented. The optimized MFH network is designed with minimized resource utilization, which also shares the centralized C-RAN architecture. The user device is simplified without the laser embedded. It helps to enhance the stability under different temperatures. The system is experimentally demonstrated with multiple transmissions coordinated, verifying a good performance suitable for future deployment.

We investigated the all-spectrum coordination and integration technologies in both MFH and user access scenarios, as the final phase of the fiber-wireless integrated system. It provides the ultimate system capacity, improved reliability with low-latency, as well extra functions including high-precision positioning.

# CHAPTER 5
# CONCLUSION

This final chapter concludes research works in the fiber-wireless integrated systems, to achieve high capacity, low latency, and improved reliability. Future research topics are summarized as well.

With the proliferation of Internet-connected devices and the emerging all types of wireless services requiring high bandwidth, low latency and reliability, the next-generation 5G wireless communication system is actively researched and standardized. The overwhelming exploration of the wireless traffic largely relies on the advanced optical backbone networks. As separate optical and wireless systems, the legacy RAN from the 3G system cannot fulfill the requirement for both users and service providers. To enhance the system performance, improve the capacity, reduce the latency and also enable multi-cell coordination, the fiber-wireless integrated system is proposed and actively investigated in the 4G era. However, with diversified application scenarios in 5G, the existing fiber-wireless integrated system cannot fulfill the capacity requirement in eMBB, the user density needs in mMTC, or latency and reliability requirements in URLLC. The goal of this dissertation work is to design and optimize the fiber-wireless integrated system fulfilling future needs, in all three phases of the implementation in our view.

## 5.1 Technical Contributions

This dissertation studies and investigates the advanced system design and DSP technology for the fiber-wireless integrated system. Based on implementation phases of the future fiber-wireless integrated system, several groups of technical contributions are summarized.

### 5.1.1 Advanced Mobile Fronthaul

The first implementation phase is based on 4G and 5G wireless standards running on low RF bands below 6-GHz. Massive MIMO and CA are extensively used, and the network is densified geographically with massively deployed small cells. More carriers with increased bandwidth should be supported with reduced cost for deployment and operation.

Two major approaches exist for MFH: analog MFH and digital MFH. They are suitable for macro or small cells. We design advanced DSP schemes to enhance both of the approaches. The analog MFH provides high spectral efficiency and low latency but suffers from high PAPR in signals. Adaptively, we propose and implement a phase pre-distortion DSP scheme to reduce the PAPR maintaining the compatibility of standard 4G/5G devices. Utilizing the powerful DSP in centralized BBU, the signal is processed and optimized centrally. The computational complexity is further minimized by the searching algorithm, still maintaining the low-latency feature by analog MFH. In digital MFH scope, the CPRI based solution is preferred in our view for its simplicity and backward compatibility. With more carriers delivered and increased channel BER introduced by high-speed PAM-4 links, we observe severe degradations with CPRI or compressed CPRI. An adaptive digitization and channel coding scheme are designed with the idea of optimizing the optical network and carried service jointly. The digitization and channel coding parameters are changed based on the optical MFH channel conditions. Huge sensitivity and capacity improvements are demonstrated experimentally.

The trend of the small cell makes current P2P MFH insufficient, and the WDM solution shows its benefit with reduced latency, increased data rate and more RRHs supported with single trunk fiber. The challenge comes from its uplink tunable laser, which is costly and requires fine temperature control. We design a novel RRH structure with the WRC-FPLD embedded using injection locking technique. The RRH stably locks the downlink wavelength and remodulates the uplink signal. It is color insensitive, cost efficiency and capable of providing a good service quality per existing standards.

### 5.1.2 Millimeter-Wave Fiber-Wireless Integrated Systems

The congested low-frequency channels cannot fulfill user needs in the long term. Hence, MMW wireless communication with fiber-wireless integration is actively studied with advanced physical system design, providing low-cost high-bandwidth channels.

As one of the major technical contributions of this dissertation, we extend the research of advanced physical layer waveforms to the MMW fiber-wireless integrated system. The waveform design also fits into the new application trends included in the 5G system. With capacity focused eMBB using CA, we propose to use the GFDM modulation utilizing both electrical and optical carriers for wireless signals generation. Subcarrier-wise shaping is applied for reducing OOB leakage. It reduces the guard band overhead in CA operation. For reliability enhanced URLLC, the orthogonal/sparse CDM is adaptively designed by replacing the orthogonal frequency modulation kernels with digital chirps. Stronger robustness with interferences and uneven noise floors are observed, still with compatibility to eMBB. Both modulations are demonstrated experimentally, with measured results showing significantly improved performance when compared with current OFDM.

For multiple user support, the PD-NOMA is proposed and applied in the integrated system. With power division multiple access in addition to existing frequency and time division, more users can be served within the same cell. Moreover, by digitally changing the power ratio to/from different users, the tunability of the equivalent reception signal quality is enabled. The service quality with multiple users is optimized and improved, as a result. It is demonstrated in the theory, simulations, and experimental measurements. The power ratio calculation process is simplified with the proposed iteration scheme. In addition to the synchronized downlink PD-NOMA, we also design the uplink asynchronous PD-NOMA, to favor both the improved performance by NOMA and reduced latency by the asynchronous uplink transmission.

### 5.1.3 All-Spectrum Fiber-Wireless System

For the phase three implementation of the fiber-wireless integrated system, we propose the all-spectrum system, which utilizes multiple EM wave bands from low RF to VLC. Based on current P2P wireless transmission technology, we propose advanced DSP and system design for both MFH and wireless access applications.

For MFH, the LED transmitter with VLC technology is proposed to deliver analog MFH information between RRHs in the indoor environment. The feature of VLC fits into this application with limited distance and bandwidth, but very low device costs. The DSP based pre-equalization is investigated in detail with centralized or distributed processing. On the contrary, lightwave technologies in wireless MFH for outdoor application suffers from reliability due to the uncontrolled weather conditions. We design the inter-dimensional ADCT in converged MMW/FSO MFH to increase the power margin thus better reliability is achieved.

With all-spectrum wireless access, we design the complete system including both MFH and user access. The MFH is implemented with minimized wavelength usage, by utilizing advanced multiplexing and DSP technologies. The user device design is implemented to maximize the data rate while reducing the power consumption and device cost. Different spectral resources are allocated based on the user type, mobility, capacity and reliability requirement, such that an optimal design of the system is demonstrated. Both all-spectrum MFH and user access are experimentally demonstrated with increased data rate and better reliability.

The technical contributions in the dissertation work are theory derivations, simulation studies and experimental verifications on the novel DSP and system design to improve the fiber-wireless integrated system, for increased capacity, improved reliability, and reduced latency, in all three provisioned implementation phases.

## 5.2 Future Research Topics

### 5.2.1 Waveforms in All-Spectrum Systems

The research of all-spectrum fiber-wireless systems is limited to advanced system design and DSP. It makes the complex system practical in implementation for both operators and device vendors at the current stage, but all based on legacy OFDM or PAM modulations. In the future, based on various channel models and system requirements, advanced beyond-OFDM modulations and multiple access schemes can be extended to this system to enhance the performance and capacity further.

### 5.2.2 Machine Learning for DSP Scheme Design

A significant part of the dissertation work is the advanced DSP design for the future fiber-wireless integrated system. We study the system requirements, design the channel coding, mapping, modulation and multiple access schemes separately. Recently, the rapid development of machine learning technologies and platforms has drawn considerable attention from both industry and academia. With the high-performance central processing unit (CPU), graphics processing unit (GPU), tensor processing unit (NPU) or FPGA, the machine learning and artificial intelligence (AI) platform can design and optimize applications automatically, and show its significant improvement in applications like computer vision [133], speech recognition [134], automatic translation [135] and data mining. In telecommunication industries, the AI already shows its advantage in managing and controlling the network [136, 137].

For our expertise, we believe a proper machine learning model of the DSP chain can be built adapting to different channel models, shown in Fig. 5.1. No strict separation between channel coding, modulation and equalization exists. Instead, the DSP chain is built using a deep neural network, as a unified model. With proper training by comparing the input/output information, all model parameters can be optimized. More importantly, this

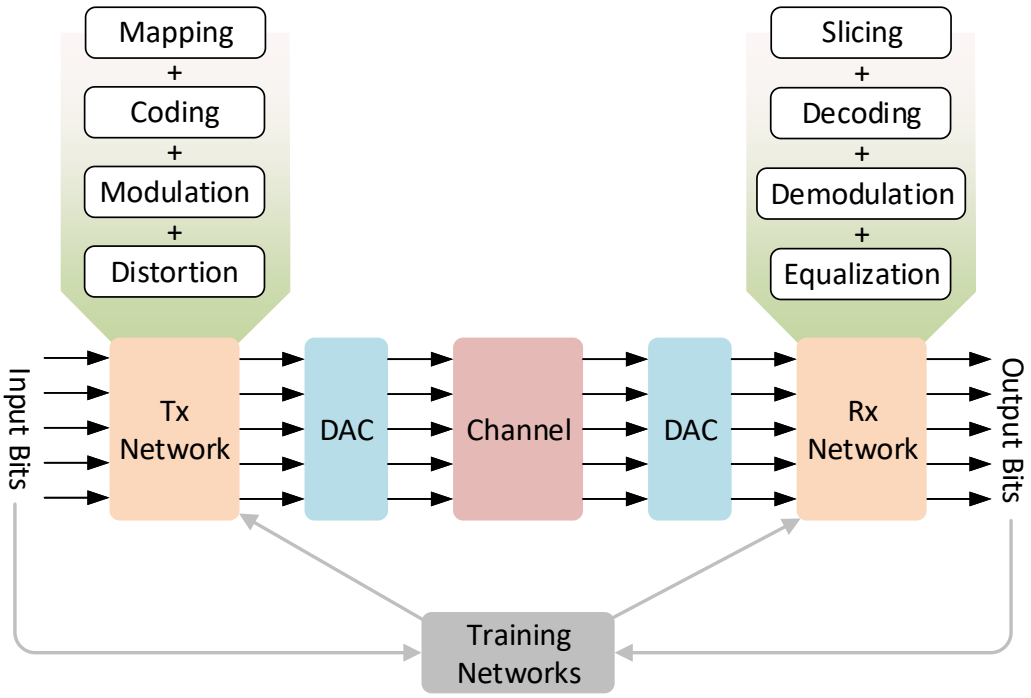


Figure 5.1: Schematic of machine learning based signal transmission/reception DSP design and model training.

process is fully automatic without manual tuning or mathematical derivation. Based on current mature modulation and coding schemes, the machine learning generated DSP scheme should have improved performance since more parameters can be adaptively optimized.

The design, train, and application of the neural network in physical layer signal design and recovery remain to be a good topic for future research in the fiber-wireless integrated system.

# REFERENCES


[1] "Cisco visual networking index: Global mobile data traffic forecast update, 2016-2021," Tech. Rep., Mar. 2017.

[2] C.-X. Wang, F. Haider, X. Gao, X.-H. You, Y. Yang, D. Yuan, H. Aggoune, H. Haas, S. Fletcher, and E. Hepsaydir, "Cellular architecture and key technologies for 5g wireless communication networks," *IEEE Communications Magazine*, vol. 52, no. 2, pp. 122–130, 2014.

[3] *2017 telecommunications trends*, `https://www.strategyand.pwc.com/trend/2017-telecommunications-industry-trends`, Accessed: 2017-12-18.

[4] J. Gubbi, R. Buyya, S. Marusic, and M. Palaniswami, "Internet of things (iot): A vision, architectural elements, and future directions," *Future generation computer systems*, vol. 29, no. 7, pp. 1645–1660, 2013.

[5] Y. Okumura and J. Terada, "Optical network technologies and architectures for backhaul / fronthaul of future radio access supporting big mobile data," in *Optical Fiber Communication Conference*, Optical Society of America, 2014, Tu3F–1.

[6] A. De La Oliva, X. C. Pérez, A. Azcorra, A. Di Giglio, F. Cavaliere, D. Tiegelbekkers, J. Lessmann, T. Haustein, A. Mourad, and P. Iovanna, "Xhaul: Toward an integrated fronthaul/backhaul architecture in 5g networks," *IEEE Wireless Communications*, vol. 22, no. 5, pp. 32–40, 2015.

[7] K. Kao and G. A. Hockham, "Dielectric-fibre surface waveguides for optical frequencies," in *Proceedings of the Institution of Electrical Engineers*, IET, vol. 113, 1966, pp. 1151–1158.

[8] H. Holma and A. Toskala, *HSDPA/HSUPA for UMTS: high speed radio access for mobile communications*. John Wiley & Sons, 2007.

[9] F. Lu, B. Zhang, Y. Yue, J. Anderson, and G.-K. Chang, "Investigation of pre-equalization technique for pluggable cfp2-aco transceivers in beyond 100 gb/s transmissions," *Journal of Lightwave Technology*, vol. 35, no. 2, pp. 230–237, 2017.

[10] N. Carapellese, M Shamsabardeh, M. Tornatore, and A. Pattavina, "Bbu hotelling in centralized radio access networks," in *Fiber-Wireless Convergence in Next-Generation Communication Networks*, Springer, 2017, pp. 265–291.

[11] "Exploring 5g new radio: Use cases capabilities and timeline," Tech. Rep., Mar. 2016.

[12] T. Taleb and A. Kunz, "Machine type communications in 3gpp networks: Potential, challenges, and solutions," *IEEE Communications Magazine*, vol. 50, no. 3, 2012.

[13] K. Zheng, S. Ou, J. Alonso-Zarate, M. Dohler, F. Liu, and H. Zhu, "Challenges of massive access in highly dense lte-advanced networks with machine-to-machine communications," *IEEE Wireless Communications*, vol. 21, no. 3, pp. 12–18, 2014.

[14] N. A. Johansson, Y.-P. E. Wang, E. Eriksson, and M. Hessler, "Radio access for ultra-reliable and low-latency 5g communications," in *Communication Workshop (ICCW), 2015 IEEE International Conference on*, IEEE, 2015, pp. 1184–1189.

[15] S. A. Ashraf, F. Lindqvist, R. Baldemair, and B. Lindoff, "Control channel design trade-offs for ultra-reliable and low-latency communication system," in *Globecom Workshops (GC Wkshps), 2015 IEEE*, IEEE, 2015, pp. 1–6.

[16] *Technical specifications and technical reports for a utran-based 3gpp system*, 3GPP, 2006.

[17] M. Iwamoto, S. Matsuoka, H. Iwasaki, and H. Otsuka, "Transmission performance of ofdm with 1024-qam in the presence of evm degradation," in *Wireless and Mobile, 2014 IEEE Asia Pacific Conference on*, IEEE, 2014, pp. 12–16.

[18] P. Mogensen, K. Pajukoski, E. Tiirola, E. Lahetkangas, J. Vihriala, S. Vesterinen, M. Laitila, G. Berardinelli, G. W. Da Costa, L. G. Garcia, *et al.*, "5g small cell optimized radio design," in *Globecom Workshops (GC Wkshps), 2013 IEEE*, IEEE, 2013, pp. 111–116.

[19] L. Guangjie, Z. Senjie, Y. Xuebin, L. Fanglan, N. Tin-fook, Z. Sunny, and K. Chen, "Architecture of gpp based, scalable, large-scale c-ran bbu pool," in *Globecom Workshops (GC Wkshps), 2012 IEEE*, IEEE, 2012, pp. 267–272.

[20] I Chih-Lin, J. Huang, R. Duan, C. Cui, J. X. Jiang, and L. Li, "Recent progress on c-ran centralization and cloudification," *IEEE Access*, vol. 2, pp. 1030–1039, 2014.

[21] R. Wang, H. Hu, and X. Yang, "Potentials and challenges of c-ran supporting multi-rats toward 5g mobile networks," *IEEE Access*, vol. 2, pp. 1187–1195, 2014.

[22] J. Bartelt, P. Rost, D. Wubben, J. Lessmann, B. Melis, and G. Fettweis, "Fronthaul and backhaul requirements of flexibly centralized radio access networks," *IEEE Wireless Communications*, vol. 22, no. 5, pp. 105–111, 2015.

[23] M. Peng, C. Wang, V. Lau, and H. V. Poor, "Fronthaul-constrained cloud radio access networks: Insights and challenges," *IEEE Wireless Communications*, vol. 22, no. 2, pp. 152–160, 2015.

[24] T. Pfeiffer, "Next generation mobile fronthaul architectures," in *Optical Fiber Communication Conference*, Optical Society of America, 2015, M2J–7.

[25] P. Chanclou, A. Pizzinat, F. Le Clech, T.-L. Reedeker, Y. Lagadec, F. Saliou, B. Le Guyader, L. Guillo, Q. Deniel, S. Gosselin, *et al.*, "Optical fiber solution for mobile fronthaul to achieve cloud radio access network," in *Future Network and Mobile Summit (FutureNetworkSummit), 2013*, IEEE, 2013, pp. 1–11.

[26] H. Al-Raweshidy and S. Komaki, *Radio over fiber technologies for mobile communications networks*. Artech House, 2002.

[27] R. Waterhouse and D. Novack, "Realizing 5g: Microwave photonics for 5g mobile wireless systems," *IEEE Microwave Magazine*, vol. 16, no. 8, pp. 84–92, 2015.

[28] S.-H. Cho, H. Park, H. S. Chung, K.-H. Doo, S. S. Lee, and J. H. Lee, "Cost-effective next generation mobile fronthaul architecture with multi-if carrier transmission scheme," in *Optical Fiber Communication Conference*, Optical Society of America, 2014, Tu2B–6.

[29] M. Zhu, X. Liu, N. Chand, F. Effenberger, and G.-K. Chang, "High-capacity mobile fronthaul supporting lte-advanced gation and $8 \times 8$ mimo," in *Optical Fiber Communications Conference and Exhibition (OFC)*, Optical Society of America, 2015, M2J–3.

[30] J. Zhang, J. Wang, M. Xu, F. Lu, L. Chen, J. Yu, and G.-k. Chang, "Full-duplex asynchronous quasi-gapless carrier-aggregation using filter-bank multi-carrier in mmw radio-over-fiber heterogeneous mobile access networks," in *Optical Fiber Communications Conference and Exhibition (OFC)*, Optical Society of America, 2016, TU2B–2.

[31] C. Liu, L. Zhang, M. Zhu, J. Wang, L. Cheng, and G.-K. Chang, "A novel multi-service small-cell cloud radio access network for mobile backhaul and computing based on radio-over-fiber technologies," *Journal of Lightwave Technology*, vol. 31, no. 17, pp. 2869–2875, 2013.

[32] X. Liu, H. Zeng, N. Chand, and F. Effenberger, "Cpri-compatible efficient mobile fronthaul transmission via equalized tdma achieving 256 gb/s cpri-equivalent data rate in a single 10-ghz-bandwidth im-dd channel," in *Optical Fiber Communications Conference and Exhibition (OFC)*, Optical Society of America, 2016, W1H–3.

[33] F. Lu, M. Xu, L. Cheng, J. Wang, S. Shen, C. Su, and G.-K. Chang, "Efficient mobile fronthaul serving massive mimo new radio services using single-if with sample-wise tdm for reduced rrh complexity and ultra-low latency," in *Optical Fiber Communication Conference*, Optical Society of America, 2017, Th3A–4.

[34] J. Zhang, J. Wang, M. Xu, F. Lu, L. Chen, J. Yu, and G.-k. Chang, "Memory-polynomial digital pre-distortion for linearity improvement of directly-modulated multi-if-over-fiber lte mobile fronthaul," in *Optical Fiber Communications Conference and Exhibition (OFC)*, Optical Society of America, 2016, TU2B–3.

[35] C. Han, S.-H. Cho, H. S. Chung, and J. H. Lee, "Linearity improvement of directly-modulated multi-if-over-fibre lte-a mobile fronthaul link using shunt diode predistorter," in *Optical Communication (ECOC), 2015 European Conference on*, IEEE, 2015, pp. 1–3.

[36] J. Wang, C. Liu, J. Zhang, M. Zhu, M. Xu, F. Lu, L. Cheng, and G.-K. Chang, "Nonlinear inter-band subcarrier intermodulations of multi-rat ofdm wireless services in 5g heterogeneous mobile fronthaul networks," *Journal of Lightwave Technology*, vol. 34, no. 17, pp. 4089–4103, 2016.

[37] T. Jiang and Y. Wu, "An overview: Peak-to-average power ratio reduction techniques for ofdm signals," *IEEE Transactions on broadcasting*, vol. 54, no. 2, pp. 257–268, 2008.

[38] K. Yang and S.-I. Chang, "Peak-to-average power control in ofdm using standard arrays of linear block codes," *IEEE Communications letters*, vol. 7, no. 4, pp. 174–176, 2003.

[39] S. H. Han and J. H. Lee, "Papr reduction of ofdm signals using a reduced complexity pts technique," *IEEE Signal Processing Letters*, vol. 11, no. 11, pp. 887–890, 2004.

[40] Y. Xiao, X. Lei, Q. Wen, and S. Li, "A class of low complexity pts techniques for papr reduction in ofdm systems," *IEEE Signal Processing Letters*, vol. 14, no. 10, pp. 680–683, 2007.

[41] D.-W. Lim, J.-S. No, C.-W. Lim, and H. Chung, "A new slm ofdm scheme with low complexity for papr reduction," *IEEE signal processing letters*, vol. 12, no. 2, pp. 93–96, 2005.

[42] J.-C. Chen and C.-P. Li, "Tone reservation using near-optimal peak reduction tone set selection algorithm for papr reduction in ofdm systems," *IEEE Signal Processing Letters*, vol. 17, no. 11, pp. 933–936, 2010.

[43] T. Wattanasuwakull and W. Benjapolakul, "Papr reduction for ofdm transmission by using a method of tone reservation and tone injection," in *Information, Communications and Signal Processing, 2005 Fifth International Conference on*, IEEE, 2005, pp. 273–277.

[44] *Common public radio interface (cpri) v7.0; interface specification*, 2015.

[45] S. H. Kim, H. S. Chung, and S. M. Kim, "Experimental demonstration of cpri data compression based on partial bit sampling for mobile front-haul link in c-ran," in *Optical Fiber Communication Conference*, Optical Society of America, 2016, W1H–5.

[46] M. Xu, F. Lu, J. Wang, L. Cheng, D. Guidotti, and G.-K. Chang, "Key technologies for next-generation digital rof mobile fronthaul with statistical data compression and multiband modulation," *Journal of Lightwave Technology*, vol. 35, no. 17, pp. 3671–3679, 2017.

[47] T. Jiang, Y. Yang, and Y.-H. Song, "Companding technique for papr reduction in ofdm systems based on an exponential function," in *Global Telecommunications Conference, 2005. GLOBECOM'05. IEEE*, IEEE, vol. 5, 2005, 4–pp.

[48] L. Zhang, X. Pang, O. Ozolins, A. Udalcovs, R. Schatz, U. Westergren, G. Jacobsen, S. Popov, L. Wosinska, S. Xiao, *et al.*, "Digital mobile fronthaul employing differential pulse code modulation with suppressed quantization noise," *Optics Express*, vol. 25, no. 25, pp. 31 921–31 936, 2017.

[49] H. Si, B. L. Ng, M. S. Rahman, and J. Zhang, "A vector quantization based compression algorithm for cpri link," in *Global Communications Conference (GLOBECOM), 2015 IEEE*, IEEE, 2015, pp. 1–6.

[50] T. Jiang, Y. Yang, and Y.-H. Song, "Exponential companding technique for papr reduction in ofdm systems," *IEEE Transactions on broadcasting*, vol. 51, no. 2, pp. 244–248, 2005.

[51] X. Wang, T. T. Tjhung, C. S. Ng, and A. A. Kassim, "On the ser analysis of a-law companded ofdm system," in *Global Telecommunications Conference, 2000. GLOBECOM'00. IEEE*, IEEE, vol. 2, 2000, pp. 756–760.

[52] N. J. Gomes, P. Chanclou, P. Turnbull, A. Magee, and V. Jungnickel, "Fronthaul evolution: From cpri to ethernet," *Optical Fiber Technology*, vol. 26, pp. 50–58, 2015.

[53] K. Miyamoto, S. Kuwano, J. Terada, and A. Otaka, "Performance evaluation of mobile fronthaul optical bandwidth reduction and wireless transmission in split-phy processing architecture," in *Optical Fiber Communication Conference*, Optical Society of America, 2016, W1H–4.

[54] ——, "Split-phy processing architecture to realize base station coordination and transmission bandwidth reduction in mobile fronthaul," in *Optical Fiber Communications Conference and Exhibition (OFC)*, Optical Society of America, 2015, M2J–4.

[55] J. Wang, Z. Yu, K. Ying, J. Zhang, F. Lu, M. Xu, L. Cheng, X. Ma, and G.-K. Chang, "Digital mobile fronthaul based on delta–sigma modulation for 32 lte carrier aggregation and fbmc signals," *Journal of Optical Communications and Networking*, vol. 9, no. 2, A233–A244, 2017.

[56] J. Wang, Z. Yu, K. Ying, J. Zhang, F. Lu, M. Xu, and G.-K. Chang, "Delta-sigma modulation for digital mobile fronthaul enabling carrier aggregation of 32 4g-lte/30 5g-fbmc signals in a single-$\lambda$ 10-gb/s im-dd channel," in *Optical Fiber Communications Conference and Exhibition (OFC)*, Optical Society of America, 2016, W1H–2.

[57] J. Wang, Z. Yu, K. Ying, J. Zhang, F. Lu, M. Xu, L. Cheng, X. Ma, and G.-K. Chang, "10-gbaud ook/pam4 digital mobile fronthaul based on one-bit/two-bit delta-sigma modulation supporting carrier aggregation of 32 lte-a signals," in *42nd European Conference on Optical Communication*, VDE, 2016, pp. 914–916.

[58] J. Wang, Z. Jia, L. A. Campos, C. Knittle, and G.-K. Chang, "Optical coherent transmission of 20x192-mhz docsis 3.1 channels with 16384qam based on delta-sigma digitization," in *Optical Fiber Communication Conference*, Optical Society of America, 2017, Th1K–1.

[59] Y. Luo, X. Zhou, F. Effenberger, X. Yan, G. Peng, Y. Qian, and Y. Ma, "Time-and wavelength-division multiplexed passive optical network (twdm-pon) for next-generation pon stage 2 (ng-pon2)," *Journal of Lightwave Technology*, vol. 31, no. 4, pp. 587–593, 2013.

[60] M. Zhu, F. Li, F. Lu, J. Yu, C. Su, G. Gu, and G.-K. Chang, "Wavelength resource sharing in bidirectional optical mobile fronthaul," *Journal of Lightwave Technology*, vol. 33, no. 15, pp. 3182–3188, 2015.

[61] F. Saliou, G. Simon, P. Chanclou, M. Brunero, L. Marazzi, P. Parolari, M. Martinelli, R. Brenot, A. Maho, S. Barbet, *et al.*, "Self-seeded rsoas wdm pon field trial for business and mobile fronthaul applications," in *Optical Fiber Communication Conference*, Optical Society of America, 2015, M2A–2.

[62] G. Yuan, X. Zhang, W. Wang, and Y. Yang, "Carrier aggregation for lte-advanced mobile communication systems," *IEEE Communications Magazine*, vol. 48, no. 2, 2010.

[63] A. J. Paulraj, D. A. Gore, R. U. Nabar, and H. Bolcskei, "An overview of mimo communications-a key to gigabit wireless," *Proceedings of the IEEE*, vol. 92, no. 2, pp. 198–218, 2004.

[64] G. Papagiannakis, G. Singh, and N. Magnenat-Thalmann, "A survey of mobile and wireless technologies for augmented reality systems," *Computer Animation and Virtual Worlds*, vol. 19, no. 1, pp. 3–22, 2008.

[65] A. Liu and V. K. Lau, "Cache-enabled opportunistic cooperative mimo for video streaming in wireless systems," *IEEE Transactions on Signal Processing*, vol. 62, no. 2, pp. 390–402, 2014.

[66] F. Lu, J. Wang, L. Cheng, M. Xu, M. Zhu, and G.-K. Chang, "Millimeter-wave radio-over-fiber access architecture for implementing real-time cloud computing service," in *Conference on Lasers and Electro-Optics (CLEO)*, IEEE, 2014, STu1J–1.

[67] *Leading towards next generation "5g" mobile services*, `https://www.fcc.gov/news-events/blog/2015/08/03/leading-towards-next-generation-5g-mobile-services.`, Accessed: 2017-03-07.

[68] *Tg3c channel modeling sub-committee final report*, IEEE, 2007.

[69] R. Van Nee, "Breaking the gigabit-per-second barrier with 802.11 ac," *IEEE Wireless Communications*, vol. 18, no. 2, 2011.

[70] E. Perahia and M. X. Gong, "Gigabit wireless lans: An overview of ieee 802.11 ac and 802.11 ad," *ACM SIGMOBILE Mobile Computing and Communications Review*, vol. 15, no. 3, pp. 23–33, 2011.

[71] *Status of project ieee 802.11ay*, `http://www.ieee802.org/11/Reports/tgay_update.htm`, Accessed: 2017-03-07.

[72] *Status of ieee 802.11 next generation 60ghz (ng60) study group*, `http://www.ieee802.org/11/Reports/ng60_update.htm`, Accessed: 2017-03-07.

[73] E. Ben-Dor, T. S. Rappaport, Y. Qiao, and S. J. Lauffenburger, "Millimeter-wave 60 ghz outdoor and vehicle aoa propagation measurements using a broadband channel sounder," in *Global Telecommunications Conference (GLOBECOM 2011), 2011 IEEE*, IEEE, 2011, pp. 1–6.

[74] X. Li, Z. Dong, J. Yu, N. Chi, Y. Shao, and G. Chang, "Fiber-wireless transmission system of 108 gb/sdata over 80 km fiber and 2 $\times$ 2 multiple-input multiple-output wireless links at 100 ghz w-band frequency," *Optics letters*, vol. 37, no. 24, pp. 5106–5108, 2012.

[75] X. Li, J. Yu, J. Zhang, F. Li, Y. Xu, Z. Zhang, and J. Xiao, "Fiber-wireless-fiber link for 100-gb/s pdm-qpsk signal transmission at w-band," *IEEE Photon. Technol. Lett.*, vol. 26, no. 18, pp. 1825–1828, 2014.

[76] J. Yu, X. Li, J. Zhang, and J. Xiao, "432-gb/s pdm-16qam signal wireless delivery at w-band using optical and antenna polarization multiplexing," in *Optical Communication (ECOC), 2014 European Conference on*, IEEE, 2014, We.3.6.6.

[77] M. Fujishima, M. Motoyoshi, K. Katayama, K. Takano, N. Ono, and R. Fujimoto, "98 mw 10 gbps wireless transceiver chipset with d-band cmos circuits," *IEEE Journal of Solid-State Circuits*, vol. 48, no. 10, pp. 2273–2284, 2013.

[78] I. F. Akyildiz, J. M. Jornet, and C. Han, "Terahertz band: Next frontier for wireless communications," *Physical Communication*, vol. 12, pp. 16–32, 2014.

[79] J. Yu, Z. Jia, L. Xu, L. Chen, T. Wang, and G.-K. Chang, "Dwdm optical millimeter-wave generation for radio-over-fiber using an optical phase modulator and an optical interleaver," *IEEE photonics technology letters*, vol. 18, no. 13, pp. 1418–1420, 2006.

[80] J. Yu, Z. Jia, L. Yi, Y. Su, G.-K. Chang, and T. Wang, "Optical millimeter-wave generation or up-conversion using external modulators," *IEEE Photonics Technology Letters*, vol. 18, no. 1, pp. 265–267, 2006.

[81] X. Pang, A. Caballero, A. Dogadaev, V. Arlunno, R. Borkowski, J. S. Pedersen, L. Deng, F. Karinou, F. Roubeau, D. Zibar, *et al.*, "100 gbit/s hybrid optical fiber-wireless link in the w-band (75–110 ghz)," *Optics Express*, vol. 19, no. 25, pp. 24 944–24 949, 2011.

[82] X. Li, Y. Xu, J. Xiao, and J. Yu, "A 2$\times$ 2 mimo optical wireless system at d-band," in *Optical Fiber Communications Conference and Exhibition (OFC)*, Optical Society of America, 2016, Th4A–7.

[83] J. Yu, Z. Jia, T. Wang, and G. K. Chang, "Centralized lightwave radio-over-fiber system with photonic frequency quadrupling for high-frequency millimeter-wave generation," *IEEE Photonics Technology Letters*, vol. 19, no. 19, pp. 1499–1501, 2007.

[84] X. Li, J. Zhang, J. Xiao, Z. Zhang, Y. Xu, and J. Yu, "W-band 8qam vector signal generation by mzm-based photonic frequency octupling," *IEEE Photonics Technology Letters*, vol. 27, no. 12, pp. 1257–1260, 2015.

[85] C.-T. Lin, P.-T. Shih, J. Chen, W.-Q. Xue, P.-C. Peng, and S. Chi, "Optical millimeter-wave signal generation using frequency quadrupling technique and no optical filtering," *IEEE Photonics Technology Letters*, vol. 20, no. 12, pp. 1027–1029, 2008.

[86] J. Xiao, X. Li, Y. Xu, Z. Zhang, L. Chen, and J. Yu, "W-band ofdm photonic vector signal generation employing a single mach-zehnder modulator and precoding," *Optics express*, vol. 23, no. 18, pp. 24 029–24 034, 2015.

[87] J. Zhang, J. Yu, N. Chi, Z. Dong, X. Li, and G.-K. Chang, "Multichannel 120-gb/s data transmission over 2 $\times$ 2 mimo fiber-wireless link at w-band," *IEEE Photon. Technol. Lett*, vol. 25, no. 8, pp. 780–783, 2013.

[88] G. Fettweis, M. Krondorf, and S. Bittner, "Gfdm-generalized frequency division multiplexing," in *Vehicular Technology Conference, 2009. VTC Spring 2009. IEEE 69th*, IEEE, 2009, pp. 1–4.

[89] N. Michailow, M. Matthé, I. S. Gaspar, A. N. Caldevilla, L. L. Mendes, A. Festag, and G. Fettweis, "Generalized frequency division multiplexing for 5th generation cellular networks," *IEEE Transactions on Communications*, vol. 62, no. 9, pp. 3045–3061, 2014.

[90] N. Michailow, M. Lentmaier, P. Rost, and G. Fettweis, "Integration of a gfdm secondary system in an ofdm primary system," in *Future Network & Mobile Summit (FutureNetw), 2011*, IEEE, 2011, pp. 1–8.

[91] F. Schaich, "Filterbank based multi carrier transmission (fbmc)evolving ofdm: Fbmc in the context of wimax," in *Wireless Conference (EW), 2010 European*, IEEE, 2010, pp. 1051–1058.

[92] B. Farhang-Boroujeny, "Ofdm versus filter bank multicarrier," *IEEE signal processing magazine*, vol. 28, no. 3, pp. 92–112, 2011.

[93] V. Vakilian, T. Wild, F. Schaich, S. ten Brink, and J.-F. Frigon, "Universal-filtered multi-carrier technique for wireless systems beyond lte," in *Globecom Workshops (GC Wkshps), 2013 IEEE*, IEEE, 2013, pp. 223–228.

[94] F. Schaich, T. Wild, and Y. Chen, "Waveform contenders for 5g-suitability for short packet and low latency transmissions," in *Vehicular Technology Conference (VTC Spring), 2014 IEEE 79th*, IEEE, 2014, pp. 1–5.

[95] R Zayani, Y Medjahdi, H Shaiek, and D Roviras, "Wola-ofdm: A potential candidate for asynchronous 5g," in *Globecom Workshops (GC Wkshps), 2016 IEEE*, IEEE, 2016, pp. 1–5.

[96] Y Medjahdi, R Zayani, H Shaïek, and D Roviras, "Wola processing: A useful tool for windowed waveforms in 5g with relaxed synchronicity," in *Communications Workshops (ICC Workshops), 2017 IEEE International Conference on*, IEEE, 2017, pp. 393–398.

[97] Y. Liu and G. Liu, "User-centric wireless network for 5g," in *5G Mobile Communications*, Springer, 2017, pp. 457–473.

[98] O. Kjebon, R. Schatz, S. Lourdudoss, S. Nilsson, B Stalnacke, and L Backbom, "30 ghz direct modulation bandwidth in detuned loaded ingaasp dbr lasers at 1.55/spl mu/m wavelength," *Electronics Letters*, vol. 33, no. 6, pp. 488–489, 1997.

[99] H.-H. Lu, C.-Y. Li, C.-A. Chu, T.-C. Lu, B.-R. Chen, C.-J. Wu, and D.-H. Lin, "10 m/25 gbps lifi transmission system based on a two-stage injection-locked 680 nm vcsel transmitter," *Optics letters*, vol. 40, no. 19, pp. 4563–4566, 2015.

[100] I.-C. Lu, C.-H. Yeh, D.-Z. Hsu, and C.-W. Chow, "Utilization of 1-ghz vcsel for 11.1-gbps ofdm vlc wireless communication," *IEEE Photonics Journal*, vol. 8, no. 3, pp. 1–6, 2016.

[101] P. T. Dat, A. Kanno, and T. Kawanishi, "Radio-on-radio-over-fiber: Efficient fronthauling for small cells and moving cells," *IEEE Wireless Communications*, vol. 22, no. 5, pp. 67–75, 2015.

[102] A. Vavoulas, H. G. Sandalidis, and D. Varoutas, "Weather effects on fso network connectivity," *Journal of Optical Communications and Networking*, vol. 4, no. 10, pp. 734–740, 2012.

[103] I. I. Kim and E. Korevaar, "Availability of free space optics (fso) and hybrid fso/rf systems," in *Proc. SPIE*, vol. 4530, 2001, pp. 84–95.

[104] F. Nadeem, V. Kvicera, M. S. Awan, E. Leitgeb, S. S. Muhammad, and G. Kandus, "Weather effects on hybrid fso/rf communication link," *IEEE Journal on Selected Areas in Communications*, vol. 27, no. 9, 2009.

[105] B. He and R. Schober, "Bit-interleaved coded modulation for hybrid rf/fso systems," *IEEE Transactions on Communications*, vol. 57, no. 12, 2009.

[106] J. Zhang, J. Wang, Y. Xu, M. Xu, F. Lu, L. Cheng, J. Yu, and G.-k. Chang, "Fiber–wireless integrated mobile backhaul network based on a hybrid millimeter-wave and free-space-optics architecture with an adaptive diversity combining technique," *Optics letters*, vol. 41, no. 9, pp. 1909–1912, 2016.

[107] J. Mietzner, R. Schober, L. Lampe, W. H. Gerstacker, and P. A. Hoeher, "Multiple-antenna techniques for wireless communications-a comprehensive literature survey," *IEEE communications surveys & tutorials*, vol. 11, no. 2, 2009.

[108] H. Sampath, S. Talwar, J. Tellado, V. Erceg, and A. Paulraj, "A fourth-generation mimo-ofdm broadband wireless system: Design, performance, and field trial results," *IEEE Communications Magazine*, vol. 40, no. 9, pp. 143–149, 2002.

[109] A. Garg, M. R. Bhatnagar, O. Berder, and B. Vrigneau, "Improved beamforming for fso miso system over gamma-gamma fading with pointing errors," in *Advanced Technologies for Communications (ATC), 2016 International Conference on*, IEEE, 2016, pp. 362–368.

[110] K. Kiasaleh, "Beam-tracking in fso links impaired by correlated fading," in *Free-Space Laser Communications VI*, International Society for Optics and Photonics, vol. 6304, 2006, p. 63041I.

[111] C. H. Doan, S. Emami, A. M. Niknejad, and R. W. Brodersen, "Millimeter-wave cmos design," *IEEE Journal of solid-state circuits*, vol. 40, no. 1, pp. 144–155, 2005.

[112] H. A. Karimi, *Advanced location-based technologies and services*. CRC Press, 2013.

[113] D. Turner, S. Savage, and A. C. Snoeren, "On the empirical performance of self-calibrating wifi location systems," in *Local Computer Networks (LCN), 2011 IEEE 36th Conference on*, IEEE, 2011, pp. 76–84.

[114] *Combain positioning service*, `https://combain.com/`, Accessed: 2017-12-18.

[115] S.-H. Yang, E.-M. Jeong, D.-R. Kim, H.-S. Kim, Y.-H. Son, and S.-K. Han, "Indoor three-dimensional location estimation based on led visible light communication," *Electronics Letters*, vol. 49, no. 1, pp. 54–56, 2013.

[116] Y. S. Eroglu, I. Guvenc, N. Pala, and M. Yuksel, "Aoa-based localization and tracking in multi-element vlc systems," in *Wireless and Microwave Technology Conference (WAMICON), 2015 IEEE 16th Annual*, IEEE, 2015, pp. 1–5.

[117] C.-W. Hsu, J.-T. Wu, H.-Y. Wang, C.-W. Chow, C.-H. Lee, M.-T. Chu, and C.-H. Yeh, "Visible light positioning and lighting based on identity positioning and rf carrier allocation technique using a solar cell receiver," *IEEE Photonics Journal*, vol. 8, no. 4, pp. 1–7, 2016.

[118] C.-W. Hsu, S. Liu, F. Lu, C.-W. Chow, C.-H. Yeh, and G.-K. Chang, "Accurate indoor visible light positioning system utilizing machine learning technique with height tolerance," in *Optical Fiber Communications Conference and Exhibition (OFC)*, Optical Society of America, 2018, M2K–2.

[119] "5g in china: Outlook and regional comparisons," Tech. Rep., 2017.

[120] F. Lu, M. Xu, L. Cheng, J. Wang, S. Shen, J. Zhang, and G.-K. Chang, "Sub-band predistortion for papr reduction in spectral efficient 5g mobile fronthaul," *IEEE Photonics Technology Letters*, vol. 29, no. 1, pp. 122–125, 2017.

[121] F. Lu, M. Xu, L. Cheng, J. Wang, S. Shen, H. J. Cho, and G.-K. Chang, "Adaptive digitization and variable channel coding for enhancement of compressed digital mobile fronthaul in pam-4 optical links," *Journal of Lightwave Technology*, vol. 35, no. 21, pp. 4714–4720, 2017.

[122] A. Li, V. Meghdadi, J.-P. Cances, and C. Aupetit-Berthelemot, "High throughput ldpc decoder for c-ran optical fronthaul based on improved bit-flipping algorithm," in *Communication Systems, Networks and Digital Signal Processing (CSNDSP), 2016 10th International Symposium on*, IEEE, 2016, pp. 1–5.

[123] F. Lu, Y.-C. Chi, M. Xu, L. Cheng, J. Wang, C.-T. Tsai, G.-R. Lin, and G.-K. Chang, "Cost-effective bi-directional mobile fronthaul employing wrc-fpld for beyond lte-advanced services," in *Optical Fiber Communications Conference and Exhibition (OFC)*, Optical Society of America, 2016, TU2B.5.

[124] F. Lu, L. Cheng, M. Zhu, J. Wang, M. Xu, X. Ma, and G.-K. Chang, "Generalized frequency division multiplexing for photonic-assisted millimeter-wave carrier aggregation," in *Optical Fiber Communication Conference*, Optical Society of America, 2015, M3E–3.

[125] F. Lu, L. Cheng, M. Xu, J. Wang, S. Shen, and G.-K. Chang, "Orthogonal chirp division multiplexing in millimeter-wave fiber-wireless integrated systems for enhanced mobile broadband and ultra-reliable communications," in *Optical Fiber Communication Conference (OFC)*, Optical Society of America, 2017, Th4E–5.

[126] X. Ouyang and J. Zhao, "Orthogonal chirp division multiplexing," *IEEE Transactions on Communications*, vol. 64, no. 9, pp. 3946–3957, 2016.

[127] F. Lu, M. Xu, L. Cheng, J. Wang, J. Zhang, and G.-K. Chang, "Non-orthogonal multiple access with successive interference cancellation in millimeter-wave radio-over-fiber systems," *Journal of Lightwave Technology*, vol. 34, no. 17, pp. 4179–4186, 2016.

[128] R. Fletcher and C. M. Reeves, "Function minimization by conjugate gradients," *The computer journal*, vol. 7, no. 2, pp. 149–154, 1964.

[129] G. Wunder, P. Jung, M. Kasparick, T. Wild, F. Schaich, Y. Chen, S. Ten Brink, I. Gaspar, N. Michailow, A. Festag, *et al.*, "5gnow: Non-orthogonal, asynchronous waveforms for future mobile applications," *IEEE Communications Magazine*, vol. 52, no. 2, pp. 97–105, 2014.

[130] F. Lu, M. Xu, L. Cheng, J. Wang, and G.-K. Chang, "Power-division non-orthogonal multiple access (noma) in flexible optical access with synchronized downlink / asynchronous uplink," *Journal of Lightwave Technology*, vol. 35, no. 19, pp. 4145–4152, 2017.

[131] F. Lu, L. Cheng, J. Shi, M. Xu, J. Wang, S. Shen, and G.-k. Chang, "Efficient mobile fronthaul incorporating vlc links for coordinated densified cells," *IEEE Photonics Technology Letters*, vol. 29, no. 13, pp. 1059–1062, 2017.

[132] F. Lu, M. Xu, S. Shen, Y. M. Alfadhli, J. J. Cho, and G.-k. Chang, "Demonstration of inter-dimensional adaptive diversity combining and repetition coding in converged mmw/fso links for 5g and beyond mobile fronthaul," in *Optical Fiber Communications Conference and Exhibition (OFC)*, Optical Society of America, 2018, M3K–4.

[133] Y. LeCun, Y. Bengio, and G. Hinton, "Deep learning," *Nature*, vol. 521, no. 7553, pp. 436–444, 2015.

[134] G. E. Dahl, D. Yu, L. Deng, and A. Acero, "Context-dependent pre-trained deep neural networks for large-vocabulary speech recognition," *IEEE Transactions on audio, speech, and language processing*, vol. 20, no. 1, pp. 30–42, 2012.

[135] D. Bahdanau, K. Cho, and Y. Bengio, "Neural machine translation by jointly learning to align and translate," *arXiv preprint arXiv:1409.0473*, 2014.

[136] T. T. Nguyen and G. Armitage, "A survey of techniques for internet traffic classification using machine learning," *IEEE Communications Surveys & Tutorials*, vol. 10, no. 4, pp. 56–76, 2008.

[137] S. Zander, T. Nguyen, and G. Armitage, "Automated traffic classification and application identification using machine learning," in *Local Computer Networks, 2005. 30th Anniversary. The IEEE Conference on*, IEEE, 2005, pp. 250–257.

# PUBLICATIONS

*Journal Publications*

2017


[1] F. Lu, M. Xu, L. Cheng, J. Wang, S. Shen, H. J. Cho, and G.-K. Chang, "Adaptive digitization and variable channel coding for enhancement of compressed digital mobile fronthaul in pam-4 optical links," *Journal of Lightwave Technology*, vol. 35, no. 21, pp. 4714–4720, 2017.

[2] F. Lu, M. Xu, L. Cheng, J. Wang, and G.-K. Chang, "Power-division non-orthogonal multiple access (noma) in flexible optical access with synchronized downlink / asynchronous uplink," *Journal of Lightwave Technology*, vol. 35, no. 19, pp. 4145–4152, 2017.

[3] F. Lu, L. Cheng, M. Xu, J. Wang, S. Shen, and G.-K. Chang, "Orthogonal and sparse chirp division multiplexing for mmw fiber-wireless integrated systems," *IEEE Photonics Technology Letters*, vol. 29, no. 16, pp. 1316–1319, 2017.

[4] F. Lu, L. Cheng, J. Shi, M. Xu, J. Wang, S. Shen, and G.-k. Chang, "Efficient mobile fronthaul incorporating vlc links for coordinated densified cells," *IEEE Photonics Technology Letters*, vol. 29, no. 13, pp. 1059–1062, 2017.

[5] F. Lu, B. Zhang, Y. Yue, J. Anderson, and G.-K. Chang, "Investigation of pre-equalization technique for pluggable cfp2-aco transceivers in beyond 100 gb/s transmissions," *Journal of Lightwave Technology*, vol. 35, no. 2, pp. 230–237, 2017.

[6] F. Lu, M. Xu, L. Cheng, J. Wang, S. Shen, J. Zhang, and G.-K. Chang, "Sub-band predistortion for papr reduction in spectral efficient 5g mobile fronthaul," *IEEE Photonics Technology Letters*, vol. 29, no. 1, pp. 122–125, 2017.

[7] S. Liu, M. Xu, J. Wang, F. Lu, W. Zhang, H. Tian, and G.-K. Chang, "A multilevel artificial neural network nonlinear equalizer for millimeter-wave mobile fronthaul systems," *Journal of Lightwave Technology*, vol. 35, no. 20, pp. 4406–4417, 2017.

[8] M. Xu, F. Lu, J. Wang, L. Cheng, D. Guidotti, and G.-K. Chang, "Key technologies for next-generation digital rof mobile fronthaul with statistical data compression and multiband modulation," *Journal of Lightwave Technology*, vol. 35, no. 17, pp. 3671–3679, 2017.

[9] J. Wang, Z. Yu, K. Ying, J. Zhang, F. Lu, M. Xu, L. Cheng, X. Ma, and G.-K. Chang, "Digital mobile fronthaul based on delta–sigma modulation for 32 lte carrier aggregation and fbmc signals," *Journal of Optical Communications and Networking*, vol. 9, no. 2, A233–A244, 2017.

[10] M. Xu, J. Zhang, F. Lu, J. Wang, L. Cheng, M. I. Khalil, D. Guidotti, and G.-K. Chang, "Orthogonal multiband cap modulation based on offset-qam and advanced filter design in spectral efficient mmw rof systems," *Journal of Lightwave Technology*, vol. 35, no. 4, pp. 997–1005, 2017.

[11] J. Zhang, M. Xu, J. Wang, F. Lu, L. Cheng, H. Cho, K. Ying, J. Yu, and G.-K. Chang, "Full-duplex quasi-gapless carrier aggregation using fbmc in centralized radio-over-fiber heterogeneous networks," *Journal of Lightwave Technology*, vol. 35, no. 4, pp. 989–996, 2017.

2016

[12] F. Lu, M. Xu, L. Cheng, J. Wang, J. Zhang, and G.-K. Chang, "Non-orthogonal multiple access with successive interference cancellation in millimeter-wave radio-over-fiber systems," *Journal of Lightwave Technology*, vol. 34, no. 17, pp. 4179–4186, 2016.

[13] J. Zhang, J. Wang, Y. Xu, M. Xu, F. Lu, L. Cheng, J. Yu, and G.-k. Chang, "Fiber–wireless integrated mobile backhaul network based on a hybrid millimeter-wave and free-space-optics architecture with an adaptive diversity combining technique," *Optics letters*, vol. 41, no. 9, pp. 1909–1912, 2016.

[14] M. Xu, J.-H. Yan, J. Zhang, F. Lu, J. Wang, L. Cheng, D. Guidotti, and G.-K. Chang, "Bidirectional fiber-wireless access technology for 5g mobile spectral aggregation and cell densification," *Journal of Optical Communications and Networking*, vol. 8, no. 12, B104–B110, 2016.

[15] M. Xu, J. Zhang, F. Lu, J. Wang, L. Cheng, H. J. Cho, M. I. Khalil, D. Guidotti, and G.-K. Chang, "Fbmc in next-generation mobile fronthaul networks with centralized pre-equalization," *IEEE Photonics Technology Letters*, vol. 28, no. 18, pp. 1912–1915, 2016.

[16] J. Wang, C. Liu, J. Zhang, M. Zhu, M. Xu, F. Lu, L. Cheng, and G.-K. Chang, "Nonlinear inter-band subcarrier intermodulations of multi-rat ofdm wireless services in 5g heterogeneous mobile fronthaul networks," *Journal of Lightwave Technology*, vol. 34, no. 17, pp. 4089–4103, 2016.

[17] L. Cheng, M. M. U. Gul, F. Lu, M. Zhu, J. Wang, M. Xu, X. Ma, and G.-K. Chang, "Coordinated multipoint transmissions in millimeter-wave radio-over-fiber systems," *Journal of Lightwave Technology*, vol. 34, no. 2, pp. 653–660, 2016.

2015

[18] M. Zhu, F. Li, F. Lu, J. Yu, C. Su, G. Gu, and G.-K. Chang, "Wavelength resource sharing in bidirectional optical mobile fronthaul," *Journal of Lightwave Technology*, vol. 33, no. 15, pp. 3182–3188, 2015.

[19] M. Xu, Y.-C. Chi, J. Wang, L. Cheng, F. Lu, M. I. Khalil, C.-T. Tsai, G.-R. Lin, and G.-K. Chang, "Wavelength sharing and reuse in dual-band wdm-pon systems employing wrc-fplds," *IEEE Photonics Technology Letters*, vol. 27, no. 17, pp. 1821–1824, 2015.

2014

[20] L. Cheng, M. Zhu, J. Wang, M. Xu, F. Lu, and G.-K. Chang, "Photonic precoding for millimeter-wave multicell mimo in centralized rof system," *IEEE Photonics Technology Letters*, vol. 26, no. 11, pp. 1116–1119, 2014.

[21] J. Zheng, F. Lu, M. Xu, M. Zhu, M. I. Khalil, X. Bao, D. Guidotti, J. Liu, N. Zhu, and G.-K. Chang, "A dual-polarization coherent communication system with simplified optical receiver for udwdm-pon architecture," *Optics express*, vol. 22, no. 26, pp. 31 735–31 745, 2014.

*Conference Publications*

2018

[22] F. Lu, M. Xu, S. Shen, Y. M. Alfadhli, J. J. Cho, and G.-k. Chang, "Demonstration of inter-dimensional adaptive diversity combining and repetition coding in converged mmw/fso links for 5g and beyond mobile fronthaul," in *Optical Fiber Communications Conference and Exhibition (OFC)*, Optical Society of America, 2018, M3K–4.

[23] F. Lu, P.-C. Peng, S. Liu, M. Xu, S. Shen, and G.-k. Chang, "Integration of multivariate gaussian mixture model for enhanced pam-4 decoding employing basis expansion," in *Optical Fiber Communications Conference and Exhibition (OFC)*, Optical Society of America, 2018, M2F–1.

[24] H. J. Cho, H. Cho, M. Xu, F. Lu, S. Shen, X. Ma, and G.-K. Chang, "Asynchronous transmission using universal filtered multicarrier for multiservice applications in 5g fiber-wireless integrated mobile fronthaul," in *Optical Fiber Communications Conference and Exhibition (OFC)*, Optical Society of America, 2018, Tu3J–2.

[25] C.-W. Hsu, S. Liu, F. Lu, C.-W. Chow, C.-H. Yeh, and G.-K. Chang, "Accurate indoor visible light positioning system utilizing machine learning technique with height tolerance," in *Optical Fiber Communications Conference and Exhibition (OFC)*, Optical Society of America, 2018, M2K–2.

[26] S. Shen, T. Kanesan, F. Lu, M. Xu, L. Cheng, J. Wang, Y. M. Alfadhli, H. J. Cho, S. Mitani, and G.-K. Chang, "Efficient mobile fronthaul using windowed ofdm exhibiting high cfo tolerance and strong oob-leakage suppression with low dsp complexity," in *Optical Fiber Communications Conference and Exhibition (OFC)*, Optical Society of America, 2018, Th3G–7.

[27] S. Shen, T. Kanesan, F. Lu, M. Xu, P.-C. Peng, S. Liu, C.-W. H. Hsu, Q. Zhou, Y. M. Alfadhli, H. J. Cho, S. Mitani, J. Finkelstein, and G.-K. Chang, "Spectrum-efficient 50-gbps long-range optical access over 85-km ssmf via dml using windowed ofdm supporting quasi-gapless asynchronous multiband transmission," in *Optical Fiber Communications Conference and Exhibition (OFC)*, Optical Society of America, 2018, M2B–5.

[28] M. Xu, Z. Jia, P.-C. Peng, S. Liu, F. Lu, C. Knittle, and G.-K. Chang, "4 $\times$ 100g pam-4 transmission in faster-than-nyquist systems incorporating eigenvalue-space precoding," in *Optical Fiber Communications Conference and Exhibition (OFC)*, Optical Society of America, 2018, W1J–7.

2017

[29] F. Lu, L. Cheng, M. Xu, J. Wang, S. Shen, and G.-K. Chang, "Orthogonal chirp division multiplexing in millimeter-wave fiber-wireless integrated systems for enhanced mobile broadband and ultra-reliable communications," in *Optical Fiber Communication Conference (OFC)*, Optical Society of America, 2017, Th4E–5.

[30] F. Lu, M. Xu, L. Cheng, J. Wang, S. Shen, C. Su, and G.-K. Chang, "Efficient mobile fronthaul serving massive mimo new radio services using single-if with sample-wise tdm for reduced rrh complexity and ultra-low latency," in *Optical Fiber Communication Conference*, Optical Society of America, 2017, Th3A–4.

[31] L. Cheng, F. Lu, J. Wang, M. Xu, S. Shen, and G.-K. Chang, "Millimeter-wave radio bundling for reliable transmission in multi-section fiber-wireless mobile fronthaul," in *Optical Fiber Communications Conference and Exhibition (OFC)*, Optical Society of America, 2017, W1C–2.

[32] J. Zhang, J. Yu, J. Wang, M. Xu, L. Cheng, F. Lu, S. Shen, Y. Yan, H. Cho, D. Guidotti, *et al.*, "Enabling technologies for millimeter-wave radio-over-fiber systems in next generation heterogeneous mobile access networks," in *Broadband Access Communication Technologies XI*, International Society for Optics and Photonics, vol. 10128, 2017, 101280A.

[33] F. Lu, B. Zhang, Y. Yue, J. Anderson, and G.-k. Chang, "Study and measurement of channel impairments on beyond 100g coherent cfp2-aco pluggable optics," in *Optical Fiber Communications Conference and Exhibition (OFC)*, Optical Society of America, 2016, Th1B–2.

[34] F. Lu, Y.-C. Chi, M. Xu, L. Cheng, J. Wang, C.-T. Tsai, G.-R. Lin, and G.-K. Chang, "Cost-effective bi-directional mobile fronthaul employing wrc-fpld for beyond lte-advanced services," in *Optical Fiber Communications Conference and Exhibition (OFC)*, Optical Society of America, 2016, TU2B.5.

[35] J. Wang, Z. Yu, K. Ying, J. Zhang, F. Lu, M. Xu, and G.-K. Chang, "Delta-sigma modulation for digital mobile fronthaul enabling carrier aggregation of 32 4g-lte/30 5g-fbmc signals in a single-$\lambda$ 10-gb/s im-dd channel," in *Optical Fiber Communications Conference and Exhibition (OFC)*, Optical Society of America, 2016, W1H–2.

[36] L. Cheng, M. Xu, F. Lu, J. Wang, J. Zhang, X. Ma, and G.-K. Chang, "Millimeter-wave cell grouping for optimized coverage based on radio-over-fiber and centralized processing," in *Optical Fiber Communication Conference*, Optical Society of America, 2016, Th2A–17.

[37] M. Xu, J. Zhang, F. Lu, Y. Wang, D. Guidotti, and G.-K. Chang, "Investigation of fbmc in mobile fronthaul networks for 5g wireless with time-frequency modulation adaptation," in *Optical Fiber Communications Conference and Exhibition (OFC), 2016*, Optical Society of America, 2016, W3C–2.

[38] M. Xu, J. Zhang, F. Lu, L. Cheng, J. Wang, D. Guidotti, T. Kanesan, S. M. Mitani, and G.-K. Chang, "Multiband oqam cap modulation in mmw rof systems with enhanced spectral and computational efficiency," in *Optical Fiber Communications Conference and Exhibition (OFC), 2016*, Optical Society of America, 2016, Tu3B–3.

[39] J. Zhang, J. Wang, M. Xu, F. Lu, L. Chen, J. Yu, and G.-k. Chang, "Memory-polynomial digital pre-distortion for linearity improvement of directly-modulated multi-if-over-fiber lte mobile fronthaul," in *Optical Fiber Communications Conference and Exhibition (OFC)*, Optical Society of America, 2016, TU2B–3.

[40] J. Zhang, J. Wang, M. Xu, F. Lu, L. Chen, J. Yu, and G.-k. Chang, "Full-duplex asynchronous quasi-gapless carrier-aggregation using filter-bank multi-carrier in mmw radio-over-fiber heterogeneous mobile access networks," in *Optical Fiber Communications Conference and Exhibition (OFC)*, Optical Society of America, 2016, TU2B–2.

[41] J. Wang, Z. Yu, K. Ying, J. Zhang, F. Lu, M. Xu, L. Cheng, X. Ma, and G.-K. Chang, "10-gbaud ook/pam4 digital mobile fronthaul based on one-bit/two-bit delta-sigma

modulation supporting carrier aggregation of 32 lte-a signals," in *42nd European Conference on Optical Communication*, VDE, 2016, pp. 914–916.

2015

[42] F. Lu, L. Cheng, M. Zhu, J. Wang, M. Xu, X. Ma, and G.-K. Chang, "Generalized frequency division multiplexing for photonic-assisted millimeter-wave carrier aggregation," in *Optical Fiber Communication Conference*, Optical Society of America, 2015, M3E–3.

[43] J. Zheng, F. Lu, M. Xu, M. Zhu, I. Khalil, G.-K. Chang, *et al.*, "Photonics-assisted microwave mixing and direct detection for dual-polarization and scm based udwdm-pon," in *Optical Fiber Communication Conference*, Optical Society of America, 2015, Th2A–56.

[44] L. Cheng, M. Gul, A. Ng'oma, F. Lu, X. Ma, and G.-K. Chang, "High-diversity millimeter-wave comp transmission based on centralized sfbc in radio-over-fiber systems," in *Optical Fiber Communications Conference and Exhibition (OFC)*, Optical Society of America, 2015, W3F–5.

[45] J. Zhang, M. Xu, J. Wang, F. Lu, L. Cheng, M. Zhu, I. Khalil, J. Yu, and G.-K. Chang, "Carrier aggregation for mmw inter-rat and intra-rat in next generation heterogeneous mobile data network based on optical domain band mapping," in *41-st European Conference on Optical Communication*, IEEE, 2015, pp. 1–3.

2014

[46] F. Lu, J. Wang, L. Cheng, M. Xu, M. Zhu, and G.-K. Chang, "Millimeter-wave radio-over-fiber access architecture for implementing real-time cloud computing service," in *Conference on Lasers and Electro-Optics (CLEO)*, IEEE, 2014, STu1J–1.

# VITA

Feng Lu was born in 1990 in Wuhan, Hubei province, China. He received the B.E. degree in Electronic Information Science and Technology from the Department of Electronic Engineering, Tsinghua University, Beijing, China, in 2013, and the M.S. degree in Electrical and Computer Engineering from Georgia Institute of Technology, Atlanta, GA, in 2016. Currently, he is working toward his Ph.D. degree in Prof. Gee-Kung Chang's group at the School of Electrical and Computer Engineering of Georgia Institute of Technology, Atlanta, GA.

He joined Prof. Chang's group since fall 2013, and have worked on several projects for the National Science Foundation (NSF) Center on Fiber-Wireless Integration and Networking (FiWIN). In 2015, he was a hardware engineer intern at Juniper Networks, Sunnyvale, California; in 2016 and 2017, he was a product research and development intern at Semtech Corporation, San Jose, California. His research mainly focuses on system design and signal processing techniques for next-generation wireless and fiber-wireless integrated systems.

He has authored and co-authored more than 45 peer-reviewed journal articles and international conference papers. He is a student member of IEEE Photonics Society and Optical Society America. He also serves as an active reviewer for Journal of Lightwave Technology, Journal of Optical Communications and Networking, Optics Express, Optics Letters, Photonics Journal, Optics Communications, Optical Fiber Technology, International Journal of Electronics and Communications, and International Journal for Light and Electron Optics.